Supplementary Information (SI) for Organic & Biomolecular Chemistry.
This journal is © The Royal Society of Chemistry 2026

Supporting information

Potassium Hydrogen Sulfate Promoted One-pot Synthesis of Bis(indolyl)alkane Esters from α-Keto Carboxylic Acids: In Silico and In Vitro Anticancer Studies

Trinadh Ballanki [a], Anjali Devi Subramanian [a], Pravin Chinnappa [b], Vaishnu Suresh Kumar [c], Mohit Garg [c], Jebiti Haribabu [d], Daniel Moraga [e], and Baby Viswambharan [a*]

Department of Chemistry, National Institute of Technology, Tiruchirappalli, Tamil Nadu - 620015, India,
Corresponding author Email: babyv@nitt.edu, baby.viswam@gmail.com.
[b] Department of Chemistry, Bharathidasan University, Tiruchirappalli, Tamil Nadu, 620024, India
[c] Department of Chemical Engineering, Birla Institute of Technology and Science, Pilani, Rajasthan, 333031, India
[d] Facultad de Medicina, Universidad de Atacama, Los Carreras 1579, 1532502 Copiapó, Chile.
[e] Laboratorio de Fisiología, Departamento de Ciencias Biomédicas, Facultad de Medicina, Universidad de Tarapacá, Arica 1000000, Chile.

Table of contents

1. General information

All reactions were carried out in oven-dried glassware. All the commercially available chemicals (Sigma Aldrich, TCI, Alfa Aesar, Avra, and SRL) were used directly and freshly distilled dry solvents for anhydrous conditions. Column chromatography was performed with silica gel (200 - 300 mesh) using gradient elution with a hexane and ethyl acetate mixture as eluent. All the reactions were monitored by thin-layer chromatography (TLC) on precoated silica gel plates and visualized under a UV chamber. ESI-HRMS spectra were recorded on an Agilent Advance Bio 6545XT LC/Q-TOF mass spectrometer. NMR spectra (^{1}H and ^{13}C) were recorded on a Bruker 500MHz NMR spectrometer. The solvent signal of $CDCl_3$ was referenced at 7.26 ppm for ^{1}H NMR and 77.16 ppm for ^{13}C NMR, and DMSO-d_6 (δ 2.50 ppm at ^{1}H NMR and δ 39.92 ppm at ^{13}C NMR). Chemical shift values (δ) are quoted in ppm, and coupling constants (*J*) are recorded in hertz (Hz). The following abbreviations classify the multiplicity: s = singlet, d = doublet, t = triplet, m = multiplet, dd = doublet of doublet, q = quartet, etc. Melting points were determined by using the Stuart melting point apparatus (SMP 30) and temperatures were uncorrected.

2. Single crystal X-ray diffraction

A brown, block-like specimen of $C_{25}H_{24}N_2O_2$, with approximate dimensions 0.37 mm x 0.22 mm x 0.19 mm, was used for the X-ray crystallographic analysis. The X-ray intensity data were measured (λ = 0.71073 Å). The total exposure time was 1.5 hours. The frames were integrated with the Bruker SAINT software package using a narrow-frame algorithm. The integration of the data using a monoclinic unit cell yielded a total of 57573 reflections to a maximum θ angle of 28.3° (0.75 Å resolution), of which 5061 were independent. The final cell constants of a = 10.933 (2) Å, b = 12.500 (2) Å, c = 15.856 (3) Å, β = 107.097 (6)°, volume = 2047.7 (7) Å^3. Data were corrected for absorption effects using the multi-scan method (SADABS). The calculated minimum and maximum transmission coefficients (based on crystal size) are 0.691 and 0.746. The structure was solved and refined using the Bruker SHELXTL Software Package, using the space group $P2_1/n$, with Z = 4 for the formula unit, $C_{25}H_{24}N_2O_2$. The largest peak in the final difference electron density synthesis was 0.37 e$^-$/Å^3, and the largest hole was -0.25 e$^-$/Å^3. On the basis of the final model, the calculated density was 1.247 g/cm^3 and F(000), 816.

Figure S1. Single-crystal X-ray structure of 20 (Ellipsoids contour of probability level is 50%).

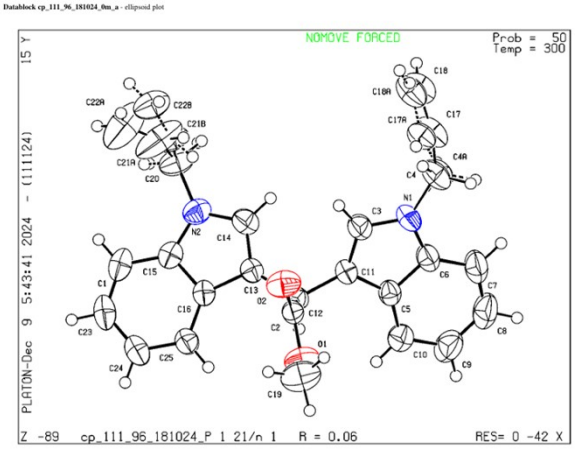

Table S1. Crystal data and structure refinement for 20.

Identification code	cp_111_96_181024_0m_a
Empirical formula	$C_{25}H_{24}N_2O_2$
Formula weight	384.46 g/mol
Crystal system	Monoclinic
Temperature	300 K
Wavelength	0.71073 Å
Crystal system, space group	Block brown, $P2_1/n$
Unit cell dimensions	a = 10.933 (2) Å alpha=90^0 b = 12.500 (2) Å beta =109.09^0 c =15.856 (3) Å gamma=90^0
Volume	2047.7 (7) $Å^3$
Z, Calculated density	4
Absorption coefficient - μ	0.08 mm^{-1}
F (000)	816
Crystal size	0.37 × 0.22 × 0.19 mm
Theta range for data collection - θ	2.6 to 27.9°
Limiting indices	-14<=h<=14, -16<=k<=16, -21<=l<=21
Reflections collected / unique	57573
Absorption correction	Multi-Scan
Independent reflections	5061 [R(int) = 0.041]
Max. and min. transmission	0.746 and 0.691
D_x	1.247 Mg m^{-3}
Refinement method	Refinement on F^2
Data / restraints / parameters	5061 / 36 / 310
R[F2 > 2σ(F^2)]	0.061
wR(F^2)	0.158
Largest diff. peak and hole	0.37 and -0.25 e$Å^{-3}$

3. Preparation of starting materials

3.1. General procedure for preparation of Indole-3-glyoxylic acid and 2-oxo-2-(1H-pyrrol-2-yl)acetic acid: [1]

To a two-necked 50 mL flask containing the indole or Pyrrole (4 mmol) in anhydrous ether (18 mL), a solution of oxalyl chloride (4 mmol) in anhydrous ether (0.64 mL) at 0 °C under an argon atmosphere was added dropwise over 10 min. The mixture was stirred for an additional 10 min; an orange precipitate formed. A saturated aqueous solution of sodium bicarbonate (6 mL) was added with caution. The mixture was heated to reflux for 30 min, cooled, and acidified with 10% HCl, resulting in the precipitation of the indole-3-glyoxylic acid in 81% yield and 2-oxo-2-(1H-pyrrol-2-yl)acetic acid in 77 %.

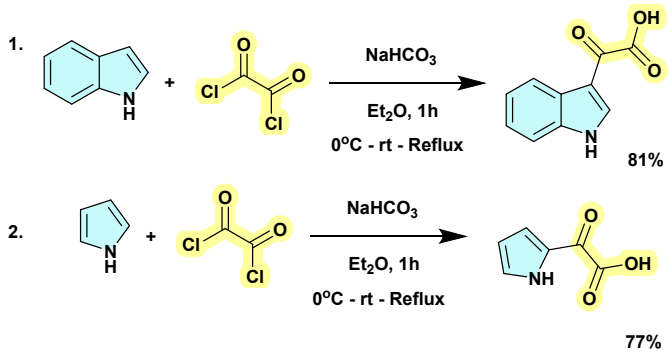

3.2. General procedure for preparation of 2-(1-methyl-1H-indol-3-yl)-2-oxoacetic acid :[2]

To a 250 mL RBF was added 1-methylindole (7.6 mmol, 1 equiv.) and anhydrous Et_2O (15 mL). The solution was cooled to 0 °C and oxalyl chloride (11.4 mmol, 1.5 equiv.) was added dropwise over a period of 10 minutes. The mixture was warmed to room temperature and stirred for 2 hours. The suspension was then cooled to 0 °C, and a saturated $NaHCO_3$ solution (5 mL) and H_2O (5 mL) were added dropwise and stirred overnight. The resulting suspension was filtered and air-dried. The filtrate was dissolved in DCM (30 mL) and extracted with 3 M NaOH solution (2 x 25 mL). The aqueous extract was cooled and acidified to pH 1-2 with concentrated HCl. The resulting precipitate was filtered, washed with cold water (2 x 10 mL), and air-dried. Pure 2-(1-methyl-1H-indol-3-yl)-2 oxoacetic acid was obtained as a light-yellow solid in 77 % yield.

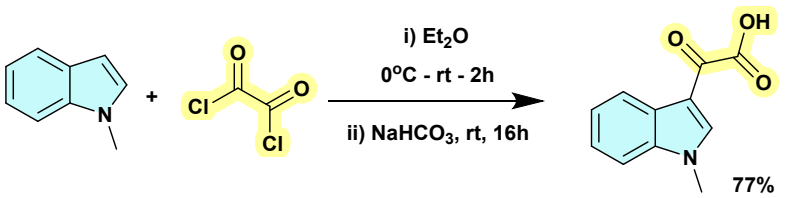

3.3. General procedure for preparation of α–Oxoacids: [2]

A flame-dried Schlenk flask with stir bar under N_2 was charged with the aryl ketone (5 mmol, 1 equiv.), SeO_2 (7.5 mmol, 1.5 equiv.) and anhydrous pyridine (12 mL). The solution was heated to 110 °C and stirred for 1 hour. After this time, the temperature was lowered to 90 °C and stirred for an additional 4 hours. Upon completion, the solution was cooled to room temperature, diluted with DCM (50 mL), and filtered. The filtrate was washed with HCl solution (1N, 20 mL), water (3 x 20 mL), and saturated NaCl solution (1 x 10 mL). The organic extract was dried over Na_2SO_4, filtered, and the solvent removed under reduced pressure. The crude α–oxo-acids were purified by silica flash chromatography in 9:1 EtOAc in hexanes and isolated as white to yellow solids.

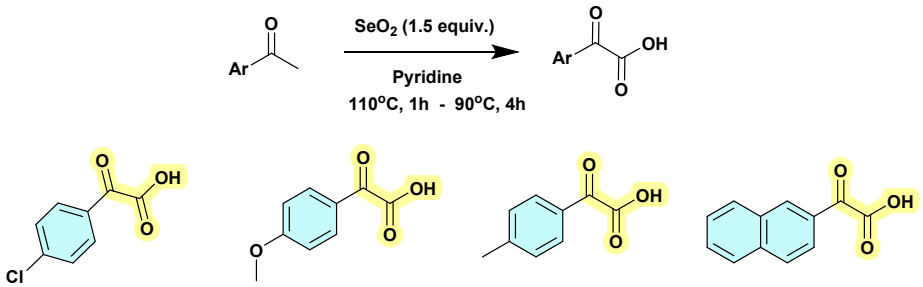

3.4. General procedure for preparation of N-Protected Amino Acids:[3]

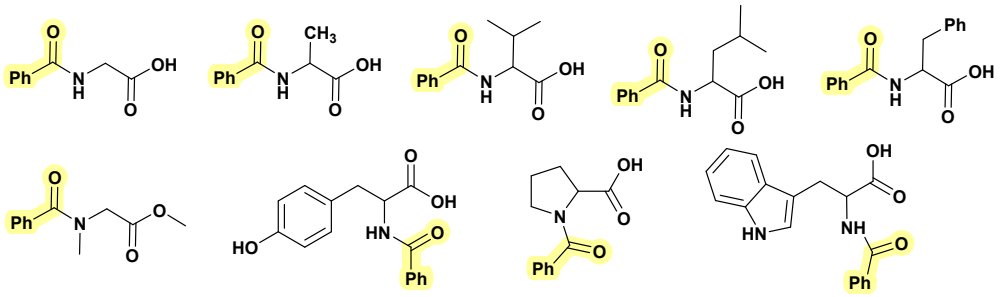

Amino acid (1 equiv., 19.4 mmol) was dissolved in 1 M NaOH aqueous solution (20 mL). The mixture was cooled to 0 °C, and then benzoyl chloride (1 equiv.) and 1 M NaOH aqueous solution (20 mL) were added dropwise simultaneously. The resulting mixture was stirred for 5h at room temperature. Then 1M HCl (60mL) was added to the reaction mixture and stirred for 10 min. The resulting solid was collected by filtration and washed with water and Et_2O. The desired product was obtained as a white solid. The following compounds were prepared in a similar manner with different yields, 80 - 98%.

4. General procedure for the methyl 2,2-di(1H-indol-3-yl)acetate (3) synthesis

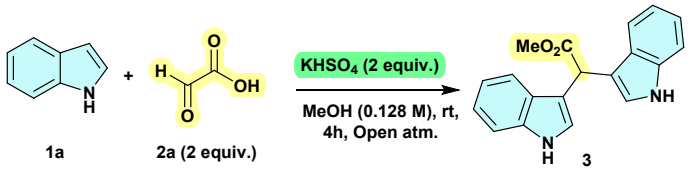

To an oven-dried 5 mL vial equipped with a magnetic stir bar and a cap were added glyoxylic acid (2.0 equiv.) and potassium bisulfate ($KHSO_4$, 2.0 equiv.) in methanol (1 mL). The mixture was stirred at room temperature for 10 minutes. A solution of indole (1a, 0.426 mmol, 1.0 equiv.) in methanol (1 mL) was then added dropwise to the above reaction mixture. The reaction was stirred at room temperature for 4 hours. The progress of the reaction was monitored by thin-layer chromatography (TLC). After complete consumption of the starting material, the reaction was quenched with water and extracted with ethyl acetate (3 × 10 mL). The combined organic layers were washed successively with saturated sodium bicarbonate ($NaHCO_3$) solution and brine, then dried over anhydrous sodium sulfate (Na_2SO_4). The solvent was removed under reduced pressure, and the crude residue was purified by column chromatography on silica gel using hexane/ethyl acetate (85:15, v/v) as the eluent to afford the pure product.

5. Gram-scale synthesis

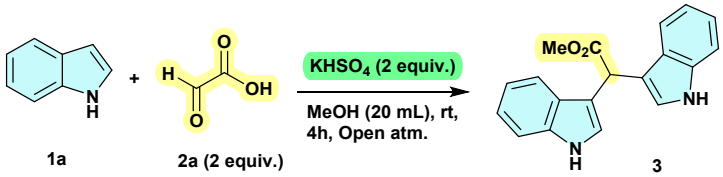

To a 100 mL round-bottom flask equipped with a magnetic stir bar and fitted with a rubber septum were added glyoxylic acid (2.0 equiv) and potassium bisulfate ($KHSO_4$, 2.0 equiv) in methanol (20 mL). The mixture was stirred at room temperature for 10 minutes. A solution of indole (1a, 8.53 mmol, 1.0 equiv) in methanol (20 mL) was then added dropwise to the reaction mixture. The reaction was stirred at room temperature for 4 hours. Reaction progress was monitored by thin-layer chromatography (TLC). After complete consumption of the starting material, the reaction was quenched with water and extracted with ethyl acetate (3 × 50 mL). The combined organic layers were washed successively with saturated sodium bicarbonate ($NaHCO_3$) solution and brine, then dried over anhydrous sodium sulfate (Na_2SO_4). The solvent was removed under reduced pressure, and the crude product was purified by column chromatography on silica gel using hexane/ethyl acetate (85:15, v/v) as the eluent to afford the desired product methyl 2,2-di(1H-indol-3-yl)acetate **(3)** in 81% yield.

6. Application of the developed strategy towards biologically relevant molecules [4]

6.a. Synthesis of 2,2-di(1H-indol-3-yl)ethan-1-ol (53)

According to the known procedure with minor modifications, A solution of the ester **3** (0.164 mmol, 1.0 equiv.) in dry ether 1 mL is added dropwise to a stirred suspension of lithium aluminium hydride (2.5 equiv.) in dry ether 1mL at 0 °C. After the addition, the reaction was stirred at room temperature for 1 hour. After complete consumption of the starting material, the reaction was quenched with saturated sodium sulfate (Na_2SO_4) and extracted with ethyl acetate (3 × 10 mL). The combined organic layers were washed with brine, then dried over anhydrous sodium sulfate (Na_2SO_4). The solvent was removed under reduced pressure, and the crude residue was purified by column chromatography on silica gel using hexane/ethyl acetate (80:20, v/v) as the eluent to afford the pure product 2,2-di(1H-indol-3-yl)ethan-1-ol (**53**) in 62% yield.

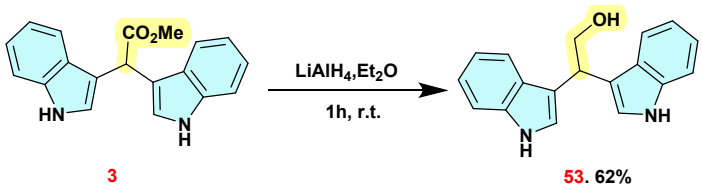

3 53. 62%

6.b. Synthesis of Sterptindole (54) and Arsindoline B (55)

According to the known procedure with minor modifications, a mixture of alcohol **53,** (0.108 mmol, 1.0 equiv.), sodium acetate (3.5 equiv.) and acetic or n-butyric anhydride (18.5 equiv.) is stirred at room temperature for 17 hours. Ethyl acetate (1 mL) and methanol (0.1 mL) are added, and the mixture is stirred overnight. Then the mixture was extracted with DCM. The combined organic layers were washed successively with water and brine, then dried over anhydrous sodium sulfate (Na_2SO_4). The solvent was removed under reduced pressure, and the crude residue was purified by column chromatography on silica gel using hexane/ethyl acetate (80:20, v/v) as the eluent to afford the pure product Streptindole (**54**) in 77% yield and Arsindoline B (**55**) in 74% yield respectively.

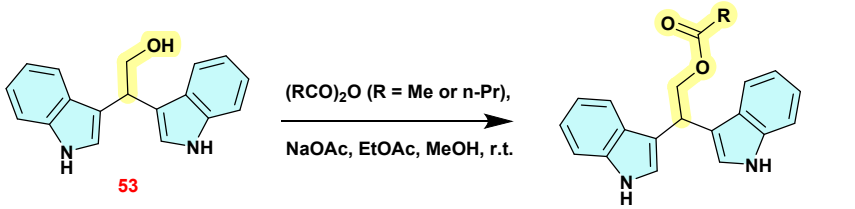

53

54. R - CH_3; Sterptindole, 77%.
55. R - n-Pr, Arsindoline B, 74%,
Antitumor agents

7. General methodology for computational studies and vitro studies

SwissADME web tool: SwissADME (www.swissadme.ch), developed by the Swiss Institute of Bioinformatics, is a free web-based tool for predicting pharmacokinetic profiles, physicochemical properties, and drug-likeness of small molecules. In this study, the synthesized ligands were submitted as SMILES notations for in-silico evaluation. The platform provided key ADME parameters (absorption, distribution, metabolism, excretion), solubility, lipophilicity, protein-binding affinity, hydration potential, and BBB permeability. Drug-likeness was validated using Lipinski, Veber, Ghose rules, QED, and CMC-50-like filters. Results were generated in tabular and graphical formats (including the BOILED-Egg and bioavailability radar), enabling efficient pre-screening and prioritization of promising candidates for synthesis and biological evaluation.

Density Functional Theory (DFT): Density Functional Theory (DFT) calculations were performed on all synthesized compounds using Gaussian09,[5] with input preparation and visualization carried out through Gauss View.[6] The goal of these investigations was to gain a better comprehension of the atomic behaviour and electronic properties of the molecules. Geometry optimization was conducted using the CAM-B3LYP functional with the 6-311+G(d,p) basis set, a technique widely recognized for forecasting molecular structures and attributes. The compounds energy levels and electronic distribution were examined using DFT, which shed light on their chemical reactivity. The highest occupied molecular orbital (HOMO) and lowest unoccupied molecular orbital (LUMO), which are crucial for assessing reactivity, stability, and molecular interactions, were also examined using Frontier Molecular Orbital (FMO) analysis. The charge distribution across the molecular surfaces was also depicted by Molecular Electrostatic Potential (MEP) maps, which highlighted areas of electron richness or deficiency and provided useful predictions about potential reactive sites.

Molecular Docking: The interactions between the synthesized compounds (**C20**, **C24-C26**) and the EGFR protein (PDB ID: 5EDQ) were investigated using molecular docking studies. Using AutoDock Vina[7] and the MGL Tools 1.5.7 interface, docking simulations were carried out. To predict advantageous binding conformations, the Lamarckian genetic algorithm search method and a stochastic scoring function were applied. The iTasser[8] server was used to fix the protein's missing atoms and residues. To ensure precise targeting of possible ligand-binding regions, the active binding pockets of EGFR were identified prior to docking using the PRankWeb[9] server, which incorporates the p2rank machine learning tool. This method gave important information about how the produced complexes might suppress EGFR activity. Several structural models of compound–protein interactions were produced by the docking experiments, which made it possible to calculate the binding free energies and identify the most stable and advantageous binding sites. All things considered, these docking studies provided important information about the synthesized complexes binding potential, confirming their applicability as potential EGFR inhibitors and directing the development of more potent anticancer drugs in the future.

Molecular Dynamics Simulations: In order to assess the dynamic behaviour of the protein-compound interactions, 100 ns molecular dynamics (MD) simulations were performed on the optimal conformations of the EGFR protein-compound complexes (**C20**, **C24**, **C25**, and **C26**) derived from molecular docking studies. The simulations were carried out using the GROMACS 2023.3[10] package, with protein and ligand topologies generated through the OPLS-AA force field.[11] Each complex was placed in a cubic box of dimensions $10 \times 10 \times 10$ nm^3 with

periodic boundary conditions applied in all directions, followed by solvation using the TIP3P water model and neutralized with NaCl. Energy minimization was performed using the steepest descent algorithm to eliminate steric clashes and unfavourable contacts. The system was then equilibrated under NPT conditions at 1 atm and 300 K, with pressure maintained using the C-rescale barostat (time constant: 1 ps) and temperature controlled by the Nose-Hoover thermostat (time constant: 0.1 ps).[12] The production MD simulation was run for 100 ns with a 2 fs timestep. The trajectories generated during the simulations were further analyzed in terms of root mean square deviation (RMSD), root mean square fluctuation (RMSF), and radius of gyration (R_{gyr}) to assess the structural stability and flexibility of the EGFR-Compound complexes.

In vitro biological activity (anticancer): The cytotoxic activities of the synthesized compounds were evaluated against two human cancer cell lines: A549 (lung cancer) and T24 (bladder cancer). Additionally, the normal breast epithelial cell line MCF-10a was used to assess selectivity. Cell lines were maintained in Dulbecco's Modified Eagle Medium (DMEM) or appropriate growth media supplemented with 10% fetal bovine serum (FBS), 1% penicillin-streptomycin, and 1% glutamine. Cells were incubated at 37°C in a humidified atmosphere containing 5% CO_2. The cytotoxicity of the compounds was determined using the MTT assay.[13] Briefly, cells were seeded into 96-well plates at a density of 5 $\times 10^3$ cells per well and allowed to adhere overnight. The following day, cells were treated with varying concentrations of the test compounds (dissolved in DMSO and diluted in media) ranging from 0 to 100 μM. DMSO (final concentration < 0.1%) was used as a vehicle control, and doxorubicin and cisplatin were included as positive controls. After 24 h of treatment, 20 μL of MTT reagent (5 mg/mL in PBS) was added to each well, and the plates were incubated at 37°C for 4 h. Following incubation, the supernatant was carefully removed, and 150 μL of DMSO was added to each well to dissolve the formazan crystals. The plates were gently shaken for 10 min to ensure complete solubilization.

8. Computational studies

8.1 SwissADME studies

The SwissADME web tool was used to assess the synthesized compounds ADME (Absorption, Distribution, Metabolism, and Excretion) characteristics, which shed light on their pharmacokinetic behaviour and potential for therapeutic potential.[14] Computational predictions of ADME parameters were combined with an evaluation of target interactions and physicochemical features in virtual screening. Lipinski's rule of five, which states that orally active compounds usually meet at least three of the following criteria: (i) ≤5 hydrogen bond donors, (ii) ≤10 hydrogen bond acceptors, (iii) molecular weight <500, and (iv) partition coefficient log P <5, was used to further analyze drug-likeness.[15] **Table 6** displays the physicochemical parameters of the chosen compounds (**C20**, **C24**, **C25**, and **C26**) that were assessed using SwissADME. The anticipated outcomes demonstrate their encouraging drug-like qualities. Lipinski's criterion for oral drug-likeness was met by all compounds, which had molecular weights between 384.47 and 461.55 g/mol, below the 500 g/mol threshold. With a high level of aromaticity, the fraction of sp^3-hybridized carbons was comparatively low (0.13–0.17). Within acceptable bounds, all derivatives had two hydrogen bond acceptors and no more than two hydrogen bond donors. Moderate molecular flexibility was indicated by the number of rotatable bonds (5–8), which also met the criterion of <9. The values of topological polar

surface area (TPSA) fell between 36.16 and 57.88 Å^2, which is within the ideal range of 20–140 Å^2 for good permeability. Compounds **C20**, **C24**, and **C25** had acceptable lipophilicity (4.62–4.70), according to the consensus LogP values, but compound **C26** exceeded the cutoff (5.96), resulting in one violation of Lipinski's rule. With a bioavailability score of 0.55, every compound demonstrated good oral bioavailability potential. According to solubility predictions (ESOL), **C20** was categorized as poorly soluble, **C24** as moderately soluble, and **C25** and **C26** as poorly soluble. It was anticipated that Gastrointestinal (GI) absorption would be low for **C26** but high for **C20**, **C24**, and **C25**. Additionally, **C20**, **C24**, and **C25** showed blood-brain barrier (BBB) permeability, while **C26** did not. All things considered, these findings imply that **C20**, **C24**, and **C25** have advantageous ADME profiles, while **C26** is constrained by high lipophilicity, decreased solubility, and poor GI absorption.

Table S2: ADME profile of compounds **C20, C24-C26**

Descriptor	Criteria	C20	C24	C25	C26
Formula	-	$C_{25}H_{24}N_2O_2$	$C_{29}H_{25}N_3O_2$	$C_{30}H_{27}N_3O_2$	$C_{31}H_{26}N_2O_2$
MW (g/mol)	<500	384.47	447.53	461.55	458.55
Csp^3 Fraction	>0.25	0.16	0.14	0.17	0.13
Hydrogen bond acceptors	≤10	2	2	2	2
Hydrogen bond donors	≤5	0	1	0	2
Number of Rotatable Bonds	<9	8	5	5	5
TPSA (Å^2)	20−140	36.16	51.95	41.09	57.88
XLOGP3	−0.7 ± 5.0	5.05	5.17	5.13	7.12
Consensus (Log P)	≤5.0	4.62	4.67	4.70	5.96
Lipinski Rule violation	≤1	0	0	0	1
Bioavailability score	0.55	0.55	0.55	0.55	0.55
ESOL (Log S)	≤6	−5.34	−6.13	−6.17	−7.43
ESOL Class	Poorly soluble	Moderately soluble	Poorly soluble	Poorly soluble	Poorly soluble
GI absorption	-	High	High	High	Low
Blood-Brain Barrier (BBB) Permeability	-	Yes	Yes	Yes	No

The synthesised compounds gastrointestinal absorption (HIA) and blood-brain barrier (BBB) permeability were evaluated using the BOILED-Egg predictive model.[16] Compounds **C20**, **C24**, and **C25** (molecules 1-3) are located in the yellow area of the plot **(Fig. S2),** suggesting a high likelihood of BBB penetration and favourable gastrointestinal absorption. Compound **C26** (molecule 4), on the other hand, is situated outside of the white (HIA) and yolk (BBB) regions, indicating decreased gastrointestinal absorption and poor brain penetration. Analysis of the P-glycoprotein (P-gp) interaction showed that compound **C26** is predicted to be a non-substrate (PGP–), whereas compounds **C20**, **C24**, and **C25** are predicted to be P-gp substrates (PGP+). These findings imply that while compound **C26** may have limited bioavailability and restricted brain access, compounds **C20**, **C24**, and **C25** have superior pharmacokinetic characteristics and possible central nervous system (CNS) activity. As shown in **Fig. S3**, the Swiss-Target Prediction tool[17] was used to assess the potential interaction profiles of the synthesized compounds expected biological target classes.[18] While enzymes, kinases, and ligand-gated ion channels contributed moderately (13.3% each), compound **C20** demonstrated a strong potential for modulating GPCR-mediated signalling through a predominant interaction with family A G protein-coupled receptors (33.3%), such as the Adenosine A3 receptor.

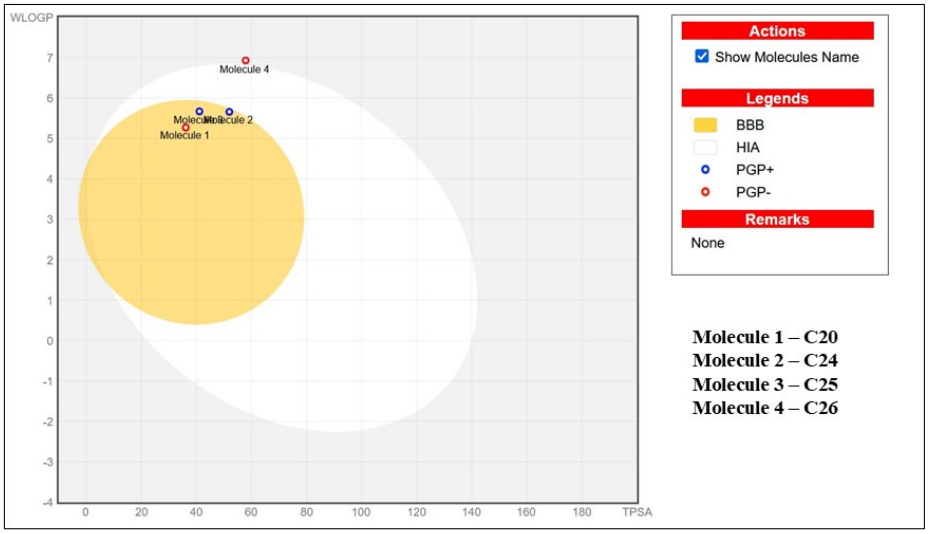

Figure. S2. ADME Profiles for C20, C24, C25 and C26 visualized using BOILED-Egg

On the other hand, **C24** showed the highest predicted affinity (26.7%) for lyases such as Carbonic anhydrase XII. Proteases, kinases, and enzymes each contribute 13.3%, which may indicate disruption of lyase-associated pathways. Compound **C25** showed a broad enzymatic orientation with multi-target potential by showing a dominant preference for cytoplasmic enzymes such as isocitrate dehydrogenase [NADP] (26.7%), followed by GPCRs, proteases, and kinases (13.3% each). Intriguingly, **C26** displayed a bifunctional profile involving both catalytic and ion-channel regulatory processes, with minor contributions from other classes (6.7%) and a dual dominance of enzymes such as Quinone reductase 2 and ligand-gated ion channels such as GABA-A receptor; alpha-1/beta-3/gamma-2 (26.7% each). All of these findings suggest that while each compound demonstrates a variety of pharmacological behaviours, their primary target classes may vary, with **C20** showing a bias toward GPCRs, **C24** showing a bias toward lyases, **C25** showing a bias toward general enzymes, and **C26** showing a bias toward enzymes and ion channels. According to these predictions taken together, **C20** and **C26** show relatively narrower target preferences, which may affect their therapeutic applicability and specificity, while **C24** and **C25** show broader polypharmacological potential. It is crucial to remember that while the SwissADME tool offers useful information about the drug-like characteristics of these compounds, these predictions are based on simplified moieties and do not take into consideration important biological complexities like metabolic stability and in vivo behaviour. Therefore, additional experimental validation is necessary to validate these results and evaluate their practicality

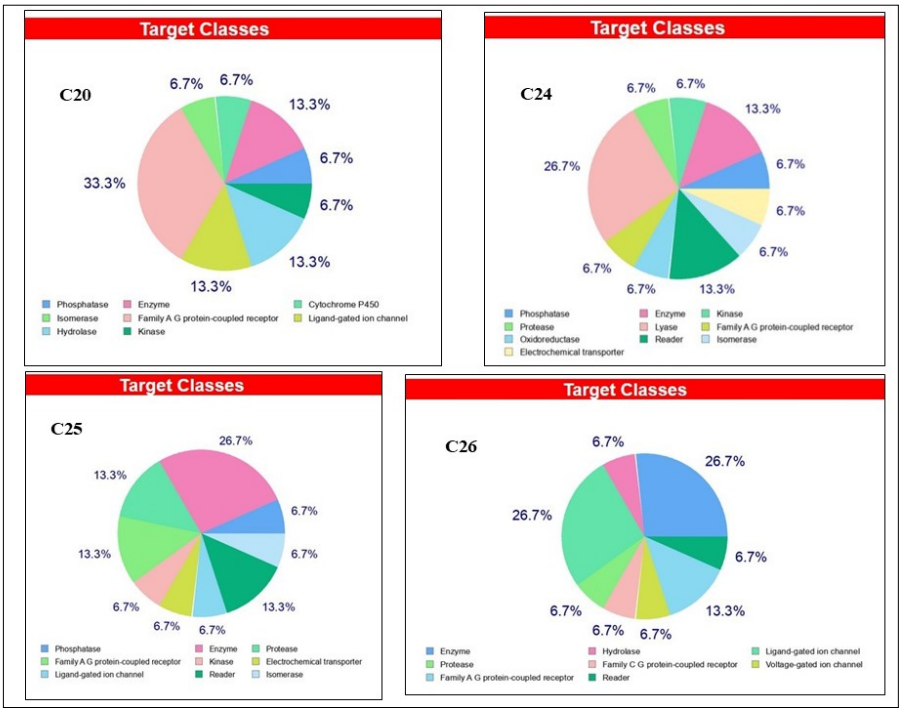

Figure. S3. Target profiling of compounds C20, C24-C26 using computational tools

Compound 20

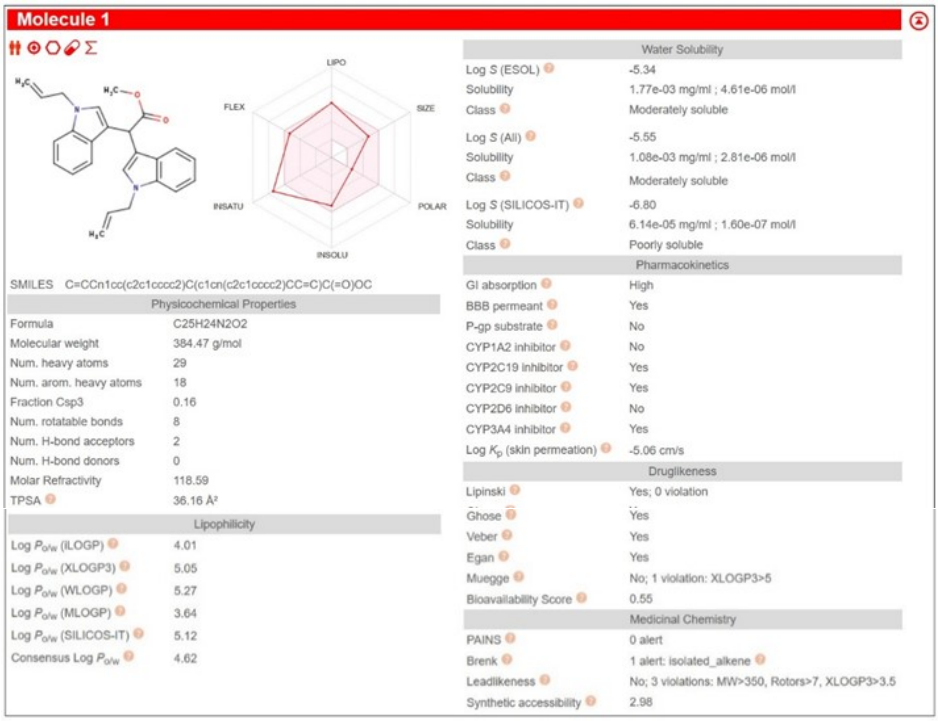

Compound 24

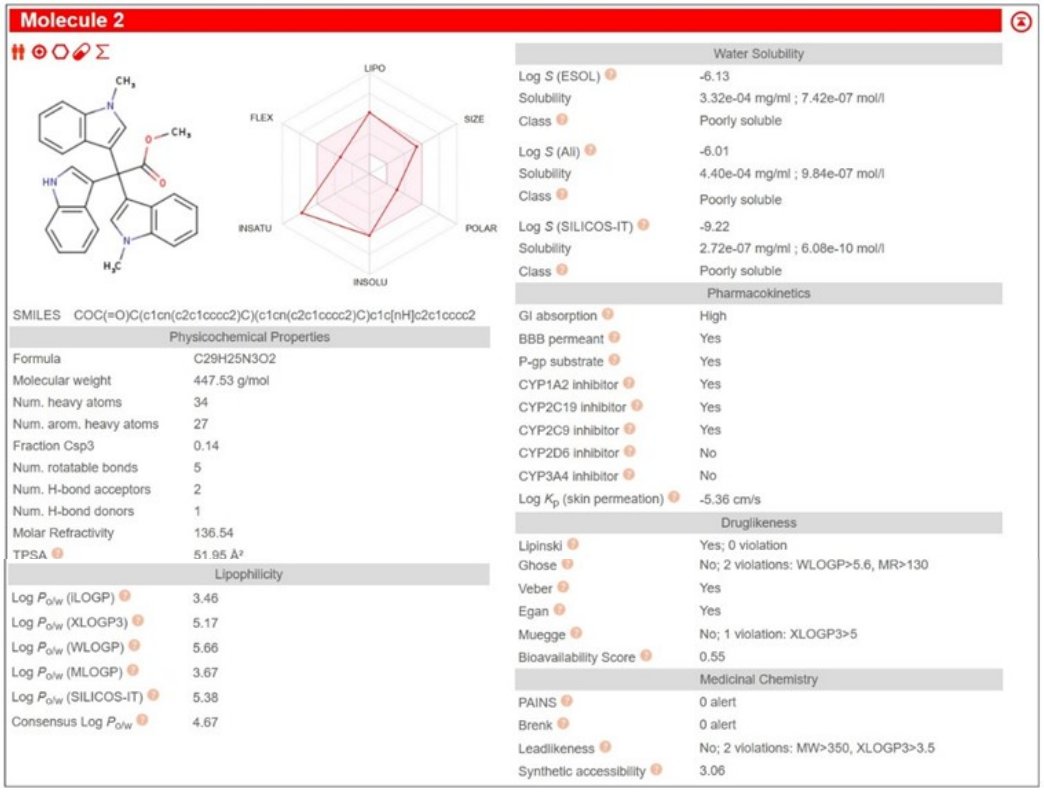

Compound 25

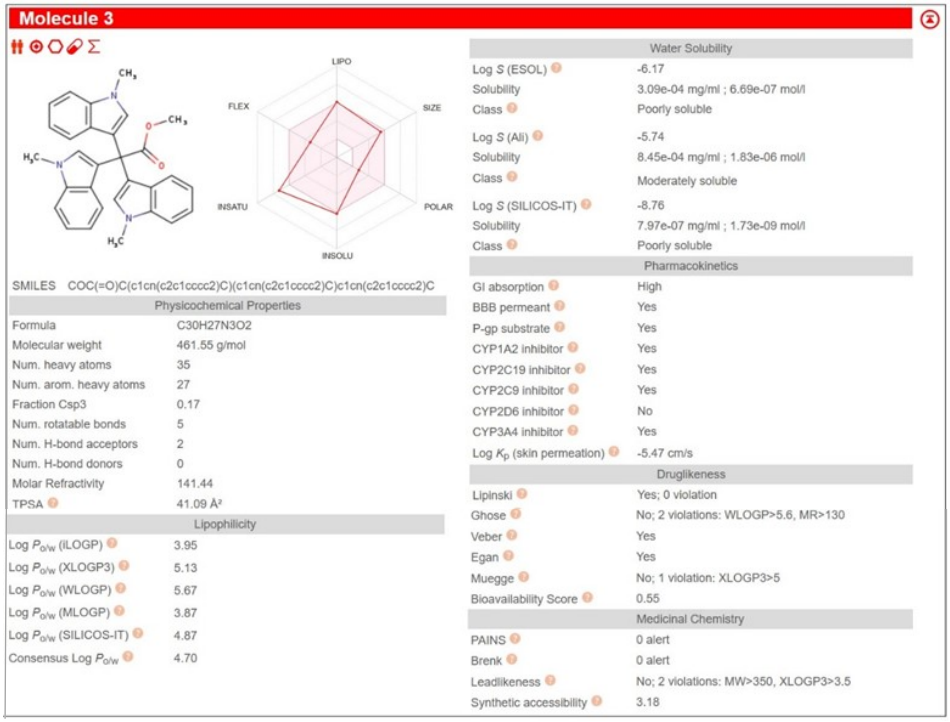

Compound 26

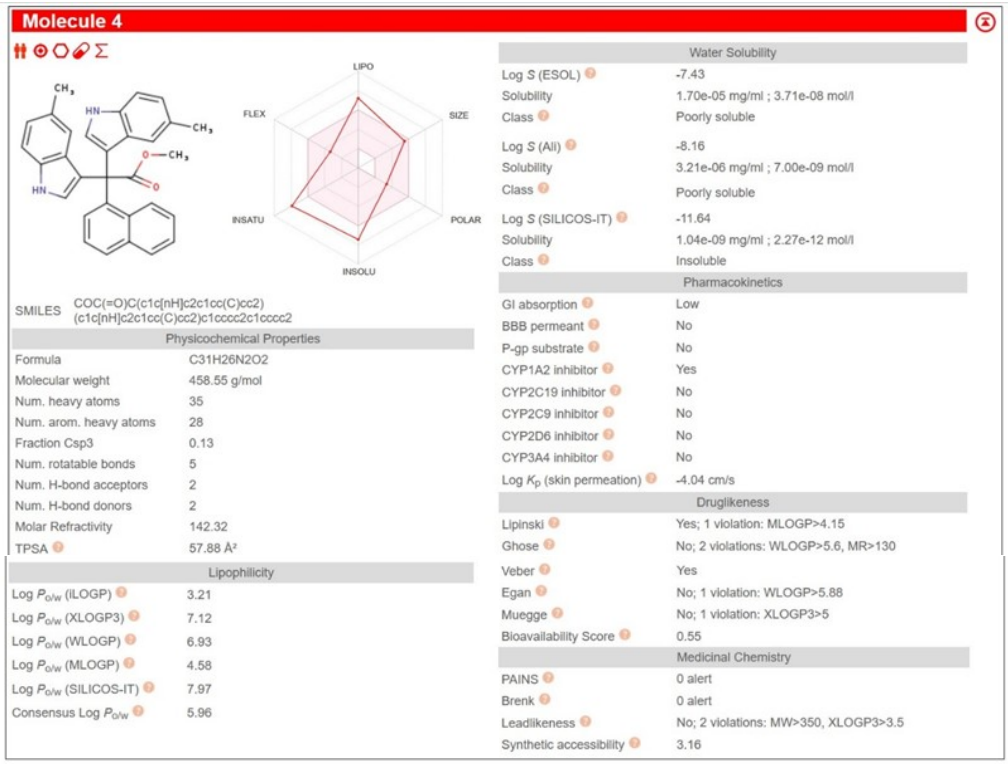

8.2 Studies using density functional theory (DFT)

DFT was used to predict the stable structures and related physicochemical properties of the as-prepared compounds (**C20**, **C24**, **C25**, and **C26**) through geometry optimization (GO) and frontier molecular orbital (FMO) analyses. These compounds optimized geometries (**Fig. S4**) were produced using the CAM-B3LYP theory and 6311+G (d, p) basis set.[19] **Fig. S5** shows the spatial distributions of the HOMO and LUMO orbitals, which are essential for forecasting electron distribution and reactivity.[20] For every complex, the energy gaps (ΔE) between HOMO and LUMO are shown. The electron density distribution for each orbital state is depicted by the molecular orbital isosurfaces in **Fig. S5**, emphasizing variations in conjugation and localization among the systems. The global reactivity descriptor and frontier molecular orbital analyses (Table 7) showed that the four compounds had different electronic properties. With large HOMO–LUMO energy gaps of 7.28, 7.20, and 7.21 eV, respectively, and high hardness values (~3.60) and low softness (~0.275), compounds **C20**, **C24**, and **C25** show comparable physicochemical characteristics. These characteristics imply that **C20**, **C24**, and **C25** have limited polarizability, high kinetic stability, and low chemical reactivity.[21] Their Global Electrophilicity Indices (GEI) (2.67–2.78) also show weak electrophilic behaviour, which is consistent with their slightly positive LUMO energies, which also show a poor tendency to accept electron density.

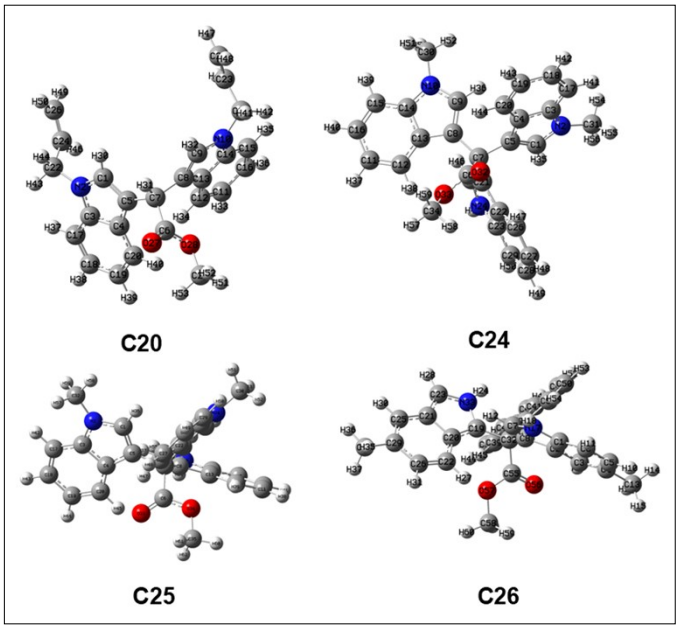

Figure. S4. DFT optimized structures of C20, C24, C25, and C26. The optimization calculation was performed using the CAM-B3LYP theory and the 6311+G (d, p) basis set.

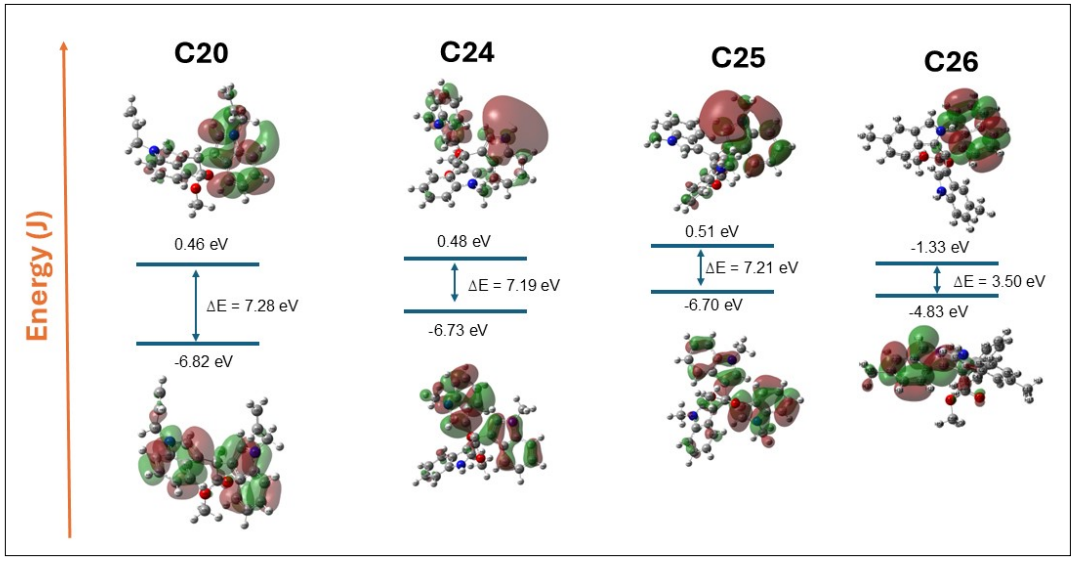

Figure. S5. The HOMO and LUMO distributions of the compounds under study are displayed in the frontier molecular orbital energy diagram (C20, C24–C26)

On the other hand, **C26** has a comparatively higher HOMO energy (−4.83 eV), a negative LUMO energy (−1.33 eV), a significantly smaller HOMO–LUMO gap (3.50 eV), lower hardness (1.75 eV), and higher softness (0.57). According to these metrics, **C26** is significantly more polarizable and chemically reactive than the other compounds. **C26** is identified as a strong electrophile with an enhanced ability to accept electron density due to the marked increase in its GEI (5.41), which suggests a higher propensity to interact with nucleophilic sites.

The following equations were used to determine the various parameters in **Table S3**: [22]

$$\text{hardness} = \Delta E/2 \quad (1)$$

$$\text{softness} = 1/\text{hardness} \quad (2)$$

electronegativity = ($|E_{HOMO} + E_{LUMO}|)/2$ (3)

chemical potential = $(-|E_{HOMO} + E_{LUMO}|)/2$ (4)

global electrophilicity index (G.E.I.) = $(\text{chemical potential})^2$ /hardness (5)

Table S3. Structural optimization and HOMO–LUMO analysis of compounds C20, C24 – C26 via DFT.

Compound	C20	C24	C25	C26
E_{opt} (eV)	-33379.9	-39033.8	-40103	-39638.8
E_{HOMO} (eV)	-6.8219	-6.72747	-6.70924	-4.82975
E_{LUMO} (eV)	0.459328	0.471846	0.503411	-1.32656
$\Delta E_{(HOMO-LUMO)}$	7.281226	7.19932	7.212654	3.503196
Hardness (H)	3.640613	3.59966	3.606327	1.751598
Softness (σ)	0.274679	0.277804	0.27729	0.570907
Electronegativity (χ)	3.181285	3.127814	3.102916	3.078154
Chemical potential (μ)	-3.18128	-3.12781	-3.10292	-3.07815
Global Electrophilicity Index (GEI)	2.779909	2.717819	2.669777	5.409364

Compounds **C20**, **C24**, **C25**, and **C26** molecular electrostatic potential (MEP) maps (**Fig. S6**) offer a visual representation of the charge distribution and potential reactive sites. Green to yellow zones indicate neutral potential, blue regions indicate electron-deficient areas vulnerable to nucleophilic attack, and red regions indicate areas of high electron density corresponding to electrophilic attack sites.[23] Compounds **C20**, **C24**, and **C25** show relatively uniform distributions with localized negative potential around heteroatoms, consistent with their large HOMO–LUMO gaps and low electrophilicity, suggesting lower reactivity. In contrast, **C26** exhibits pronounced red and blue regions, reflecting stronger charge separation and higher polarizability. These observations confirm that **C26** possesses enhanced chemical reactivity compared to **C20**, **C24**, and **C25**.

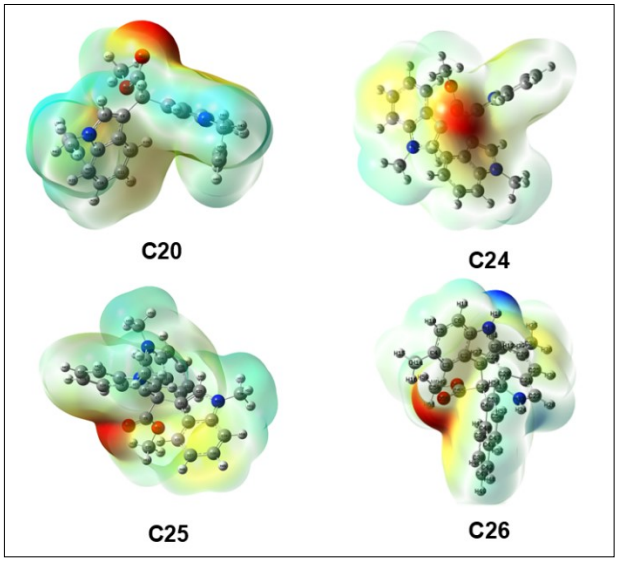

Figure. S6. Molecular electrostatic potential (MEP) maps of compounds C20, C24 – C26.

8.3 Molecular docking analysis

Lung cancer, especially non-small cell lung cancer (NSCLC), is largely caused by mutations, amplification, or overexpression of the epidermal growth factor receptor (EGFR) protein, which promotes unchecked cell growth and survival. EGFR is now a well-established therapeutic target because of its crucial role in tumour pathogenesis and its strong correlation with a poor prognosis.[24]

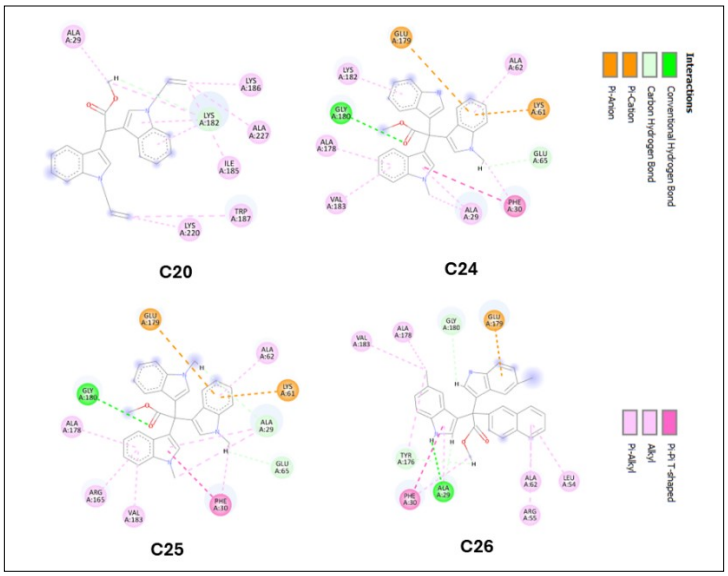

Figure. S7. 2D interaction diagrams of complexes C20, C24–C26 show important protein–ligand interactions after docking, such as hydrophobic contacts, π–π stacking, carbon–hydrogen bonds, conventional hydrogen bonds, and π-π-cations

A trustworthy method for evaluating **C20**, **C24**, **C25**, and **C26** possible anticancer qualities against lung cancer is to see how well they inhibit EGFR activity. In order to learn more about the binding affinities and interaction mechanisms of compounds **C20**, **C24**, **C25**, and **C26** within the EGFR active site, molecular docking studies[25] were conducted. Key intermolecular contacts that stabilize each ligand-protein complex are clearly shown in the two-dimensional interaction diagrams (**Fig. S7**). Compound **C20** demonstrated moderate stabilization by forming π-alkyl and π-anion interactions with Lys220, Val183, and Trp187, as well as conventional hydrogen bonds with Lys182 and Ala29. Through the formation of multiple hydrogen bonds with Gly180 and Glu179, carbon-hydrogen interactions with Ala62 and Lys61, and π–π stacking with Phe30, compound **C24** demonstrated stronger binding. Likewise, **C25** supported increased binding affinity by forming hydrophobic interactions with Ala178, Val183, and Phe30 as well as hydrogen bonds with Gly180, Glu179, and Lys61. **Compound C26** superior stabilization potential was demonstrated by its most extensive interaction network, which included hydrophobic and π-alkyl interactions with Ala62, Leu54, and Arg55, as well as hydrogen bonds with Gly180, Ala29, and Glu179. These results were further supported by the binding pocket three-dimensional surface visualizations (**Fig. S8**), which showed the hydrogen bond donor (pink) and acceptor (green) regions surrounding each ligand. While **C26** more efficiently occupies the binding cavity and forms numerous polar and hydrophobic contacts at once, compounds **C20**, **C24**, and **C25** exhibit complementary binding interactions but only cover a small portion of the donor/acceptor surfaces.

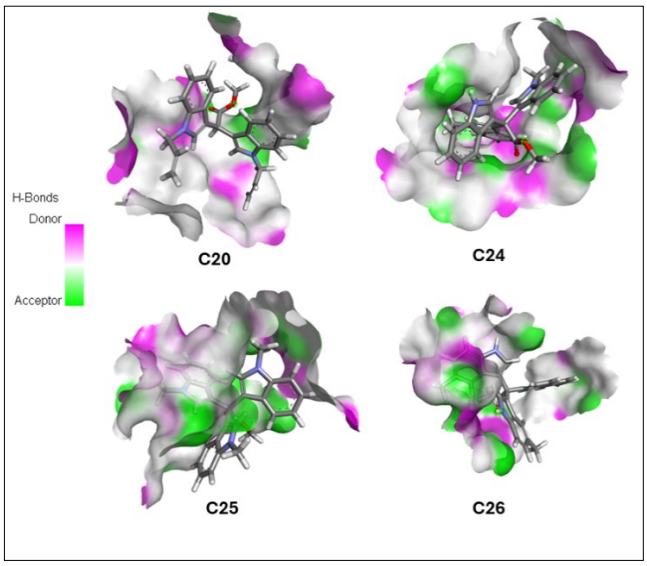

Figure S8. After docking, the donor (magenta) and acceptor (green) regions of the EGFR binding pocket interact with the amino acid residues in this three-dimensional representation of the hydrogen bond surface of C20, C24–C26

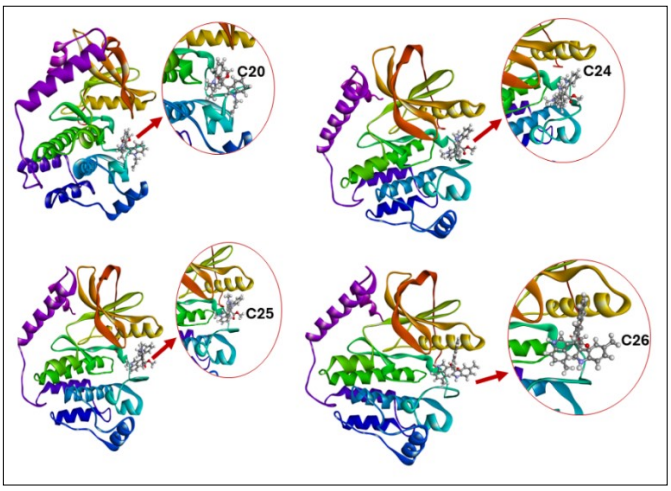

Figure. S9. 3D representation of C20, C24–C26 in the EGFR binding pocket after docking.

The overall docking conformations within the protein backbone are illustrated in **Fig. S9**. Compounds **C20**, **C24**, and **C25** exhibit moderate accommodation as they are confined either partially within the cavity or close to the surface groove. Compound **C26**, on the other hand, demonstrated ideal complementarity with the active site architecture by fitting snugly within the binding pocket. The greater docking score and binding affinity of **C26** in comparison to the other compounds are supported by this spatial orientation as well as its wide range of intermolecular contacts.

8.4 Molecular dynamics simulation

Molecular Dynamics (MD) simulations[26] were performed for 100 ns to assess the stability of EGFR–compound (**C20**, **C24–C26**) complexes in order to further validate the docking results. With the exception of **EGFR–C24**, which reached equilibrium after about 60 ns, all complexes reached equilibrium within the first 20 ns and remained stable, according to the RMSD[27] plots (**Fig. S10**, a–d). The complexes compactness was further supported by the radius of gyration (Rgyr)[28] (**Fig. S10**, e), where **EGFR–C26** showed the lowest R_{gyr} values, indicating improved structural stability. Residue-level (Cα) fluctuations assessed by RMSF[29] (**Fig. S10**, f) were minimal (<0.3 nm) across most residues, with key binding site residues such as LYS44, PHE30, THR90, GLY160, VAL150, and SER232 showing lower flexibility in the EGFR–C26 complex. These findings collectively demonstrate that compound **C26** forms the most stable and compact complex with EGFR at this temperature (303 K) and pressure (1 atm) and illustrate its superior binding affinity predicted in docking studies.

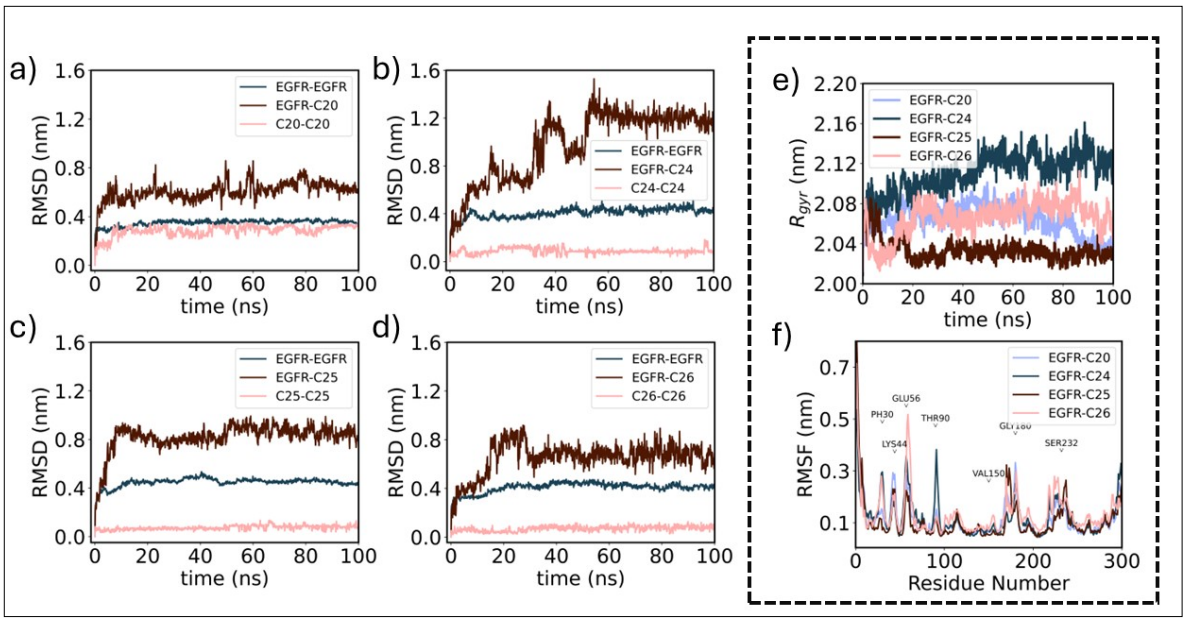

Figure. S10. RMSD trajectories for (a) EGFR-C20; (b) EGFR-C24; (c) EGFR-C25; and (d) EGFR-C26 systems; (e) R_{gyr} for the EGFR backbone in the EGFR-compound complexes; (f) RMSF of the Cα of the amino acid residues in EGFR complexed with the compounds.

9. Spectral data of compounds

Methyl 2,2-di(1H-indol-3-yl)acetate (3)[30]

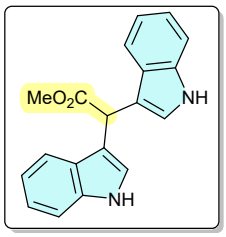

Brown solid, 36mg, 91%; mp 62−64 °C; Eluent (20% ethyl acetate in hexane); ^{1}H NMR (500 MHz, $CDCl_3$ with 0.03% v/v TMS) δ 7.92 (s, 2H), 7.59 (d, *J* = 7.9 Hz, 2H), 7.24 (d, *J* = 8.1 Hz, 2H), 7.18 – 7.12 (m, 2H), 7.10 – 7.05 (m, 2H), 6.90 (d, *J* = 2.0 Hz, 2H), 5.49 (s, 1H), 3.71 (s, 3H); ^{13}C NMR {^{1}H} (125 MHz, $CDCl_3$ with 0.03% v/v TMS) δ 173.9, 136.3, 126.6, 123.3, 122.1, 119.6, 119.2, 113.5, 111.2, 52.3, 40.4; HRMS (ESI): calcd. for $C_{19}H_{16}N_2O_2$ [M + H^+] 305.1285; found 305.1280.

Methyl 2,2-bis(5-methyl-1H-indol-3-yl)acetate (4)[30]

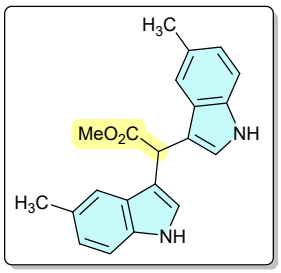

Brown solid, 29mg, 79%; mp 78−80 °C; Eluent (20% ethyl acetate in hexane); ^{1}H NMR (500 MHz, $CDCl_3$ with 0.03% v/v TMS) δ 7.90 (s, 2H), 7.39 (d, *J* = 0.7 Hz, 2H), 7.20 (d, *J* = 8.3 Hz, 2H), 7.00 (dd, *J* = 8.3, 1.5 Hz, 2H), 6.98 (d, *J* = 2.0 Hz, 2H), 5.45 (s, 1H), 3.74 (s, 3H), 2.41 (s, 6H); ^{13}C NMR {^{1}H} (125 MHz, $CDCl_3$ with 0.03% v/v TMS) δ 174.1, 134.7, 128.8, 126.9, 123.8, 123.5, 118.8, 113.0, 110.9, 52.2, 40.4, 21.5; HRMS (ESI): calcd. for $C_{21}H_{20}N_2O_2$ [M + H^+] 333.1598; found 333.1598.

Methyl 2,2-bis(5-methoxy-1H-indol-3-yl)acetate (5)

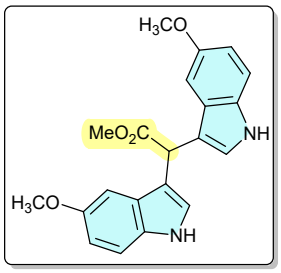

Brown semisolid, 23mg, 64%; Eluent (20% ethyl acetate in hexane); ^{1}H NMR (500 MHz, $CDCl_3$ with 0.03% v/v TMS) δ 8.00 (s, 2H), 7.22 – 7.16 (m, 2H), 7.03 (dd, *J* = 21.6, 2.4 Hz, 4H), 6.84 (dd, *J* = 8.8, 2.3 Hz, 2H), 5.40 (s, 1H), 3.78 (s, 6H), 3.75 (s, 3H); ^{13}C NMR {^{1}H} (125 MHz, $CDCl_3$ with 0.03% v/v TMS) δ 174.0, 154.0, 131.5, 127.0, 124.1, 113.1, 112.3, 112.0, 101.1, 55.9, 52.2, 40.6; HRMS (ESI): calcd. for $C_{21}H_{20}N_2O_4$ [M + H^+] 365.1496; found 365.1496.

Methyl 2,2-bis(5-(benzyloxy)-1H-indol-3-yl)acetate (6)

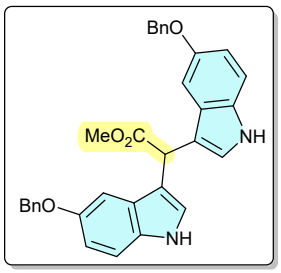

Brown semisolid, 24mg, 71%; Eluent (20% ethyl acetate in hexane); ^{1}H NMR (500 MHz, $CDCl_3$ with 0.03% v/v TMS) δ 7.86 (s, 2H), 7.35 (d, J = 7.2 Hz, 4H), 7.28 (t, *J* = 7.4 Hz, 4H), 7.22 (t, *J* = 7.3 Hz, 2H), 7.16 (d, *J* = 8.8 Hz, 2H), 7.07 (d, *J* = 2.3 Hz, 2H), 6.97 (s, 2H), 6.86 (dd, *J* = 8.8, 2.4 Hz, 2H), 5.30 (s, 1H), 4.97 (s, 4H), 3.62 (s, 3H); ^{13}C NMR {^{1}H} (125 MHz, $CDCl_3$ with 0.03% v/v TMS) δ 173.7, 153.2, 137.6, 131.6, 128.4, 127.6 (d, *J* = 14.1 Hz), 127.0, 124.1, 113.1 (d, *J* = 13.1 Hz), 111.9, 102.8, 70.8, 52.2, 40.7; HRMS (ESI): calcd. for $C_{33}H_{28}N_2O_4$ [M + Na^+] 539.1941; found 539.1947.

Methyl 2,2-bis(7-methyl-1H-indol-3-yl)acetate (7)

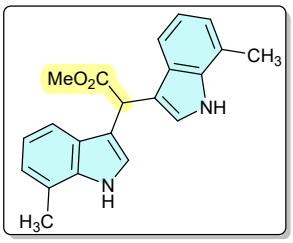

Yellow semisolid, 30mg, 76%; Eluent (20% ethyl acetate in hexane); ^{1}H NMR (500 MHz, $CDCl_3$ with 0.03% v/v TMS) δ 7.91 (s, 2H), 7.38 (d, J = 7.7 Hz, 2H), 6.95 – 6.88 (m, 6H), 5.41 (s, 1H), 3.65 (s, 3H), 2.34 (s, 6H); ^{13}C NMR {^{1}H} (125 MHz, $CDCl_3$ with 0.03% v/v TMS) δ 174.1, 135.9, 126.2, 123.1, 122.6, 120.5, 119.8, 116.9, 114.0, 52.2, 40.6, 16.5; HRMS (ESI): calcd. for $C_{21}H_{20}N_2O_2$ [M + Na^+] 355.1417; found 355.1413.

Methyl 2,2-bis(5-chloro-1H-indol-3-yl)acetate (8)

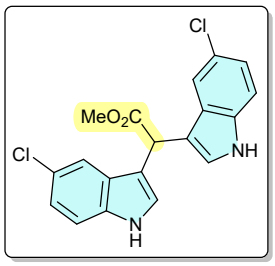

Brown semisolid, 38mg, 97%; Eluent (20% ethyl acetate in hexane); ^{1}H NMR (500 MHz, $CDCl_3$ with 0.03% v/v TMS) δ 8.15 (s, 2H), 7.55 (d, J = 1.9 Hz, 2H), 7.25 (s, 2H), 7.13 (dd, J = 8.4, 2.1 Hz, 4H), 5.38 (s, 1H), 3.77 (s, 3H); ^{13}C NMR {^{1}H} (125 MHz, $CDCl_3$ with 0.03% v/v TMS) δ 173.4, 134.7, 127.5, 125.5, 124.6, 122.7, 118.7, 112.9, 112.3, 52.4, 40.3; HRMS (ESI): calcd. for $C_{19}H_{14}Cl_2N_2O_2$ [M + K^+] 411.0064; found 411.0065.

Methyl 2,2-bis(5-bromo-1H-indol-3-yl)acetate (9)[31]

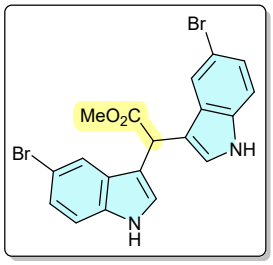

Red semisolid, 33mg, 93%; Eluent (20% ethyl acetate in hexane); ^{1}H NMR (500 MHz, $CDCl_3$ with 0.03% v/v TMS) δ 8.11 (s, 2H), 7.63 (d, J = 1.7 Hz, 2H), 7.18 (s, 1H), 7.16 (d, J = 1.8 Hz, 1H), 7.10 (d, J = 8.6 Hz, 2H), 6.98 (s, 2H), 5.29 (s, 1H), 3.69 (s, 3H); ^{13}C NMR {^{1}H} (125 MHz, $CDCl_3$ with 0.03% v/v TMS) δ 173.4, 135.0, 128.1, 125.2, 124.5, 121.7, 113.0, 112.8, 112.7, 52.5, 40.3; HRMS (ESI): calcd. for $C_{19}H_{14}Br_2N_2O_2$ [M + K^+] 498.9054; found 498.9070.

Methyl 2,2-bis(5-fluoro-1H-indol-3-yl)acetate (10)

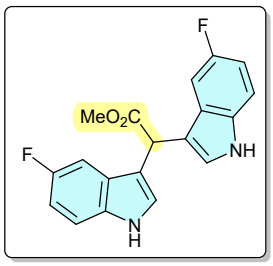

Brown semisolid, 37mg, 98%; Eluent (20% ethyl acetate in hexane); ^{1}H NMR (500 MHz, $CDCl_3$ with 0.03% v/v TMS) δ 8.04 (s, 2H), 7.18 – 7.13 (m, 4H), 7.07 (d, J = 2.5 Hz, 2H), 6.85 (td, J = 9.0, 2.4 Hz, 2H), 5.29 (s, 1H), 3.69 (s, 3H); ^{13}C NMR {^{1}H} (125 MHz, $CDCl_3$ with 0.03% v/v TMS) δ 173.5, 157.7 (d, J = 235 Hz), 132.9, 126.8 (d, J = 9.9 Hz), 125.0, 113.3 (d, J = 4.7 Hz), 111.9 (d, J = 9.7 Hz), 110.7 (d, J = 26.4 Hz), 104.3 (d, J = 23.9 Hz), 52.4, 40.5; HRMS (ESI): calcd. for $C_{19}H_{14}F_2N_2O_2$ [M + Na^+] 363.0916; found 363.0916.

Methyl 2,2-bis(6-bromo-1H-indol-3-yl)acetate (11)[31]

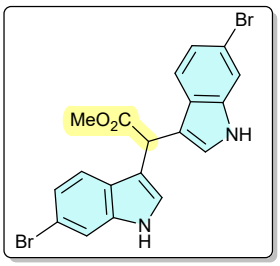

Brown solid, 34mg, 91%; mp 64−66 °C; Eluent (20% ethyl acetate in hexane); ^{1}H NMR (500 MHz, $CDCl_3$ with 0.03% v/v TMS) δ 8.05 (s, 2H), 7.41 (d, J = 1.6 Hz, 2H), 7.35 (d, J = 8.5 Hz, 2H), 7.10 (dd, J = 8.5, 1.6 Hz, 2H), 6.98 (d, J = 2.2 Hz, 2H), 5.35 (s, 1H), 3.68 (s, 3H); ^{13}C NMR {^{1}H} (125 MHz, $CDCl_3$ with 0.03% v/v TMS) δ 173.5, 137.1, 125.4, 123.8, 123.1, 120.5, 115.8, 114.2, 113.5, 52.4, 40.3; HRMS (ESI): calcd. for $C_{19}H_{14}Br_2N_2O_2$ [M + K^+] 498.9054; found 498.9096.

Methyl 2,2-bis(4-chloro-1H-indol-3-yl)acetate (12)

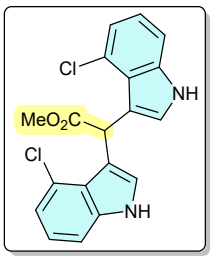

Brown semisolid, 31mg, 82%; Eluent (20% ethyl acetate in hexane); ^{1}H NMR (500 MHz, $CDCl_3$ with 0.03% v/v TMS) δ 8.19 (s, 2H), 7.02 (dd, *J* = 7.4, 1.3 Hz, 2H), 6.94 (dd, *J* = 9.5, 6.9 Hz, 4H), 6.56 (s, 1H), 6.53 (d, *J* = 2.3 Hz, 2H), 3.69 (s, 3H); ^{13}C NMR {^{1}H} (125 MHz, $CDCl_3$ with 0.03% v/v TMS) δ 175.7, 137.9, 126.1, 124.9, 123.2, 122.7, 120.7, 114.6, 110.2, 52.6, 41.1; HRMS (ESI): calcd. for $C_{19}H_{14}Cl_2N_2O_2$ [M + Na^+] 395.0325; found 395.0321.

Methyl 2,2-bis(2-methyl-1H-indol-3-yl)acetate (15)[30]

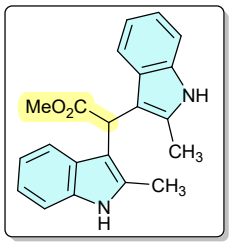

Brown solid, 22mg, 56%; mp 208-210 °C; Eluent (20% ethyl acetate in hexane); ^{1}H NMR (500 MHz, $CDCl_3$ with 0.03% v/v TMS) δ 7.78 (s, 2H), 7.36 (d, *J* = 8.0 Hz, 2H), 7.23 (d, *J* = 8.0 Hz, 2H), 7.10 – 7.04 (m, 2H), 7.02 – 6.94 (m, 2H), 5.47 (s, 1H), 3.78 (s, 3H), 2.19 (s, 6H); ^{13}C NMR {^{1}H} (125 MHz, $CDCl_3$ with 0.03% v/v TMS) δ 174.0, 134.8, 132.2, 128.2, 120.9, 119.5, 118.6, 110.2, 108.6, 52.1, 39.8, 12.3; HRMS (ESI): calcd. for $C_{21}H_{20}N_2O_2$ [M + Na^+] 355.1417; found 355.1413.

Methyl 2,2-bis(2-phenyl-1H-indol-3-yl)acetate (16)[30]

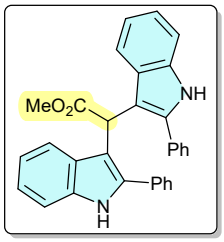

White solid, 18mg, 52%; mp 218-220 °C; Eluent (10% ethyl acetate in hexane); ^{1}H NMR (500 MHz, $CDCl_3$ with 0.03% v/v TMS) δ 8.02 (s, 2H), 7.38 – 7.31 (m, 6H), 7.29 – 7.25 (m, 8H), 7.09 (ddd, *J* = 8.1, 7.1, 1.1 Hz, 2H), 6.92 (ddd, *J* = 8.1, 7.1, 1.0 Hz, 2H), 5.71 (s, 1H), 3.52 (s, 3H); ^{13}C NMR {^{1}H} (125 MHz, $CDCl_3$ with 0.03% v/v TMS) δ 173.8, 136.1, 135.6 132.8, 128.5, 128.3, 128.2, 127.8, 121.9, 120.7, 119.8, 110.6, 109.9, 51.9, 41.3; HRMS (ESI): calcd. for $C_{31}H_{24}N_2O_2$ [M + Na^+] 479.1730; found 479.1733.

Methyl 2,2-bis(1-ethyl-1H-indol-3-yl)acetate (17)

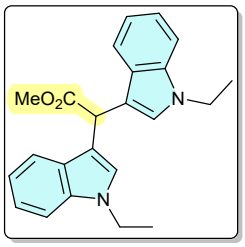

Orange semisolid, 36mg, 93%; Eluent (10% ethyl acetate in hexane); ^{1}H NMR (500 MHz, $CDCl_3$ with 0.03% v/v TMS) δ 7.63 (d, *J* = 7.9 Hz, 2H), 7.32 (d, *J* = 8.3 Hz, 2H), 7.23 – 7.18 (m, 2H), 7.12 – 7.04 (m, 4H), 5.51 (s, 1H), 4.11 (q, *J* = 7.3 Hz, 4H), 3.74 (s, 3H), 1.42 (t, *J* = 7.3 Hz, 6H); ^{13}C NMR {^{1}H} (125 MHz, $CDCl_3$ with 0.03% v/v TMS) δ 174.1, 136.1, 127.3, 126.2, 121.5, 119.5, 119.0, 112.1, 109.3, 52.2, 40.9, 40.4, 15.4; HRMS (ESI): calcd. for $C_{23}H_{24}N_2O_2$ [M + Na^+] 383.1730; found 383.1729.

Methyl 2,2-bis(1-methyl-1H-indol-3-yl)acetate (18)[30]

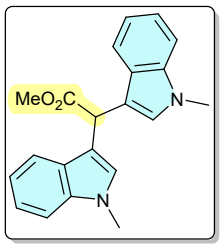

Red semisolid, 34mg, 92%; Eluent (10% ethyl acetate in hexane); ^{1}H NMR (500 MHz, $CDCl_3$ with 0.03% v/v TMS) δ 7.54 (dd, *J* = 8.0, 0.8 Hz, 2H), 7.20 (d, *J* = 8.2 Hz, 2H), 7.16 – 7.11 (m, 2H), 7.04 – 6.98 (m, 2H), 6.93 (s, 2H), 5.44 (d, J = 0.7 Hz, 1H), 3.65 (s, 3H), 3.61 (s, 6H); ^{13}C NMR {^{1}H} (125 MHz, $CDCl_3$ with 0.03% v/v TMS) δ 174.1, 137.1, 127.9, 127.1, 121.7, 119.3, 119.2, 112.2, 109.3, 52.2, 40.3, 32.7; HRMS (ESI): calcd. for $C_{21}H_{20}N_2O_2$ [M + Na^+] 355.1417; found 355.1424.

Methyl 2,2-bis(1-benzyl-1H-indol-3-yl)acetate (19)[30]

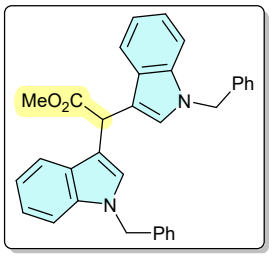

Orange semisolid, 36mg, 83%; Eluent (10% ethyl acetate in hexane); ^{1}H NMR (500 MHz, $CDCl_3$ with 0.03% v/v TMS) δ 7.56 (d, *J* = 7.9 Hz, 2H), 7.15 (dd, *J* = 9.3, 7.1 Hz, 10H), 7.05 (d, *J* = 3.2 Hz, 4H), 6.98 (d, *J* = 7.1 Hz, 4H), 5.47 (s, 1H), 5.15 (s, 4H), 3.65 (s, 3H); ^{13}C NMR {^{1}H} (125 MHz, $CDCl_3$ with 0.03% v/v TMS) δ 173.8, 137.5, 136.8, 128.7, 128.6,128.1, 127.5 – 127.4 (m), 126.7, 121.9, 119.6, 119.4, 112.7, 109.9, 52.2, 50.1, 40.6; HRMS (ESI): calcd. for $C_{33}H_{28}N_2O_2$ [M + Na^+] 507.2043; found 507.2049.

Methyl 2,2-bis(1-allyl-1H-indol-3-yl)acetate (20)

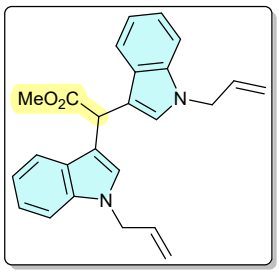

Brown semisolid, 29mg, 79%; Eluent (10% ethyl acetate in hexane); ^{1}H NMR (500 MHz, $CDCl_3$ with 0.03% v/v TMS) δ 7.54 (dd, *J* = 7.9, 0.5 Hz, 2H), 7.21 (d, *J* = 8.2 Hz, 2H), 7.11 (t, *J* = 7.6 Hz, 2H), 7.00 (dd, *J* = 7.7, 7.1 Hz, 4H), 5.87 (ddd, *J* = 22.4, 10.5, 5.4 Hz, 2H), 5.44 (s, 1H), 5.08 (d, *J* = 10.2 Hz, 2H), 4.99 (d, *J* = 17.1 Hz, 2H), 4.57 (d, *J* = 5.4 Hz, 4H), 3.66 (s, 3H); ^{13}C NMR {^{1}H} (125 MHz, $CDCl_3$ with 0.03% v/v TMS) δ 173.9, 136.5, 133.4, 127.3, 127.0, 121.7, 119.5, 119.3, 117.3, 112.4, 109.7, 52.2, 48.9, 40.4; HRMS (ESI): calcd. for $C_{25}H_{24}N_2O_2$ [M + Na^+] 407.1730; found 407.1739.

Ethyl 2,2-di(1H-indol-3-yl)acetate (21)[30]

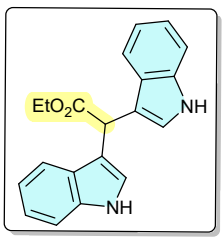

Yellow semisolid, 27mg, 59%; Eluent (15% ethyl acetate in hexane); ^{1}H NMR (500 MHz, $CDCl_3$ with 0.03% v/v TMS) δ 7.97 (s, 2H), 7.57 (d, *J* = 7.9 Hz, 2H), 7.27 (d, *J* = 8.1 Hz, 2H), 7.13 – 7.09 (m, 2H), 7.04 – 6.99 (m, 4H), 5.43 (s, 1H), 4.16 – 4.12 (m, 2H), 1.19 (s, 3H); ^{13}C NMR {^{1}H} (125 MHz, $CDCl_3$ with 0.03% v/v TMS) δ 172.4, 135.3, 125.6, 122.2, 121.1, 118.5, 118.3, 112.7, 110.1, 60.0, 39.6, 13.2; HRMS (ESI): calcd. for $C_{20}H_{18}N_2O_2$ [M + Na^+] 341.1260; found 341.1261.

Methyl 2,2-di(1H-indol-3-yl)propanoate (22)[32]

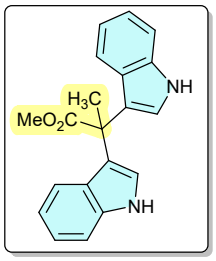

Brown semisolid, 43mg, 95%; Eluent (10% ethyl acetate in hexane); ^{1}H NMR (500 MHz, $CDCl_3$ with 0.03% v/v TMS) δ 7.91 (s, 2H), 7.42 (d, J = 8.1 Hz, 2H), 7.20 (d, J = 8.1 Hz, 2H), 7.05 (t, J = 7.6 Hz, 2H), 6.92 (t, J = 7.6 Hz, 2H), 6.72 (d, J = 2.3 Hz, 2H), 3.56 (s, 3H), 2.01 (s, 3H); ^{13}C NMR {^{1}H} (125 MHz, $CDCl_3$ with 0.03% v/v TMS) δ 176.1, 136.8, 126.0, 123.0, 121., 121.2, 119.2, 119.0, 111.3, 52.2, 46.2, 25.9; HRMS (ESI): calcd. for $C_{20}H_{18}N_2O_2$ [M + Na^+] 341.1260; found 341.1269.

Methyl 2,2-di(1H-indol-3-yl)-2-phenylacetate (23)

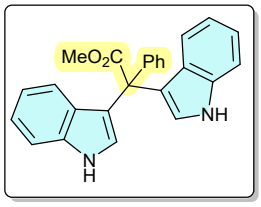

Purple semisolid, 23mg, 45%; Eluent (10% ethyl acetate in hexane); ^{1}H NMR (500 MHz, DMSO – d_6 /$CDCl_3$ (9:1 v/v)) δ 10.81 (d, J = 1.6 Hz, 2H), 7.27 (d, J = 8.1 Hz, 2H), 7.16 (s, 5H), 6.94 – 6.89 (m, 2H), 6.85 (d, J = 8.0 Hz, 2H), 6.73 – 6.65 (m, 4H), 3.59 (s, 3H); ^{13}C NMR {^{1}H} (125 MHz, DMSO – d_6/$CDCl_3$ (9:1 v/v)) δ 174.1, 142.9, 137.1, 129.2, 127.8, 127.0, 126.9, 125.3, 121.2, 121.1, 118.7, 117.6, 111.9, 56.4, 52.4; HRMS (ESI): calcd. for $C_{25}H_{20}N_2O_2$ [M + Na^+] 403.1417; found 403.1415.

Methyl 2-(1H-indol-3-yl)-2,2-bis(1-methyl-1H-indol-3-yl)acetate (24)

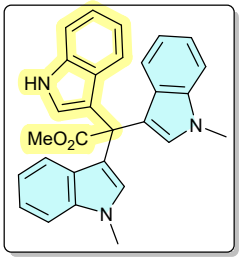

Brown semisolid, 20mg, 35%; Eluent (20% ethyl acetate in hexane); ^{1}H NMR (500 MHz, $CDCl_3$ with 0.03% v/v TMS) δ 7.85 (s, 1H), 7.22 (t, J = 7.4 Hz, 4H), 7.20 – 7.16 (m, 2H), 7.07 – 7.03 (m, 2H), 7.02 – 6.98 (m, 1H), 6.86 (d, J = 2.5 Hz, 1H), 6.83 – 6.79 (m, 3H), 6.75 (s, 2H), 3.66 (s, 3H), 3.59 (s, 6H); ^{13}C NMR {^{1}H} (125 MHz, $CDCl_3$ with 0.03% v/v TMS) δ 173.3, 136.4, 135.6, 128.1, 126.2, 125.9, 123.5, 120.7, 120.6, 120.4, 120.0, 118.1, 117.6, 117.2, 115.4, 109.9, 108.0, 51.2, 49.8, 31.7; HRMS (ESI): calcd. for $C_{29}H_{25}N_3O_2$ [M + K^+] 486.1578; found 486.1572.

Methyl 2,2,2-tris(1-methyl-1H-indol-3-yl)acetate (25)

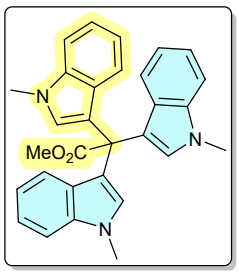

Red semisolid, 41mg, 59%; Eluent (20% ethyl acetate in hexane); ^{1}H NMR (500 MHz, $CDCl_3$ with 0.03% v/v TMS) δ 7.32 (d, J = 8.1 Hz, 2H), 7.30 – 7.27 (m, 4H), 7.17 – 7.14 (m, 3H), 6.91 (ddd, J = 8.0, 7.1, 0.9 Hz, 3H), 6.86 (s, 3H), 3.77 (s, 3H), 3.71 (s, 9H); ^{13}C NMR {^{1}H} (125 MHz, $CDCl_3$ with 0.03% v/v TMS) δ 174.4, 137.4, 129.1, 127.3, 121.8, 121.0, 118.6, 116.6, 109.0, 52.2, 50.7, 32.7; HRMS (ESI): calcd. for $C_{30}H_{27}N_3O_2$ [M + Na^+] 484.1995; found 484.1996.

Methyl 2,2-bis(5-methyl-1H-indol-3-yl)-2-(naphthalen-2-yl)acetate (26)

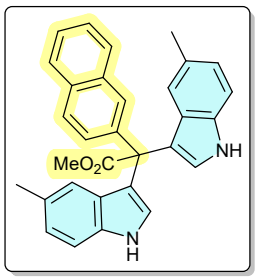

Brown semisolid, 10mg, 19%; Eluent (10% ethyl acetate in hexane); ^{1}H NMR (500 MHz, $CDCl_3$ with 0.03% v/v TMS) δ 7.83 (s, 2H), 7.77 (d, *J* = 1.5 Hz, 1H), 7.72 (d, *J* = 8.1 Hz, 1H), 7.61 (dd, *J* = 8.3, 3.7 Hz, 2H), 7.39 – 7.32 (m, 3H), 7.15 (d, *J* = 8.3 Hz, 2H), 6.94 (s, 2H), 6.88 (dd, *J* = 8.3, 1.3 Hz, 2H), 6.65 (d, *J* = 2.6 Hz, 2H), 3.72 (s, 3H), 2.16 (s, 6H); ^{13}C NMR {^{1}H} (125 MHz, $CDCl_3$ with 0.03% v/v TMS) δ 174.4, 139.5, 135.1, 133.0, 132.4, 128.5 (d, *J* = 3.3 Hz), 128.0, 127.2 (dd, *J* = 25.4, 6.8 Hz), 125.7, 125.6, 125.2, 123.5, 121.5, 118.3, 110.7, 56.6, 52.4, 21.5; HRMS (ESI): calcd. for $C_{31}H_{26}N_2O_2$ [M + Na^+] 481.1886; found 481.1899.

Methyl 2,2-di(1H-indol-3-yl)-2-(naphthalen-2-yl)acetate (27)

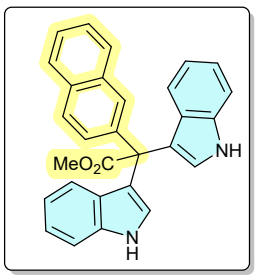

Brown semisolid, 4mg, 5%; Eluent (25% ethyl acetate in hexane); ^{1}H NMR (500 MHz, $CDCl_3$ with 0.03% v/v TMS) δ7.95 (s, 2H), 7.76 (s, 1H), 7.71 (d, *J* = 8.2 Hz, 1H), 7.60 (dd, *J* = 15.9, 8.2 Hz, 3H), 7.37 (dd, *J* = 8.6, 1.9 Hz, 2H), 7.26 (d, *J* = 8.2 Hz, 2H), 7.13 (d, *J* = 8.1 Hz, 2H), 7.04 (dd, *J* = 11.2, 4.0 Hz, 2H), 6.84 – 6.80 (m, 2H), 6.74 (d, *J* = 2.6 Hz, 2H), 3.71 (s, 3H); HRMS (ESI): calcd. for $C_{29}H_{22}N_2O_2$ [M + Na^+] 453.1573; found 453.1592.

Methyl 2,2-bis(5-chloro-1H-indol-3-yl)-2-(naphthalen-2-yl)acetate (28)

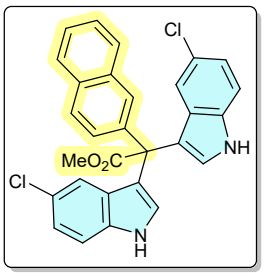

Brown semisolid, 2mg, 2%; HRMS (ESI): calcd. for $C_{22}H_{20}Cl_2N_2O_2$ [M + Na^+] 521.0794; found 521.0812.

(1-methyl-1H-indol-3-yl)(naphthalen-2-yl)methanone (29)[33]

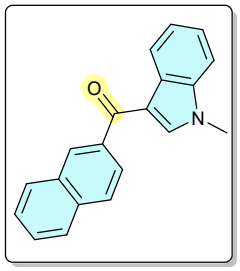

Green semisolid, 25mg, 37%; Eluent (5% ethyl acetate in hexane); ^{1}H NMR (500 MHz, $CDCl_3$ with 0.03% v/v TMS) δ 8.39 – 8.33 (m, 1H), 8.22 (s, 1H), 7.88 – 7.82 (m, 4H), 7.52 – 7.45 (m, 3H), 7.32 – 7.27 (m, 3H), 3.77 (s, 3H); ^{13}C NMR {^{1}H} (125 MHz, $CDCl_3$ with 0.03% v/v TMS) δ 190.8, 138.2, 137.8, 137.6, 134.7, 132.5, 129.1, 129.0, 128.2, 127.8, 127.5, 127.2, 126.6, 125.5, 123.7, 122.77 (d, *J* = 4.0 Hz), 115.9, 109.6, 33.5; HRMS (ESI): calcd. for $C_{20}H_{15}NO$ [M + Na^+] 286.1226; found 286.1226.

Methyl 2-(1H-indol-3-yl)-2-(1-methyl-1H-indol-3-yl)acetate (30)

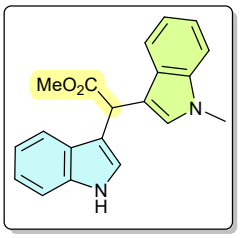

Red semisolid, 40mg, 48%; Eluent (10% ethyl acetate in hexane); ^{1}H NMR (500 MHz, $CDCl_3$ with 0.03% v/v TMS) δ 7.98 (s, 1H), 7.54 (dd, *J* = 8.0, 0.7 Hz, 2H), 7.22 (dd, *J* = 14.3, 8.2 Hz, 2H), 7.16 – 7.08 (m, 2H), 7.01 (ddd, *J* = 8.0, 5.6, 1.0 Hz, 3H), 6.90 (s, 1H), 5.44 (s, 1H), 3.66 (s, 3H), 3.60 (s, 3H); ^{13}C NMR {^{1}H} (125 MHz, $CDCl_3$ with 0.03% v/v TMS) δ 172.9, 136.1, 135.3, 126.9, 126.0, 125.6, 122.2, 121.1, 120.6, 118.5, 118.40 – 118.04 (m), 112.7, 110.9, 110.2, 108.3, 51.2, 39.3, 31.6; HRMS (ESI): calcd. for $C_{20}H_{18}N_2O_2$ [M + Na^+] 341.1260; found 341.1267.

Methyl 2-(1H-indol-3-yl)-2-(phenylamino)acetate (31)

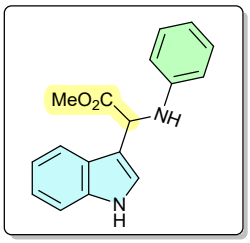

Brown semisolid, 20mg, 50%; Eluent (25% ethyl acetate in hexane); ^{1}H NMR (500 MHz, $CDCl_3$ with 0.03% v/v TMS) δ 8.06 (s, 1H), 7.36 (d, *J* = 8.0 Hz, 1H), 7.23 – 7.21 (m, 1H), 7.09 (dtd, *J* = 9.2, 7.9, 3.0 Hz, 4H), 7.02 (dd, *J* = 2.4, 0.7 Hz, 1H), 6.97 (ddd, *J* = 8.0, 7.1, 1.0 Hz, 2H), 6.53 (d, *J* = 8.5 Hz, 2H), 5.06 (s, 1H), 3.64 (s, 3H); ^{13}C NMR {^{1}H} (125 MHz, $CDCl_3$ with 0.03% v/v TMS) δ 173.9, 145.4, 136.3, 129.3, 128.5, 126.6, 123.1, 122.1, 119.6, 119.0, 115.3, 114.1 (d, *J* = 9.9 Hz), 111.2, 52.2, 48.1; HRMS (ESI): calcd. for $C_{17}H_{18}N_2O_2$ [M + H^+] 281.1285; found 281.1288.

Methyl (E)-2-(phenylimino)acetate (32)

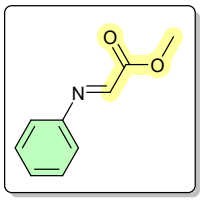

Red semisolid; HRMS (ESI): calcd. for $C_9H_9NO_2$ [M + H^+] 164.0706; found 164.0711.

Methyl (E)-2-(3H-indol-3-ylidene)acetate (33)

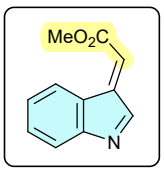

Green semisolid, 27mg, 82%; ^{1}H NMR (500 MHz, $CDCl_3$ with 0.03% v/v TMS) δ 8.21 (s, 1H), 7.62 (d, *J* = 7.9 Hz, 1H), 7.26 (d, *J* = 8.1 Hz, 1H), 7.16 – 7.12 (m, 1H), 7.09 – 7.04 (m, 1H), 5.41 (s, 1H), 3.68 (s, 3H); ^{13}C NMR {^{1}H} (125 MHz, $CDCl_3$ with 0.03% v/v TMS) δ 174.5, 136.4, 125.3, 123.4, 122.6, 120.2, 119.3, 113.6, 111.4, 67.2, 52.8; HRMS (ESI): calcd. for $C_{11}H_9NO_2$ [M + H^+] 188.0706; found 188.0715.

Methyl 2-oxo-2-phenylacetate (34)[34]

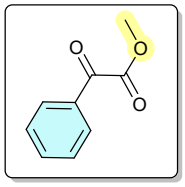

Yellow semisolid, 15mg, 47%; Eluent (10% ethyl acetate in hexane); ^{1}H NMR (500 MHz, $CDCl_3$ with 0.03% v/v TMS) δ 8.01 – 7.88 (m, 2H), 7.63 – 7.57 (m, 1H), 7.48 – 7.42 (m, 2H), 3.91 (s, 3H); ^{13}C NMR {^{1}H} (125 MHz, $CDCl_3$ with 0.03% v/v TMS) δ 186.0, 164.0, 135.0, 132.4, 130.1, 128.9, 52.8.

Methyl 2-(4-methoxyphenyl)-2-oxoacetate (35)[34]

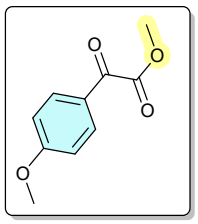

White semisolid, 46mg, 68%; Eluent (5% ethyl acetate in hexane); ^{1}H NMR (500 MHz, $CDCl_3$ with 0.03% v/v TMS) δ 7.93 (d, J = 9.1 Hz, 2H), 6.89 (d, J = 9.0 Hz, 2H), 3.88 (s, 3H), 3.81 (s, 3H); ^{13}C NMR {^{1}H} (125 MHz, $CDCl_3$ with 0.03% v/v TMS) δ 184.4, 165.1, 164.3, 132.6, 125.5, 114.2, 55.6, 52.6.

Methyl 2-oxo-2-(p-tolyl)acetate (36)[34]

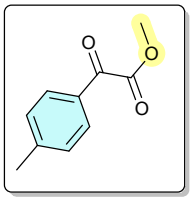

Yellow semisolid, 20mg, 53%; Eluent (10% ethyl acetate in hexane); ^{1}H NMR (500 MHz, $CDCl_3$ with 0.03% v/v TMS) δ 7.84 (d, J = 8.2 Hz, 2H), 7.23 (dd, J = 8.5, 0.6 Hz, 2H), 3.89 (s, 3H), 2.36 (s, 3H); ^{13}C NMR {^{1}H} (125 MHz, $CDCl_3$ with 0.03% v/v TMS) δ 185.6, 164.2, 146.3, 130.2, 129.6, 126.6, 52.6, 21.8.

Methyl 2-(4-chlorophenyl)-2-oxoacetate (37)[35]

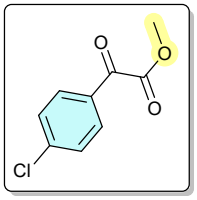

Pink semisolid, 27mg, 62%; Eluent (10% ethyl acetate in hexane); ^{1}H NMR (500 MHz, $CDCl_3$ with 0.03% v/v TMS) δ7.95 – 7.88 (m, 2H), 7.45 – 7.38 (m, 2H), 3.91 (s, 3H); ^{13}C NMR {^{1}H} (125 MHz, $CDCl_3$ with 0.03% v/v TMS) 184.4, 163.4, 141.7, 131.4, 130.8, 129.3, 52.9.

Methyl 2-(1H-indol-3-yl)-2-oxoacetate (38)[36]

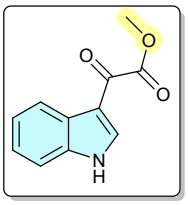

Brown solid, 31mg, 96%; Eluent (20% ethyl acetate in hexane); ^{1}H NMR (500 MHz, DMSO-d_6) δ 12.42 (s, 1H), 8.46 (d, J = 3.1 Hz, 1H), 8.18 (d, J = 7.1 Hz, 1H), 7.56 (d, J = 7.3 Hz, 1H), 7.30 (dd, J = 9.9, 4.0 Hz, 2H), 3.90 (s, 3H); ^{13}C NMR {^{1}H} (125 MHz, DMSO-d_6) δ 179.1, 164.4 138.8, 137.1, 125.9, 124.3, 123.3, 121.6, 113.2, 112.9, 52.9; HRMS (ESI): calcd. for $C_{11}H_9NO_3$ [M + Na^+] 226.0475; found 226.0475.

Methyl 2-(1-methyl-1H-indol-3-yl)-2-oxoacetate (39)[36]

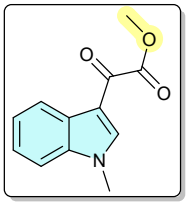

Yellow semisolid, 30mg, 88%; Eluent (20% ethyl acetate in hexane); ^{1}H NMR (500 MHz, $CDCl_3$ with 0.03% v/v TMS) δ 8.35 – 8.31 (m, 1H), 8.19 (s, 1H), 7.28 – 7.22 (m, 3H), 3.85 (s, 3H), 3.74 (s, 3H); ^{13}C NMR {^{1}H} (125 MHz, $CDCl_3$ with 0.03% v/v TMS) δ 176.8, 163.3, 140.4, 137.3, 127.0, 124.1, 123.5, 122.7, 112.7, 109.9, 52.7, 33.7; HRMS (ESI): calcd. for $C_{12}H_{11}NO_3$ [M + Na^+] 240.0631; found 240.0635.

Methyl 2-oxo-2-(1H-pyrrol-2-yl)acetate (40)[37]

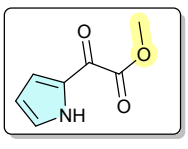

Yellow semisolid, 24mg, 87%; Eluent (10% ethyl acetate in hexane); ^{1}H NMR (500 MHz, $CDCl_3$ with 0.03% v/v TMS) δ 10.04 (s, 1H), 7.36 (s, 1H), 7.15 (s, 1H), 6.31 (d, J = 2.1 Hz, 1H), 3.88 (s, 3H); ^{13}C NMR {^{1}H} (125 MHz, $CDCl_3$ with 0.03% v/v TMS) δ 171.5, 162.6, 129.4, 128.4, 122.8, 112.3, 53.0.

Methyl 2-(naphthalen-2-yl)-2-oxoacetate (41)[38]

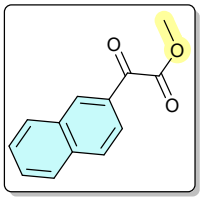

Red semisolid, 20mg, 62%; Eluent (5% ethyl acetate in hexane); ^{1}H NMR (500 MHz, $CDCl_3$ with 0.03% v/v TMS) δ 8.48 (s, 1H), 7.97 (dd, *J* = 8.6, 1.7 Hz, 1H), 7.90 (d, *J* = 8.2 Hz, 1H), 7.85 (d, *J* = 8.6 Hz, 1H), 7.81 (d, *J* = 8.2 Hz, 1H), 7.57 (ddd, *J* = 8.2, 6.9, 1.2 Hz, 1H), 7.52 – 7.47 (m, 1H), 3.95 (s, 3H); ^{13}C NMR {^{1}H} (125 MHz, $CDCl_3$ with 0.03% v/v TMS) δ 185.9, 164.1, 136.4, 133.6, 132.3, 130.0, 129.8, 129.6, 128.9, 127.9, 127.2, 124.0, 52.8.

Methyl cinnamate (42)[39]

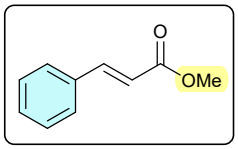

White semisolid, 27mg, 50%; ^{1}H NMR (500 MHz, $CDCl_3$ with 0.03% v/v TMS) δ 7.62 (d, *J* = 16.0 Hz, 1H), 7.47 – 7.41 (m, 2H), 7.30 (dd, *J* = 4.1, 2.5 Hz, 3H), 6.36 (d, *J* = 16.0 Hz, 1H), 3.72 (s, 3H); ^{13}C NMR {^{1}H} (125 MHz, $CDCl_3$ with 0.03% v/v TMS) δ 167.4, 144.8, 134.4, 130.2, 128.8, 128.0, 117.8, 51.6.

Methyl benzoylglycinate (43)[40]

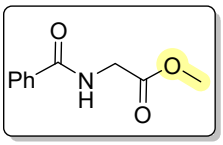

White semisolid, 16mg, 30%; Eluent (25% ethyl acetate in hexane); ^{1}H NMR (500 MHz, $CDCl_3$ with 0.03% v/v TMS) δ 7.77 – 7.72 (m, 2H), 7.47 – 7.42 (m, 1H), 7.37 (ddd, *J* = 6.7, 4.5, 1.2 Hz, 2H), 6.64 (s, 1H), 4.18 (d, *J* = 5.1 Hz, 2H), 3.73 (s, 3H); ^{13}C NMR {^{1}H} (125 MHz, $CDCl_3$ with 0.03% v/v TMS) δ 170.5, 167.4, 133.7, 131.8, 128.6, 127.0, 52.4, 41.7; HRMS (ESI): calcd. for $C_{10}H_{11}NO_3$ [M + Na^+] 216.0631; found 216.0632.

Methyl benzoylalaninate (44)[43]

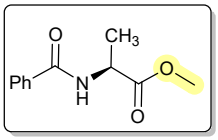

Yellow semisolid, 10mg, 30%; Eluent (10% ethyl acetate in hexane); ^{1}H NMR (500 MHz, $CDCl_3$ with 0.03% v/v TMS) δ 7.73 (d, *J* = 7.7 Hz, 2H), 7.41 (t, *J* = 7.4 Hz, 1H), 7.33 (t, *J* = 7.6 Hz, 2H), 6.88 (d, *J* = 5.9 Hz, 1H), 4.72 (p, *J* = 7.2 Hz, 1H), 3.69 (s, 3H), 1.43 (d, *J* = 7.2 Hz, 3H; ^{13}C NMR {^{1}H} (125 MHz, $CDCl_3$ with 0.03% v/v TMS) δ 172.7, 165.9, 132.8, 130.6, 127.5, 126.0, 51.5, 47.4, 17.4; HRMS (ESI): calcd. for $C_{11}H_{13}NO_3$ [M + H^+] 208.0974; found 208.0976.

Methyl benzoylvalinate (45)[40]

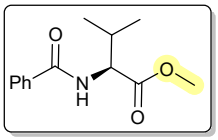

Pale yellow semisolid, 34mg, 64%; Eluent (10% ethyl acetate in hexane); ^{1}H NMR (500 MHz, $CDCl_3$ with 0.03% v/v TMS) δ 7.88 – 7.76 (m, 2H), 7.52 (t, *J* = 7.4 Hz, 1H), 7.45 (t, *J* = 7.4 Hz, 2H), 6.67 (d, *J* = 5.2 Hz, 1H), 4.79 (dd, *J* = 8.6, 4.9 Hz, 1H), 3.77 (s, 3H), 2.33 – 2.21 (m, 1H), 1.00 (dd, *J* = 11.7, 6.9 Hz, 6H); ^{13}C NMR {^{1}H} (125 MHz, $CDCl_3$ with 0.03% v/v TMS) δ 172.6, 167.2, 134.1, 131.7, 128.6, 127.0, 57.4, 52.2, 31.6, 19.0, 17.9; HRMS (ESI): calcd. for $C_{13}H_{17}NO_3$ [M + H^+] 236.1287; found 236.1289.

Methyl benzoylleucinate (46)[40]

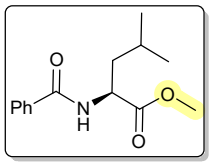

White semisolid, 38mg, 72%; Eluent (10% ethyl acetate in hexane); ^{1}H NMR (500 MHz, $CDCl_3$ with 0.03% v/v TMS) δ 7.73 (dd, *J* = 5.3, 3.2 Hz, 2H), 7.44 (dd, *J* = 8.4, 6.4 Hz, 1H), 7.36 (t, *J* = 7.6 Hz, 2H), 6.54 (d, *J* = 6.7 Hz, 1H), 4.84 – 4.73 (m, 1H), 3.70 (s, 3H), 1.73 – 1.64 (m, 2H), 1.18 (s, 1H), 0.91 (dd, *J* = 9.7, 6.2 Hz, 6H); ^{13}C NMR {^{1}H} (125 MHz, $CDCl_3$ with 0.03% v/v TMS) δ 172.7, 166.1, 132.6, 130.7, 127.5, 126.0, 51.3, 50.1, 40.8, 23.9, 21.8, 21.0; HRMS (ESI): calcd. for $C_{14}H_{19}NO_3$ [M + H$^+$] 250.1443; found 250.1446.

Methyl benzoylphenylalaninate (47)[43]

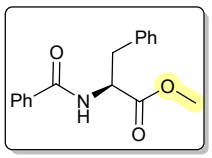

Pale yellow semisolid, 43mg, 82%; Eluent (10% ethyl acetate in hexane); ^{1}H NMR (500 MHz, $CDCl_3$ with 0.03% v/v TMS) δ 7.65 (d, *J* = 7.3 Hz, 2H), 7.43 (t, *J* = 7.4 Hz, 1H), 7.34 (t, *J* = 7.7 Hz, 2H), 7.24 – 7.17 (m, 3H), 7.06 (d, *J* = 6.8 Hz, 2H), 6.54 (d, *J* = 5.9 Hz, 1H), 5.02 (dd, *J* = 13.2, 5.6 Hz, 1H), 3.69 (s, 3H), 3.19 (ddd, *J* = 34.3, 13.9, 5.6 Hz, 2H); ^{13}C NMR {^{1}H} (125 MHz, $CDCl_3$ with 0.03% v/v TMS) δ 172.0, 166.8, 135.5, 133.9, 131.8, 129.3, 128.6, 127.2, 127.0, 53.5, 52.4, 37.9; HRMS (ESI): calcd. for $C_{17}H_{17}NO_3$ [M + H$^+$] 284.1287; found 284.1289.

Methyl N-benzoyl-N-methylglycinate (48)[40]

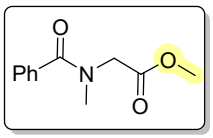

Yellow semisolid, 40mg, 65% as a mixture of conformers (1: 2); Eluent (25% ethyl acetate in hexane); ^{1}H NMR (500 MHz, $CDCl_3$ with 0.03% v/v TMS) δ 7.39 (s, 2.45 H), 7.33 (d, *J* = 17.6 Hz, 5H), 3.92 (s, 0.96H), 4.21 (s, 2H), 3.66 (s, 1.61 H), 3.71 (s, 3H), 3.04 (s, 1.49 H), 2.97 (s, 3H); ^{13}C NMR {^{1}H} (125 MHz, $CDCl_3$ with 0.03% v/v TMS) δ 172.1, 169.5, 135.4, 129.8, 128.5 (d, *J* = 30.9 Hz), 127.1, 126.5, 53.1, 52.2 (d, *J* = 20.1 Hz), 49.0, 38.6; HRMS (ESI): calcd. for $C_{11}H_{13}NO_3$ [M + Na$^+$] 230.0788; found 230.0799.

Methyl benzoyltyrosinate (49)[41]

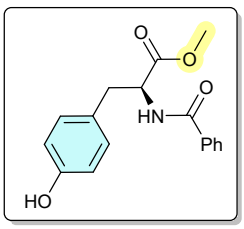

White solid, 30mg, 66%; Eluent (25% ethyl acetate in hexane); ^{1}H NMR (500 MHz, DMSO – d_6) δ 9.21 (s, 1H), 8.78 (d, *J* = 7.8 Hz, 1H), 7.82 (d, *J* = 7.3 Hz, 2H), 7.56 – 7.52 (m, 1H), 7.47 (dd, *J* = 10.3, 4.6 Hz, 2H), 7.10 (d, *J* = 8.4 Hz, 2H), 6.67 (d, *J* = 8.4 Hz, 2H), 4.67 – 4.50 (m, 1H), 3.64 (s, 3H), 3.03 (ddd, *J* = 23.8, 13.8, 7.7 Hz, 2H); ^{13}C NMR {^{1}H} (125 MHz, DMSO – d_6) δ 172.8, 166.9, 156.4, 134.2, 131.9, 130.4, 128.7, 128.1, 127.8, 115.5, 55.1, 52.3, 36.0; HRMS (ESI): calcd. for $C_{17}H_{17}NO_4$ [M + Na$^+$] 322.1050; found 322.1066.

Methyl benzoylprolinate (50)[40]

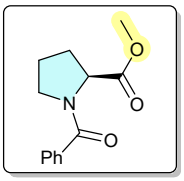

White solid, 36mg, 72%; Eluent (25% ethyl acetate in hexane); ^{1}H NMR (500 MHz, $CDCl_3$ with 0.03% v/v TMS) δ 7.49 (d, *J* = 6.5 Hz, 2H), 7.36 – 7.30 (m, 3H), 4.60 (dd, *J* = 8.3, 5.2 Hz, 1H), 3.70 (s, 3H), 3.57 (dt, *J* = 10.1, 7.0 Hz, 1H), 3.46 (dd, *J* = 8.6, 4.0 Hz, 1H), 2.25 (dd, *J* = 14.7, 6.9 Hz, 1H), 1.98 – 1.93 (m, 2H), 1.85 – 1.77 (m, 1H); ^{13}C NMR {^{1}H} (125 MHz, $CDCl_3$ with 0.03% v/v TMS) δ 172.7, 169.6, 136.1, 130.1, 128.2, 127.2, 59.1, 52.2, 49.9, 29.3, 25.3; HRMS (ESI): calcd. for $C_{13}H_{15}NO_3$ [M + Na^+] 256.0944; found 256.0957.

Methyl benzoyltryptophanate (51)[43]

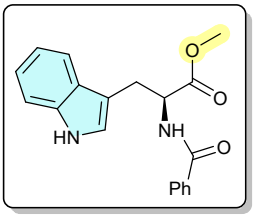

White semisolid, 46mg, 88%; Eluent (25% ethyl acetate in hexane); ^{1}H NMR (500 MHz, $CDCl_3$ with 0.03% v/v TMS) δ 8.60 (s, 1H), 7.71 (d, *J* = 7.3 Hz, 2H), 7.58 (d, *J* = 7.9 Hz, 1H), 7.48 (d, *J* = 7.5 Hz, 1H), 7.37 (dd, *J* = 16.4, 8.4 Hz, 3H), 7.20 (t, *J* = 7.6 Hz, 1H), 7.10 (t, *J* = 7.5 Hz, 1H), 6.99 (d, *J* = 2.3 Hz, 1H), 6.79 (d, *J* = 7.5 Hz, 1H), 5.22 – 5.13 (m, 1H), 3.73 (s, 3H), 3.47 (t, *J* = 5.1 Hz, 2H); ^{13}C NMR {^{1}H} (125 MHz, $CDCl_3$ with 0.03% v/v TMS) δ 172.4, 167.1, 136.2, 133.8, 131.7, 128.5, 127.6, 127.1, 123.0, 122.2, 119.6, 118.5, 111.4, 109.7, 53.6, 52.4, 27.6; HRMS (ESI): calcd. for $C_{19}H_{18}N_2O_3$ [M + Na^+] 345.1210; found 345.1218.

Methyl acetylcysteinate (52)[43]

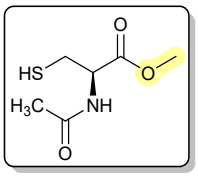

White semisolid, 14mg, 43% as a mixture of conformers (1: 0.7); Eluent (50% ethyl acetate in hexane); ^{1}H NMR (500 MHz, $CDCl_3$ with 0.03% v/v TMS) δ 6.53 (d, *J* = 7.1 Hz, 1H), 6.38 (s, 0.75H), 4.82 (tt, *J* = 7.5, 4.6 Hz, 1.77H), 3.73 (s, 2.38H), 3.71 (s, 3H), 3.19 – 3.09 (m, 2H), 2.95 (ddd, *J* = 8.9, 4.1, 3.3 Hz, 1.53H), 2.01 (s, 3H), 2.00 (s, 2.39H), 1.19 (s, 1H); ^{13}C NMR {^{1}H} (125 MHz, $CDCl_3$ with 0.03% v/v TMS) δ 170.9, 170.6, 170.1, 169.9), 53.5, 52.8 (d, *J* = 3.2 Hz), 51.7, 40.7, 26.8, 23.1 (d, *J* = 7.1 Hz); HRMS (ESI): calcd. for $C_6H_{11}NO_3S$ [M + Na^+] 178.0532; found 178.0531.

2,2-di(1H-indol-3-yl)ethan-1-ol (53)[44]

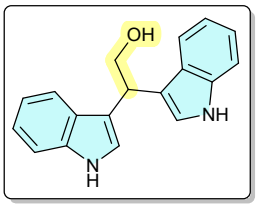

Red semisolid, 28mg, 62%; Eluent (20% ethyl acetate in hexane); ^{1}H NMR (500 MHz, $CDCl_3$ with 0.03% v/v TMS) δ 7.91 (s, 2H), 7.48 (d, *J* = 8.0 Hz, 2H), 7.19 (d, *J* = 8.1 Hz, 2H), 7.07 (t, *J* = 7.6 Hz, 2H), 6.96 (t, *J* = 7.5 Hz, 2H), 6.81 (s, 2H), 4.65 (t, J = 6.1 Hz, 1H), 4.15 (d, *J* = 6.1 Hz, 2H), 4.04 (qd, *J* = 7.1, 1.2 Hz, 1H).

2,2-di(1H-indol-3-yl)ethyl acetate (Streptindole, 54)[44]

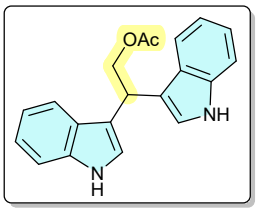

White solid, 16mg, 77%; mp 56-58 °C; Eluent (20% ethyl acetate in hexane); ^{1}H NMR (500 MHz, $CDCl_3$ with 0.03% v/v TMS) δ 7.87 (s, 2H), 7.53 (d, *J* = 8.0 Hz, 2H), 7.23 (d, *J* = 8.1 Hz, 2H), 7.10 – 7.06 (m, 2H), 6.98 (ddd, *J* = 8.0, 7.1, 1.0 Hz, 2H), 6.82 (d, *J* = 1.5 Hz, 2H), 4.85 (t, *J* = 7.1 Hz, 1H), 4.64 (d, *J* = 7.1 Hz, 2H), 1.89 (s, 3H); ^{13}C NMR {^{1}H} (125 MHz, $CDCl_3$ with 0.03% v/v TMS) δ 170.3, 135.3, 125.9, 121.1, 120.9, 118.4, 118.3, 115.1, 110.1, 66.3, 32.5, 20.0; HRMS (ESI): calcd. for $C_{20}H_{18}N_2O_2$ [M + H$^+$] 319.1441; found 319.1443.

2,2-di(1H-indol-3-yl)ethyl butyrate (Arsindoline B, 55)[44]

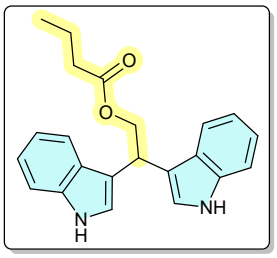

Brown semisolid, 27mg, 74%; Eluent (20% ethyl acetate in hexane); ^{1}H NMR (500 MHz, $CDCl_3$ with 0.03% v/v TMS) δ 7.89 (s, 2H), 7.54 (d, *J* = 8.2 Hz, 2H), 7.26 (d, *J* = 8.1 Hz, 2H), 7.11 – 7.07 (m, 2H), 6.98 (ddd, *J* = 8.0, 7.1, 1.0 Hz, 2H), 6.88 (d, *J* = 1.7 Hz, 2H), 4.87 (t, *J* = 7.1 Hz, 1H), 4.67 (d, *J* = 7.1 Hz, 2H), 2.13 (t, *J* = 7.4 Hz, 2H), 1.47 (dd, *J* = 14.9, 7.4 Hz, 2H), 0.75 (t, *J* = 7.4 Hz, 3H); ^{13}C NMR {^{1}H} (125 MHz, $CDCl_3$ with 0.03% v/v TMS) δ 172.9, 135.4, 126.0, 121.0, 120.0, 118.5, 118.3, 115.3, 110.0, 66.0, 35.2, 32.6, 17.3, 12.5; HRMS (ESI): calcd. for $C_{22}H_{22}N_2O_2$ [M + H$^+$] 369.1573; found 369.1575.

10. ^{1}H and ^{13}C NMR spectra of compounds

Methyl 2,2-di(1H-indol-3-yl)acetate (3)

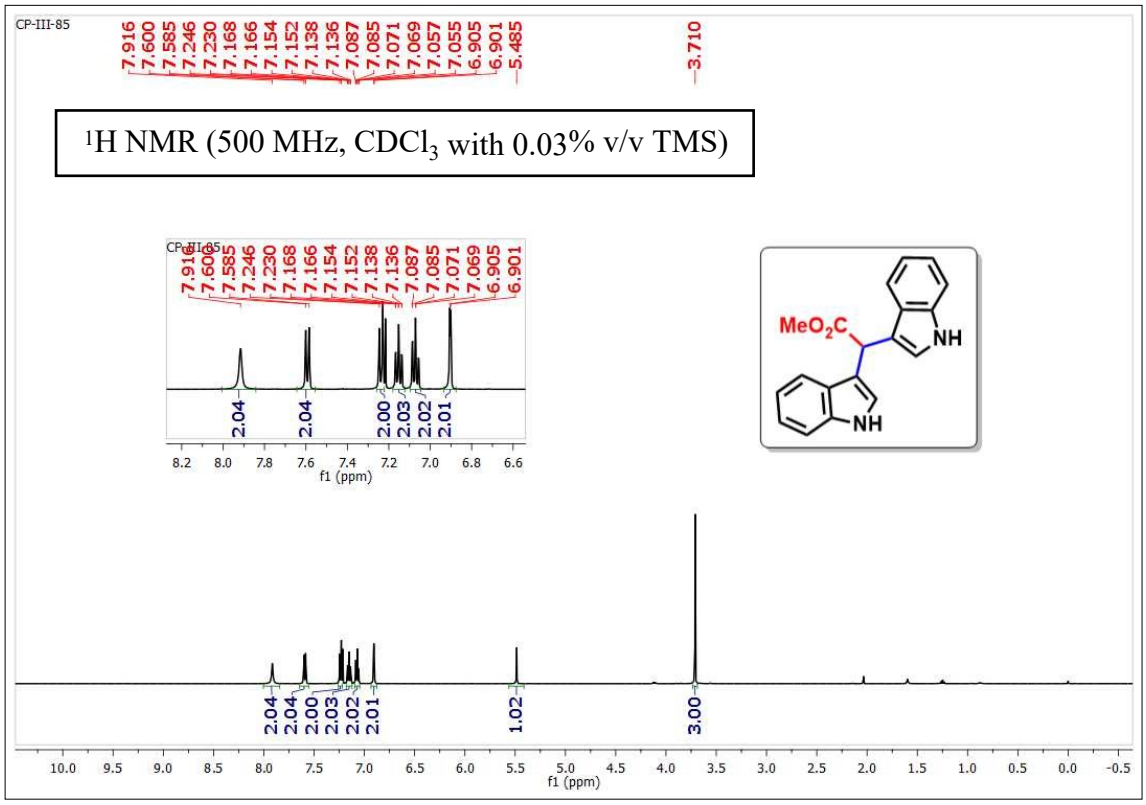

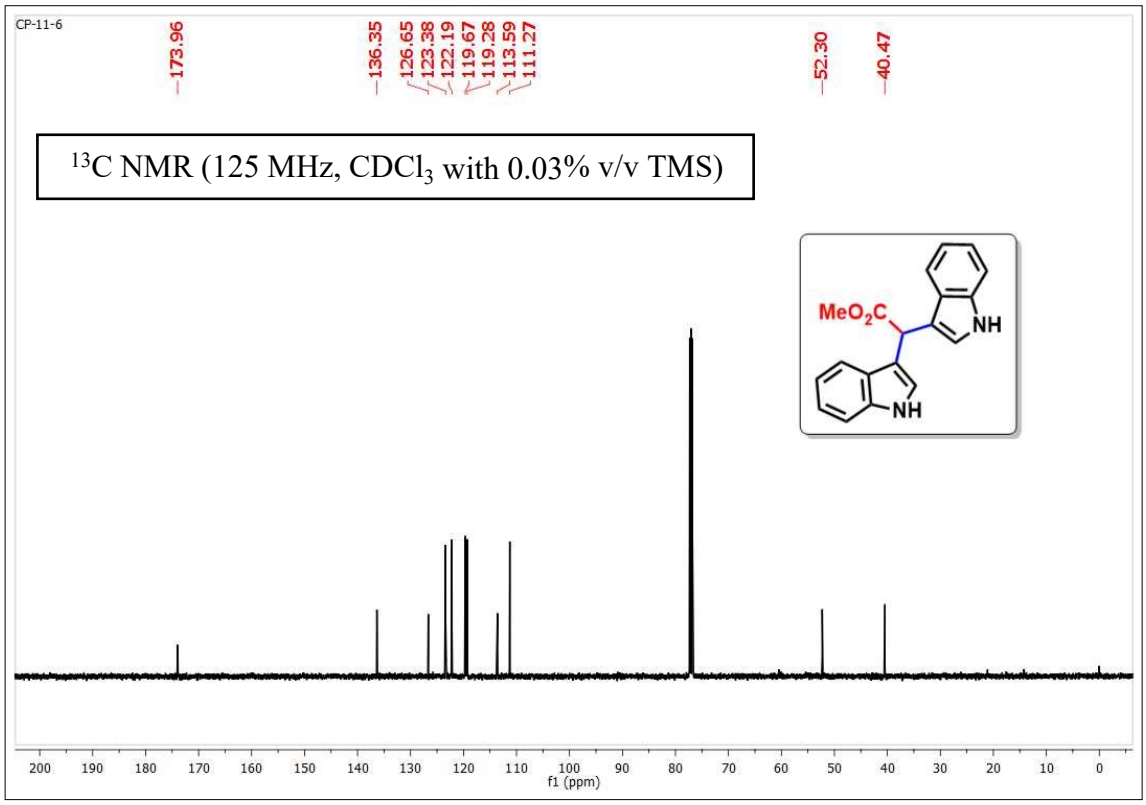

Methyl 2,2-bis(5-methyl-1H-indol-3-yl)acetate (4)

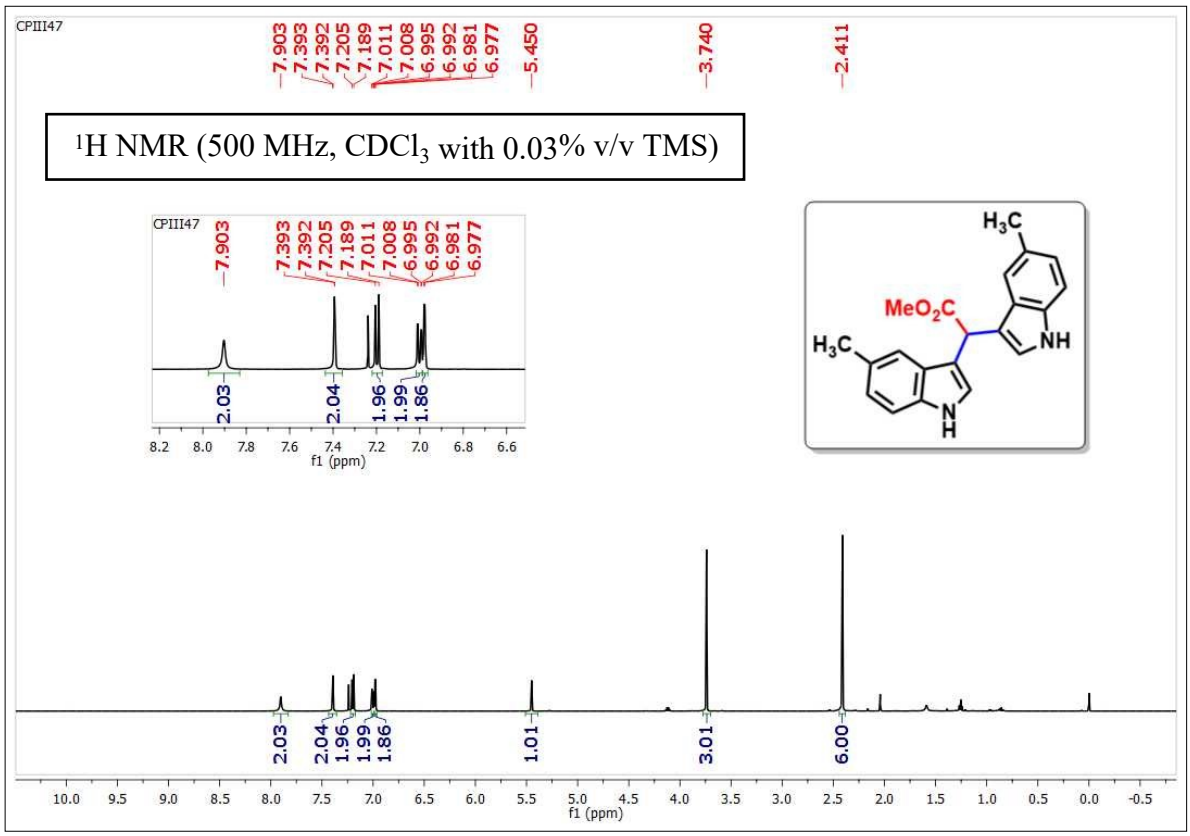

^{1}H NMR (500 MHz, $CDCl_3$ with 0.03% v/v TMS)

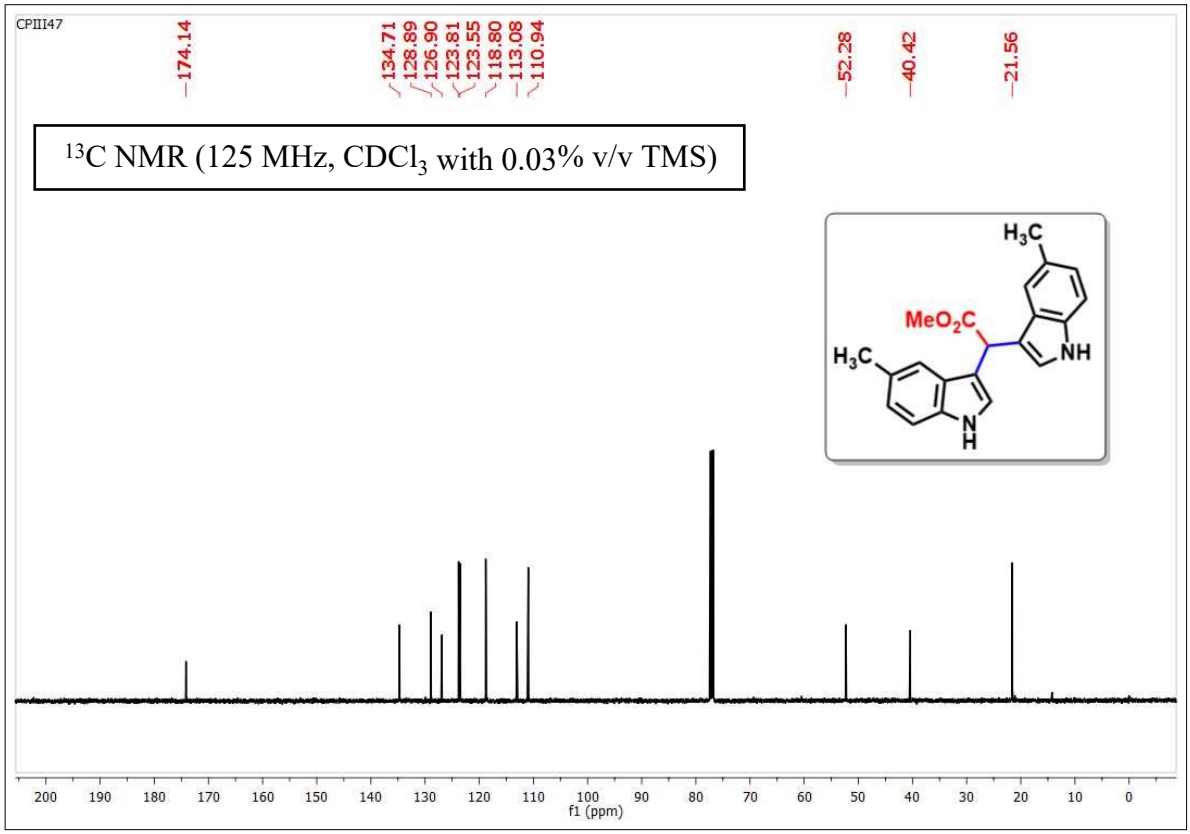

^{13}C NMR (125 MHz, $CDCl_3$ with 0.03% v/v TMS)

Methyl 2,2-bis(5-methoxy-1H-indol-3-yl)acetate (5)

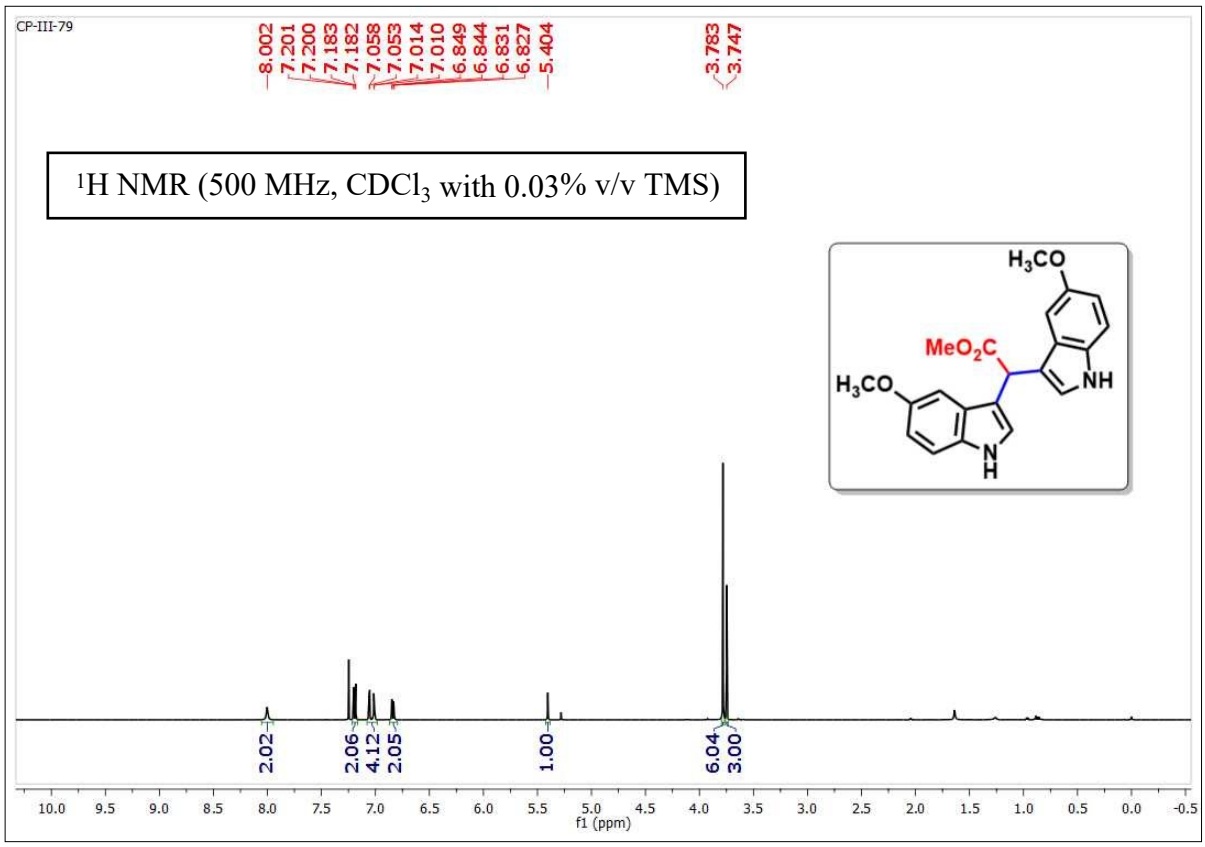

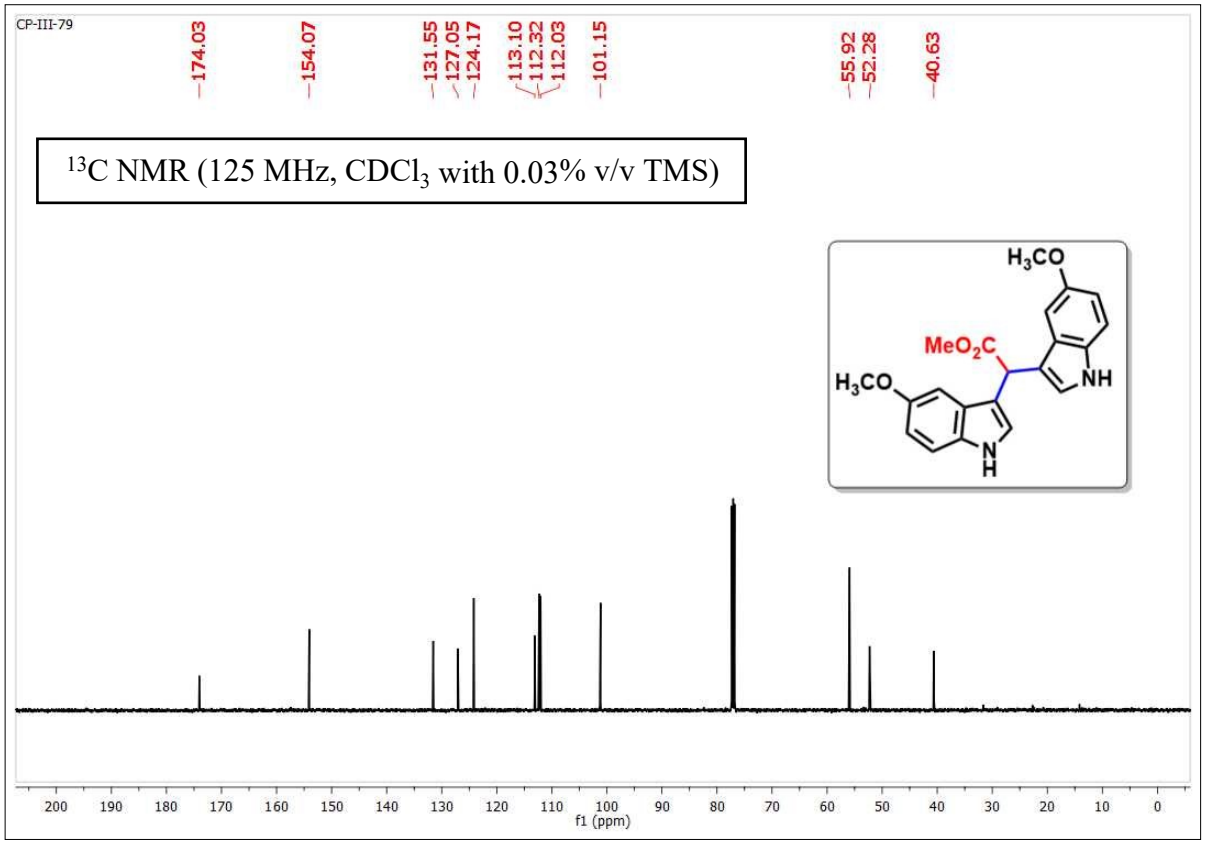

Methyl 2,2-bis(5-(benzyloxy)-1H-indol-3-yl)acetate (6)

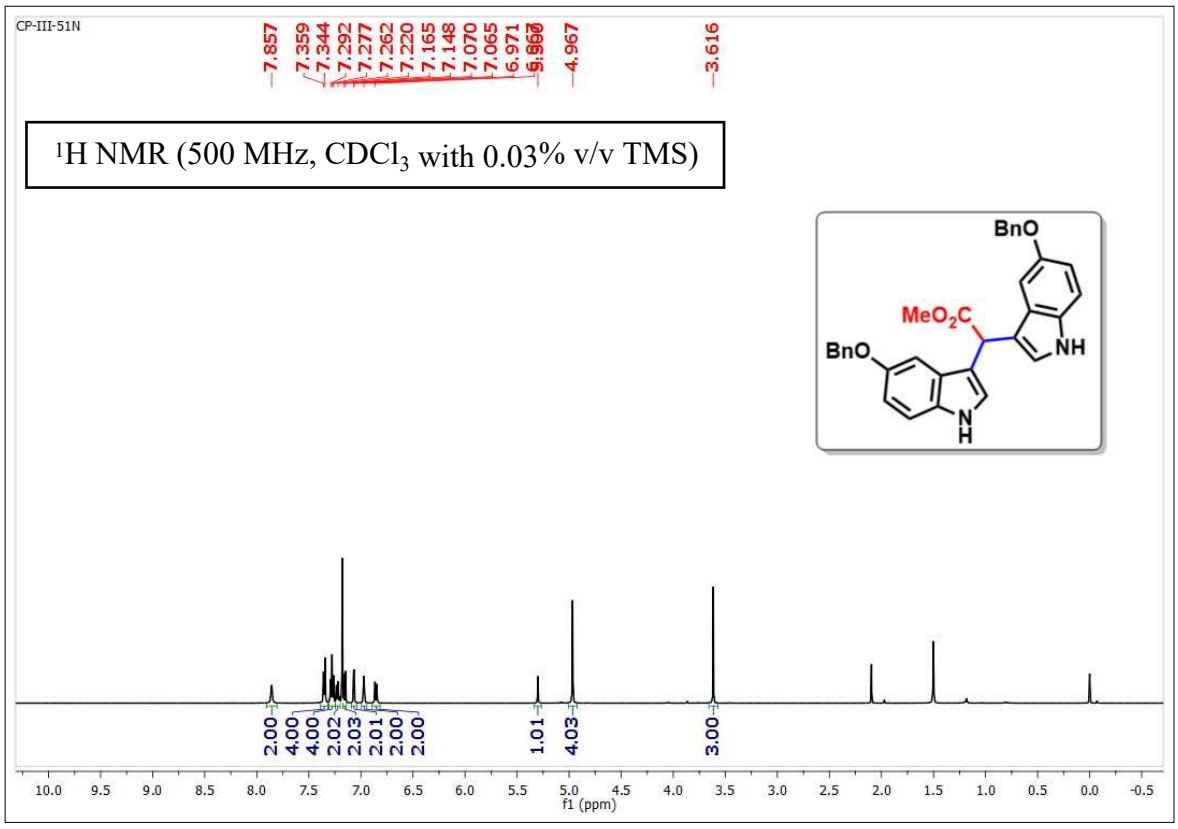

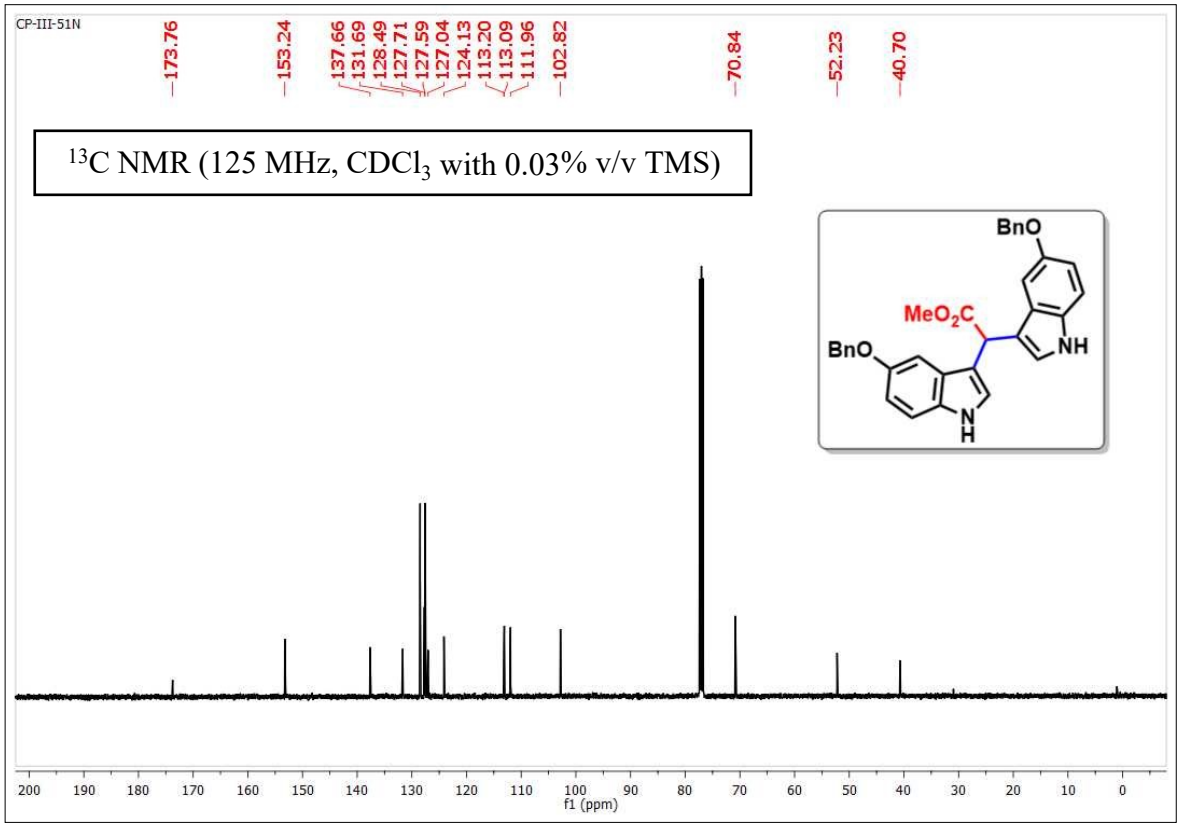

Methyl 2,2-bis(7-methyl-1H-indol-3-yl)acetate (7)

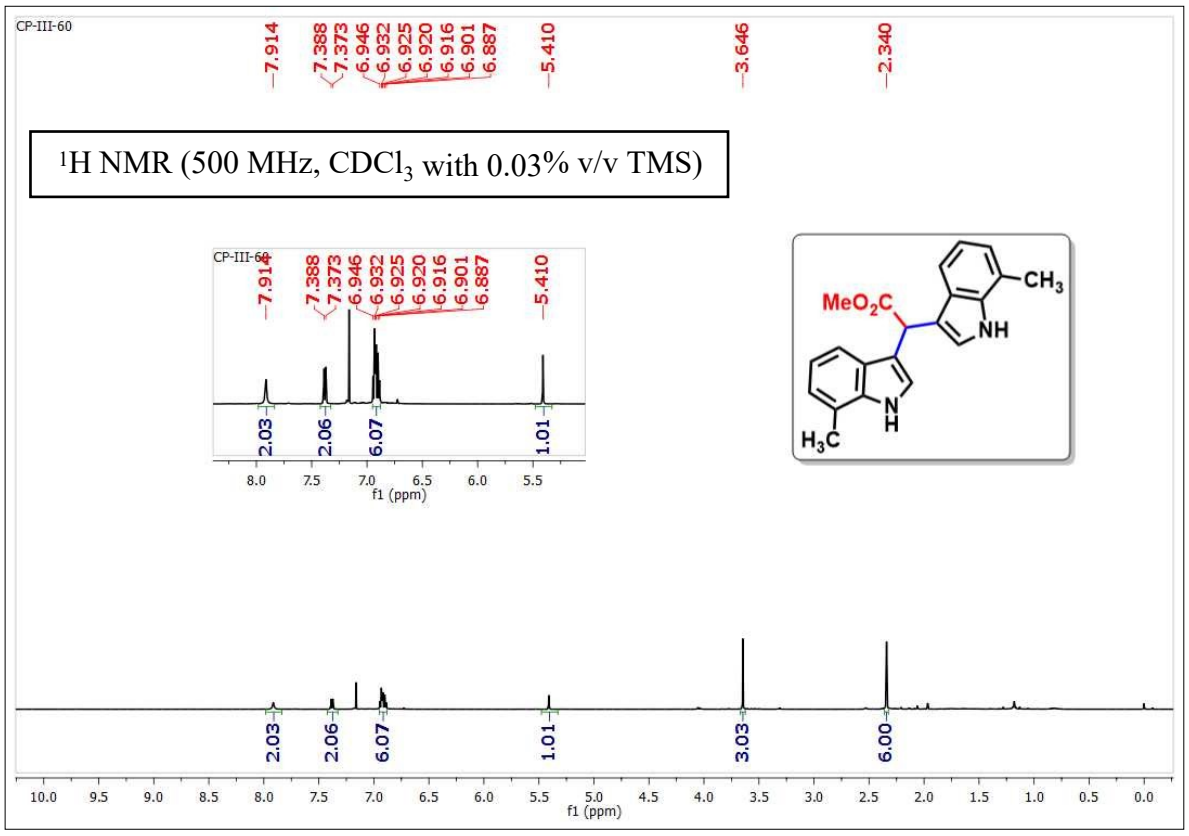

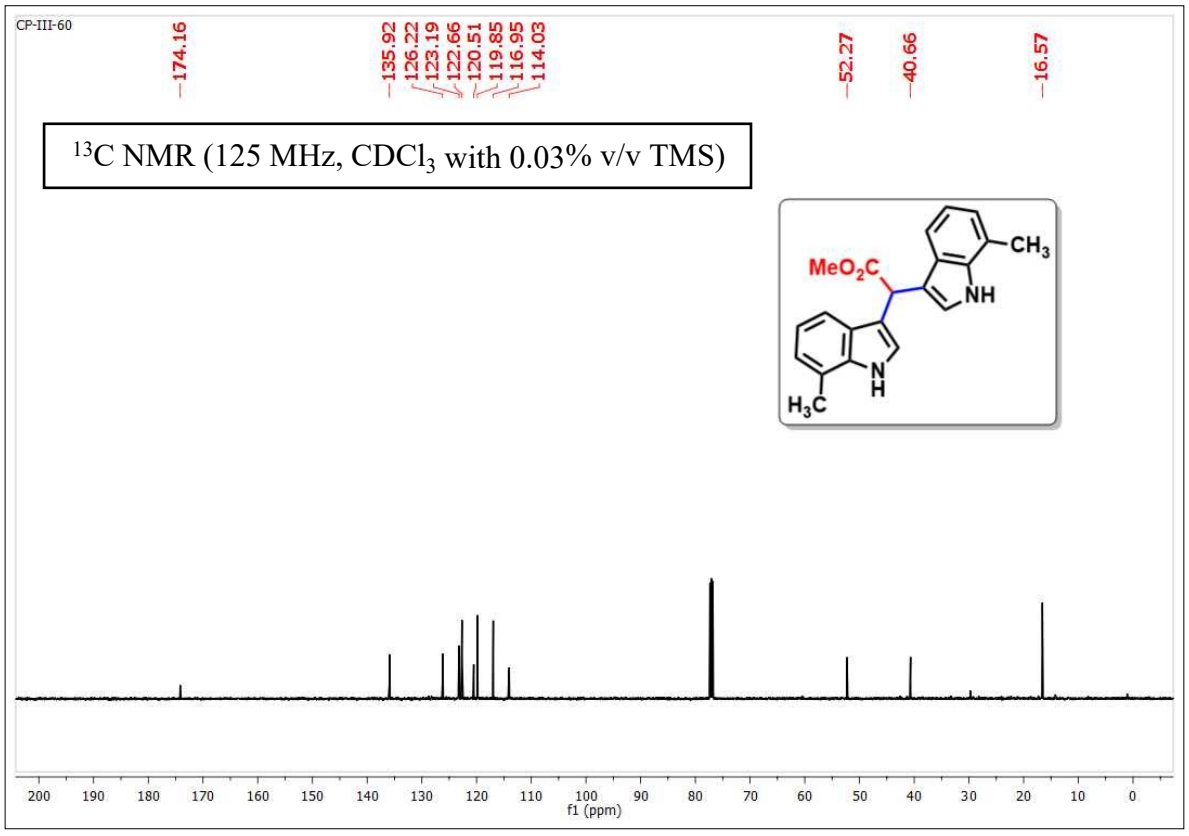

Methyl 2,2-bis(5-chloro-1H-indol-3-yl)acetate (8)

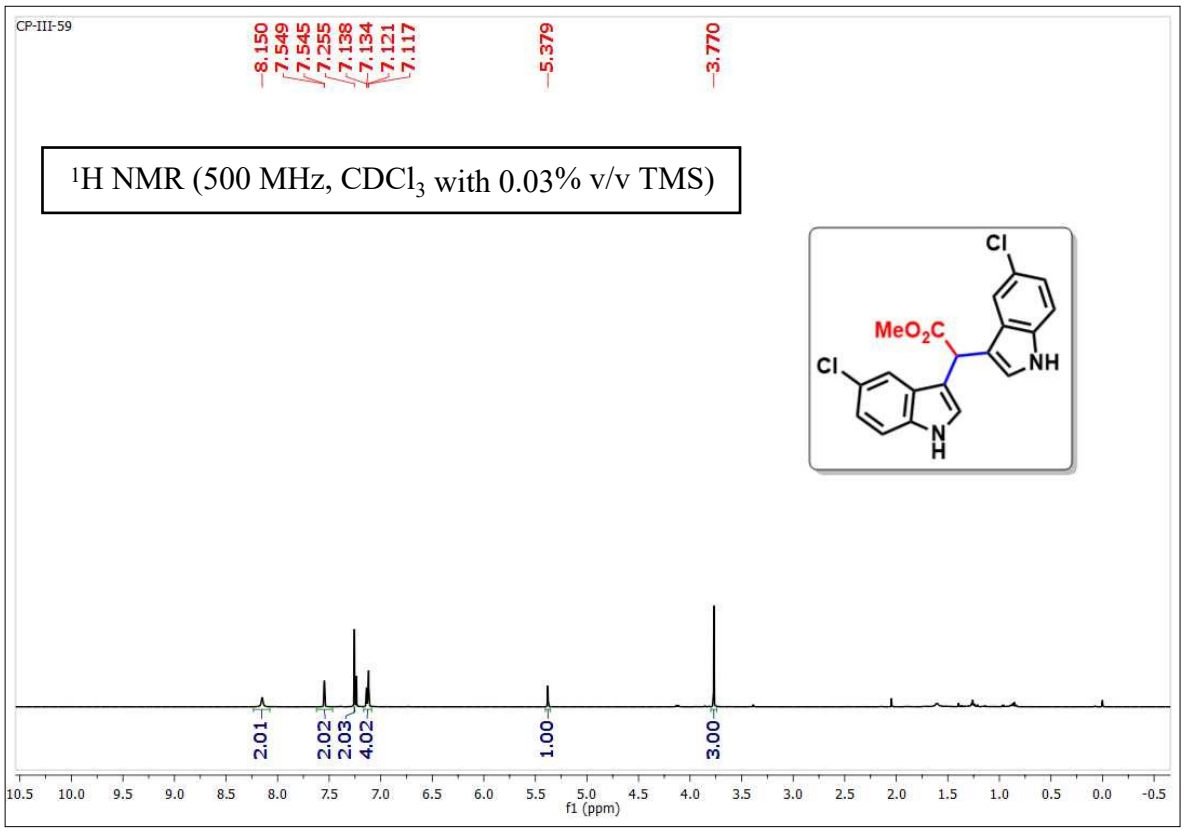

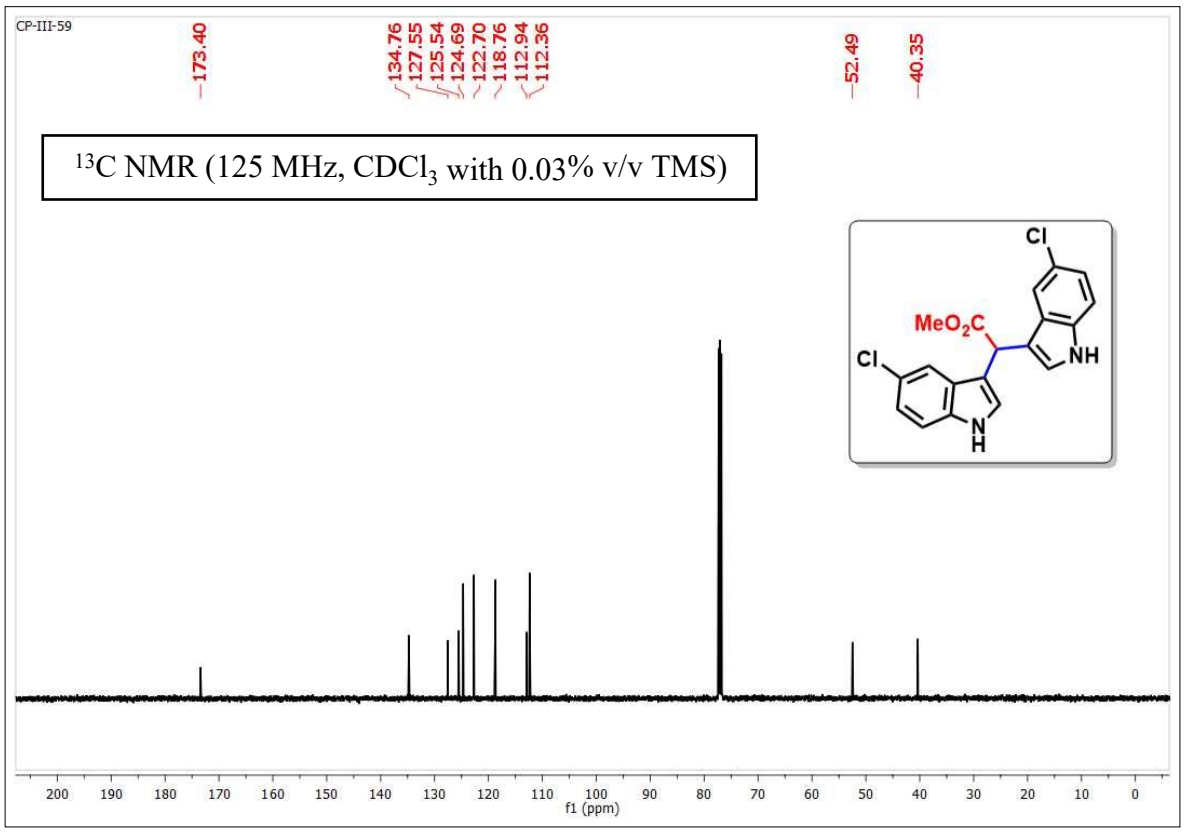

Methyl 2,2-bis(5-bromo-1H-indol-3-yl)acetate (9)

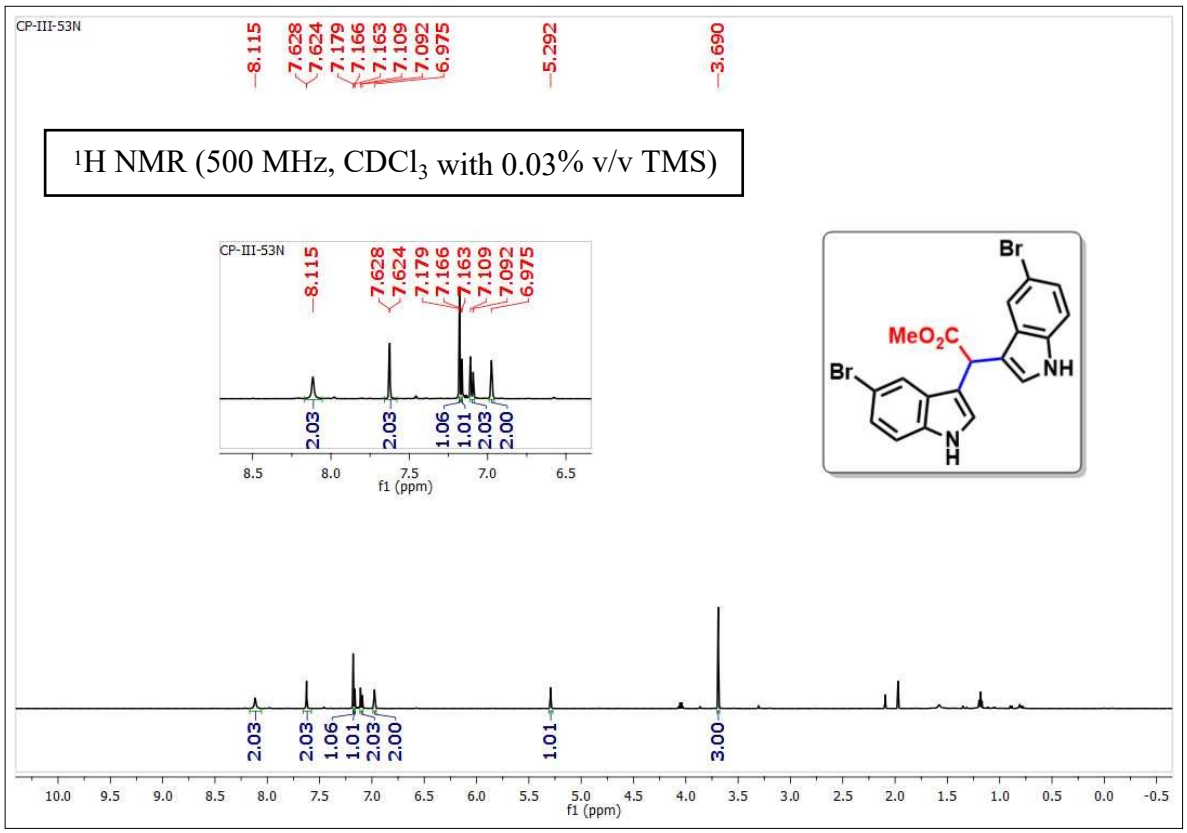

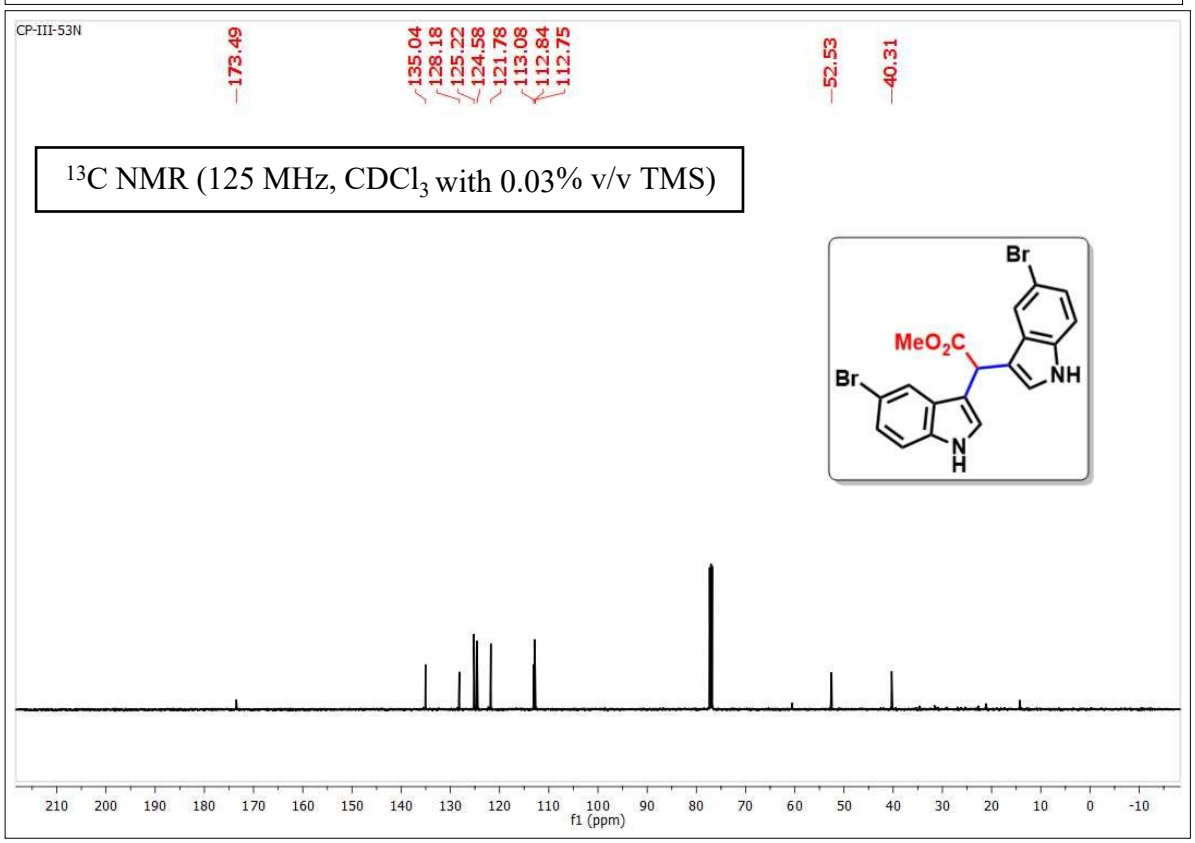

Methyl 2,2-bis(5-fluoro-1H-indol-3-yl)acetate (10)

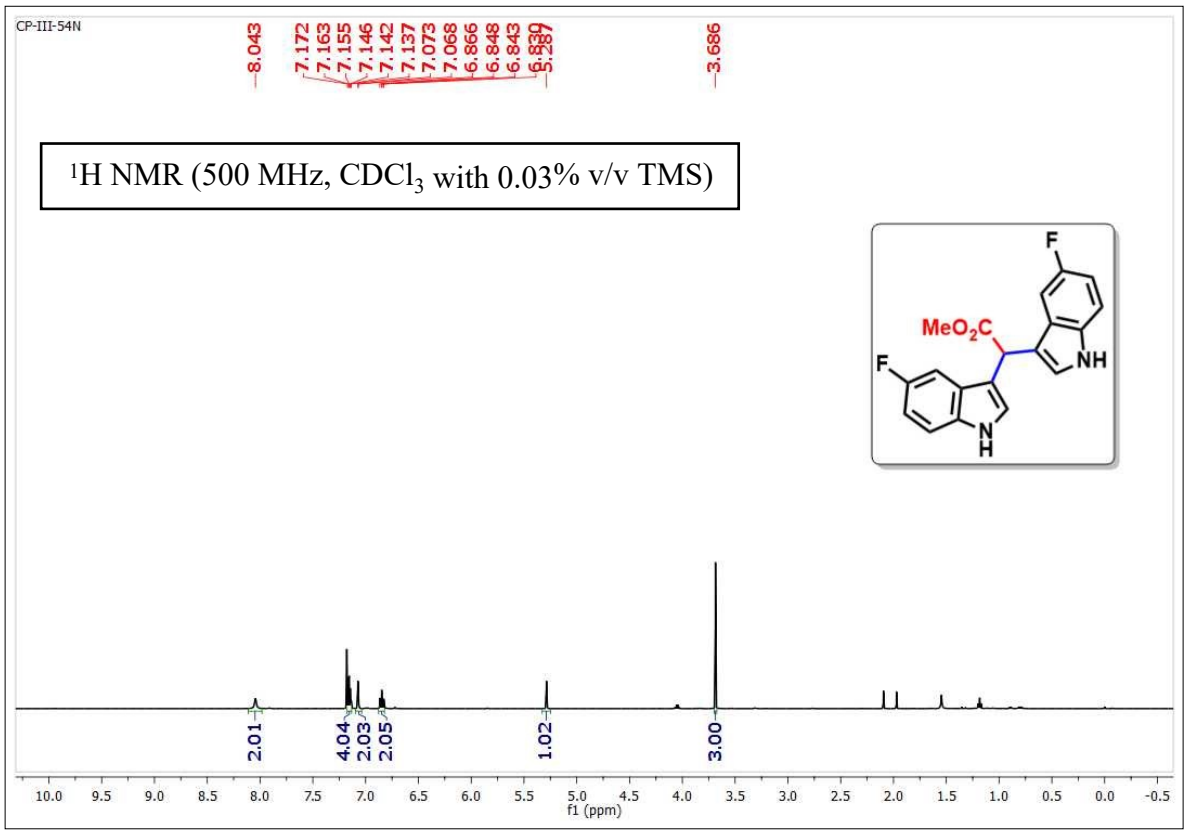

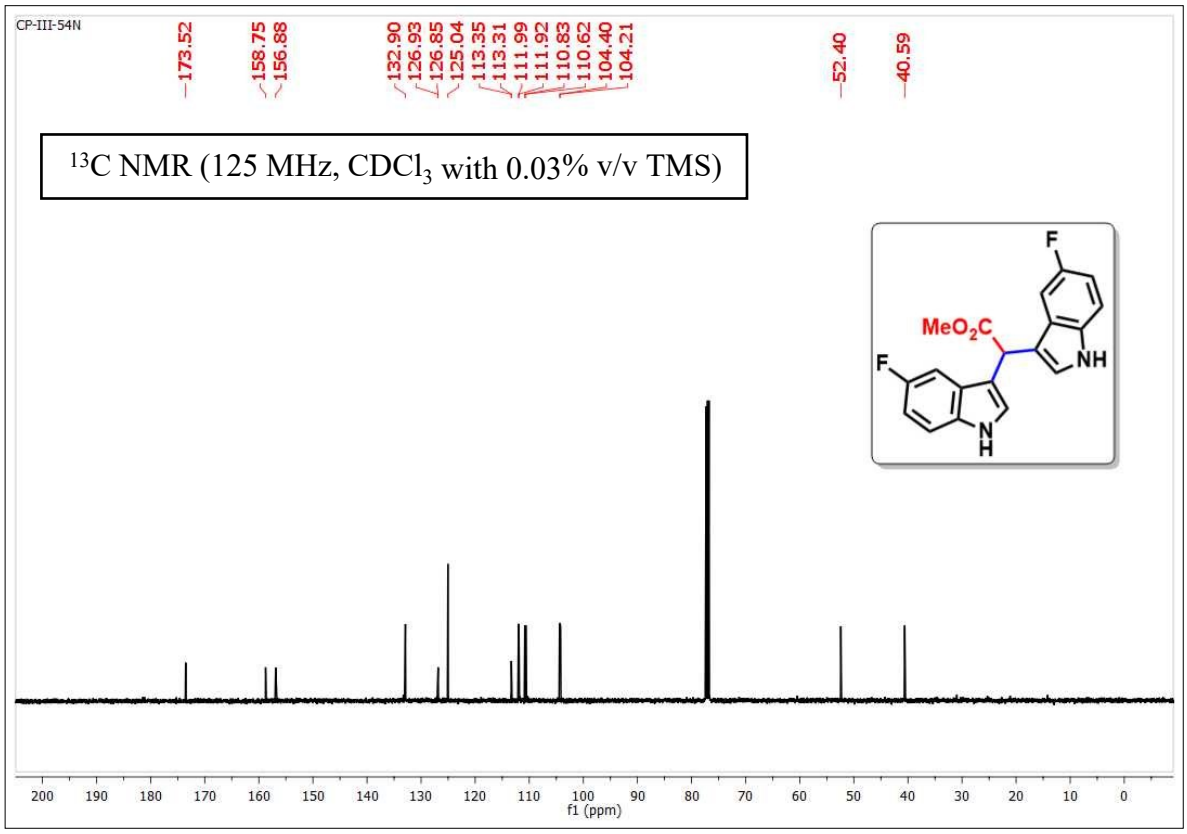

Methyl 2,2-bis(6-bromo-1H-indol-3-yl)acetate (11)

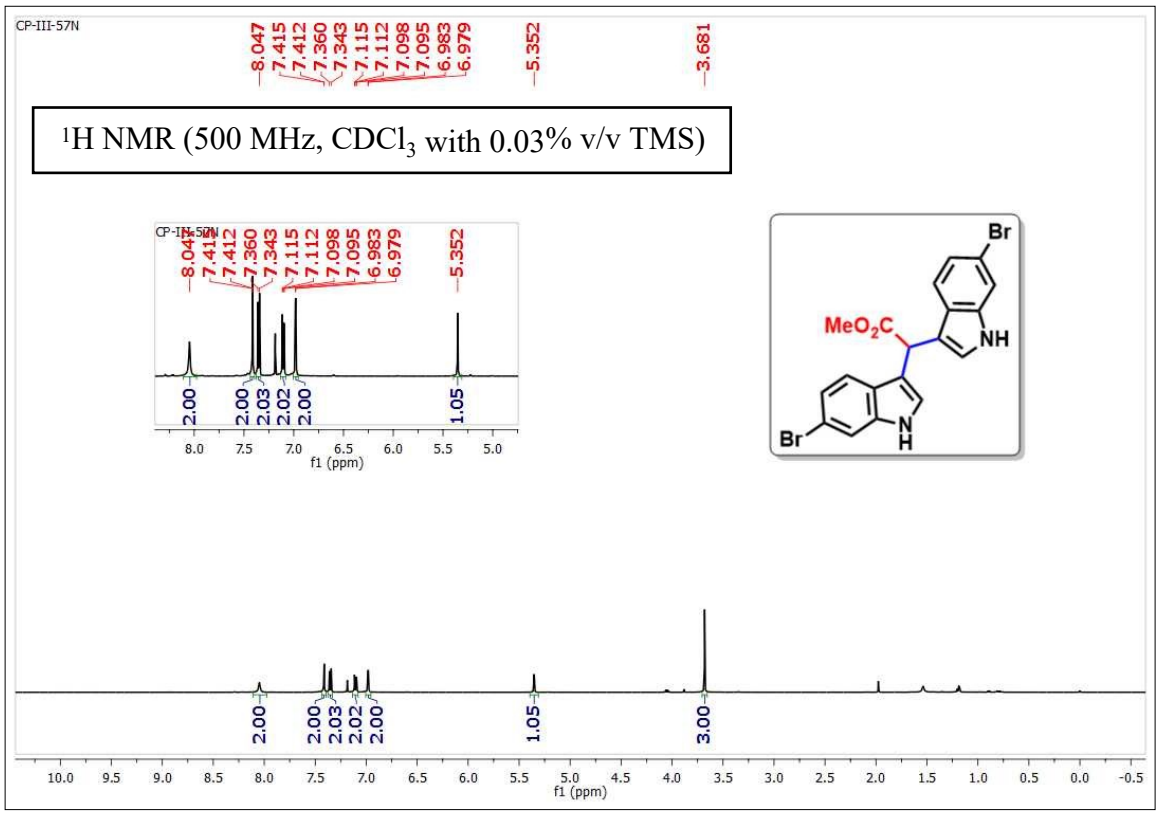

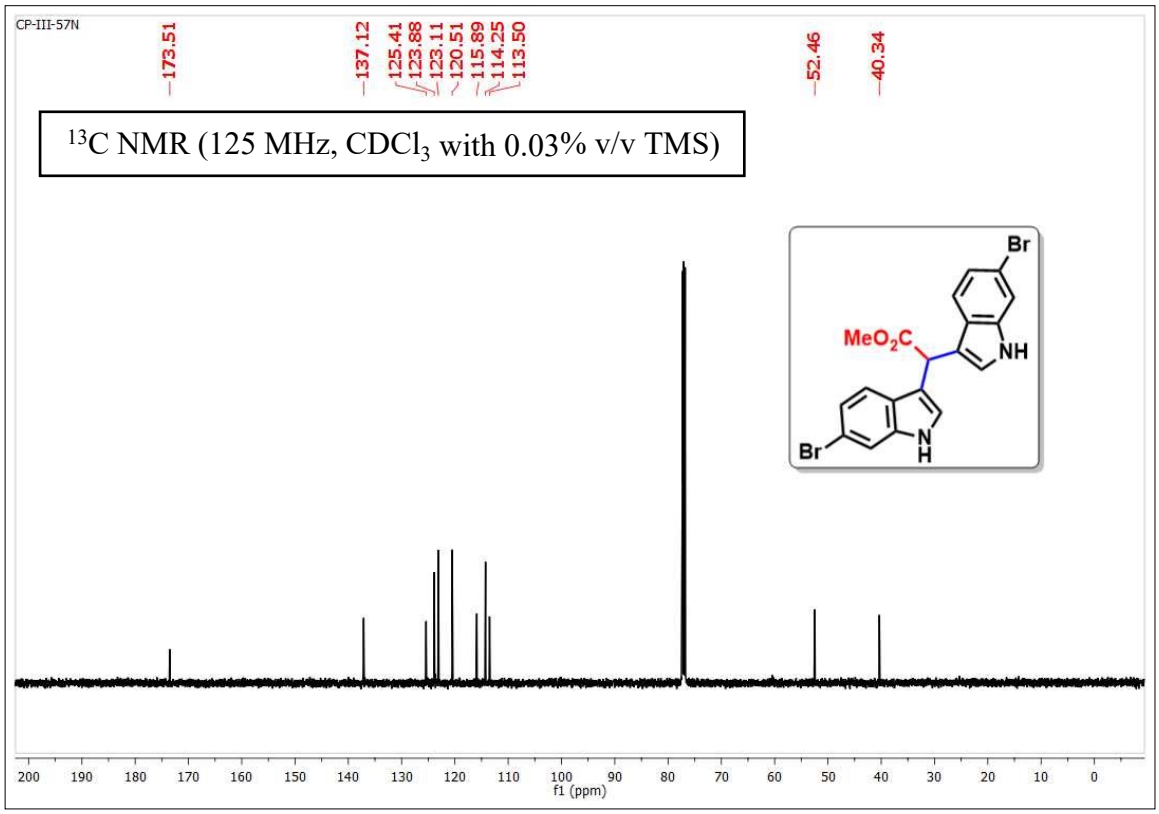

Methyl 2,2-bis(4-chloro-1H-indol-3-yl)acetate (12)

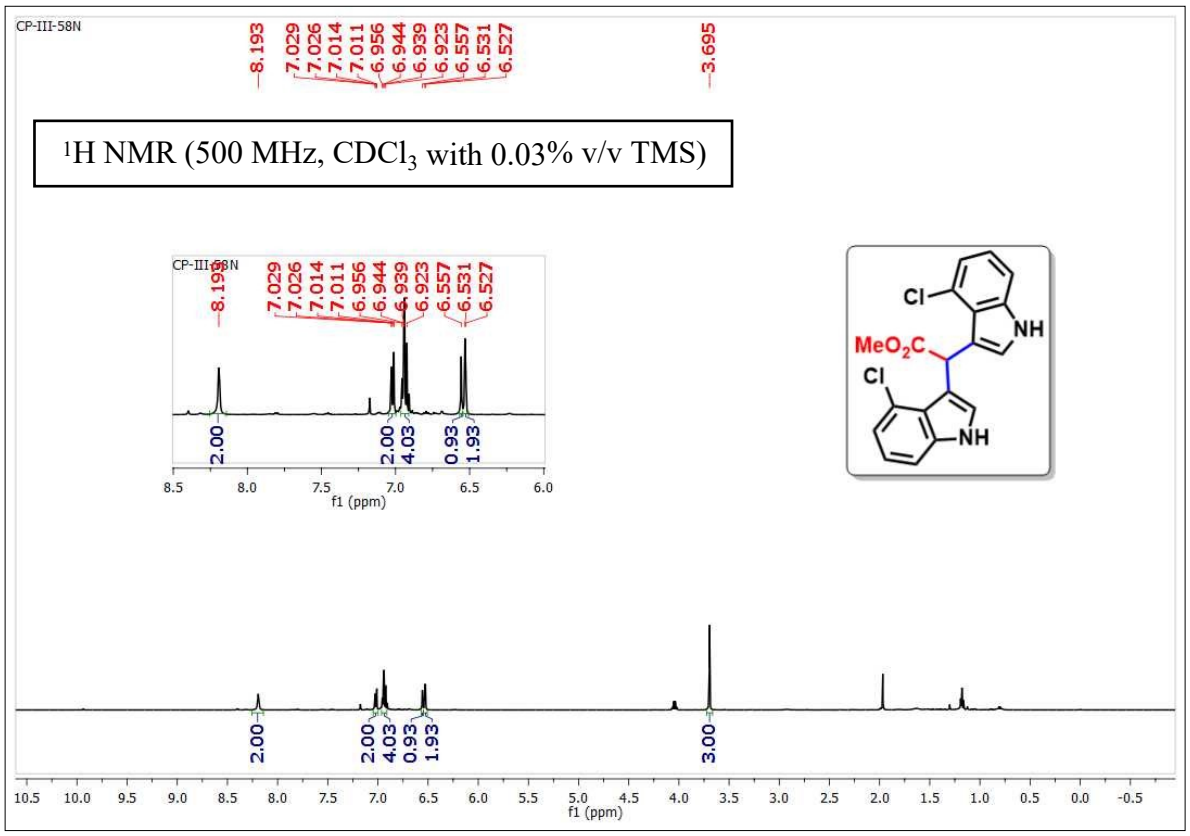

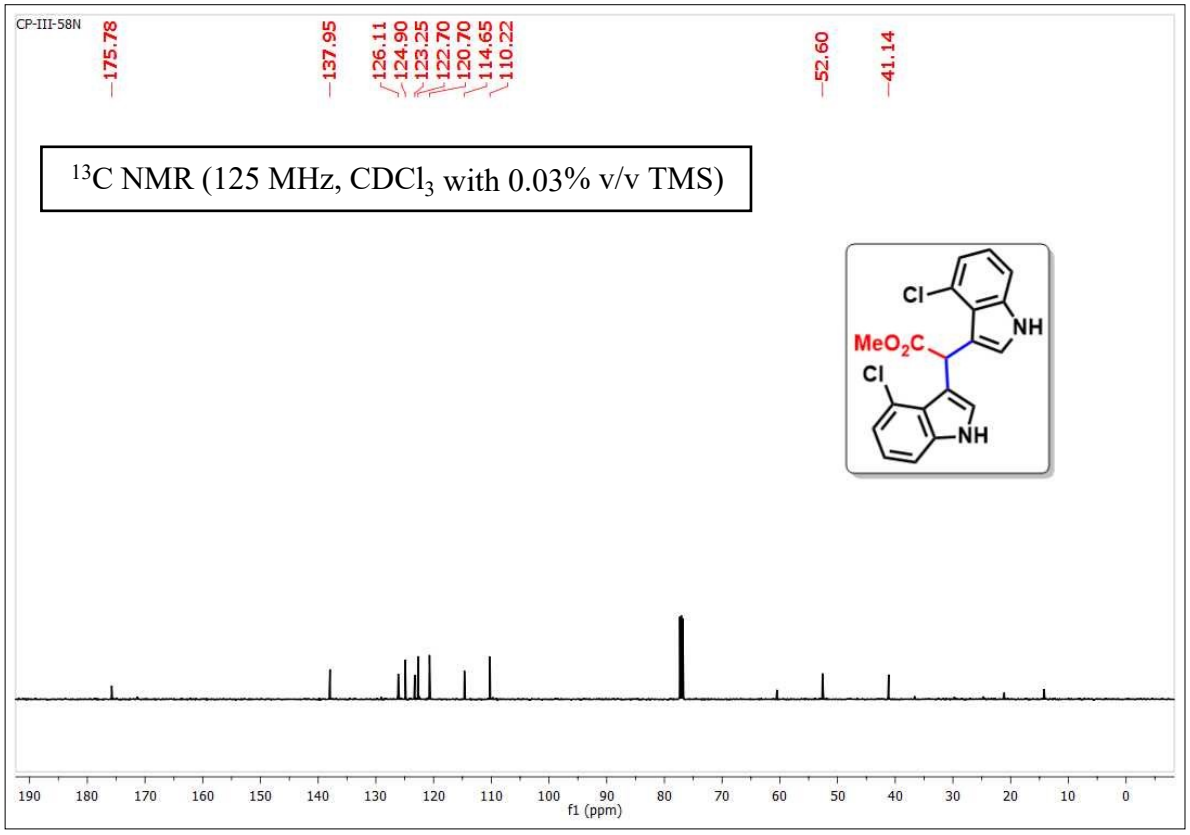

Methyl 2,2-bis(2-methyl-1H-indol-3-yl)acetate (15)

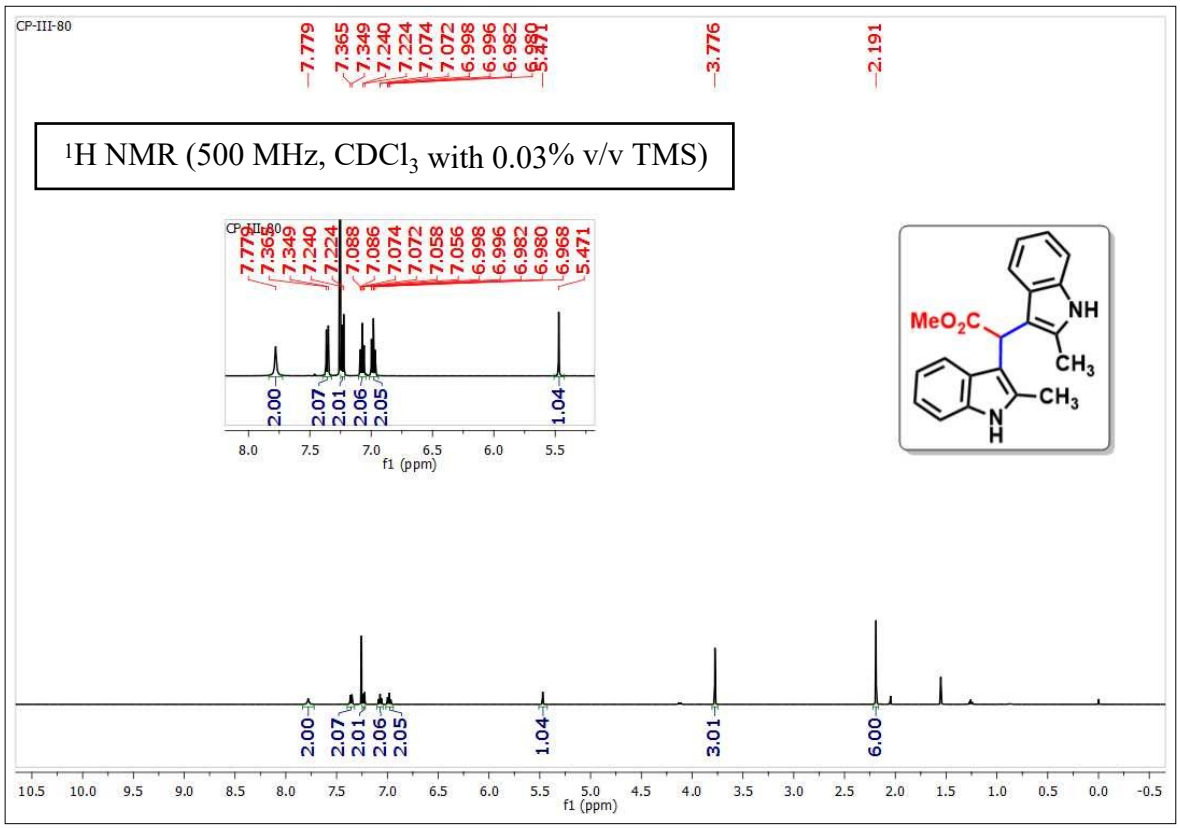

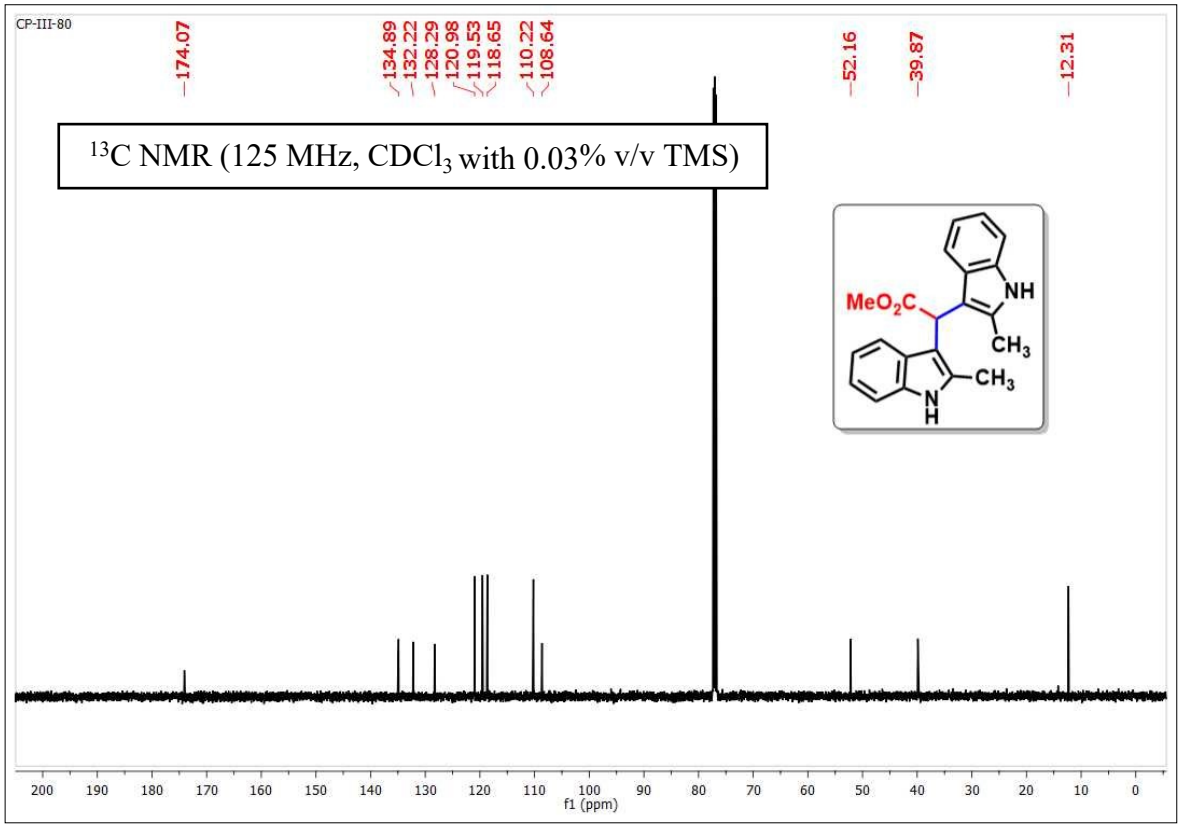

Methyl 2,2-bis(2-phenyl-1H-indol-3-yl)acetate (16)

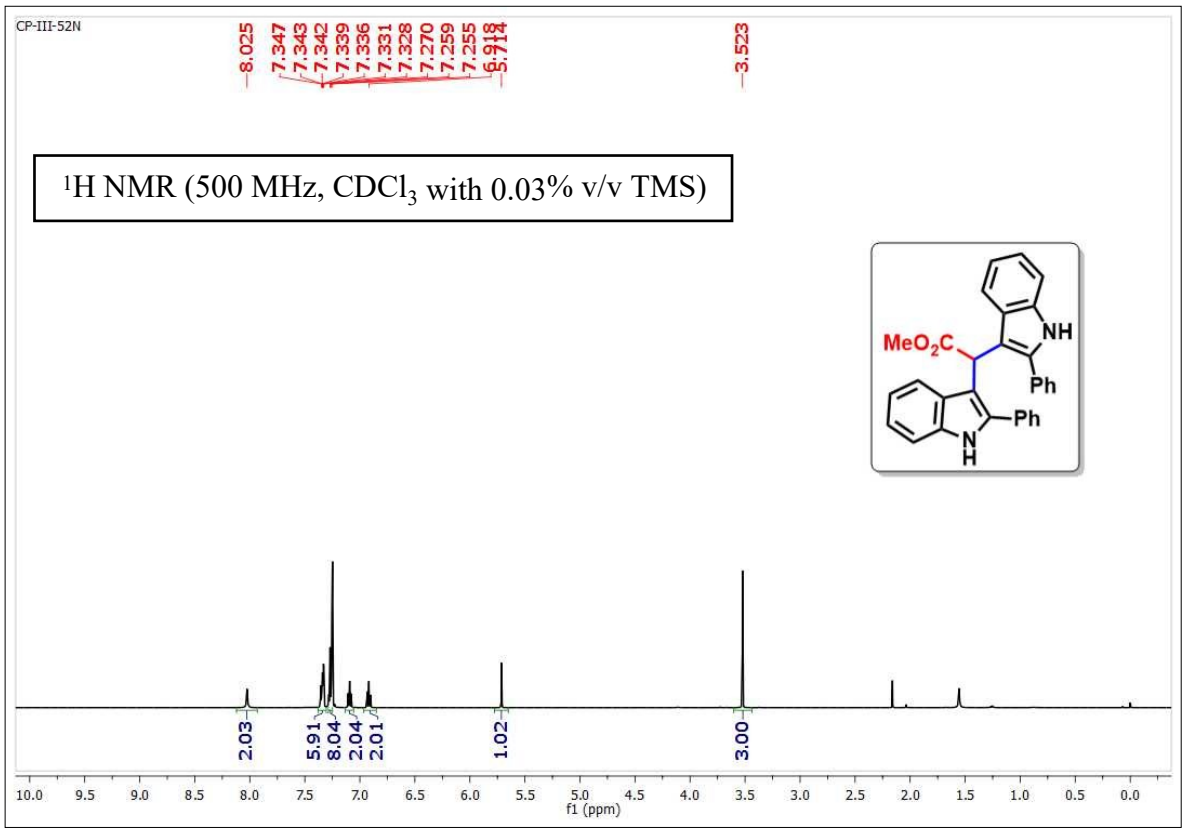

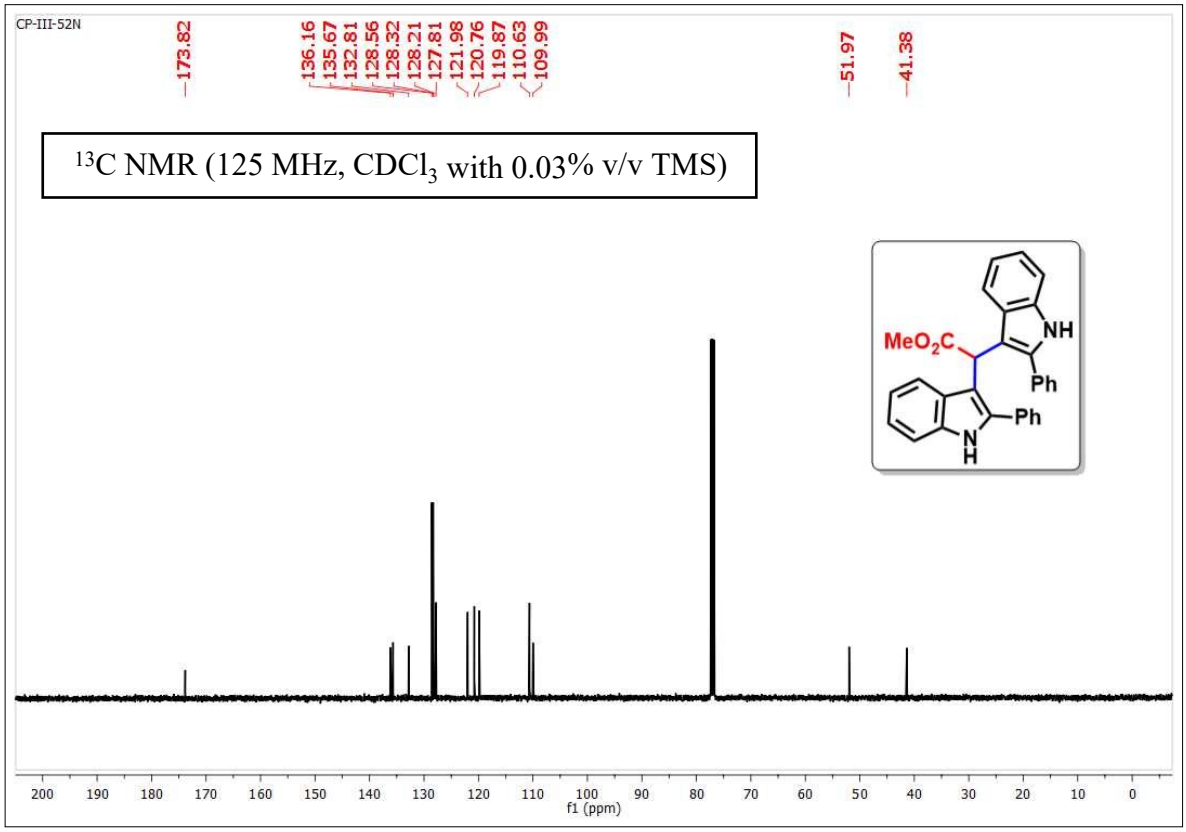

Methyl 2,2-bis(1-ethyl-1H-indol-3-yl)acetate (17)

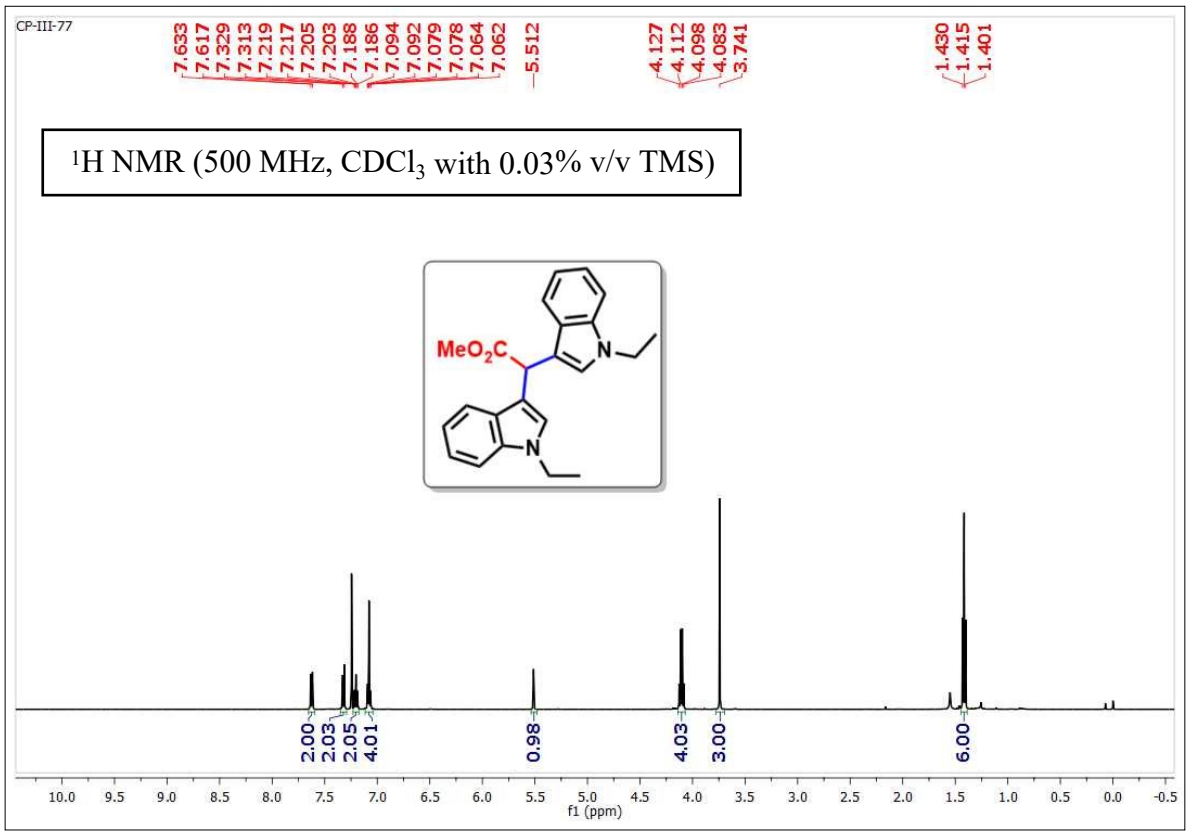

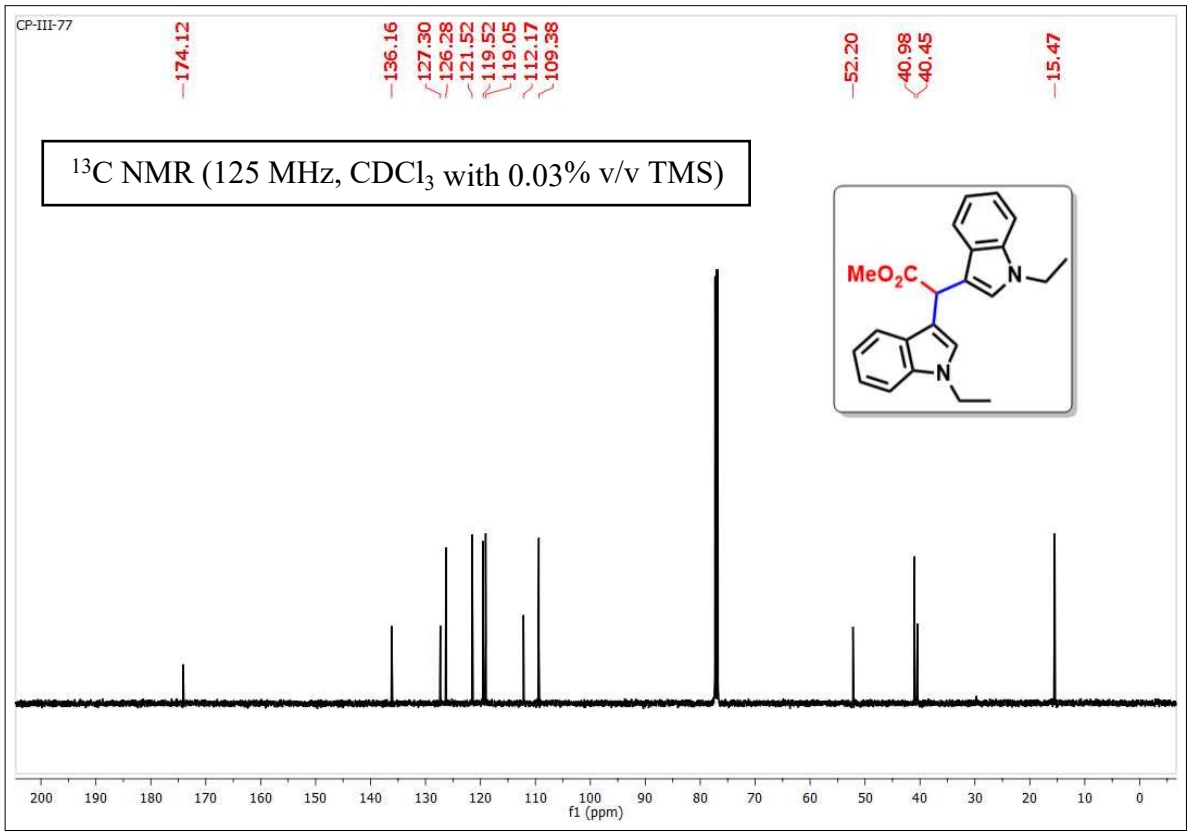

Methyl 2,2-bis(1-methyl-1H-indol-3-yl)acetate (18)

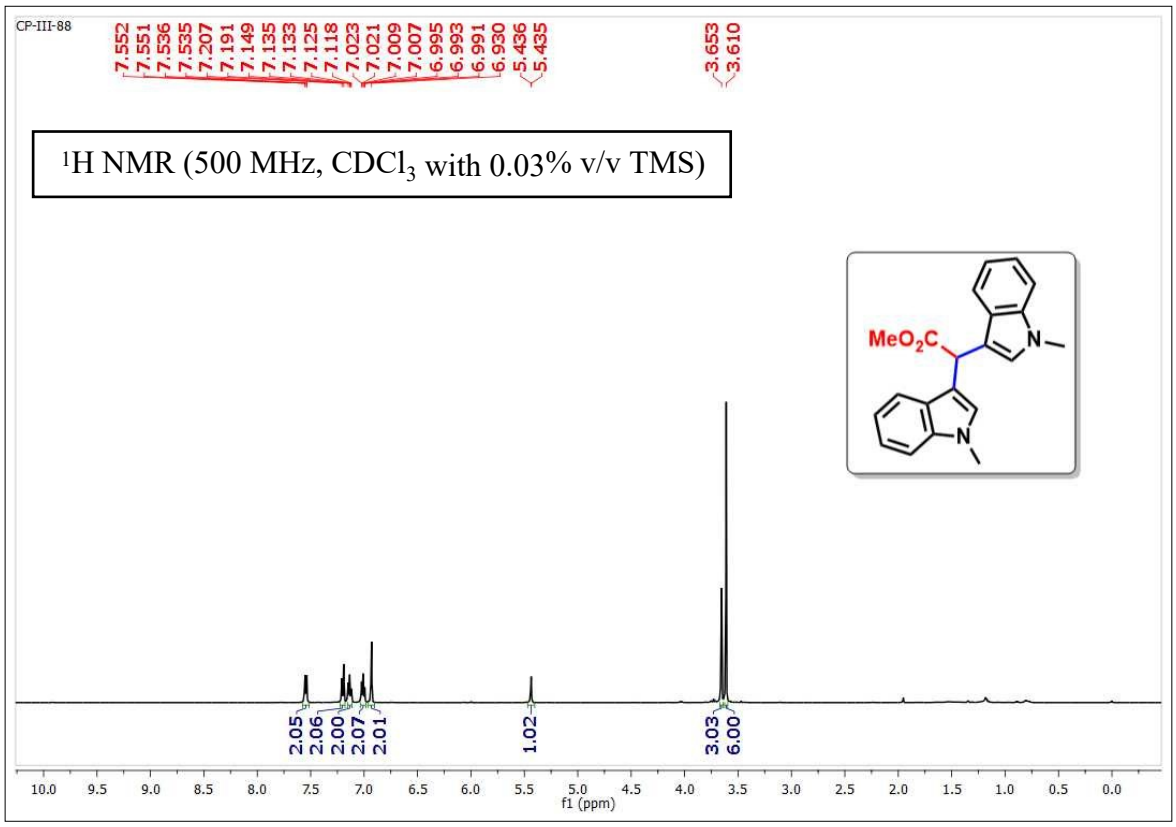

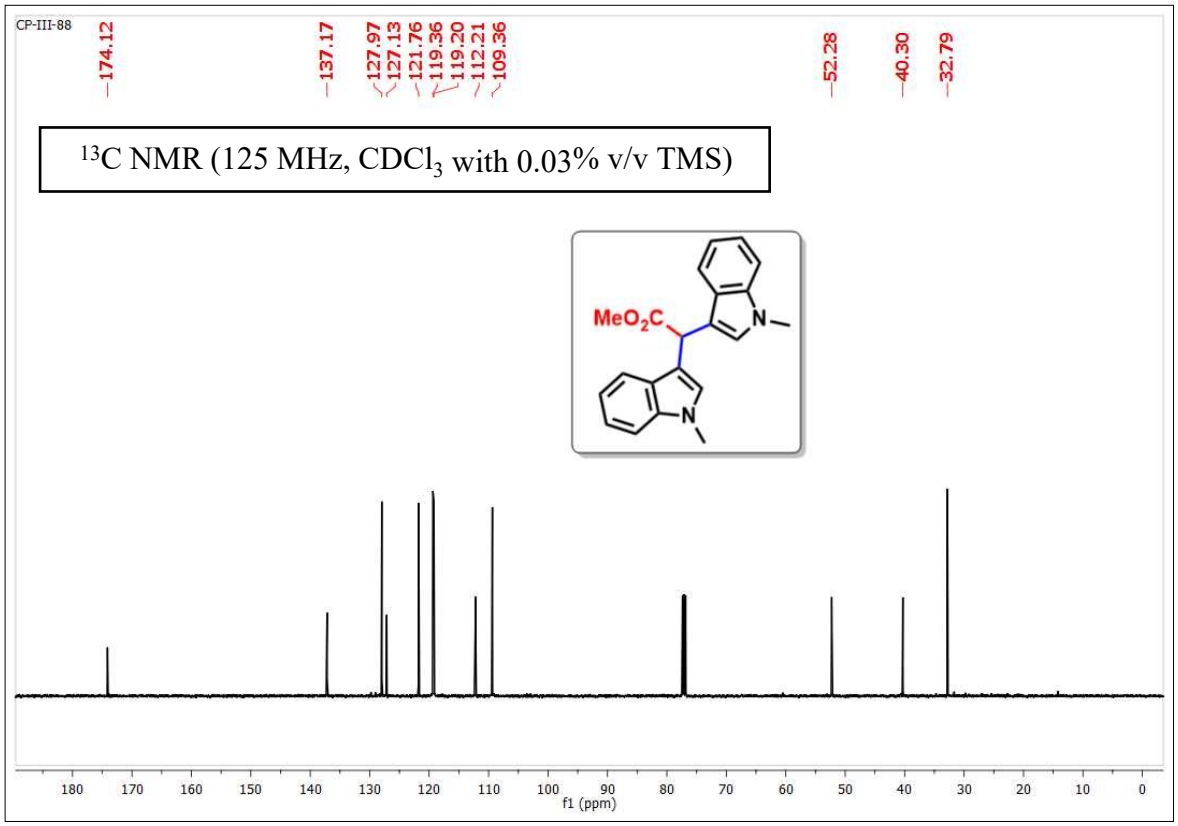

Methyl 2,2-bis(1-benzyl-1H-indol-3-yl)acetate (19)

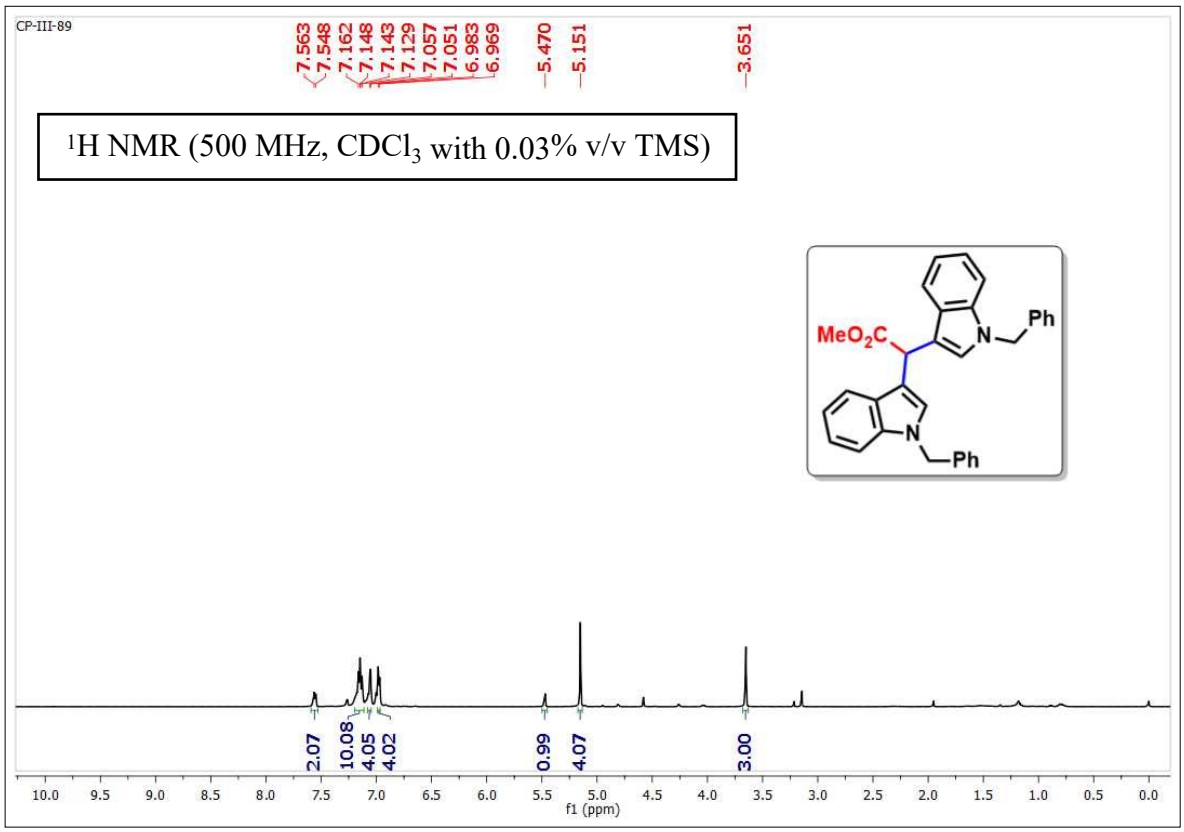

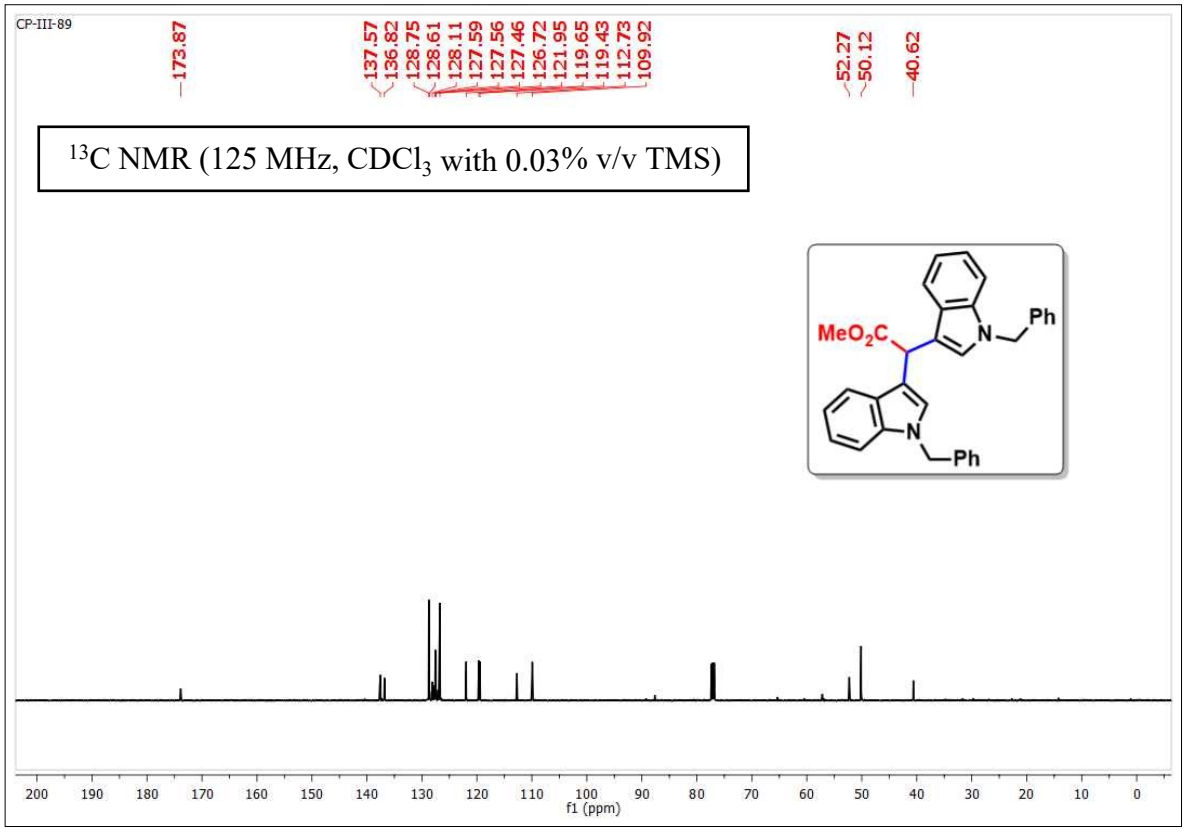

Methyl 2,2-bis(1-allyl-1H-indol-3-yl)acetate (20)

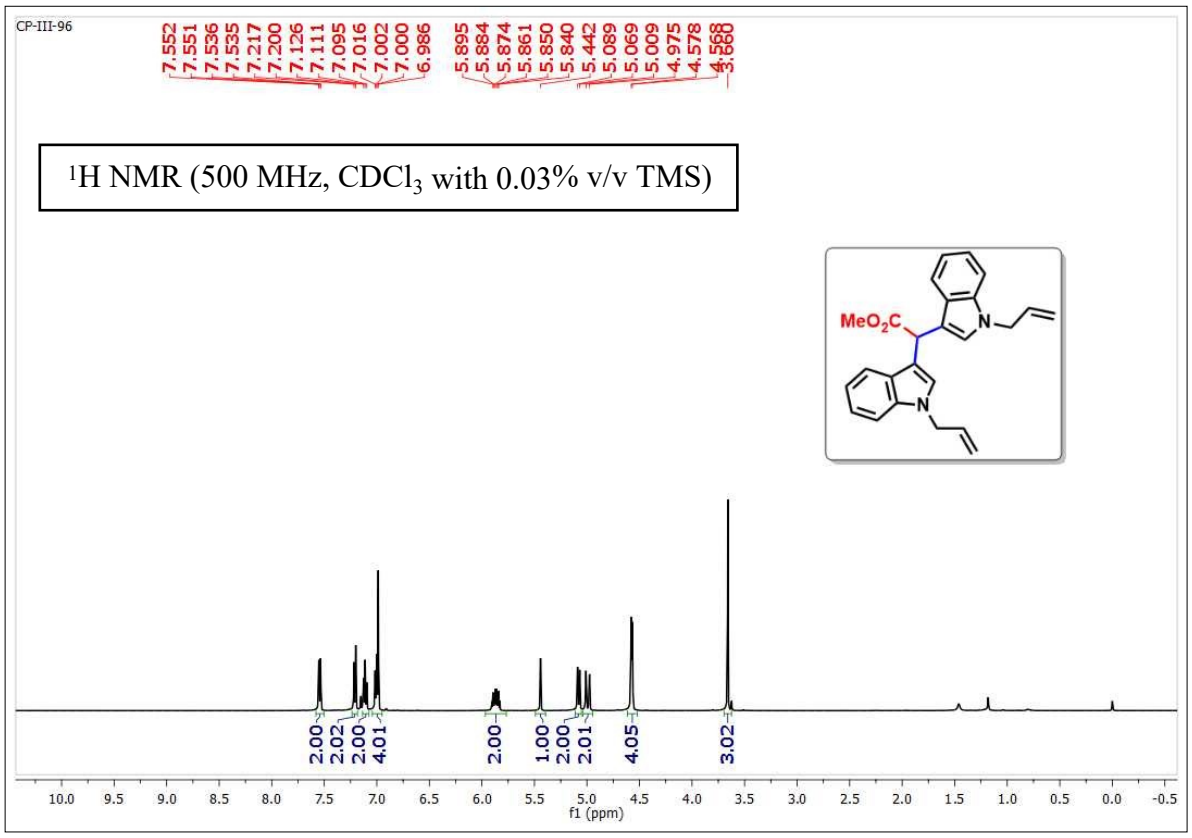

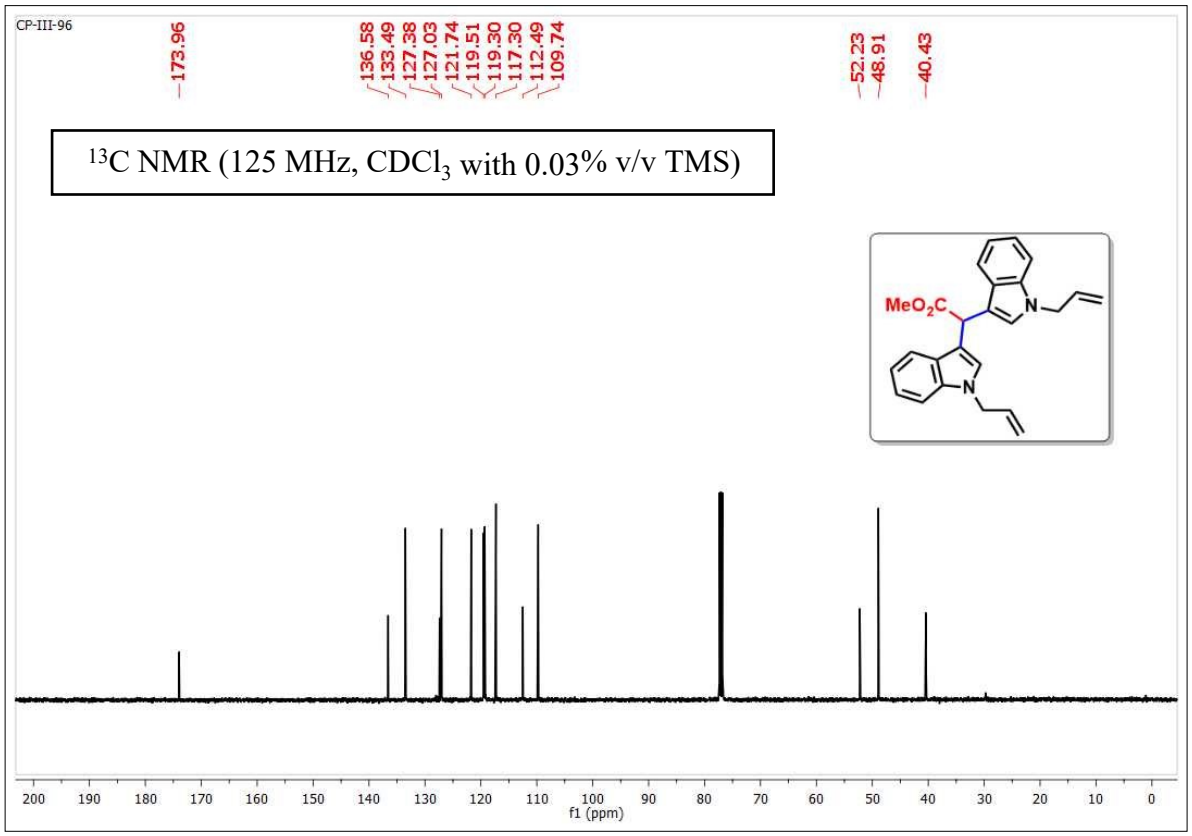

Ethyl 2,2-di(1H-indol-3-yl)acetate (21)

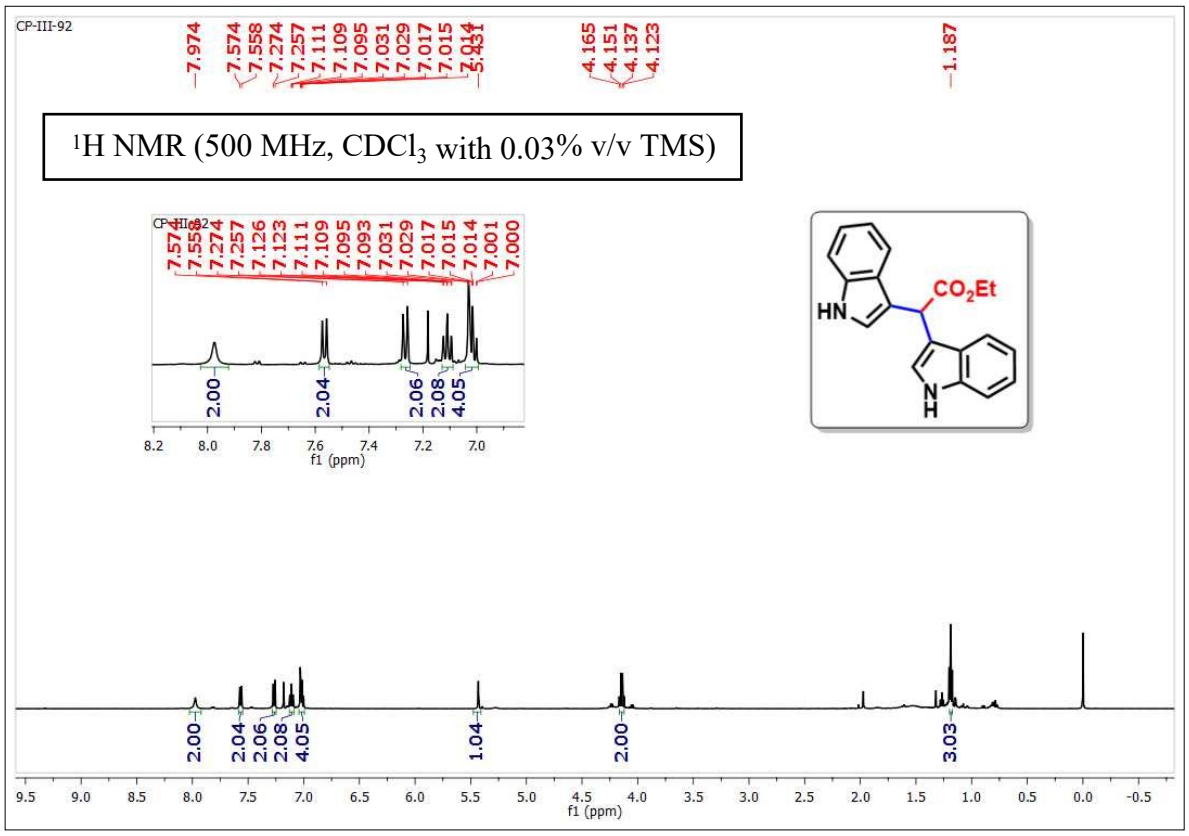

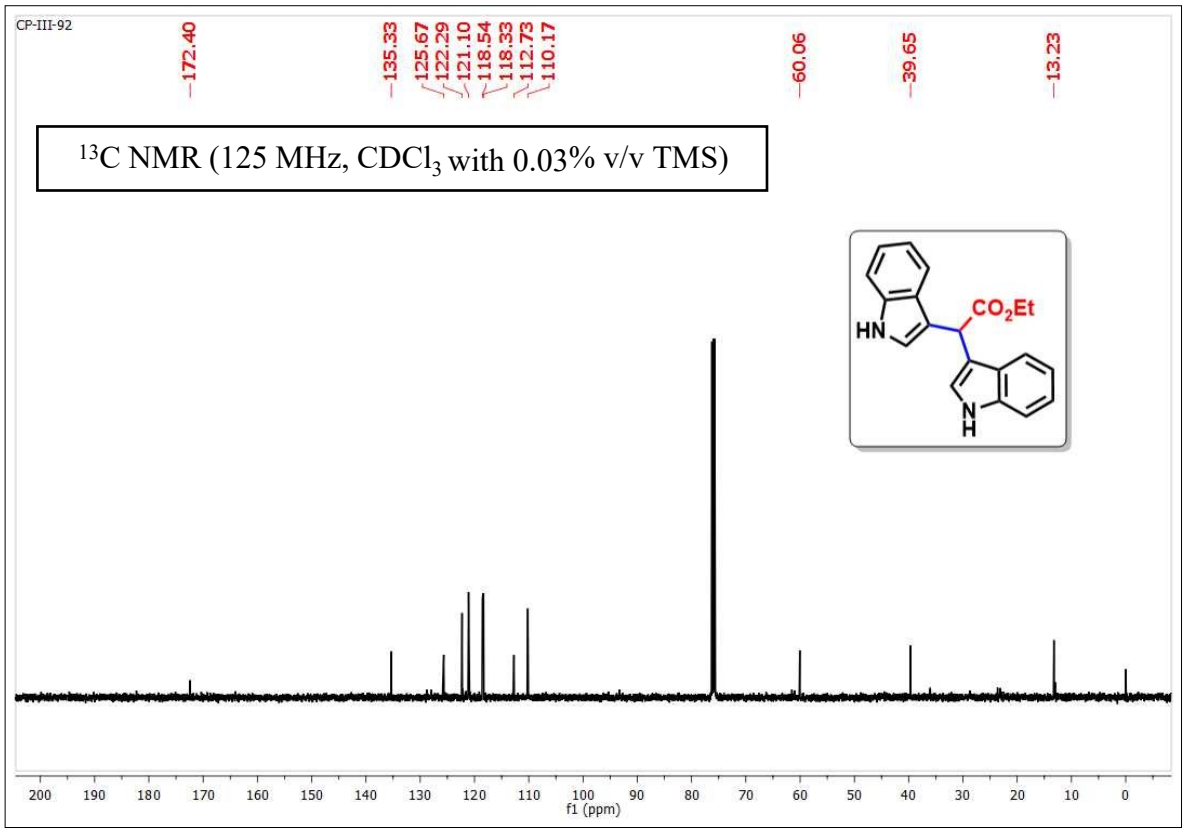

Methyl 2,2-di(1H-indol-3-yl)propanoate (22)

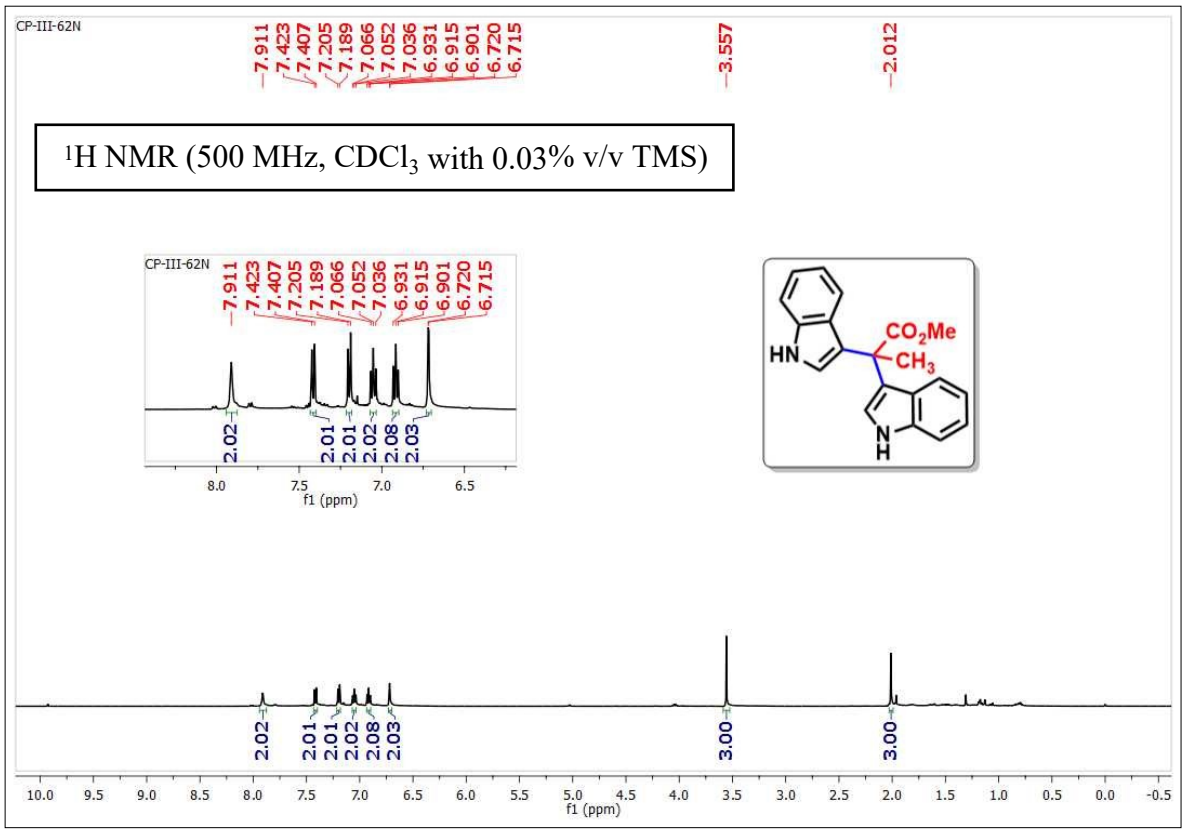

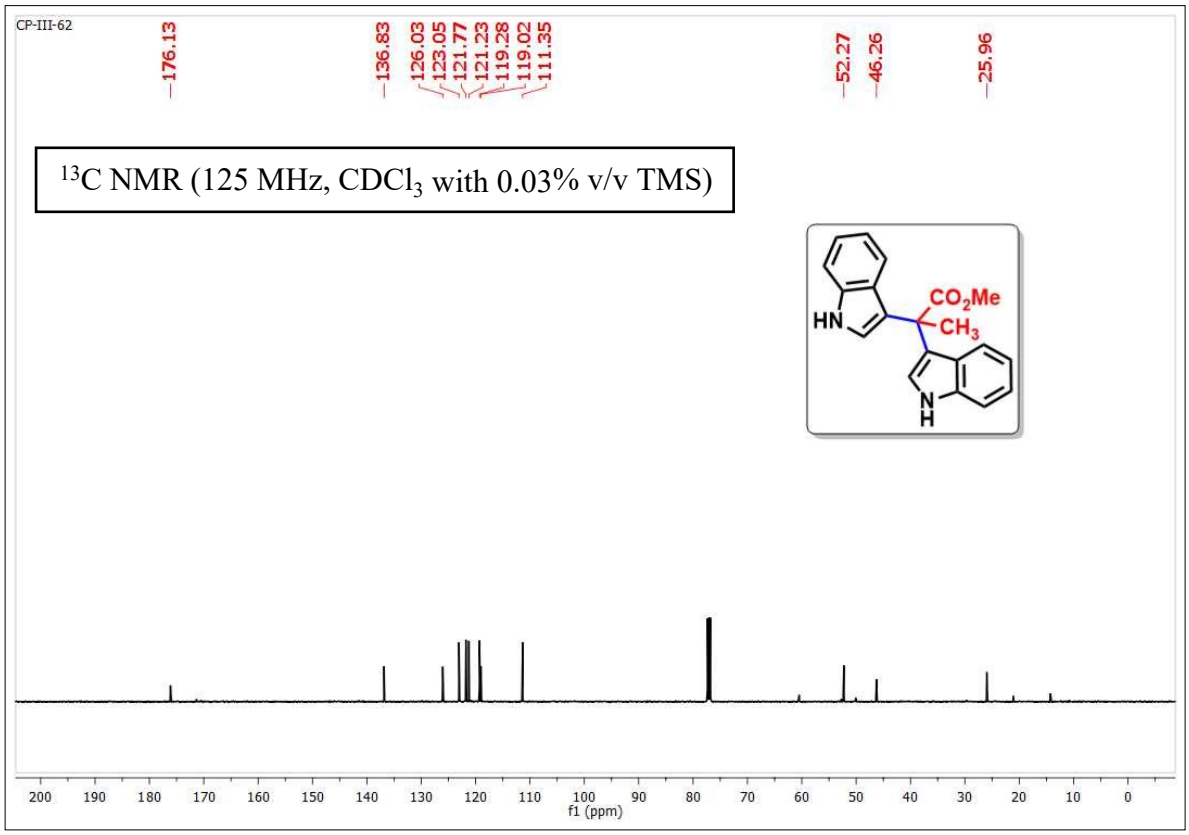

Methyl 2,2-di(1H-indol-3-yl)-2-phenylacetate (23)

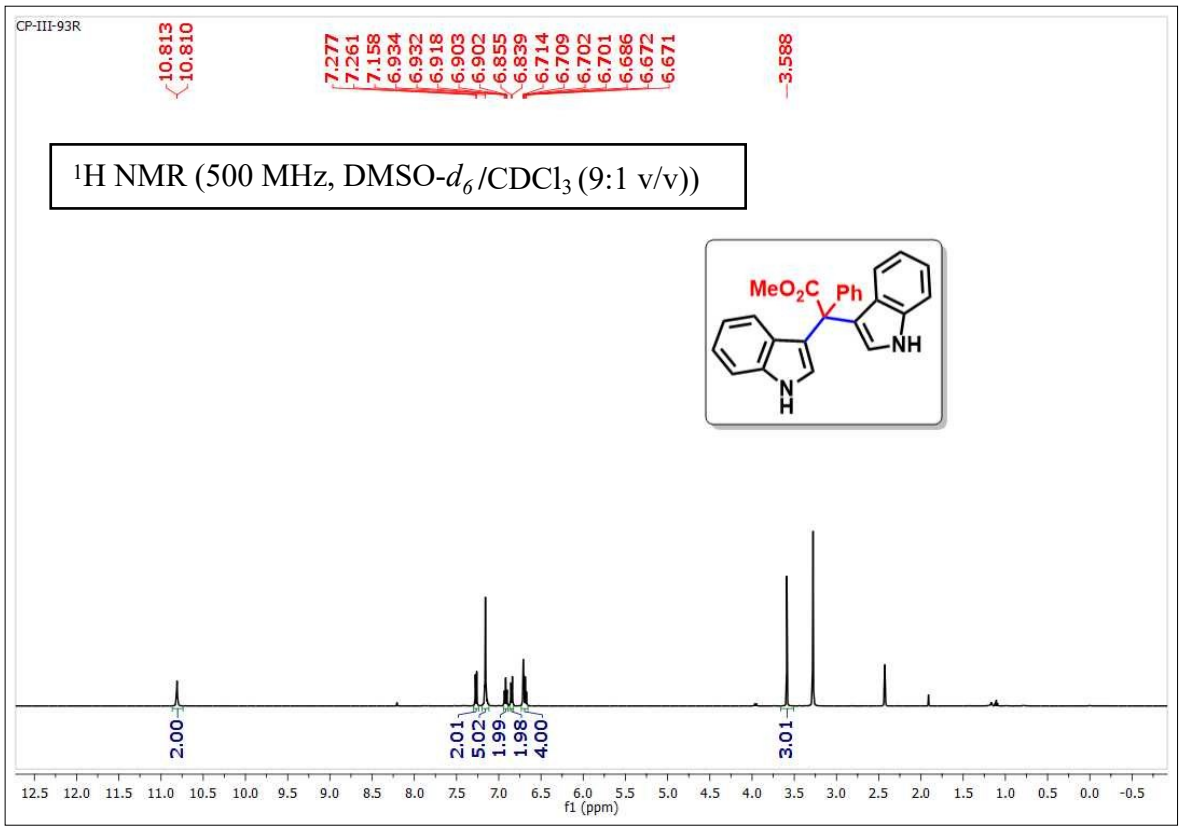

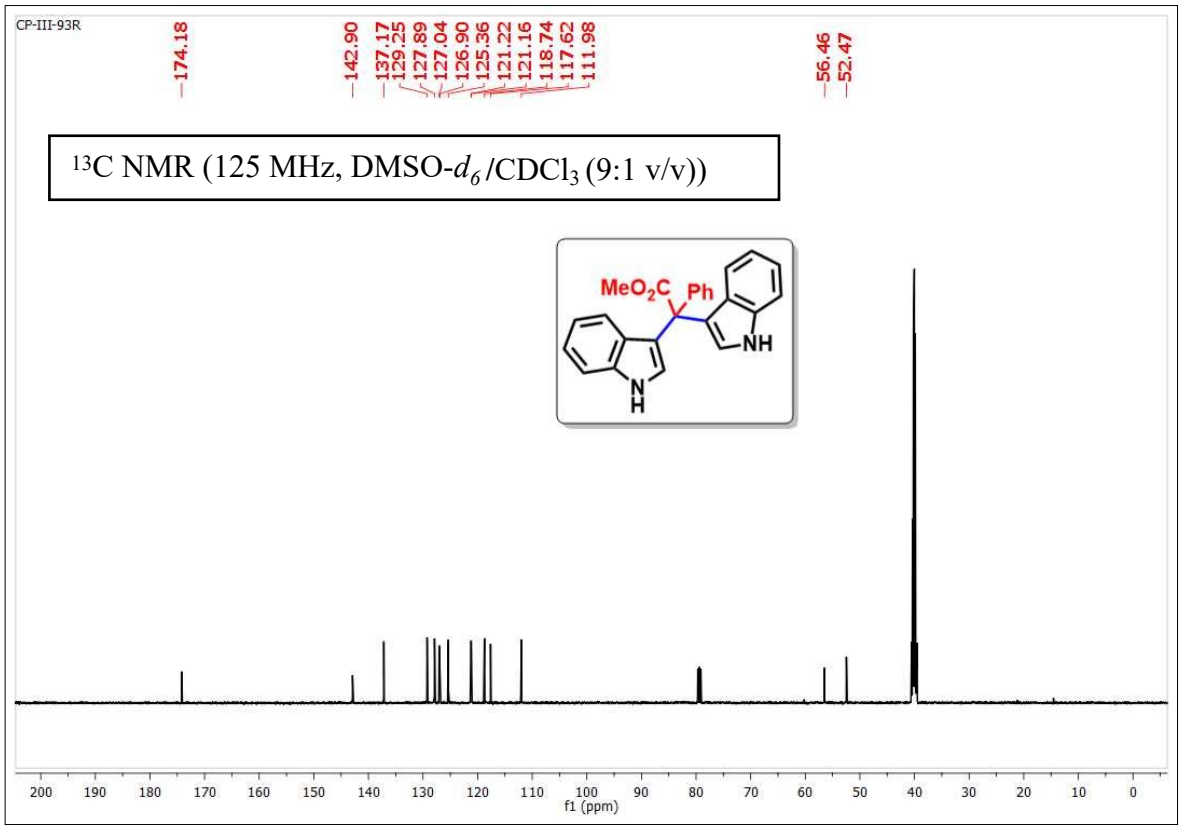

Methyl 2-(1H-indol-3-yl)-2,2-bis(1-methyl-1H-indol-3-yl)acetate (24)

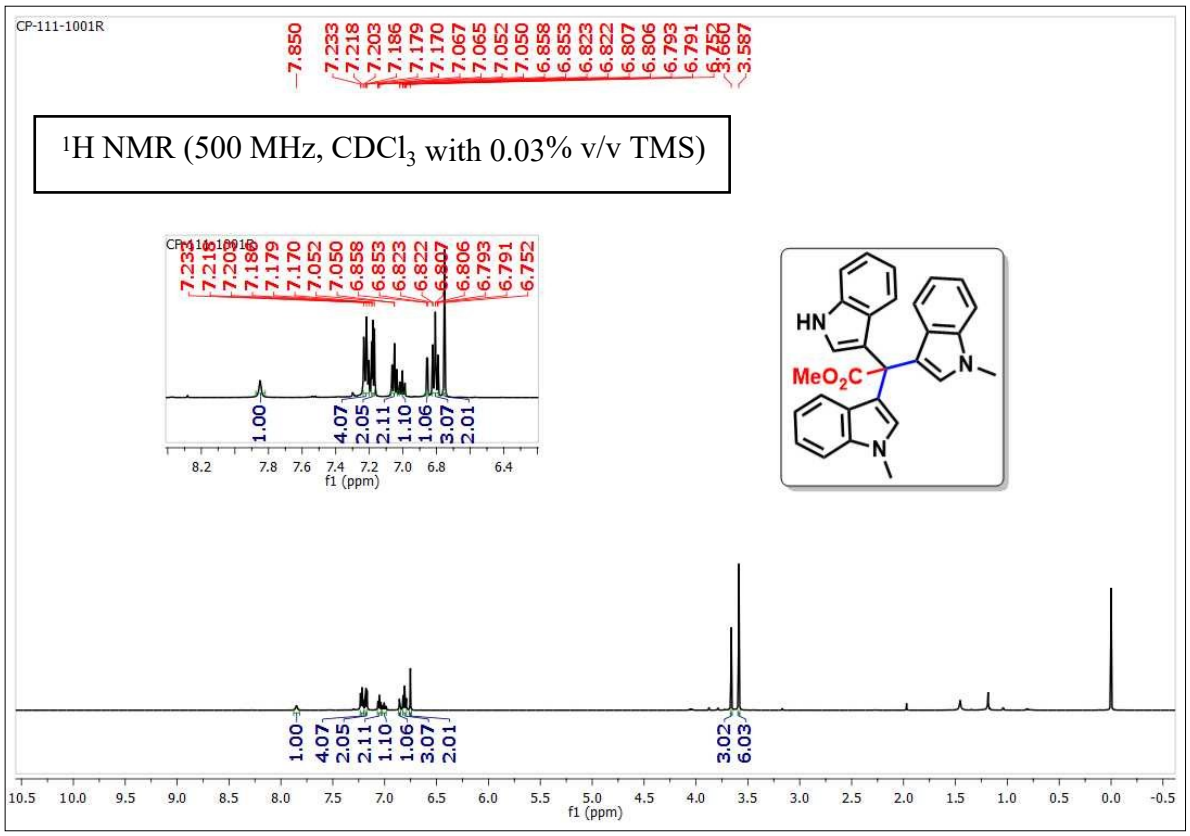

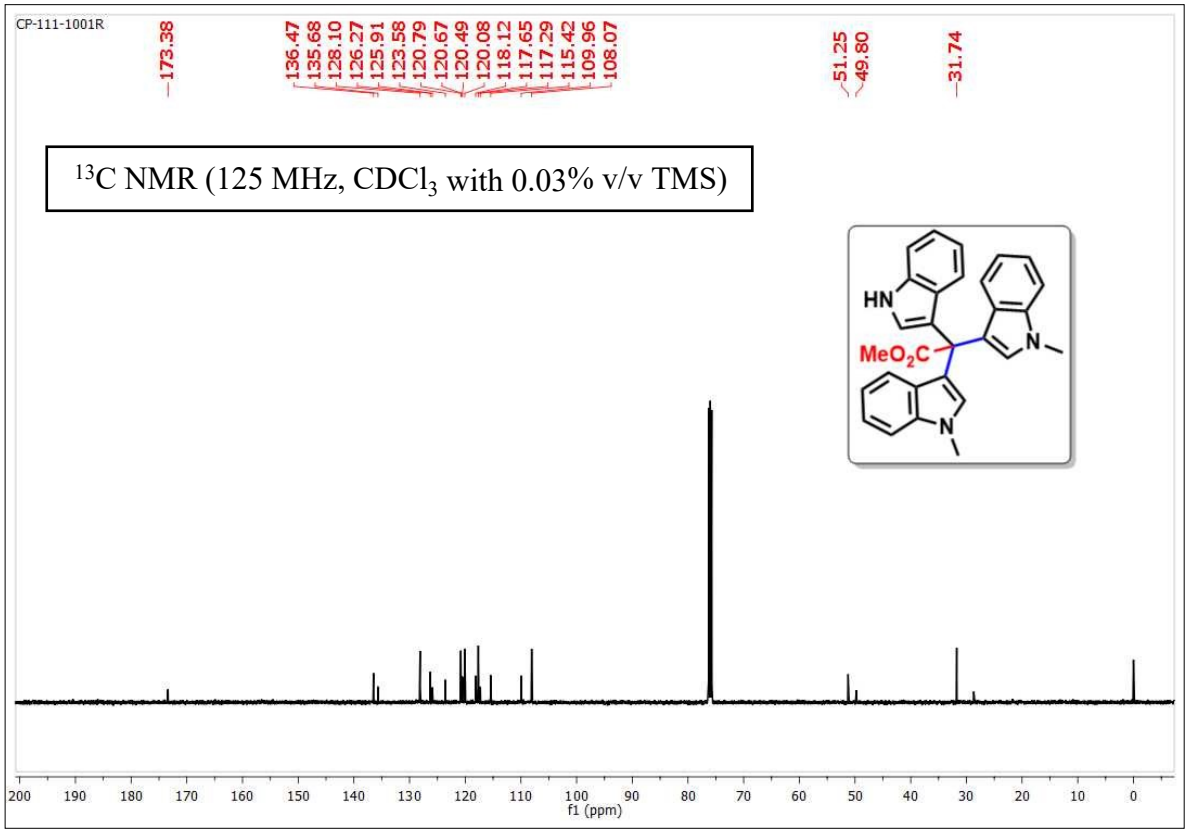

Methyl 2,2,2-tris(1-methyl-1H-indol-3-yl)acetate (25)

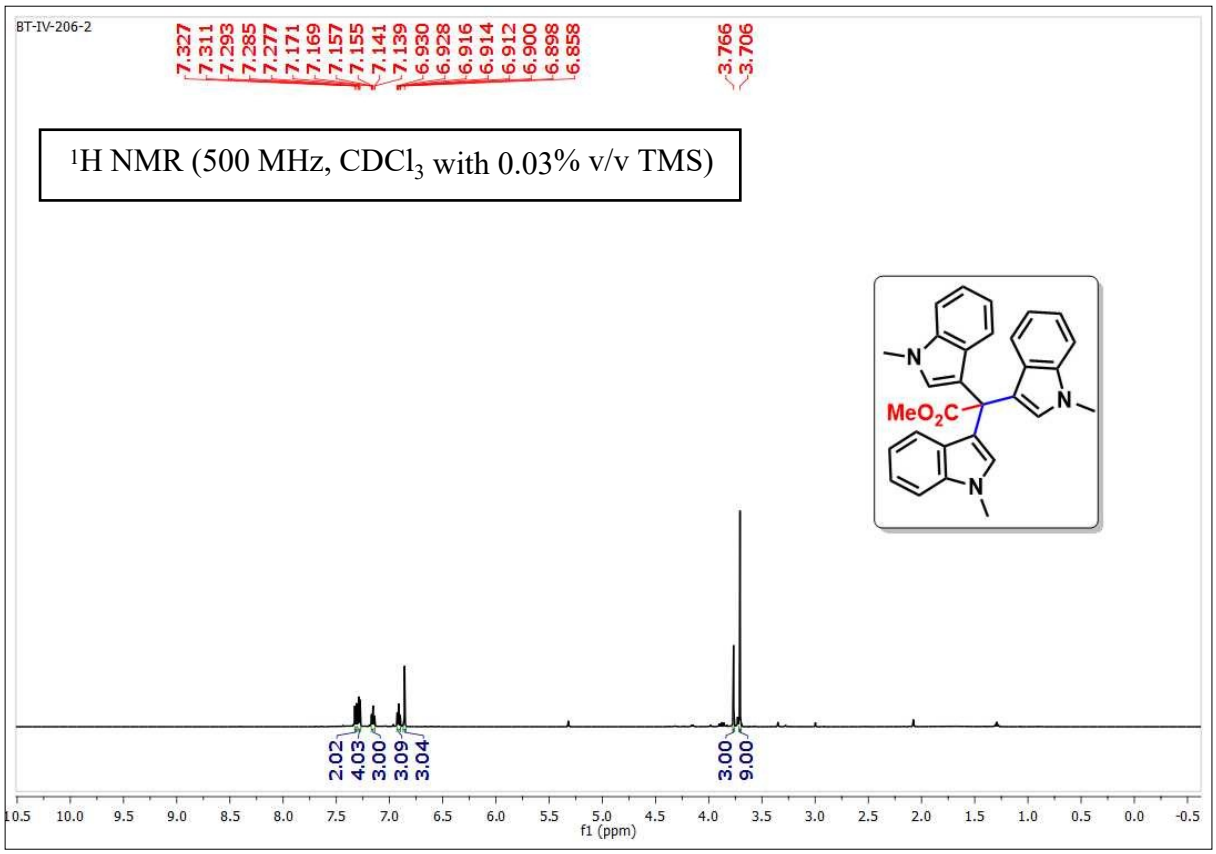

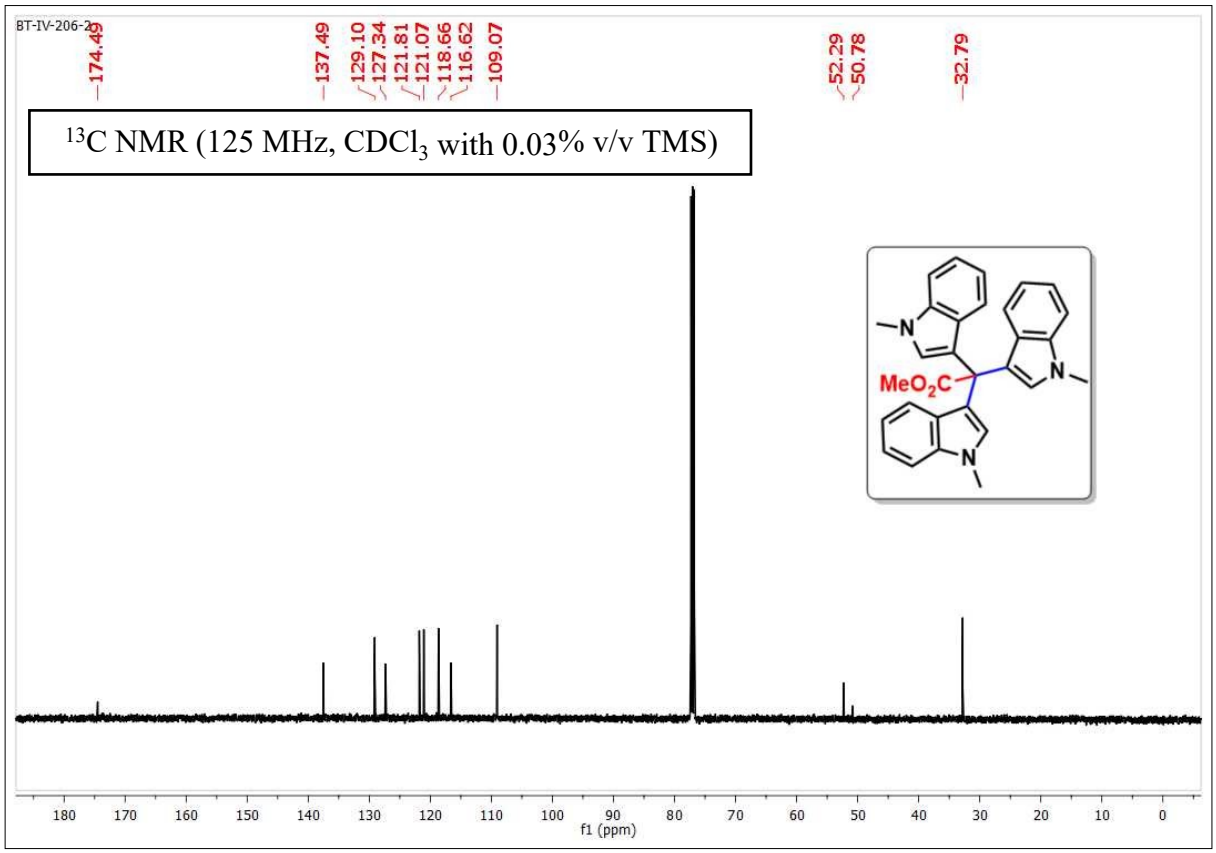

Methyl 2,2-bis(5-methyl-1H-indol-3-yl)-2-(naphthalen-2-yl)acetate (26)

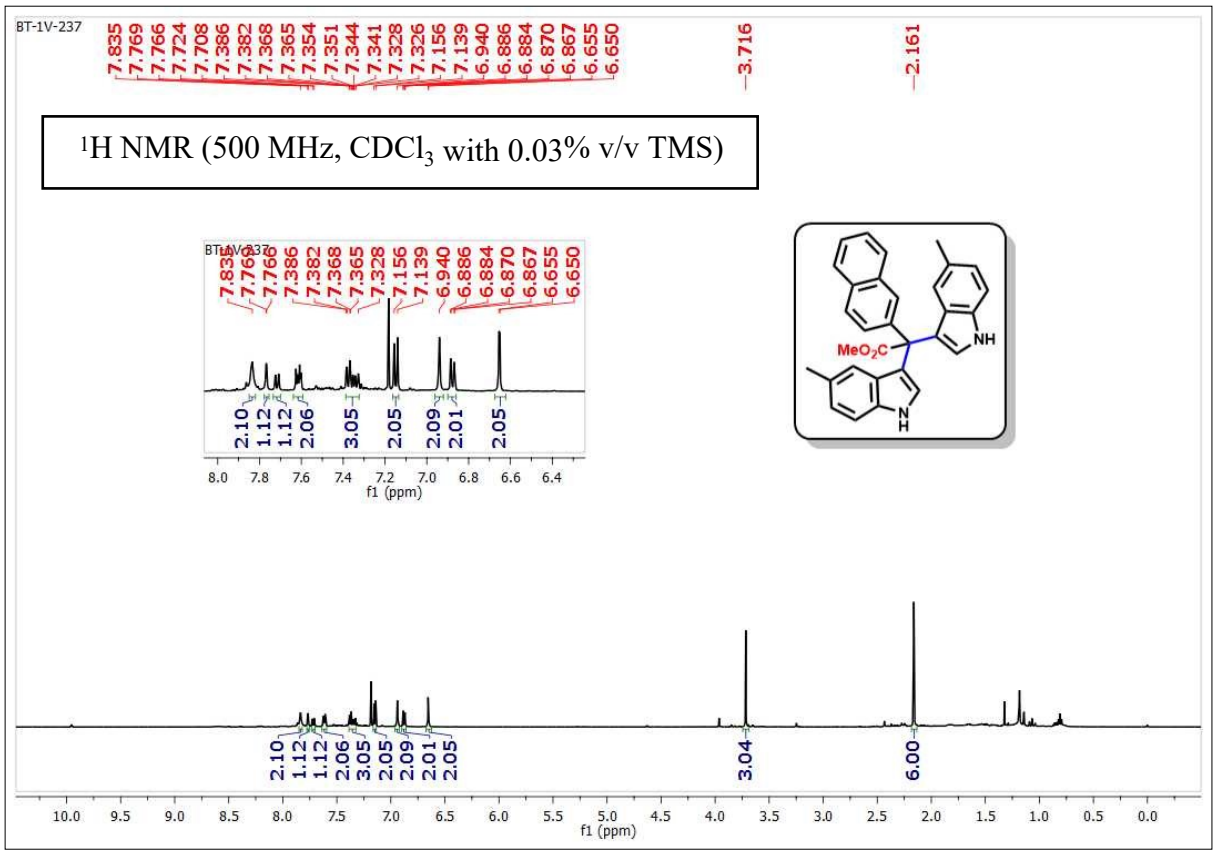

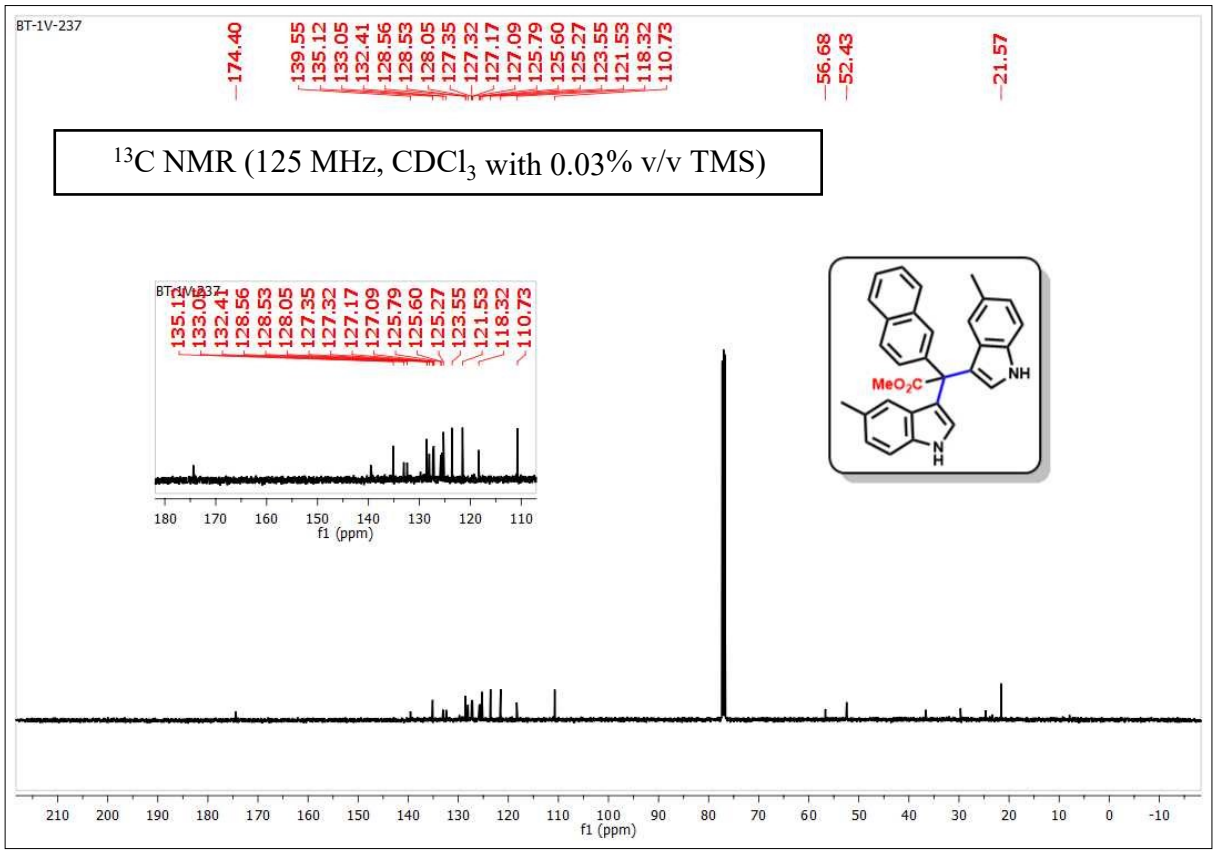

Methyl 2,2-di(1H-indol-3-yl)-2-(naphthalen-2-yl)acetate (27)

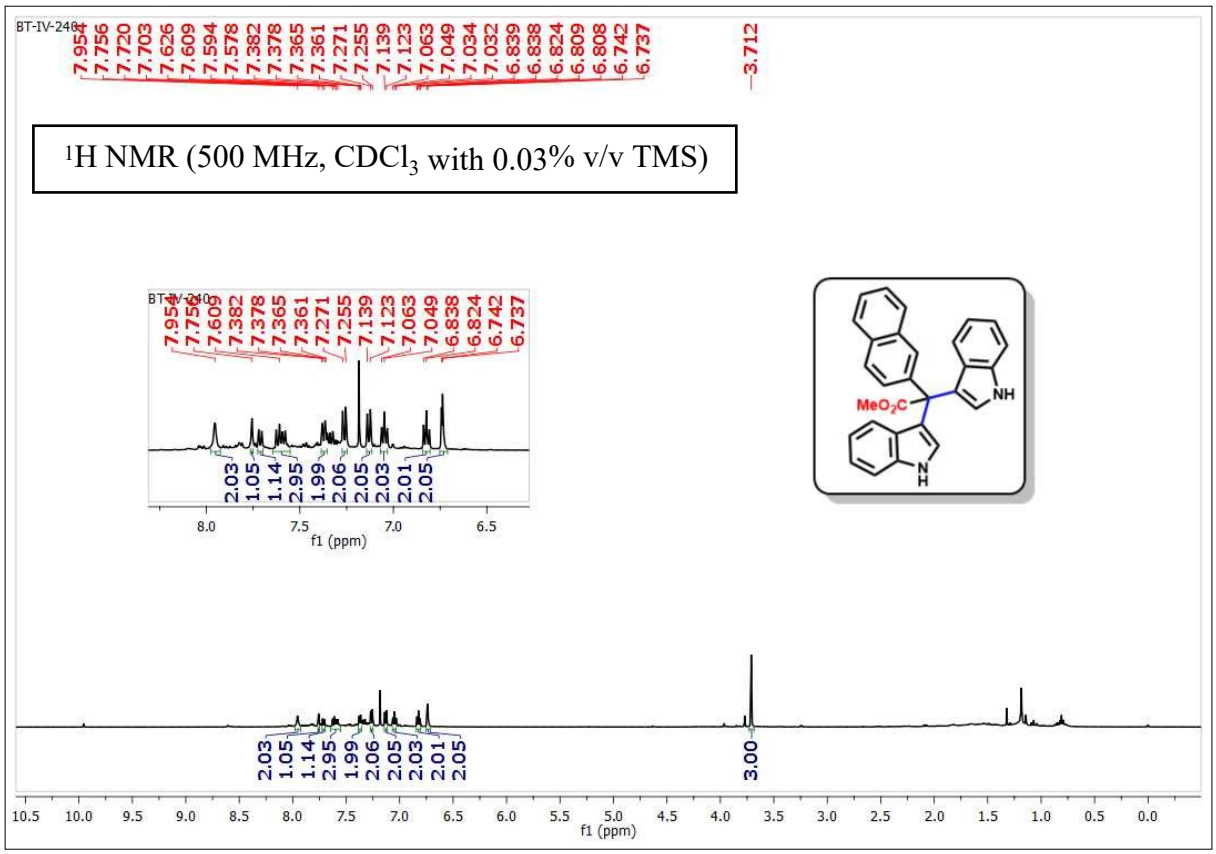

Methyl 2,2-bis(5-chloro-1H-indol-3-yl)-2-(naphthalen-2-yl)acetate (28)

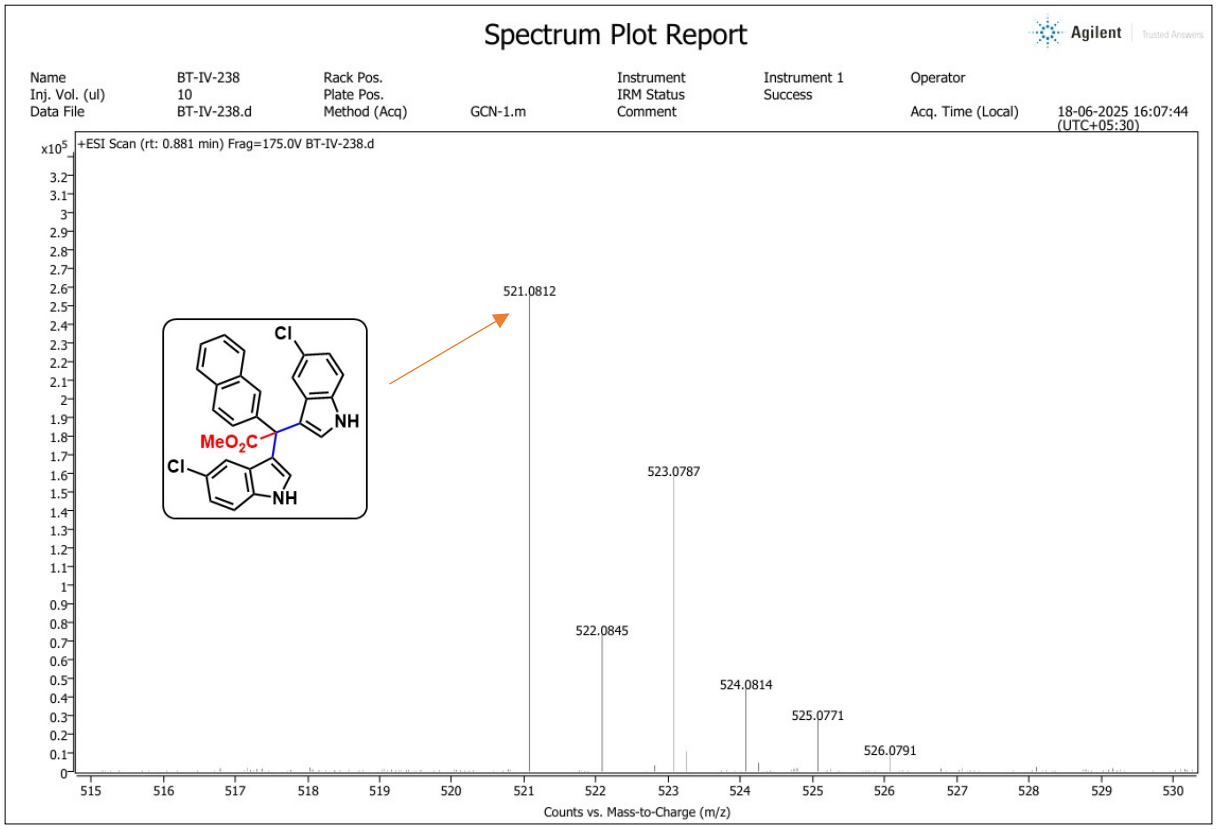

(1-methyl-1H-indol-3-yl)(naphthalen-2-yl)methanone (29)

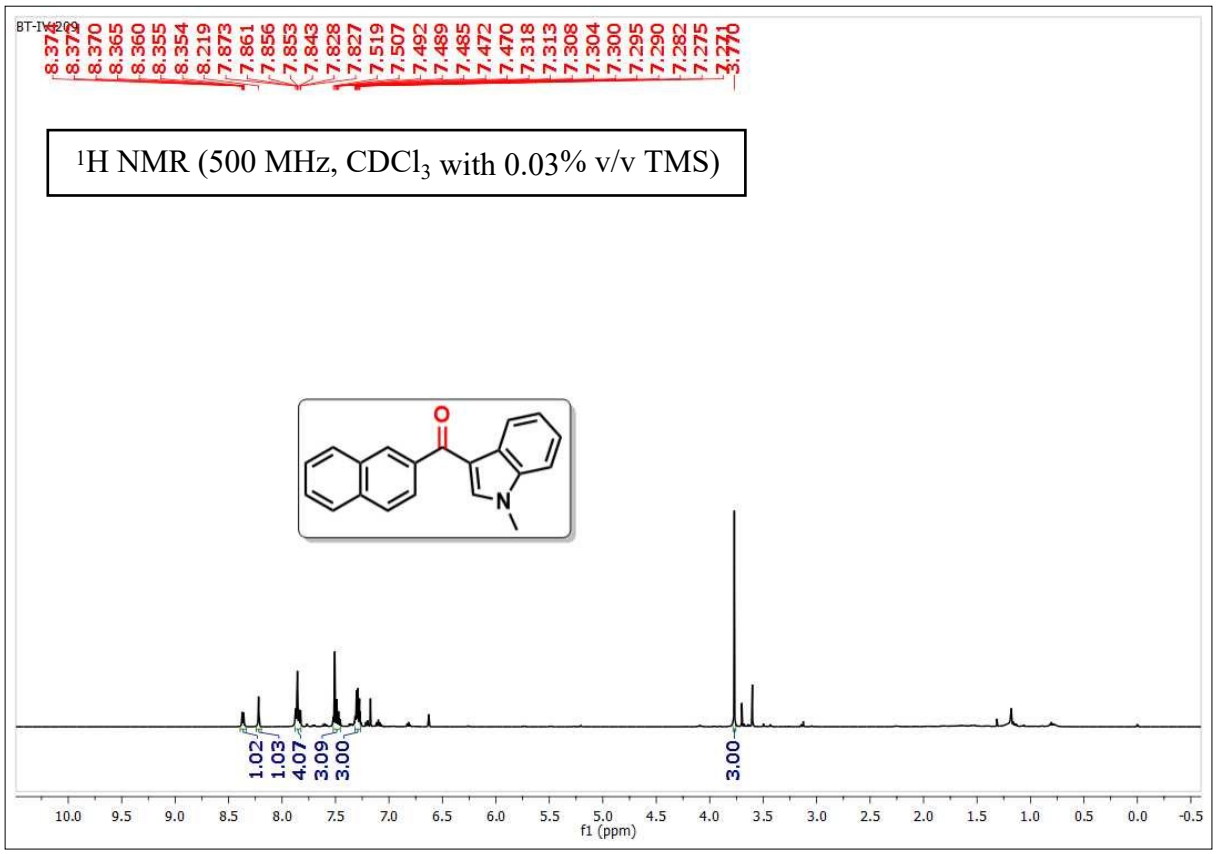

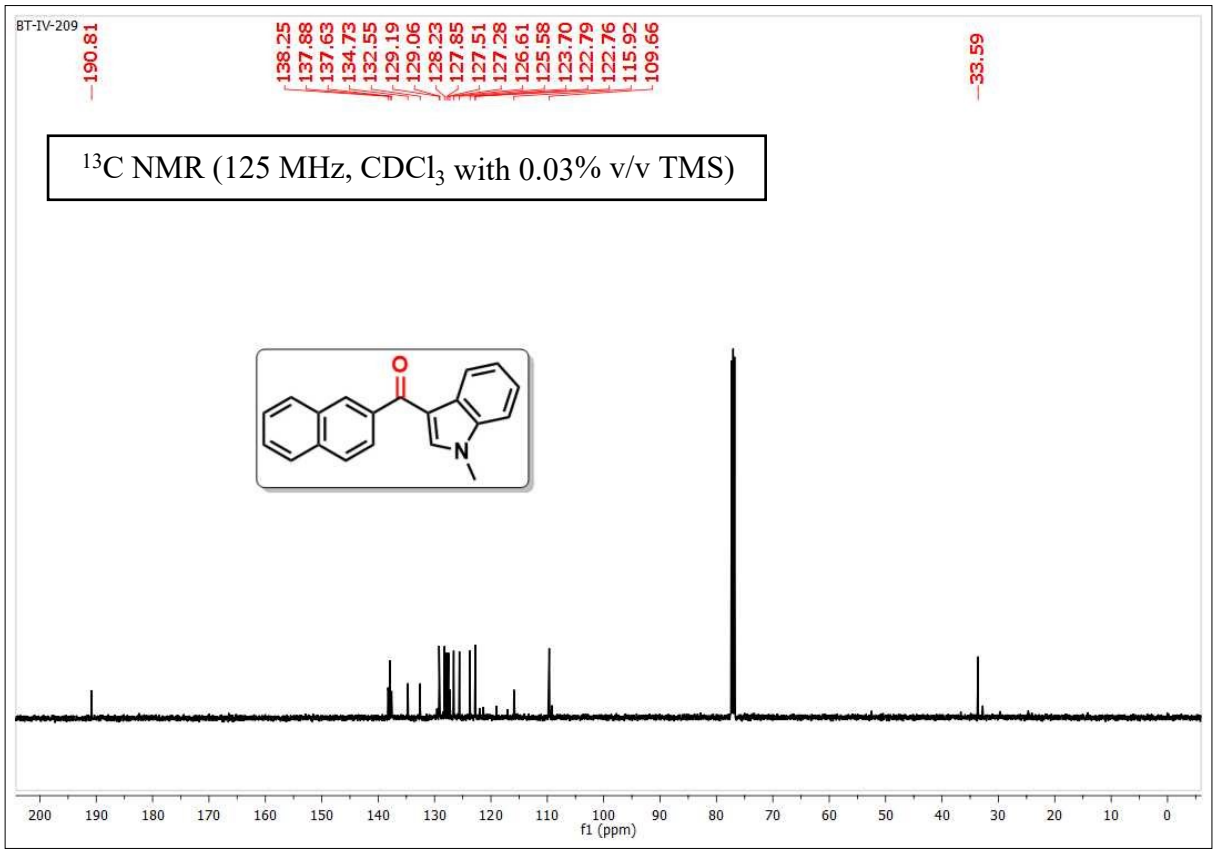

Methyl 2-(1H-indol-3-yl)-2-(1-methyl-1H-indol-3-yl)acetate (30)

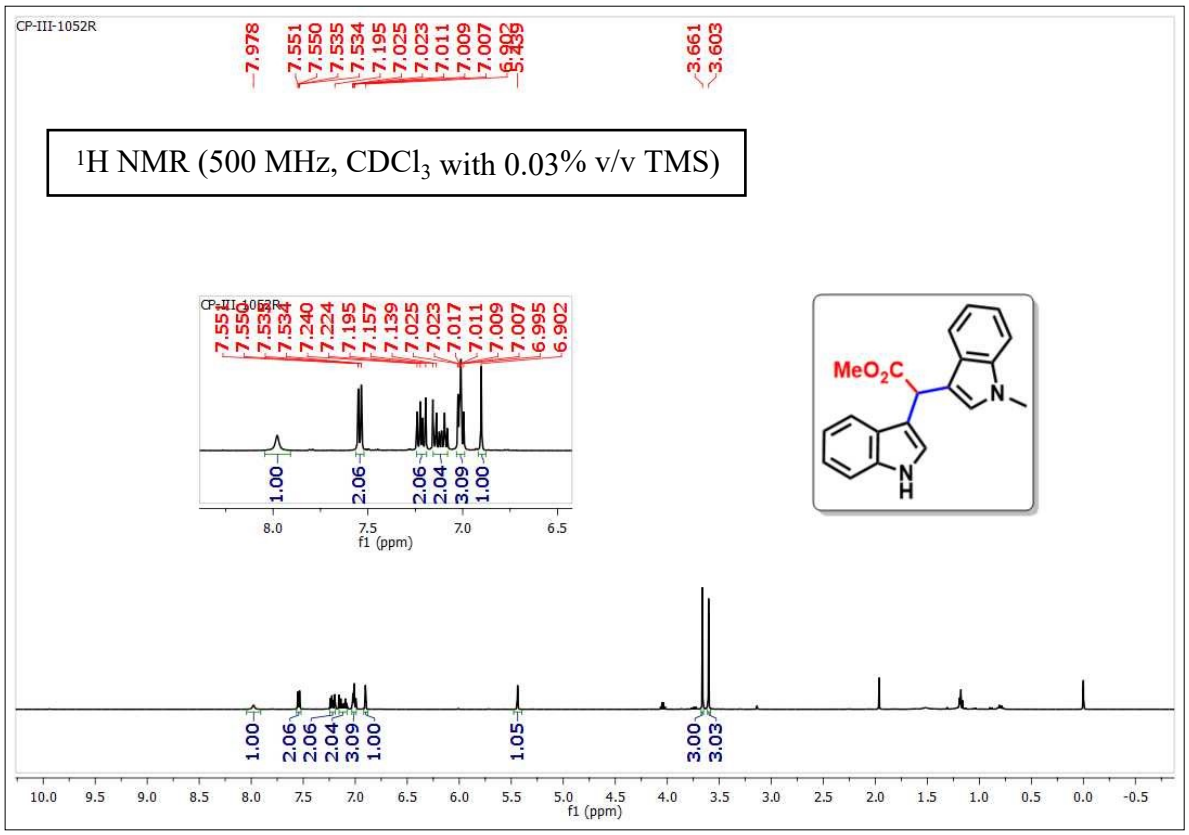

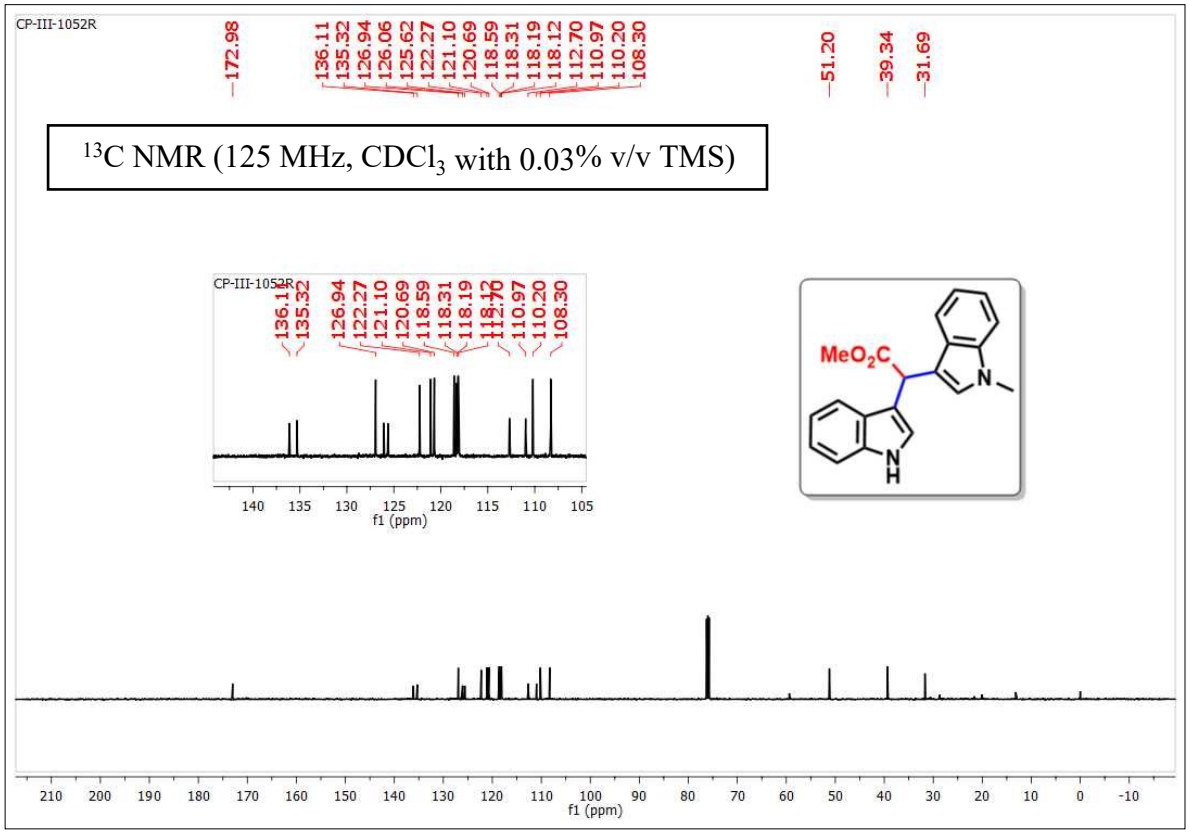

Methyl 2-(1H-indol-3-yl)-2-(phenylamino)acetate (31)

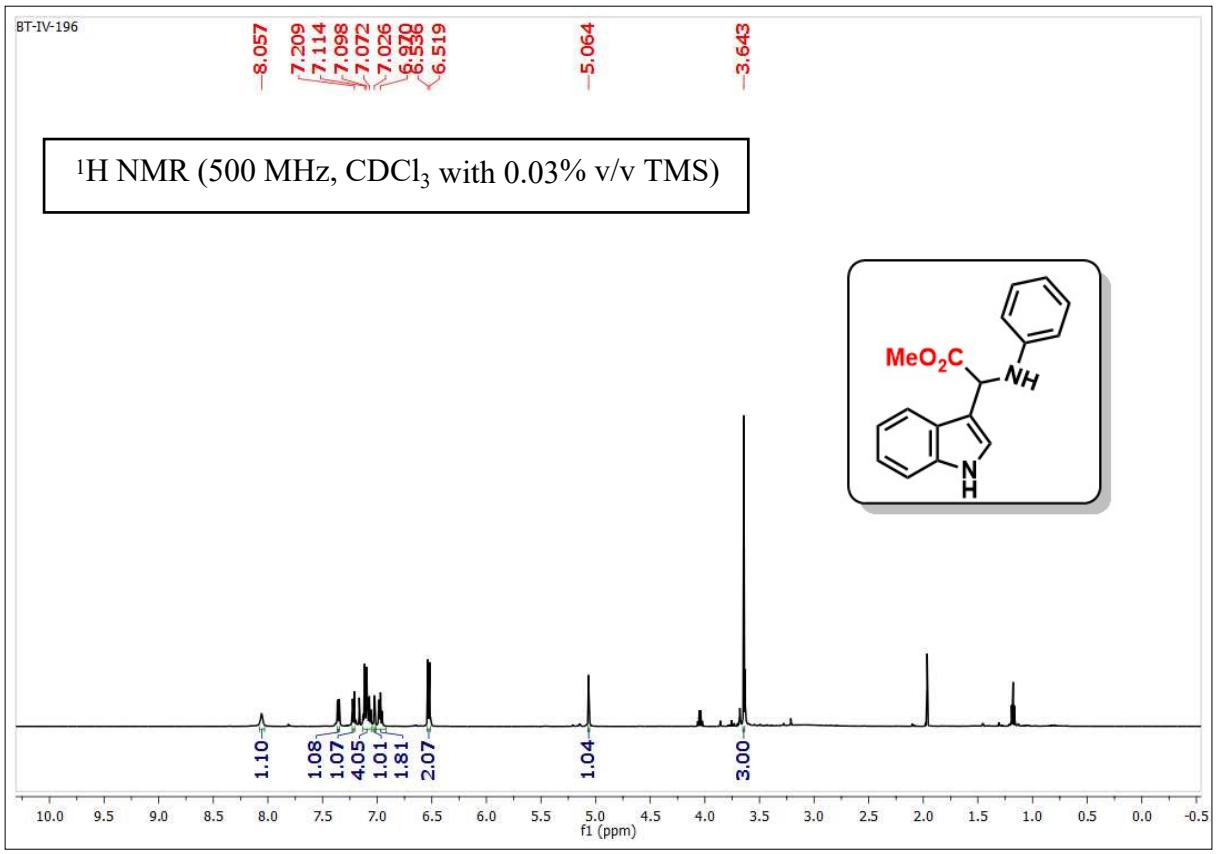

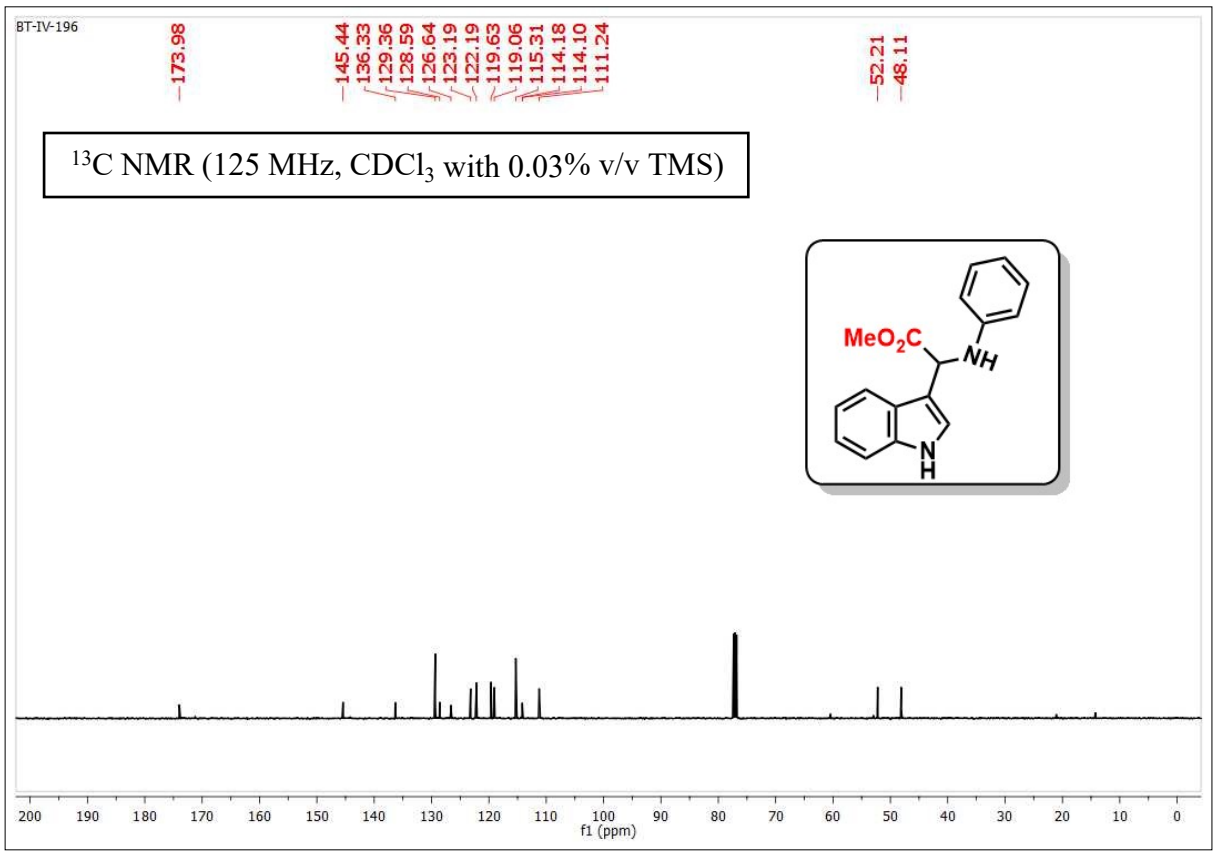

Methyl (E)-2-(phenylimino)acetate (32)

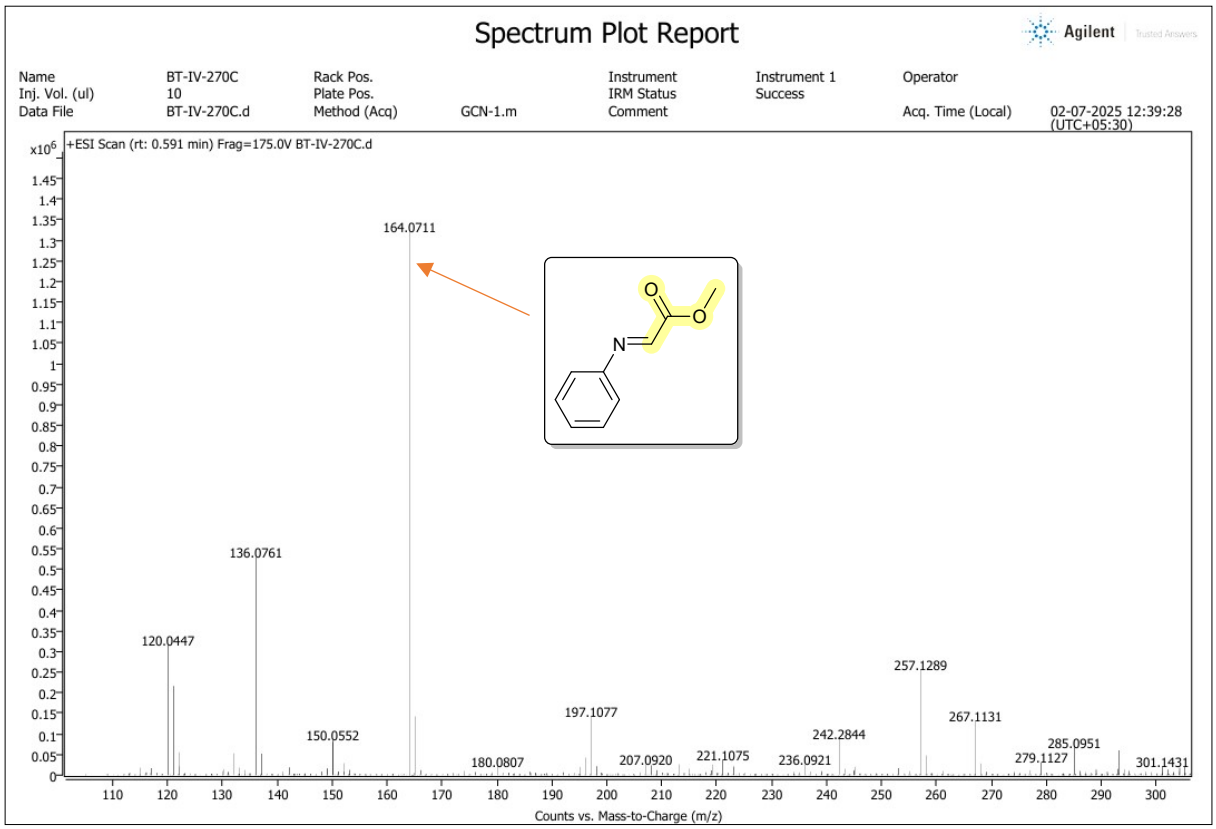

Methyl (E)-2-(3H-indol-3-ylidene)acetate (33)

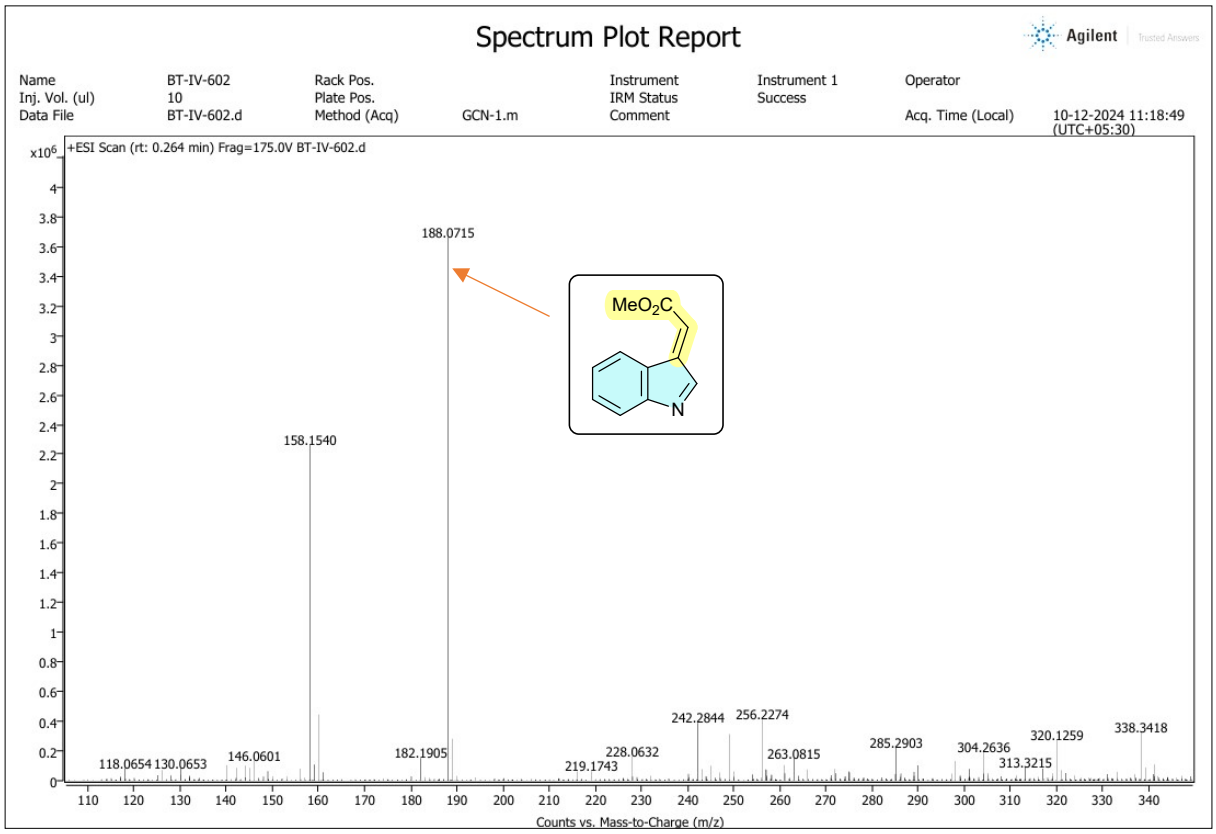

Methyl (E)-2-(3H-indol-3-ylidene)acetate (33)

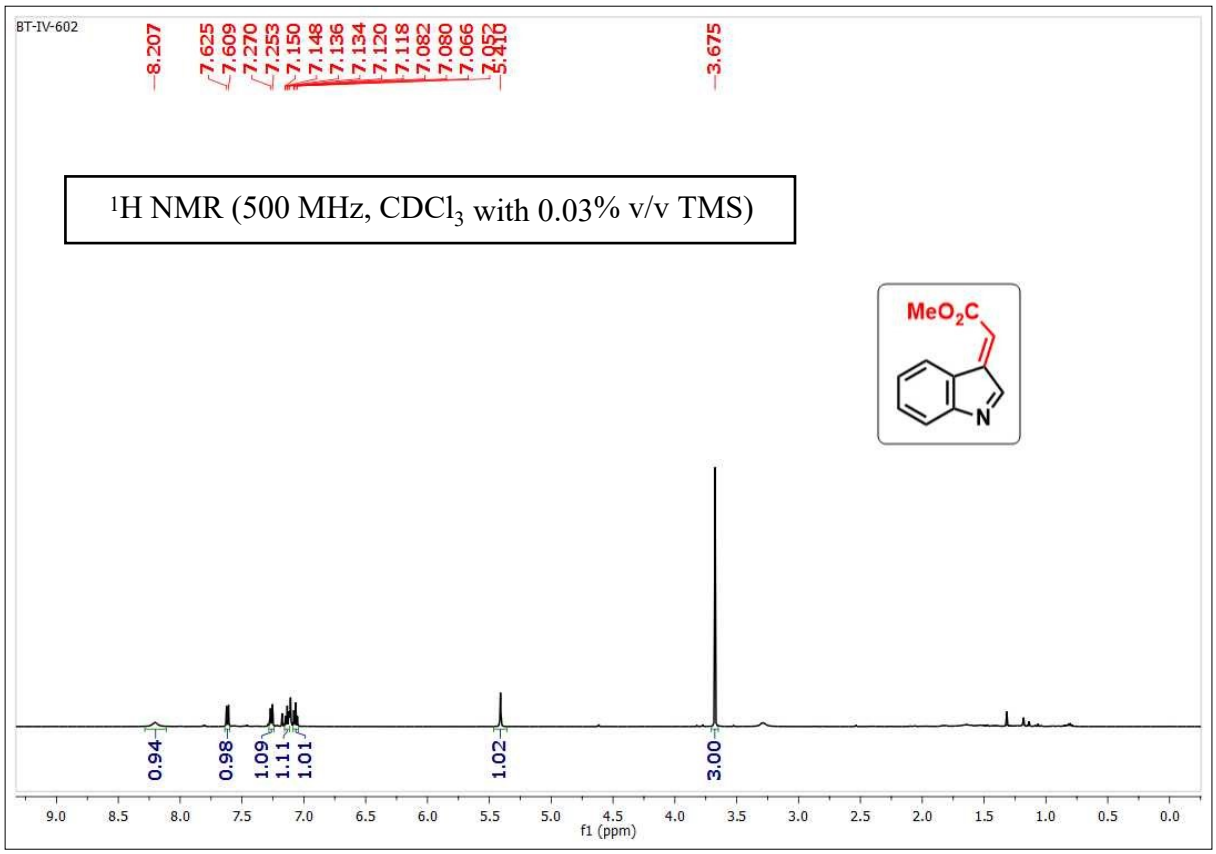

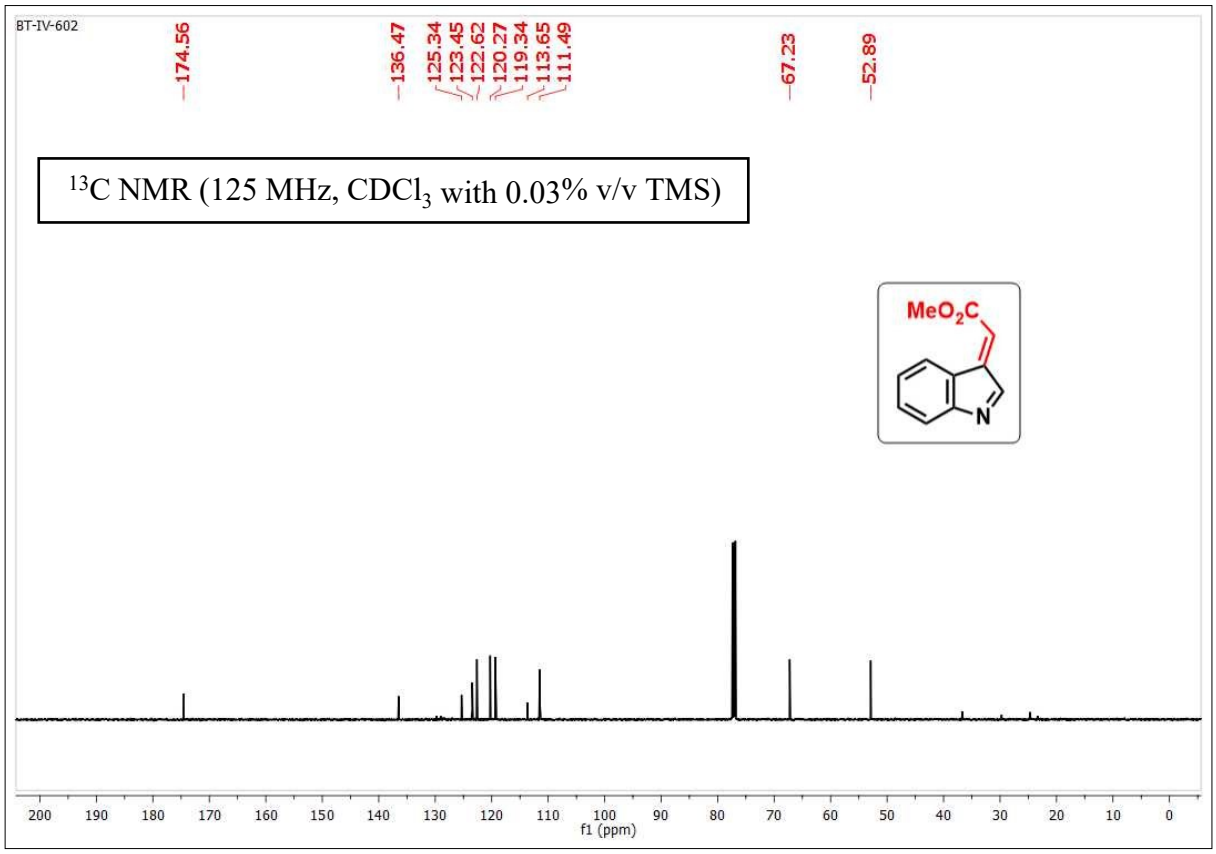

Methyl 2-oxo-2-phenylacetate (34)

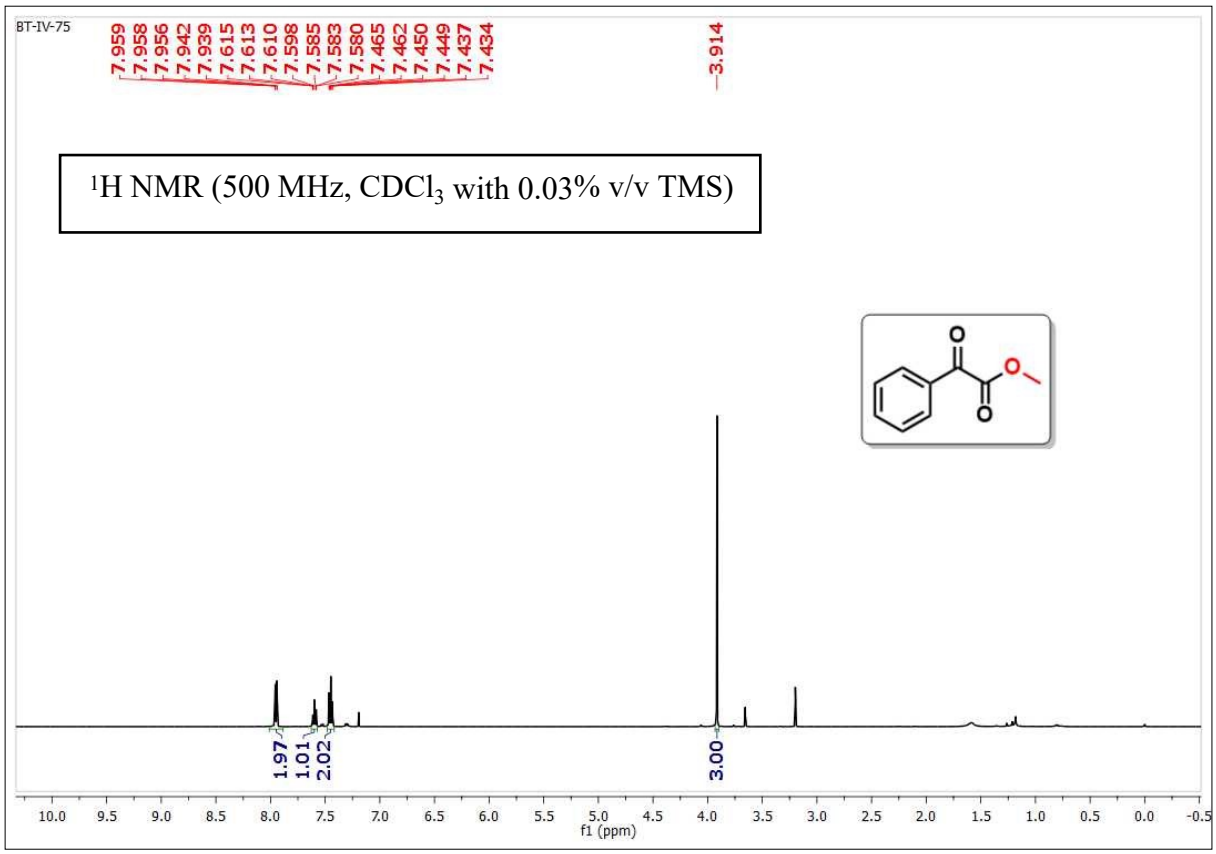

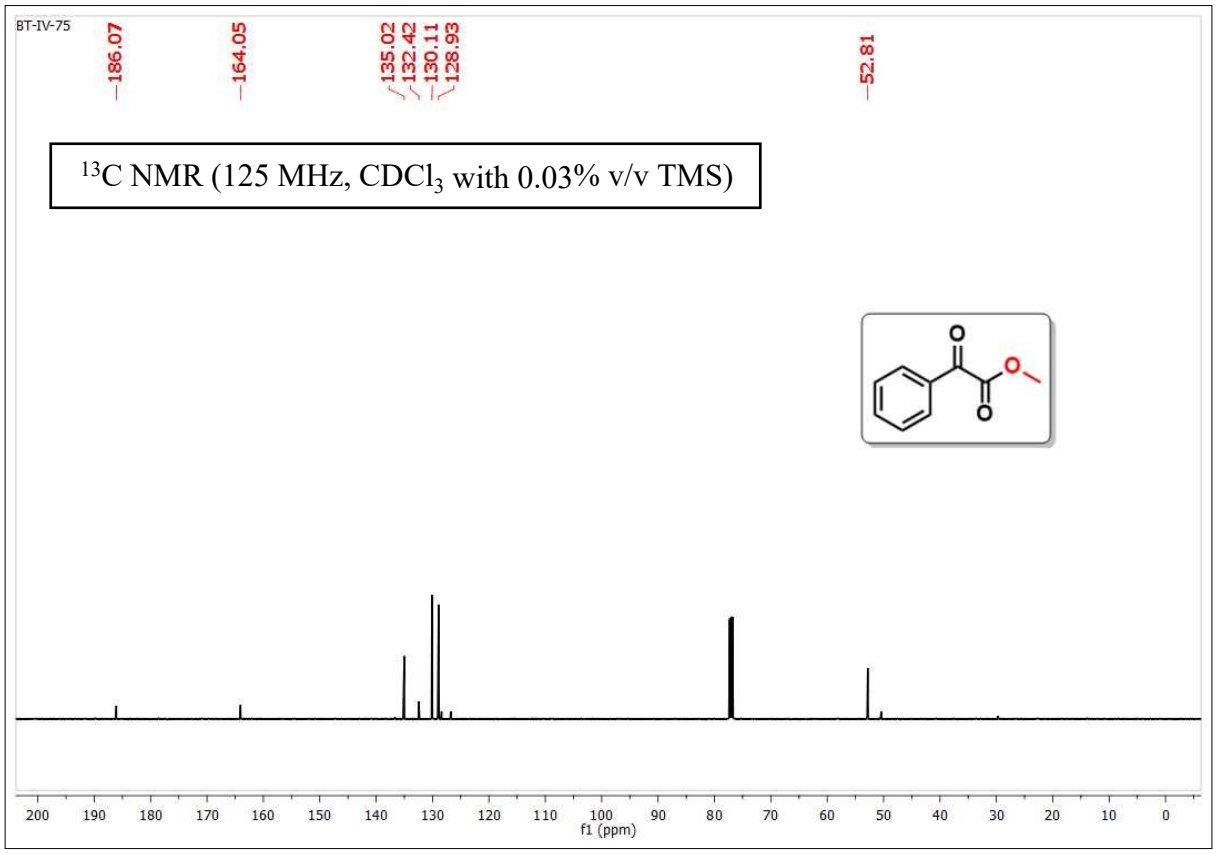

Methyl 2-(4-methoxyphenyl)-2-oxoacetate (35)

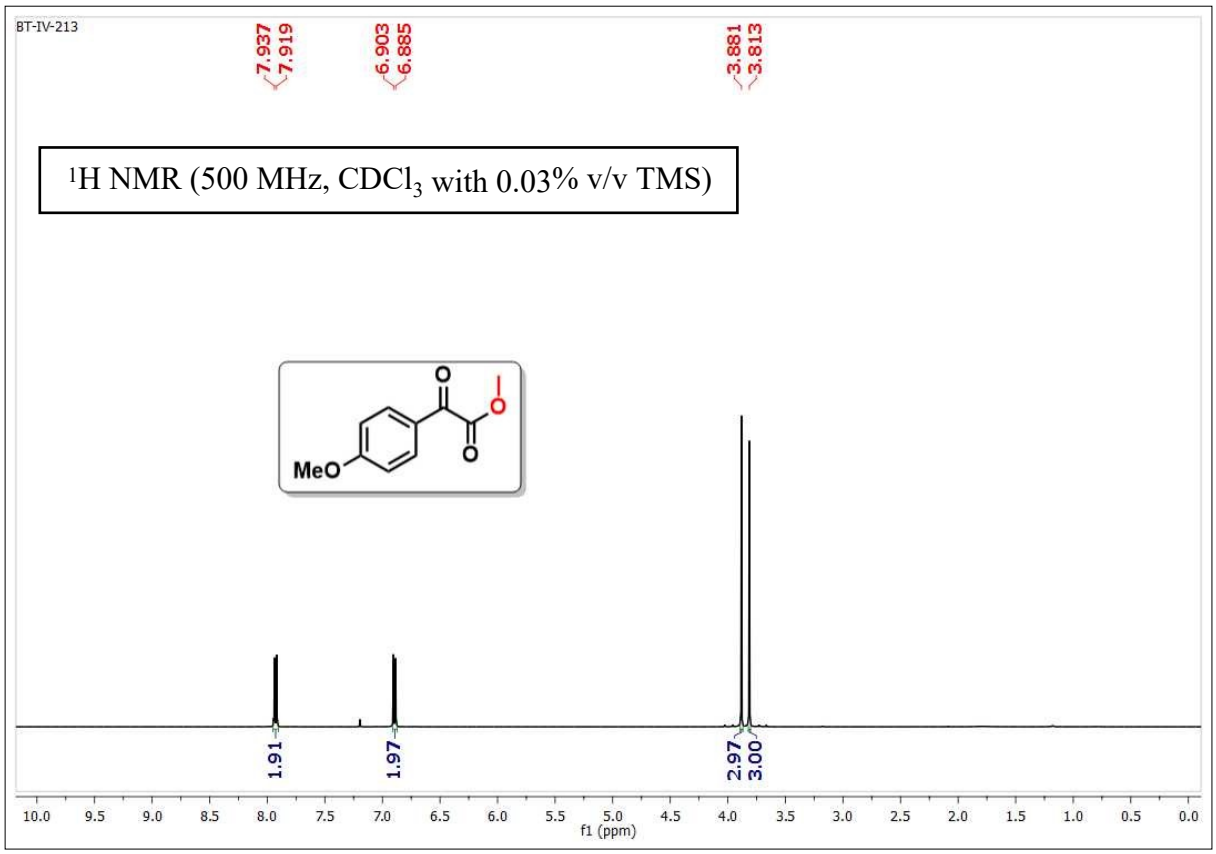

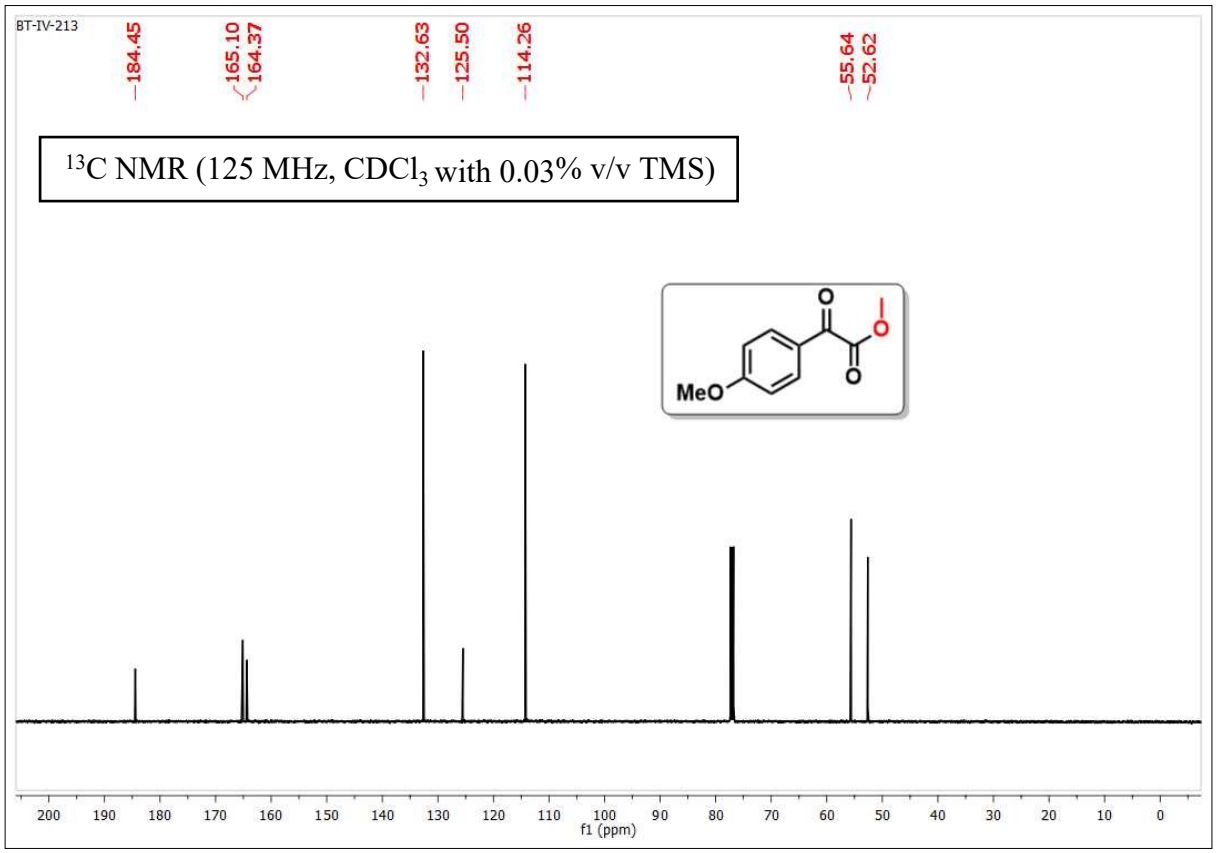

Methyl 2-oxo-2-(p-tolyl)acetate (36)

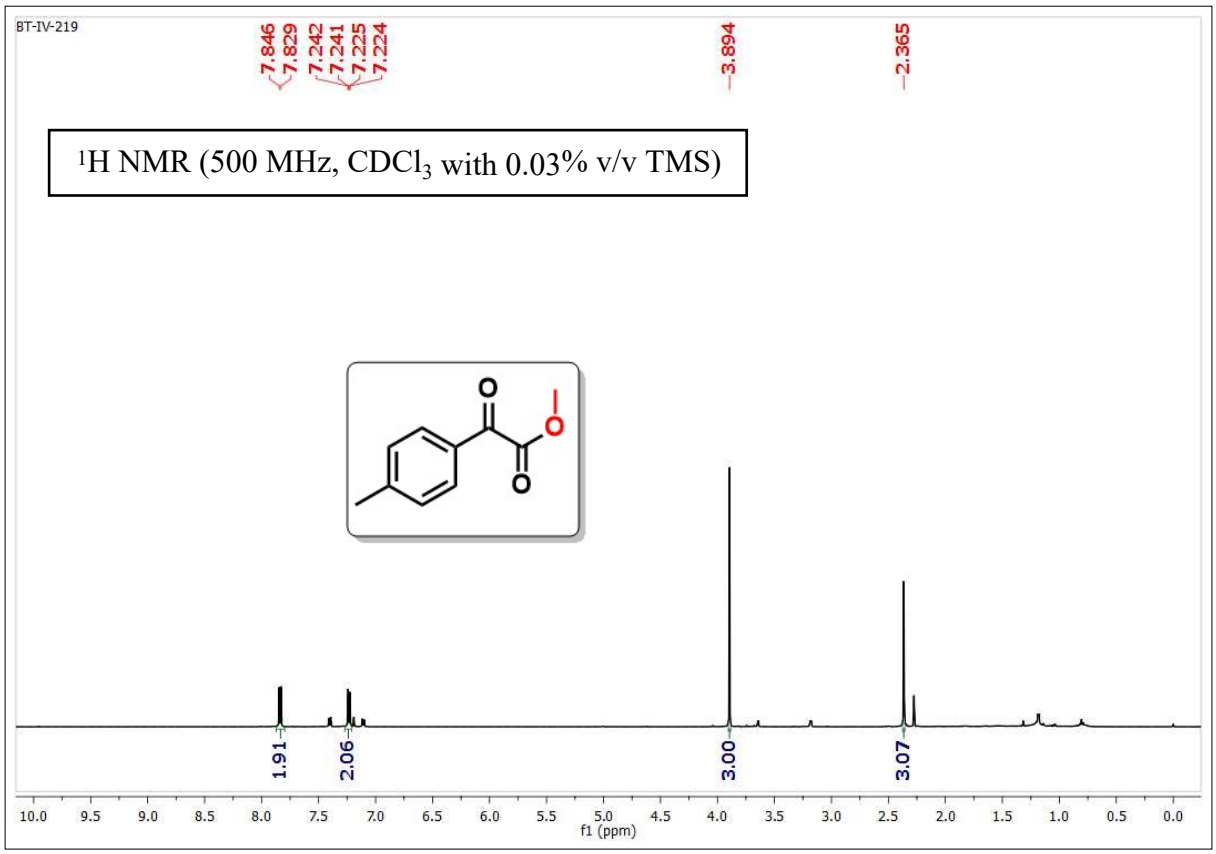

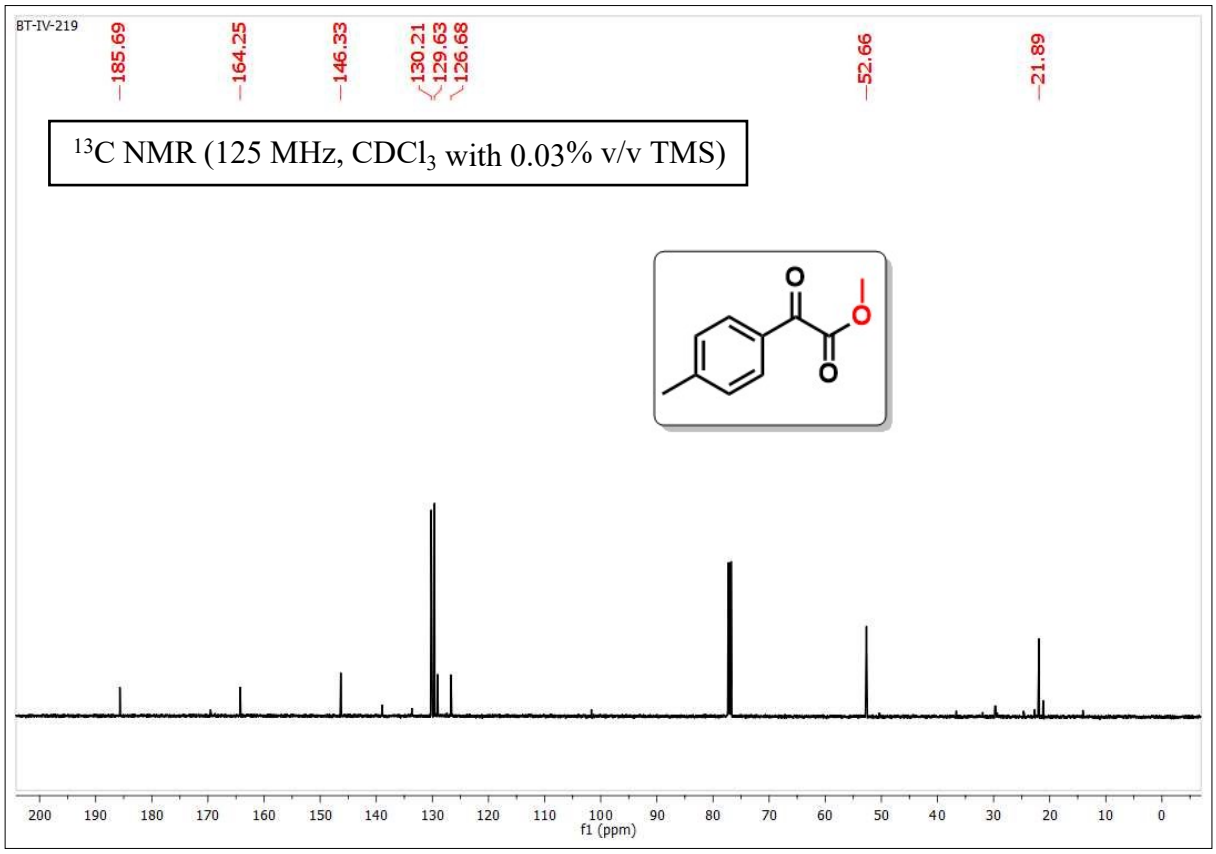

Methyl 2-(4-chlorophenyl)-2-oxoacetate (37)

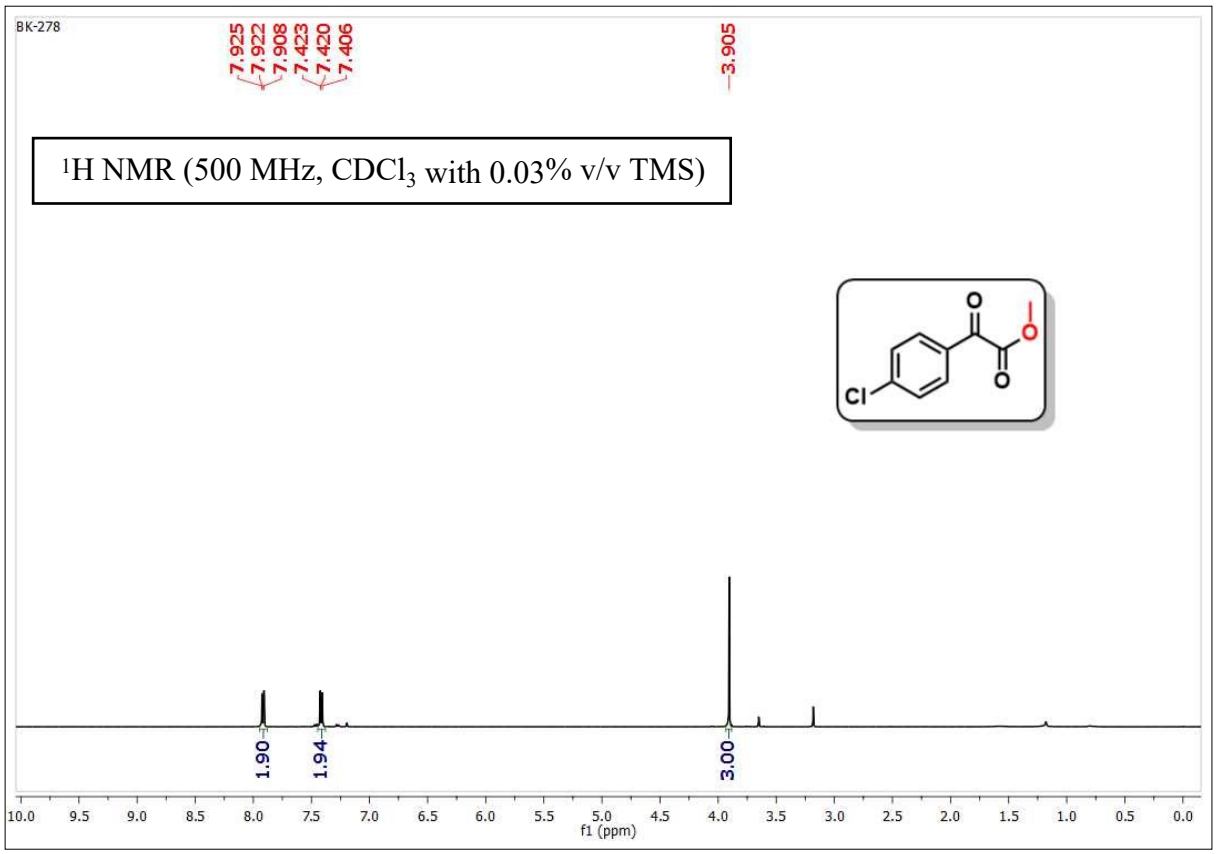

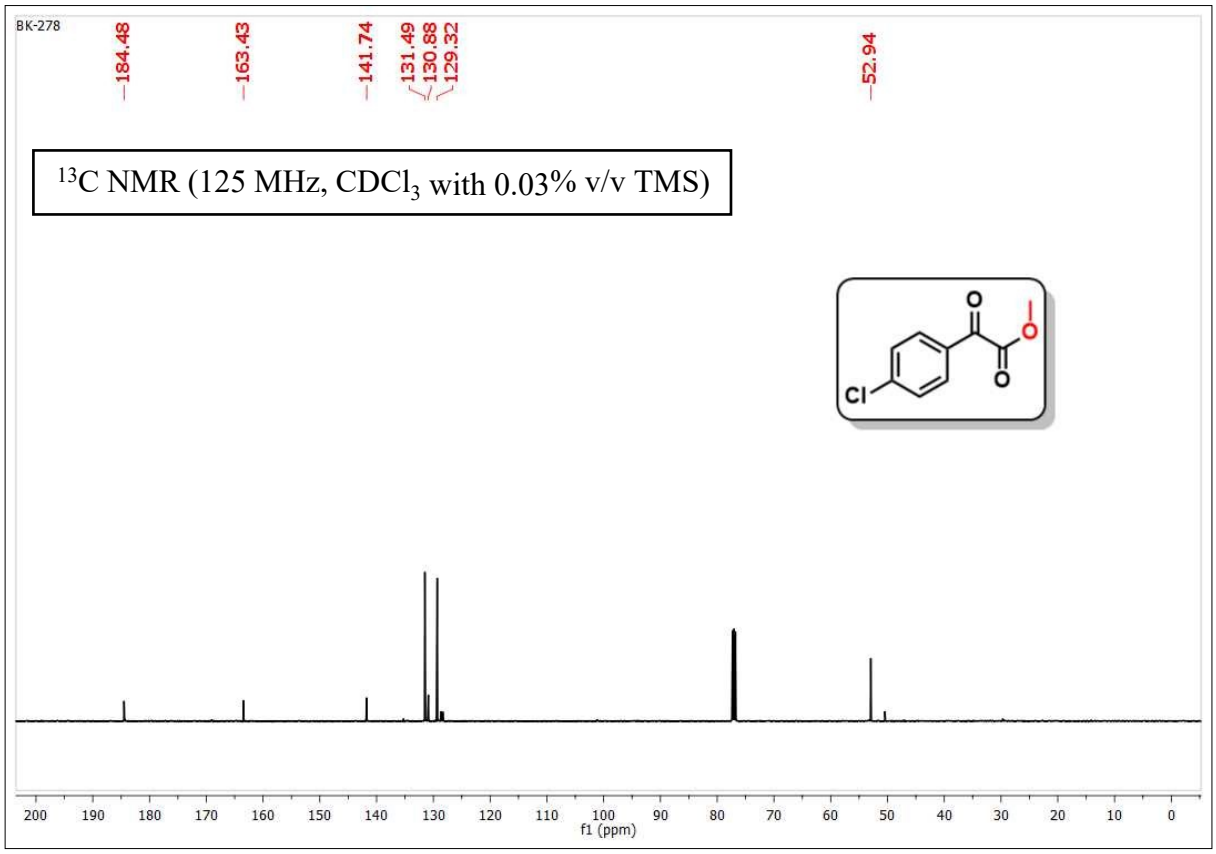

Methyl 2-(1H-indol-3-yl)-2-oxoacetate (38)

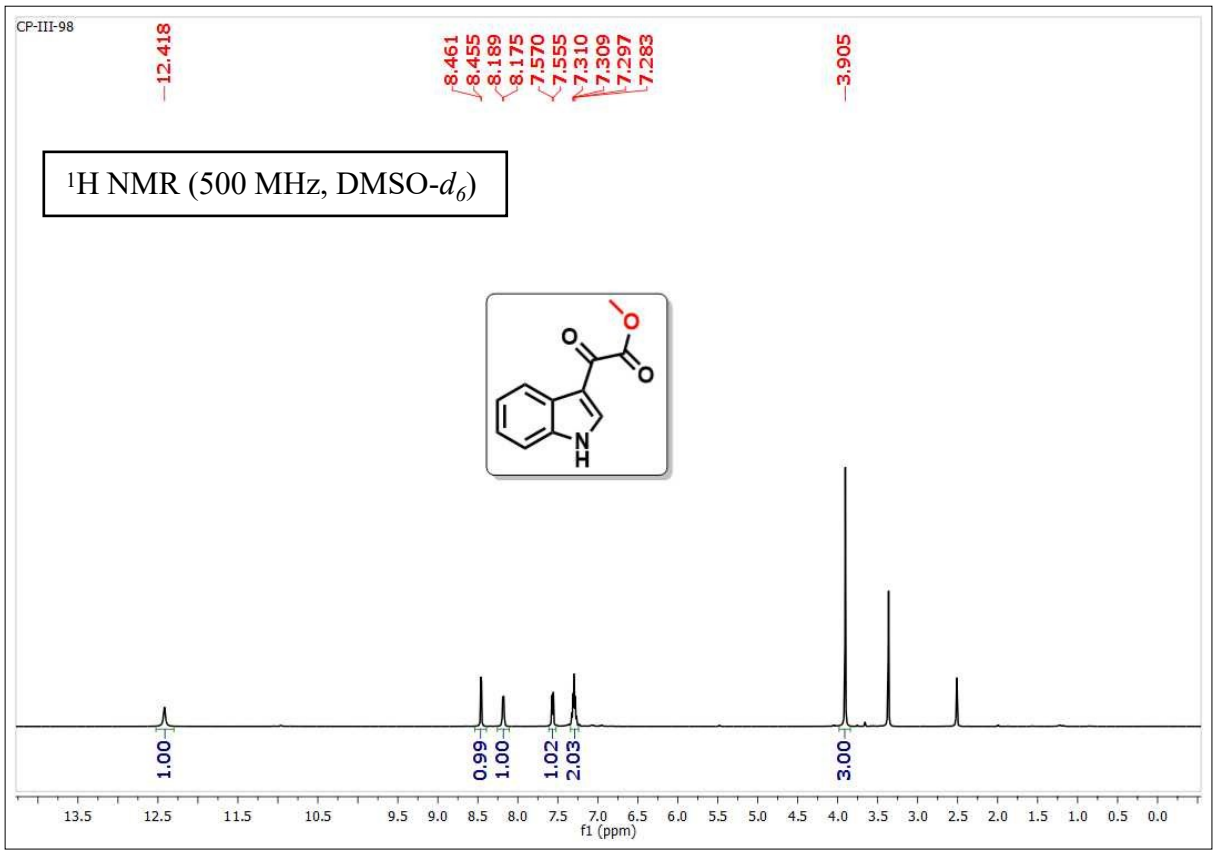

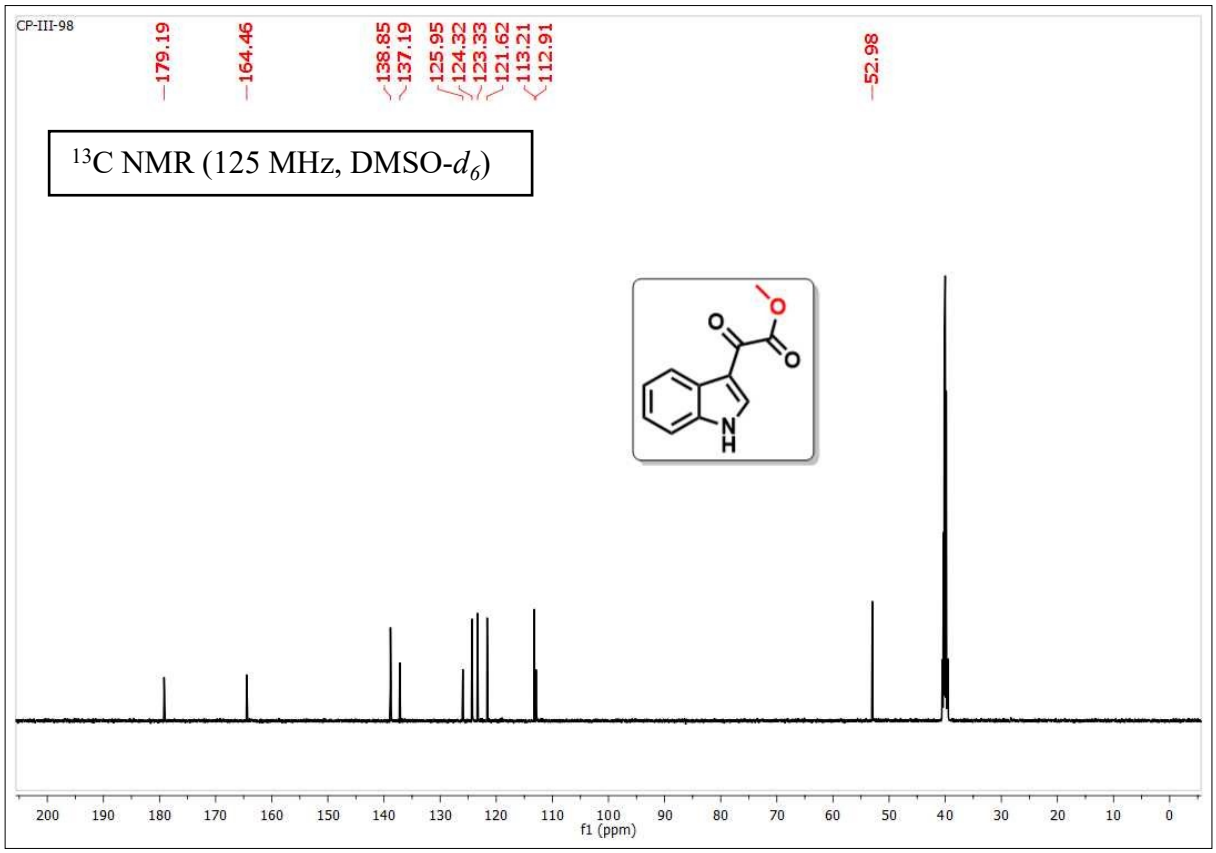

Methyl 2-(1-methyl-1H-indol-3-yl)-2-oxoacetate (39)

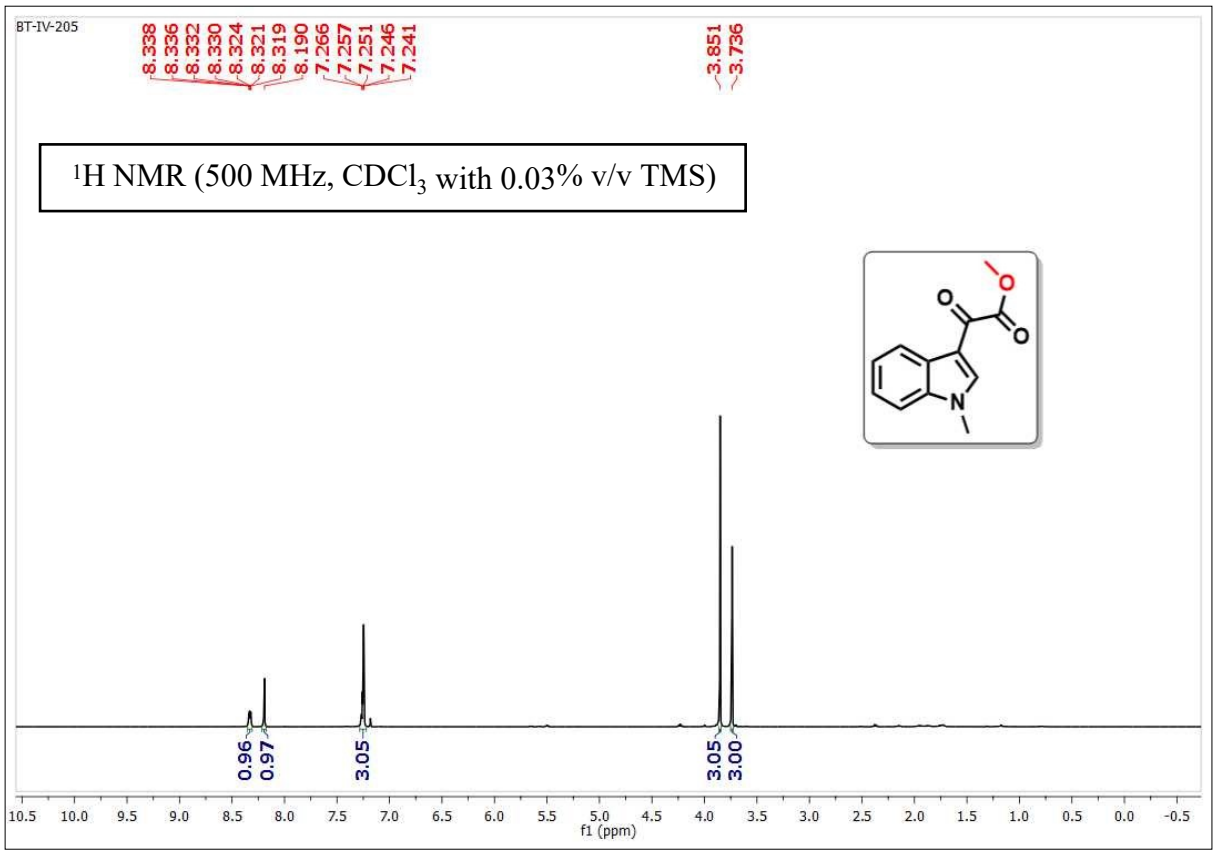

^{1}H NMR (500 MHz, $CDCl_3$ with 0.03% v/v TMS)

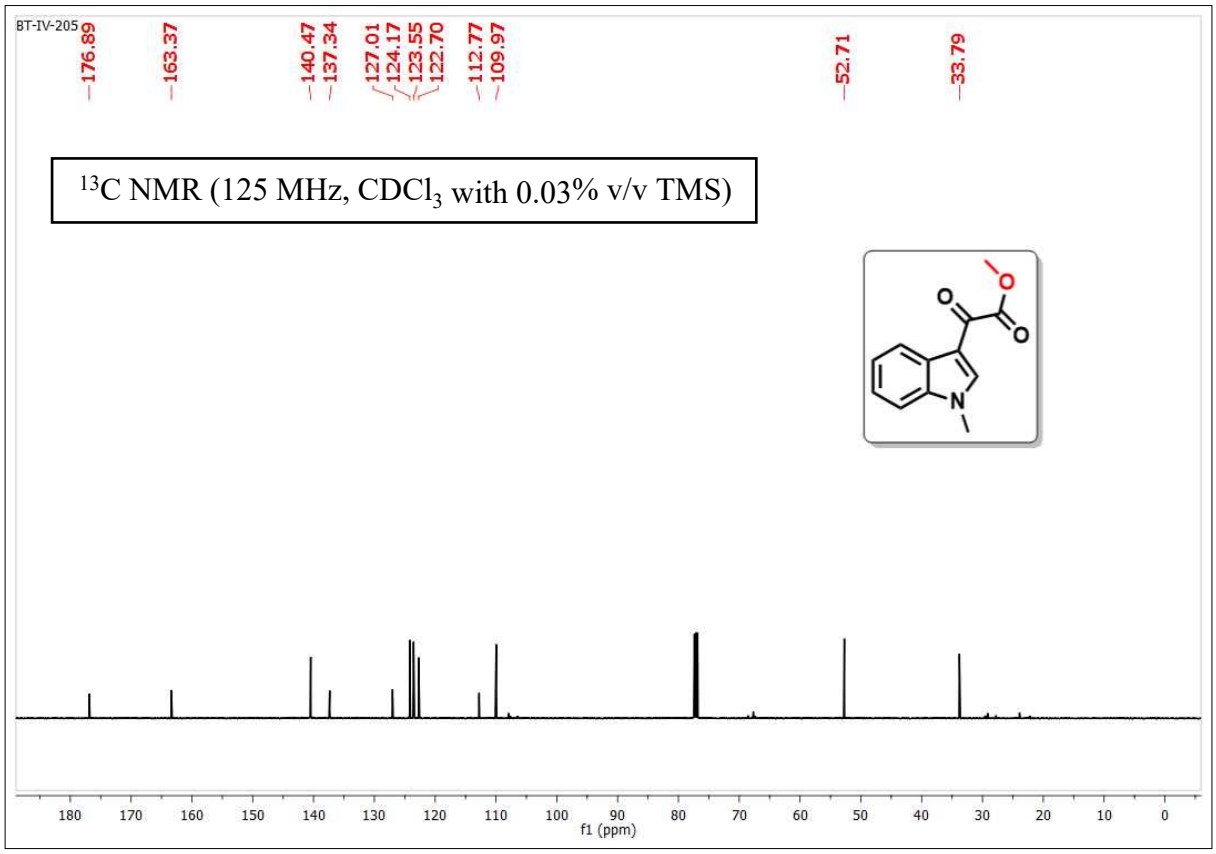

^{13}C NMR (125 MHz, $CDCl_3$ with 0.03% v/v TMS)

Methyl 2-oxo-2-(1H-pyrrol-2-yl)acetate (40)

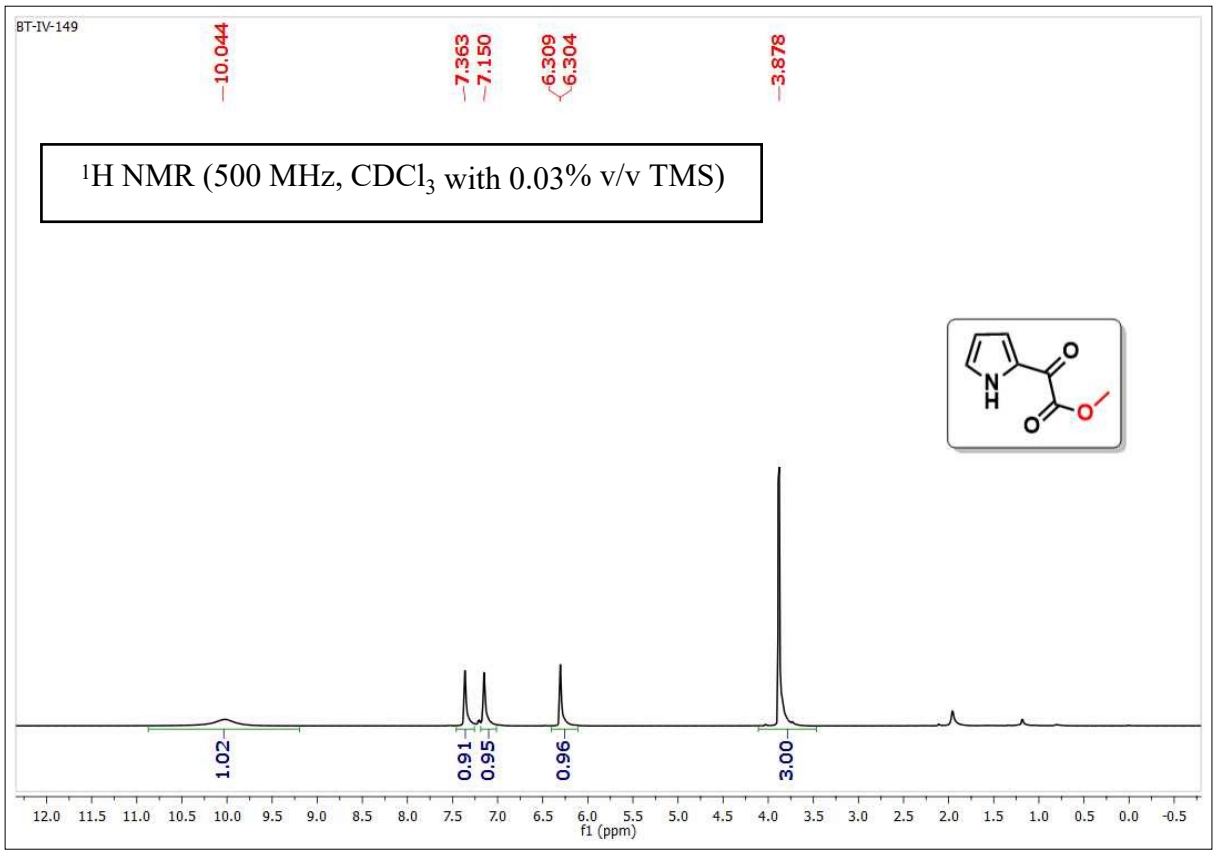

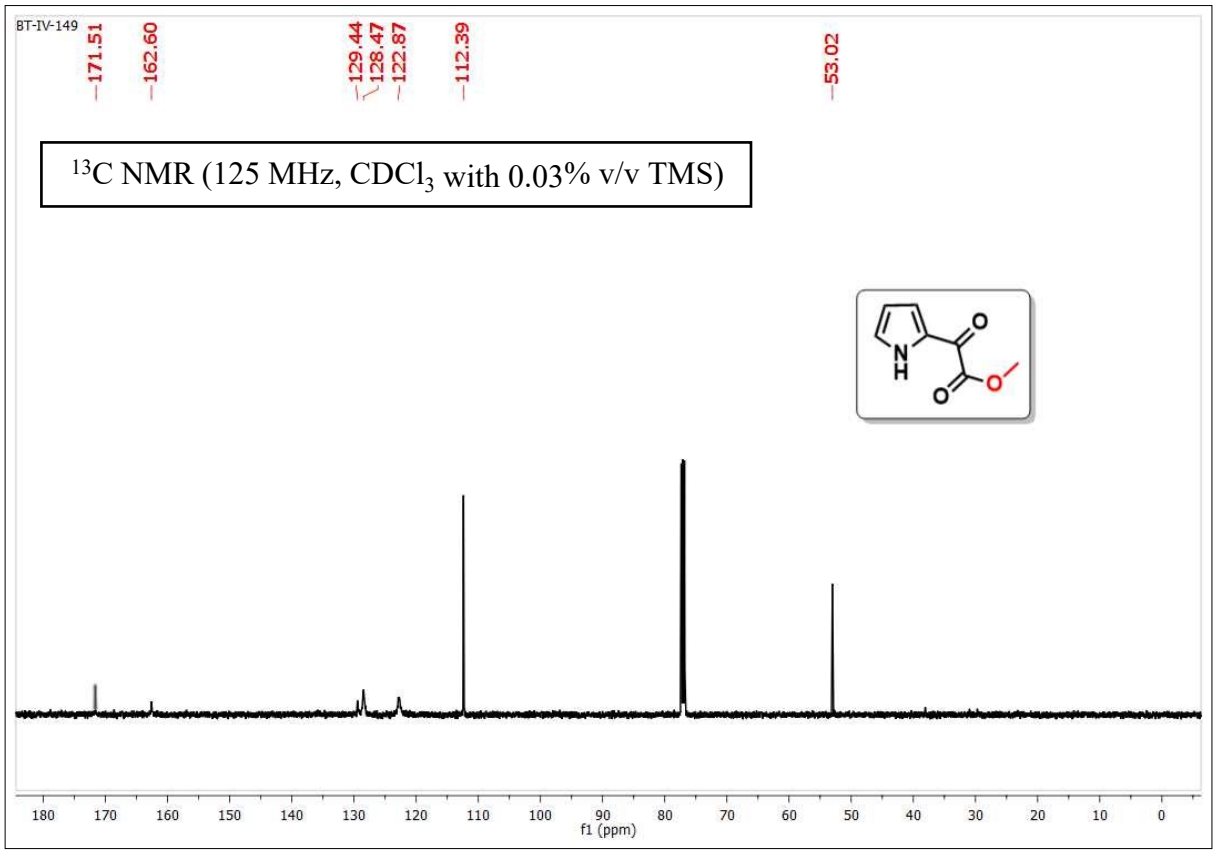

Methyl 2-(naphthalen-2-yl)-2-oxoacetate (41)

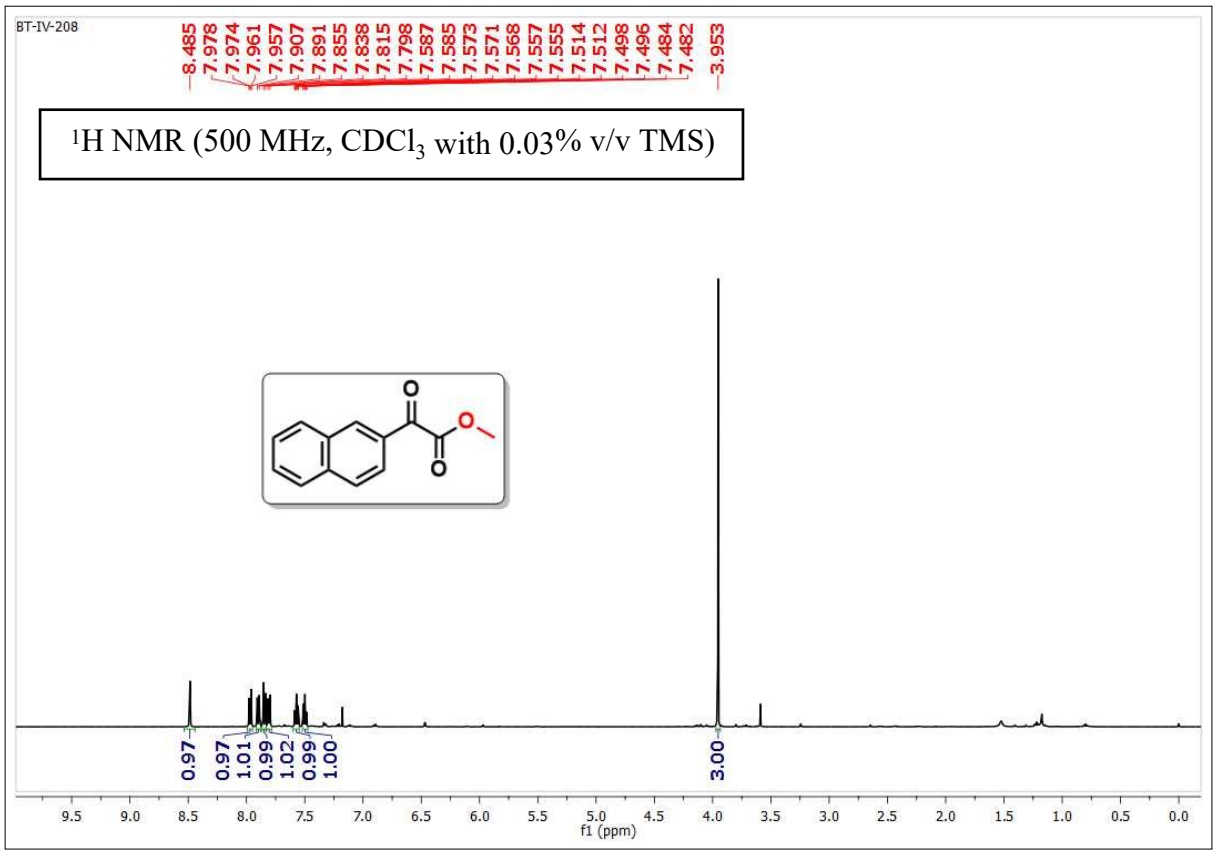

^{1}H NMR (500 MHz, $CDCl_3$ with 0.03% v/v TMS)

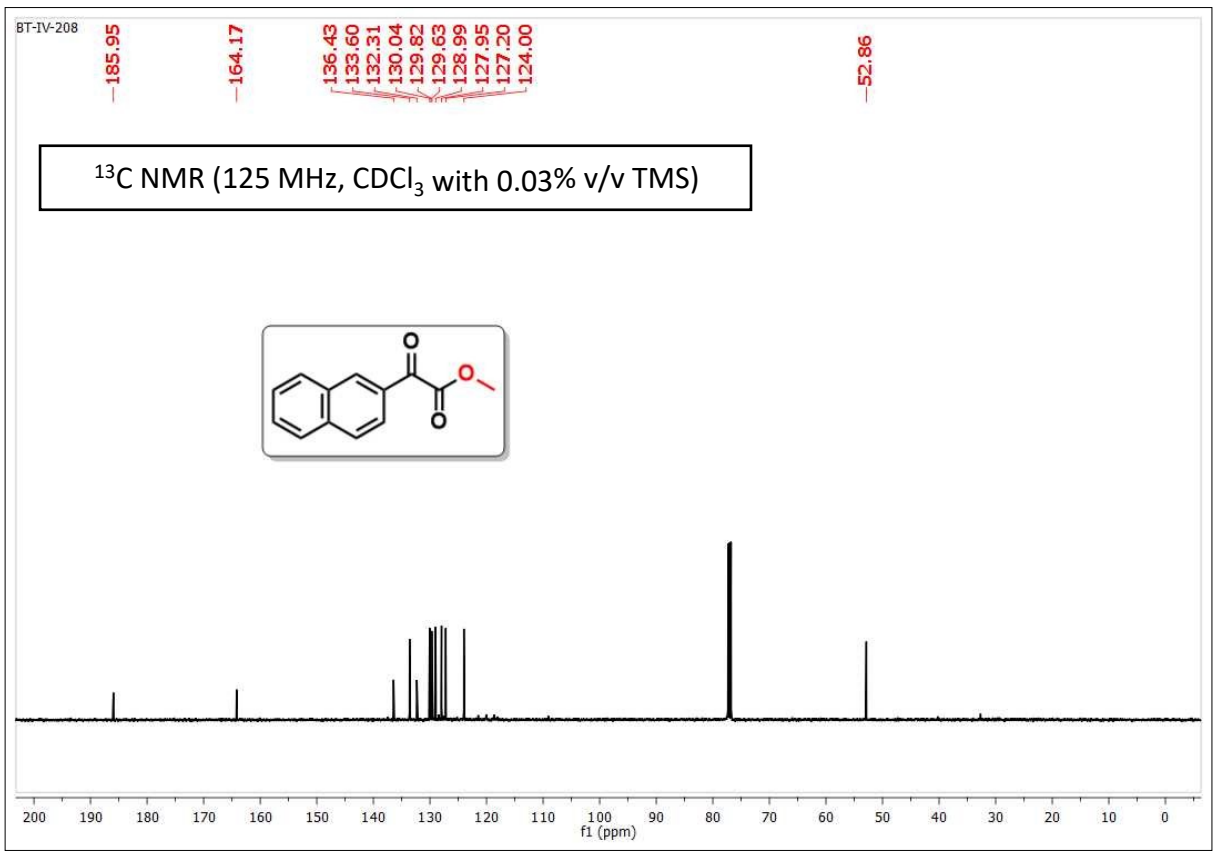

^{13}C NMR (125 MHz, $CDCl_3$ with 0.03% v/v TMS)

Methyl cinnamate (42)

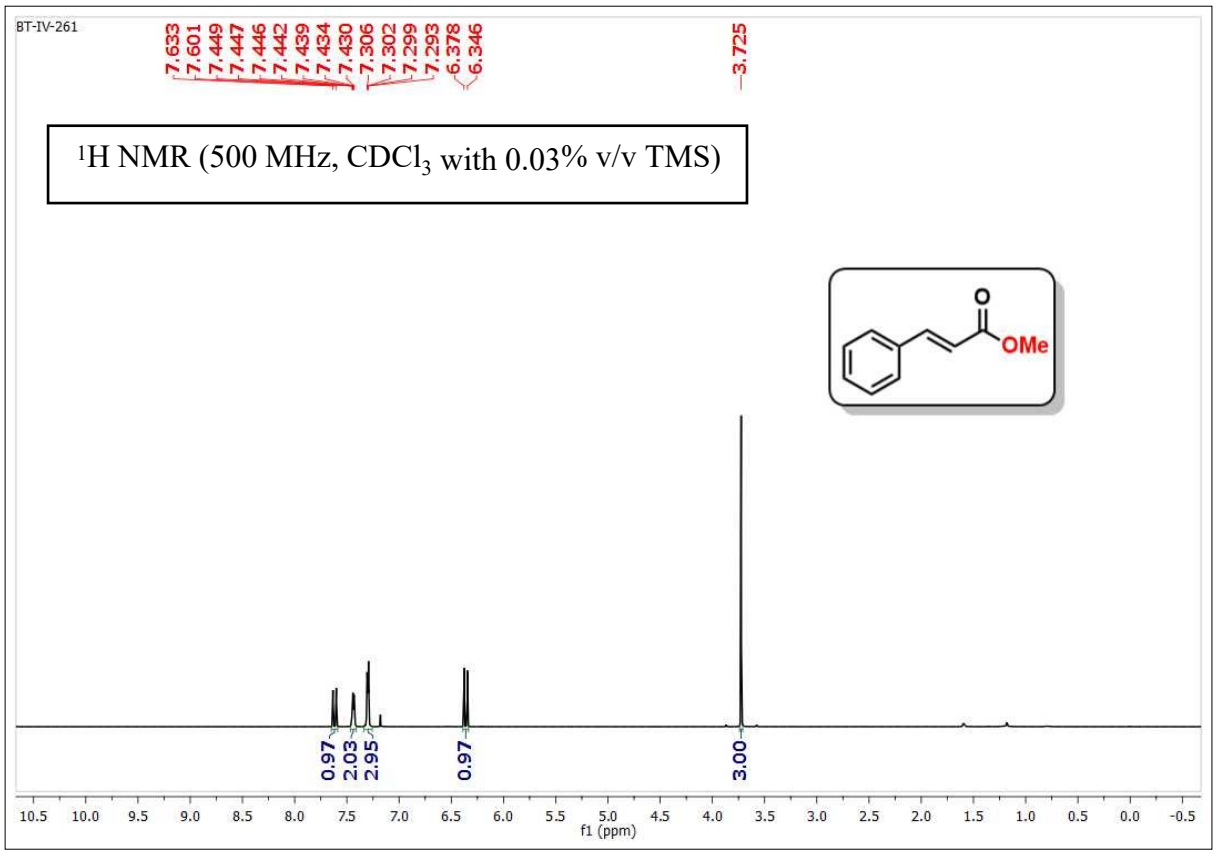

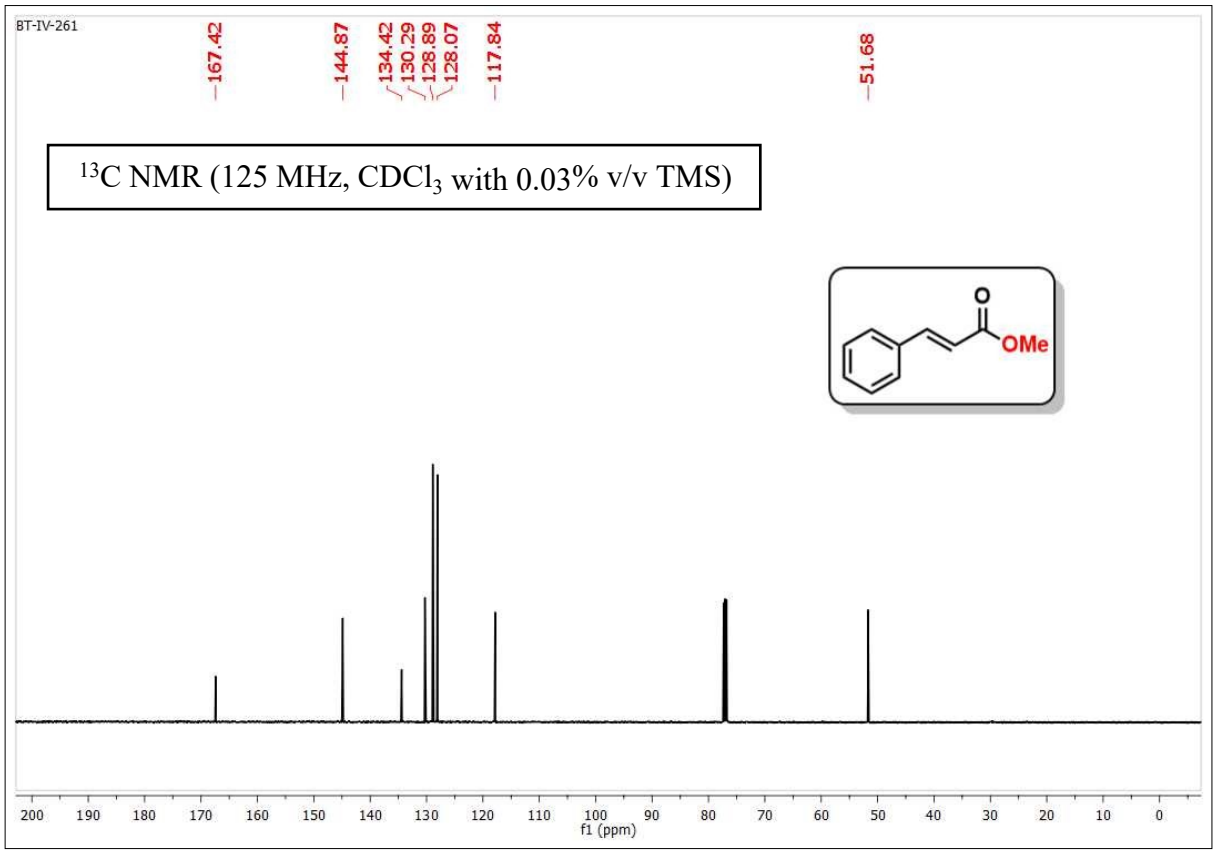

Methyl benzoylglycinate (43)

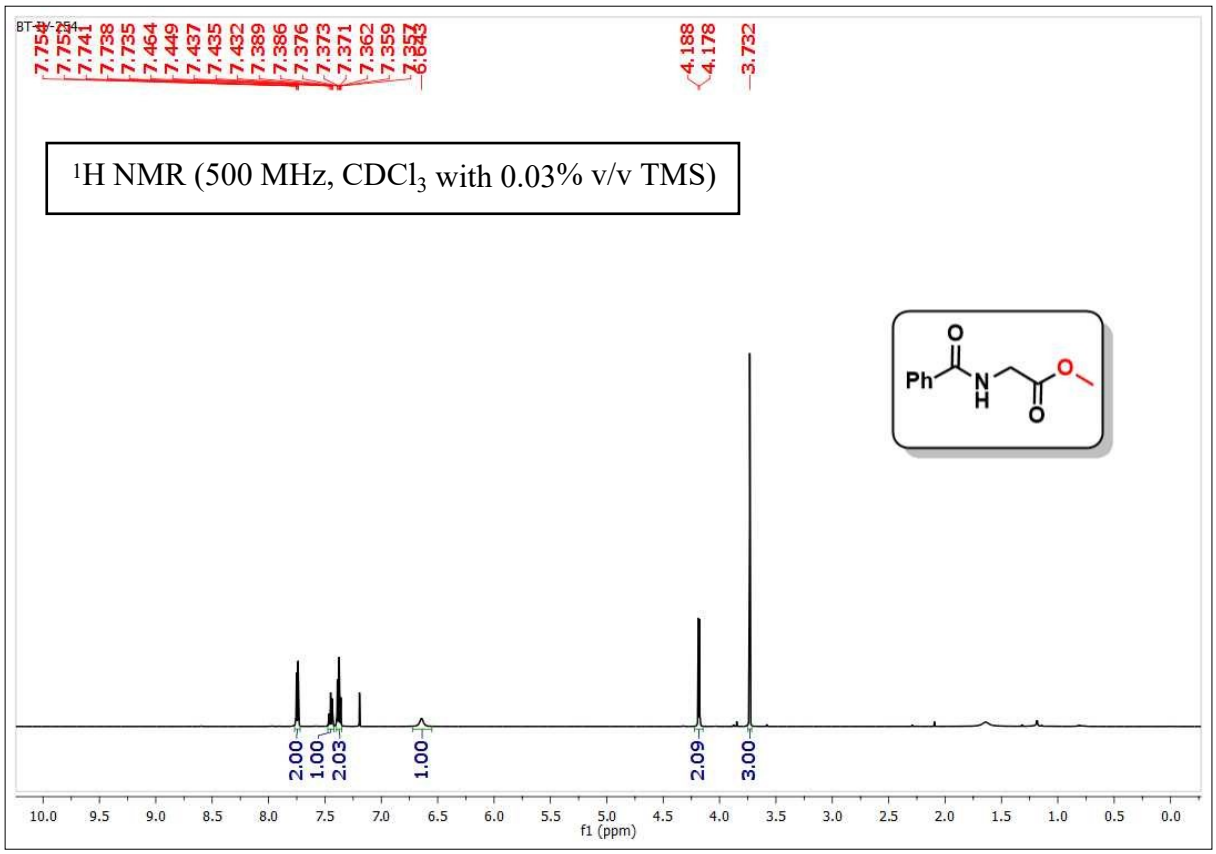

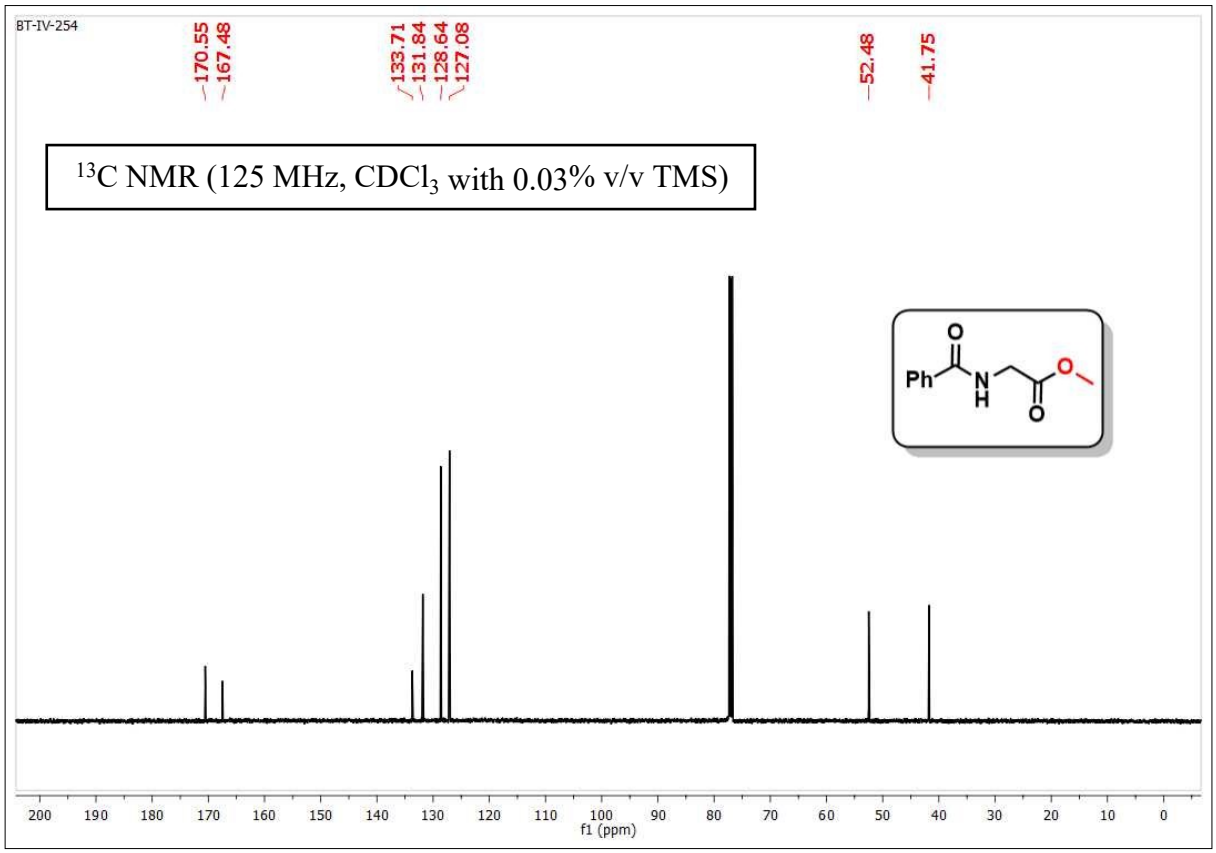

Methyl benzoylalaninate (44)

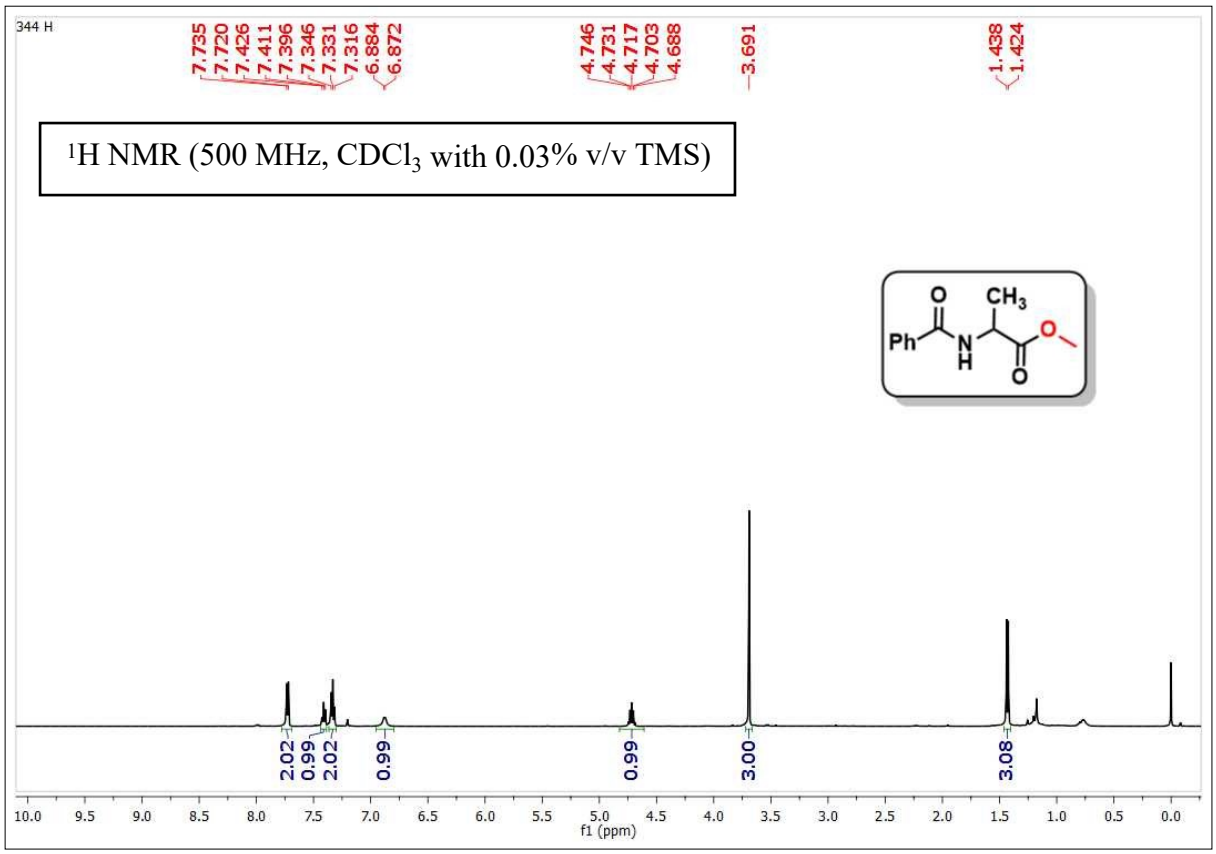

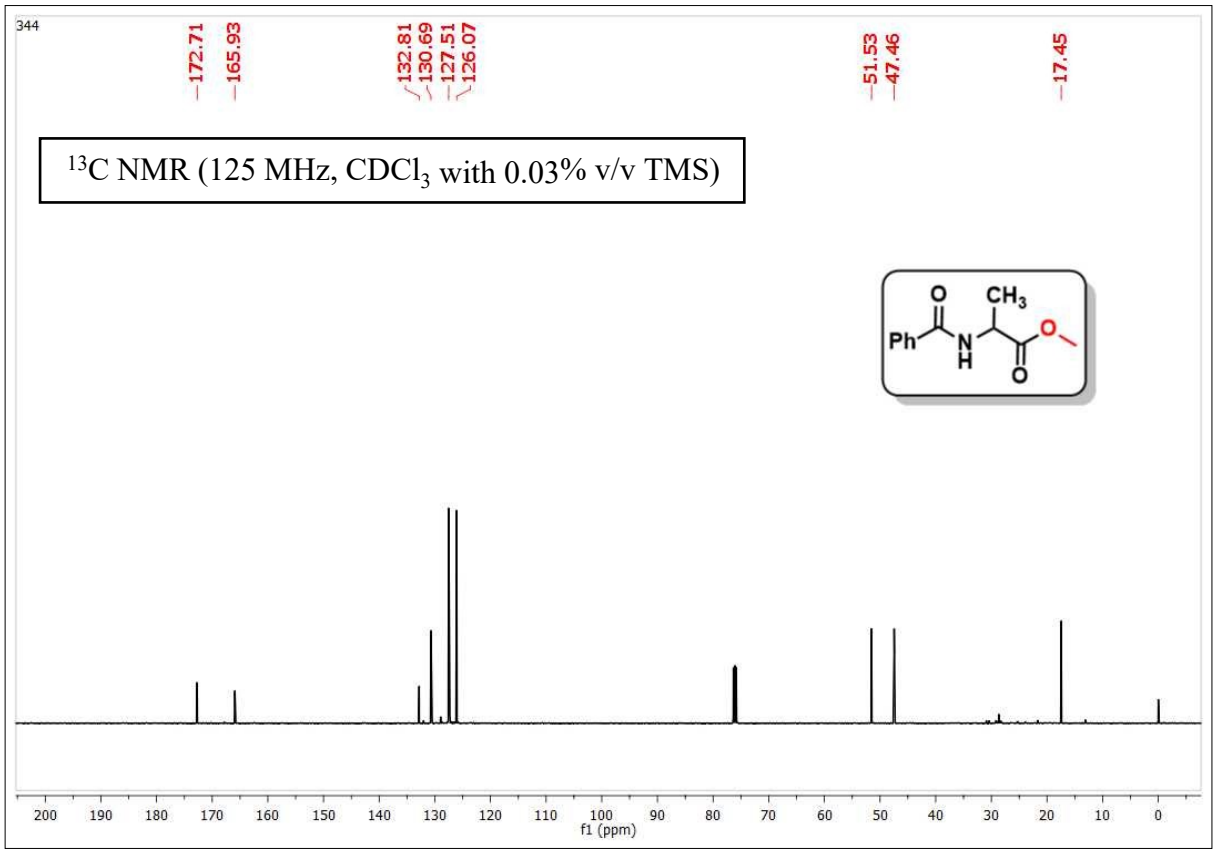

Methyl benzoylvalinate (45)

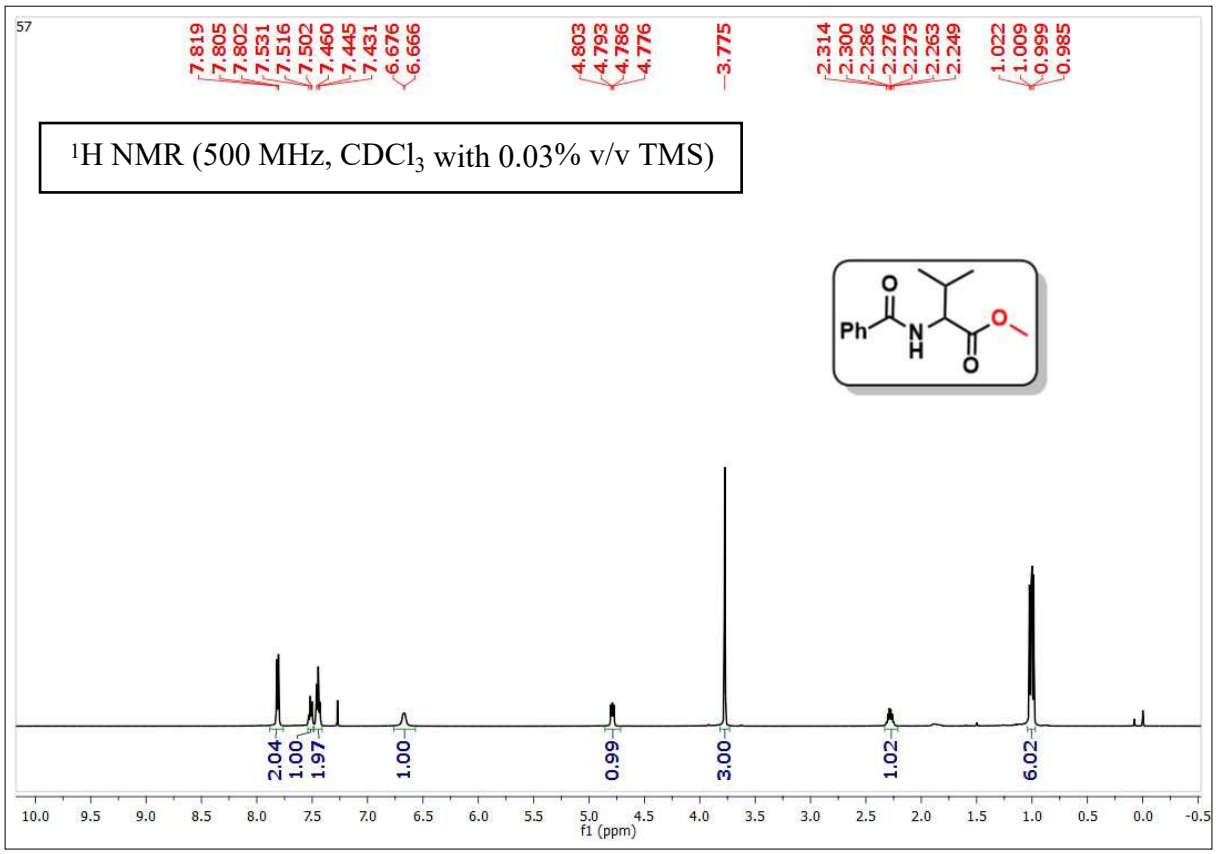

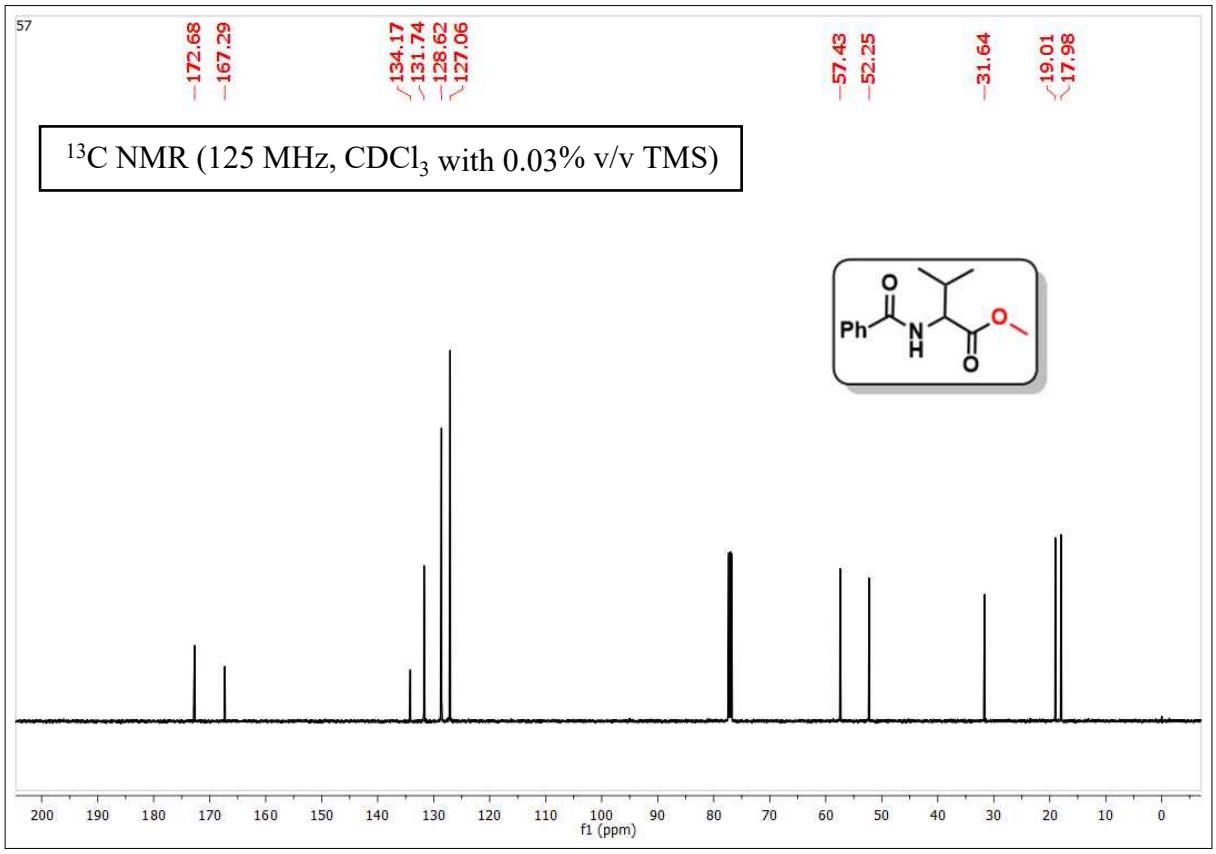

Methyl benzoylleucinate (46)

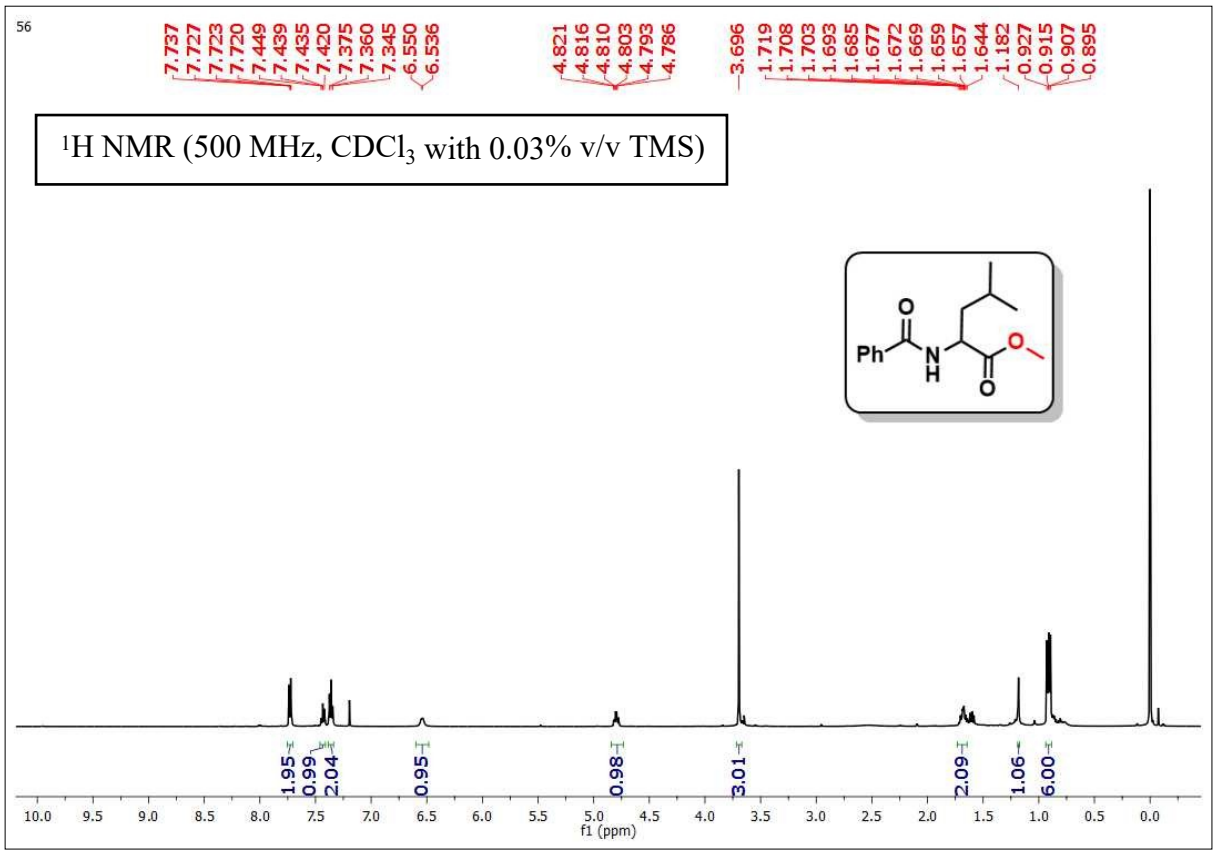

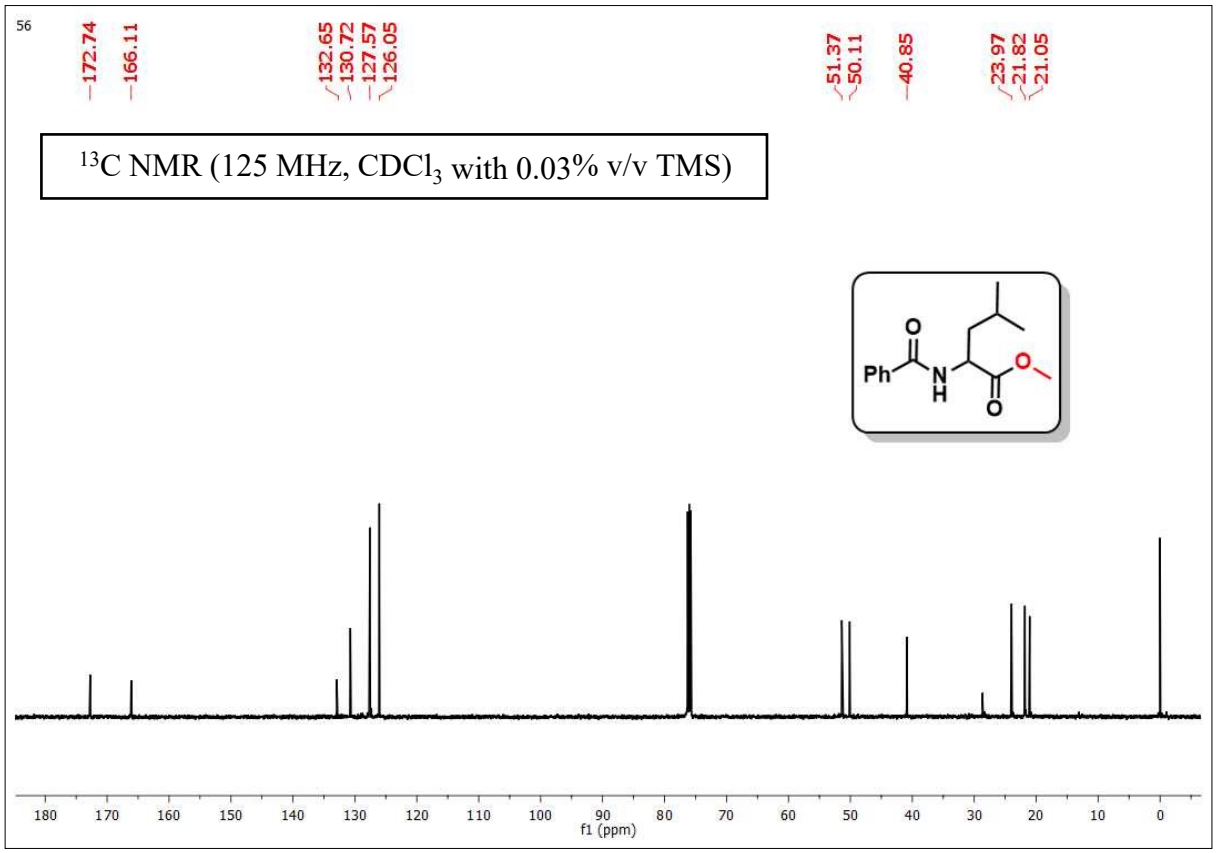

Methyl benzoylphenylalaninate (47)

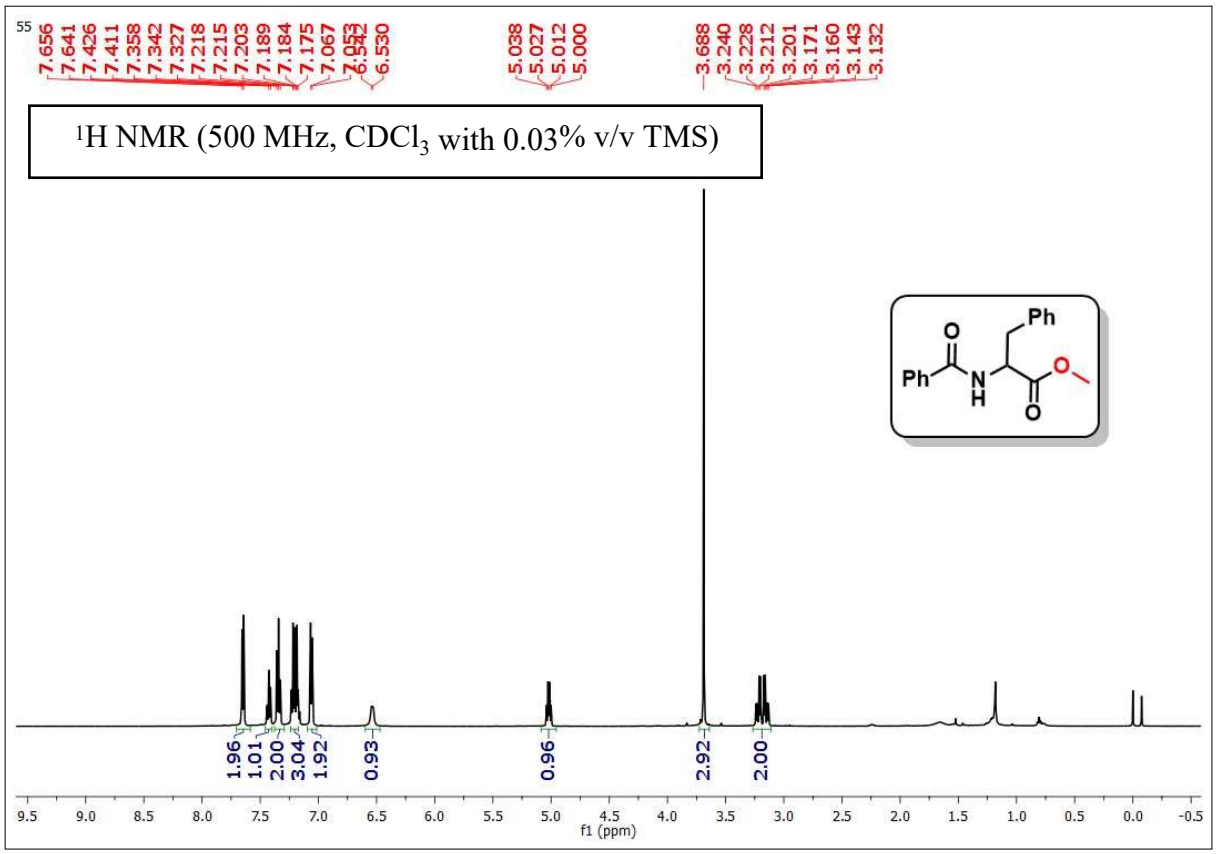

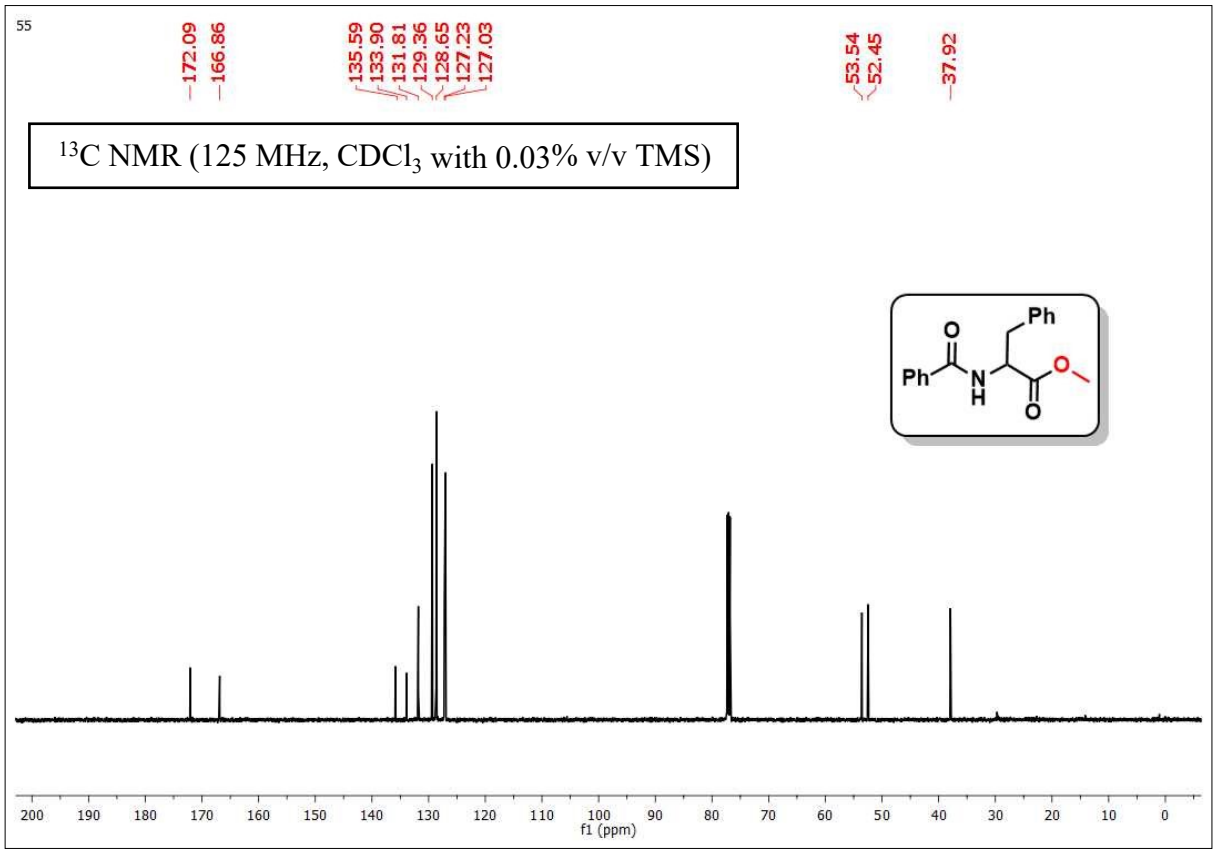

Methyl N-benzoyl-N-methylglycinate (48)

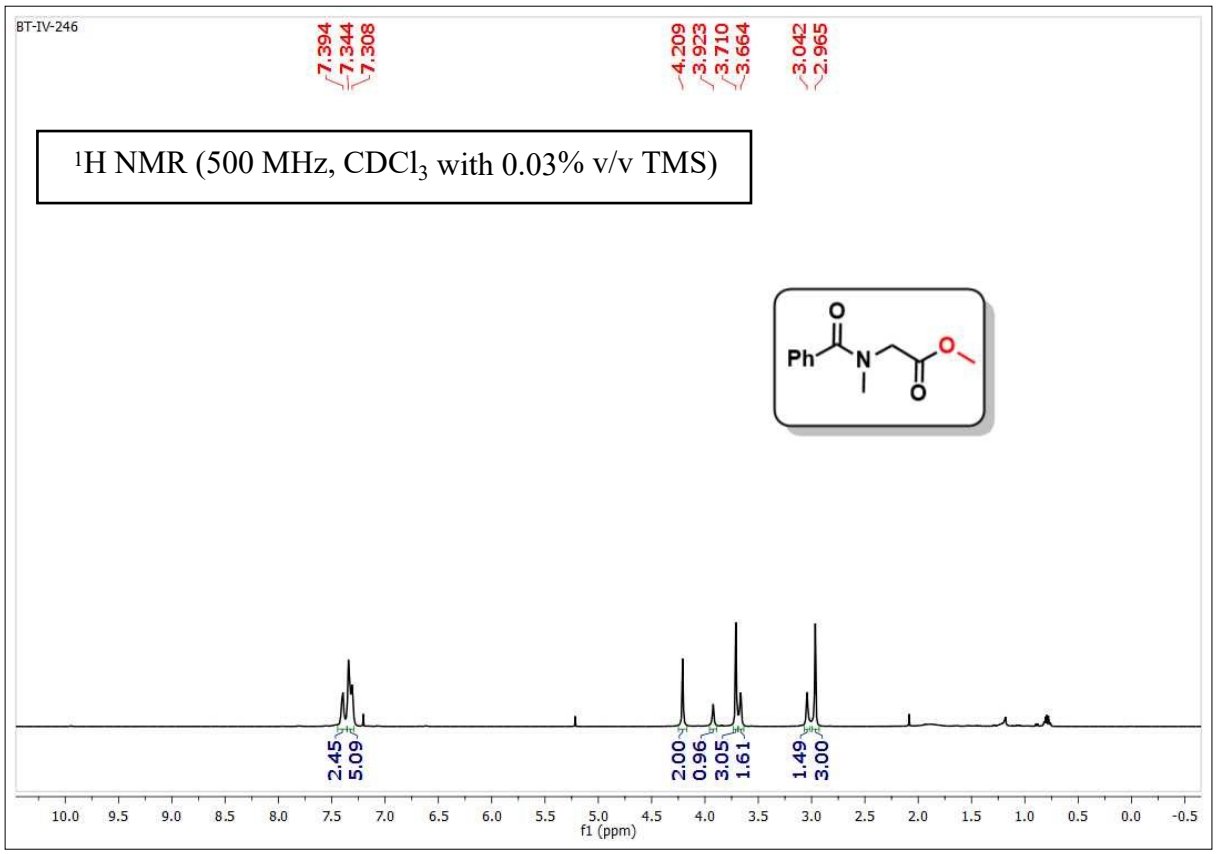

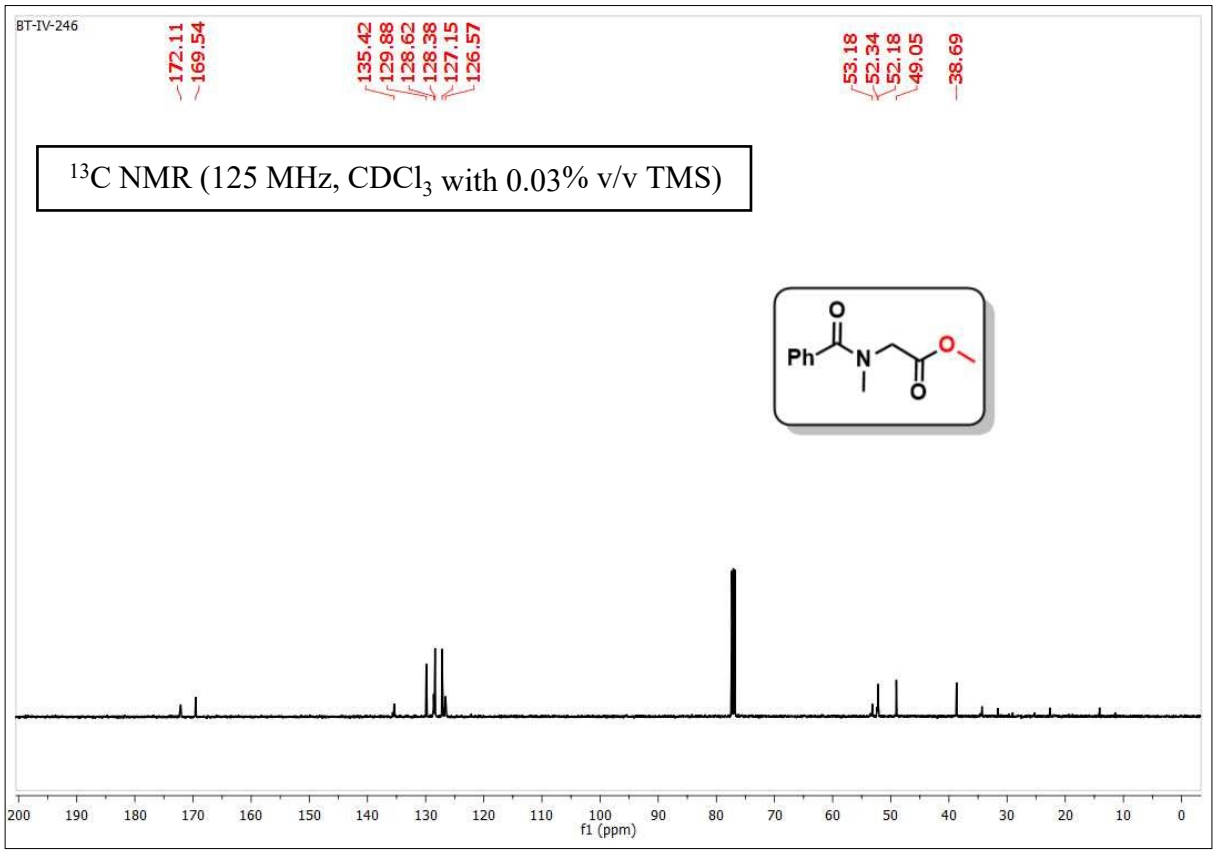

Methyl benzoyltyrosinate (49)

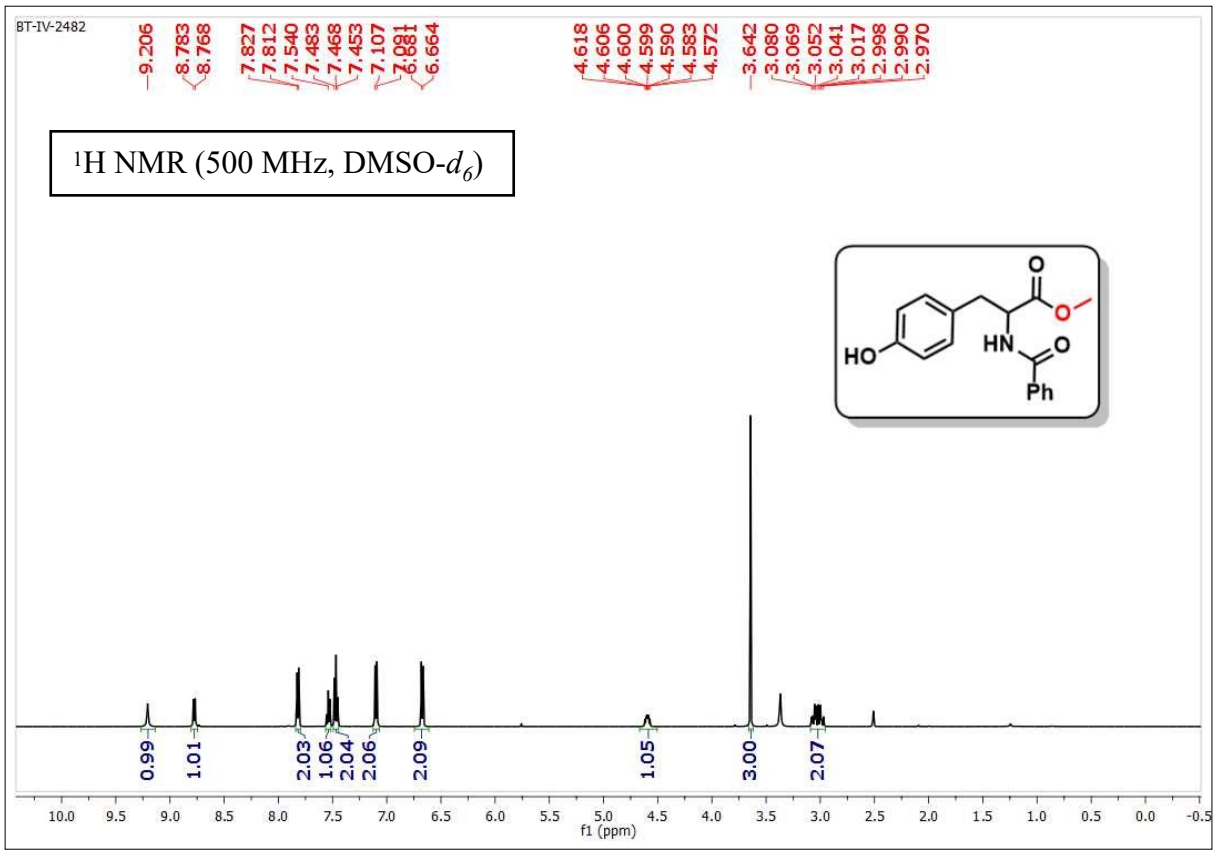

^{1}H NMR (500 MHz, DMSO-d_6)

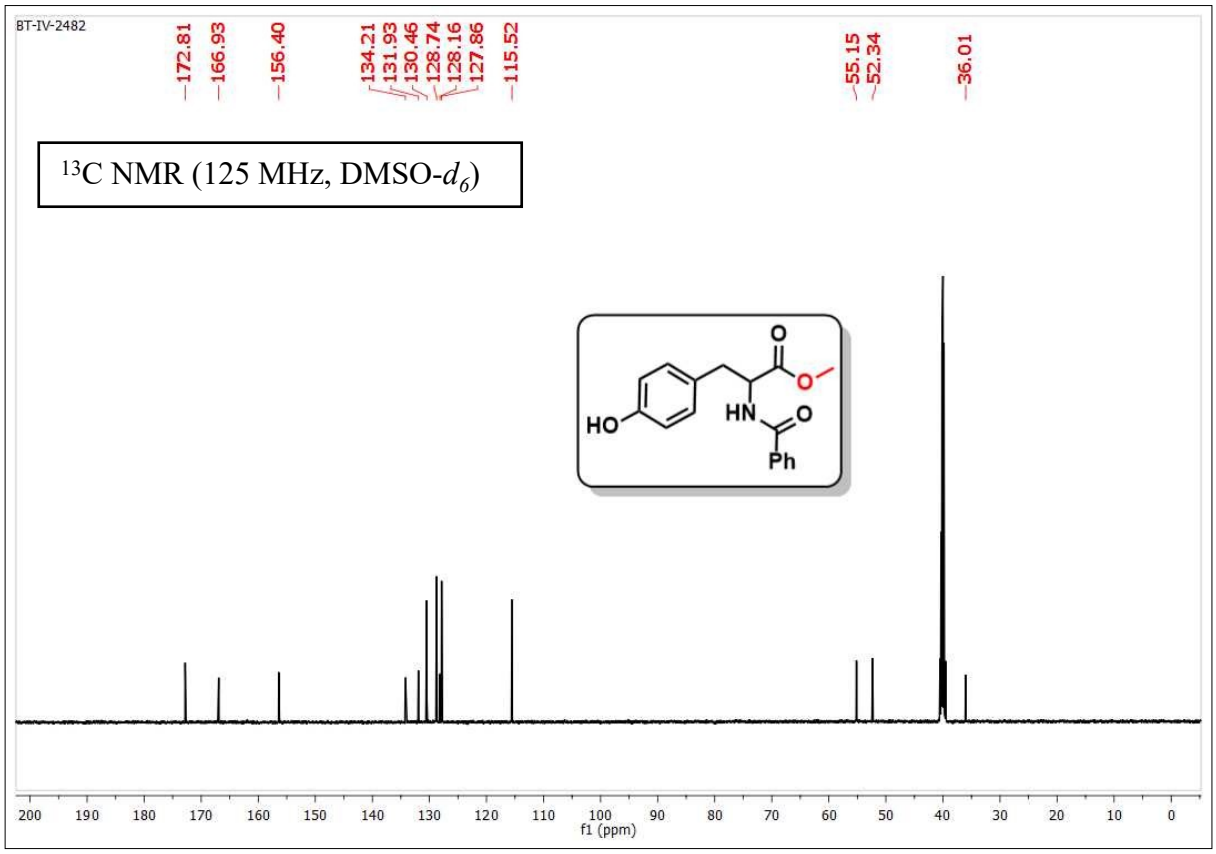

^{13}C NMR (125 MHz, DMSO-d_6)

Methyl benzoylprolinate (50)

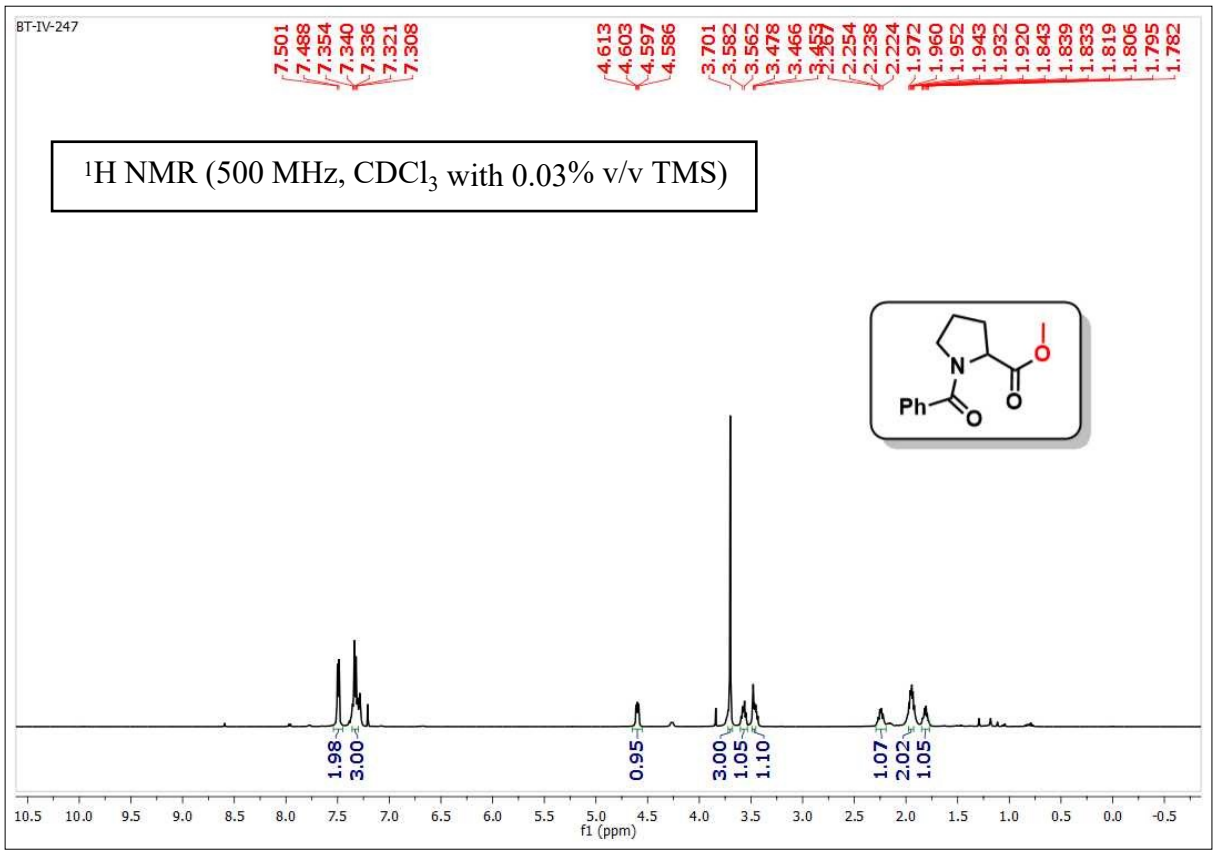

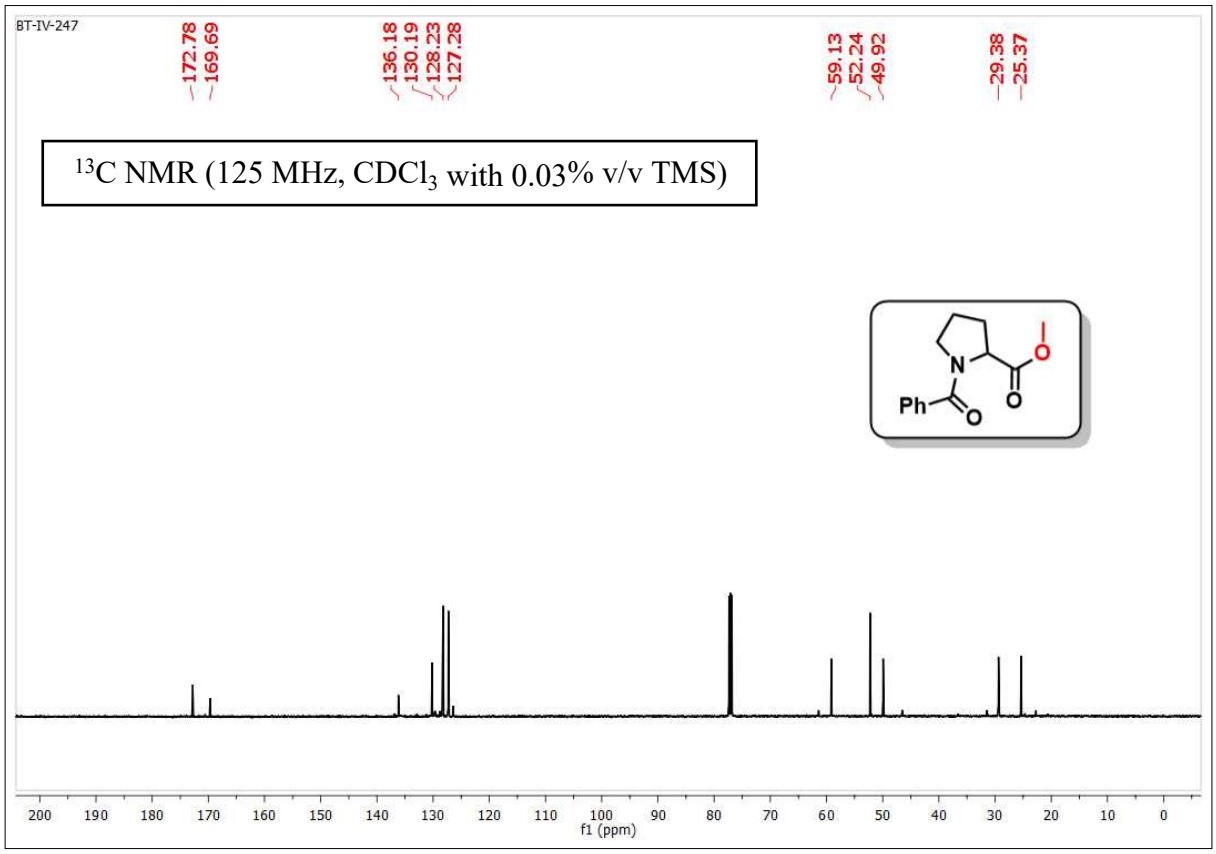

Methyl benzoyltryptophanate (51)

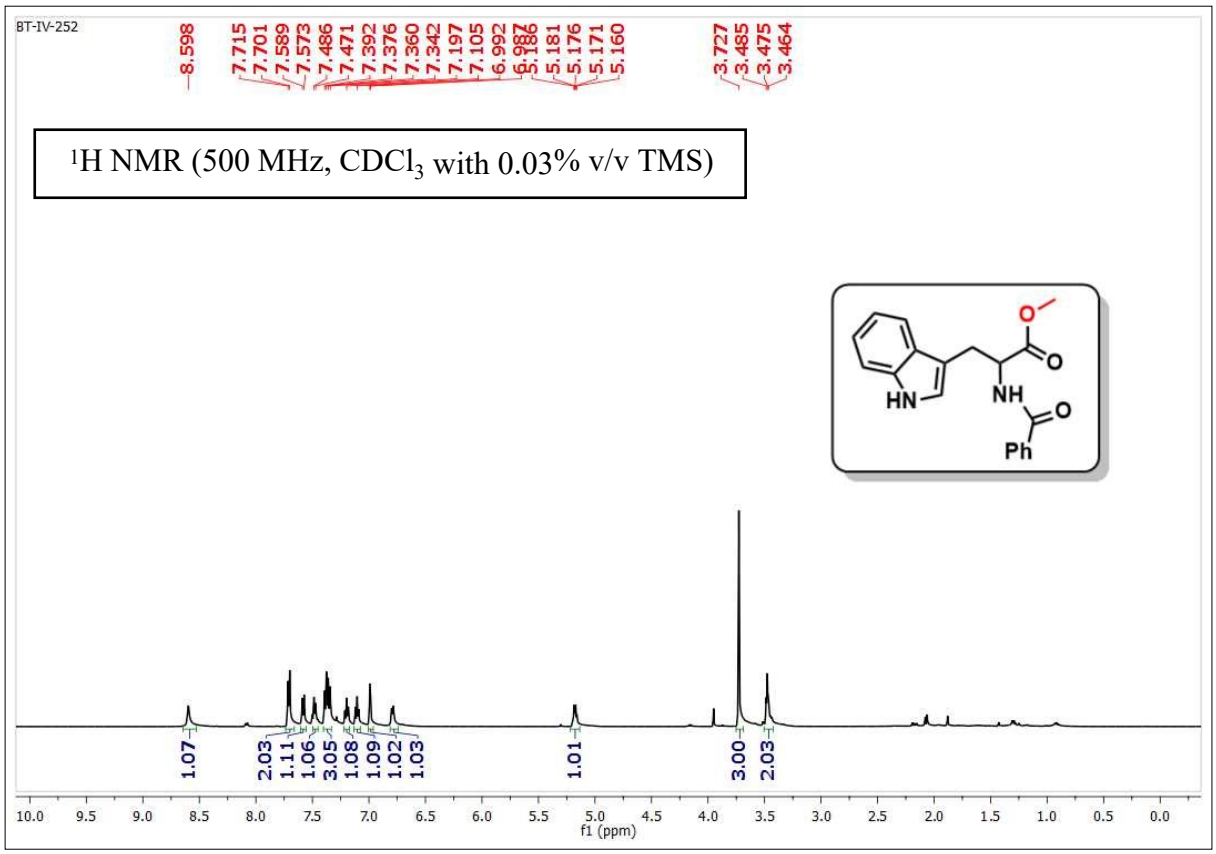

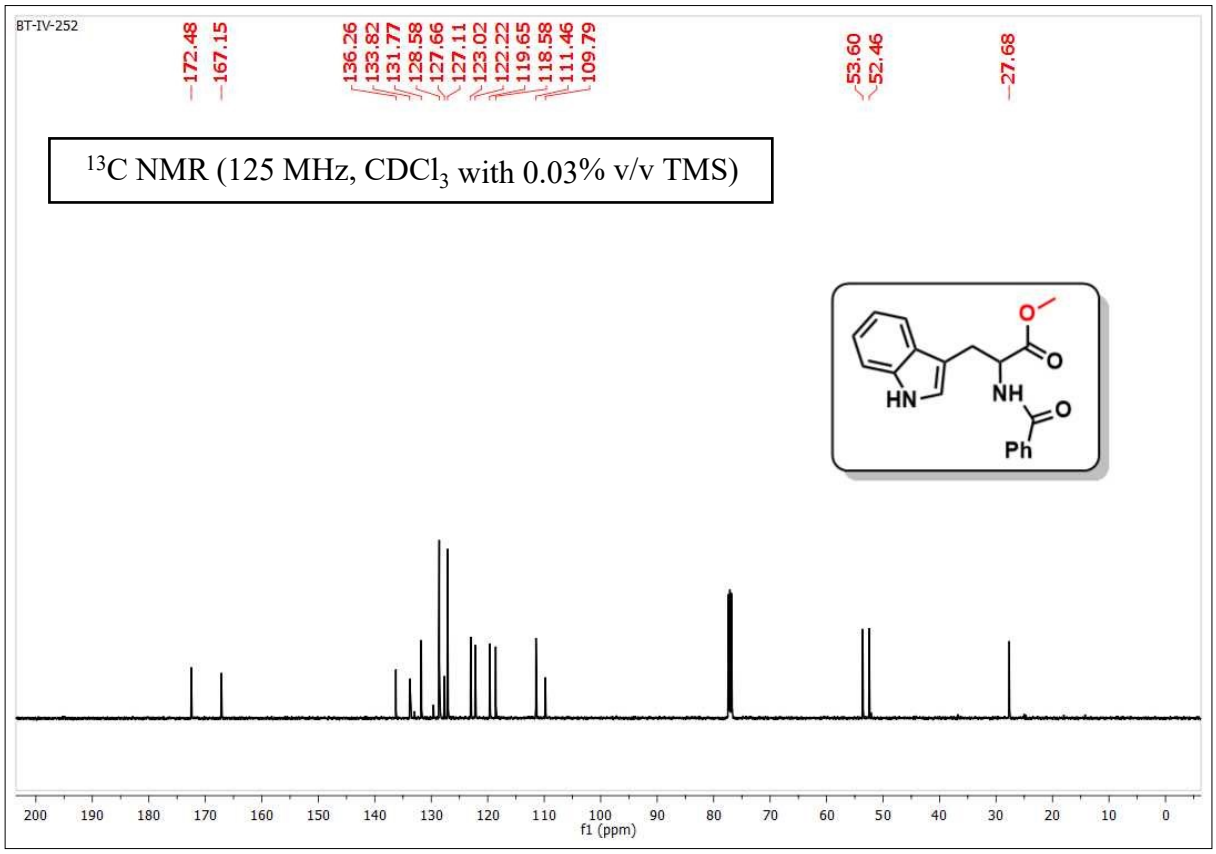

Methyl acetylcysteinate (52)

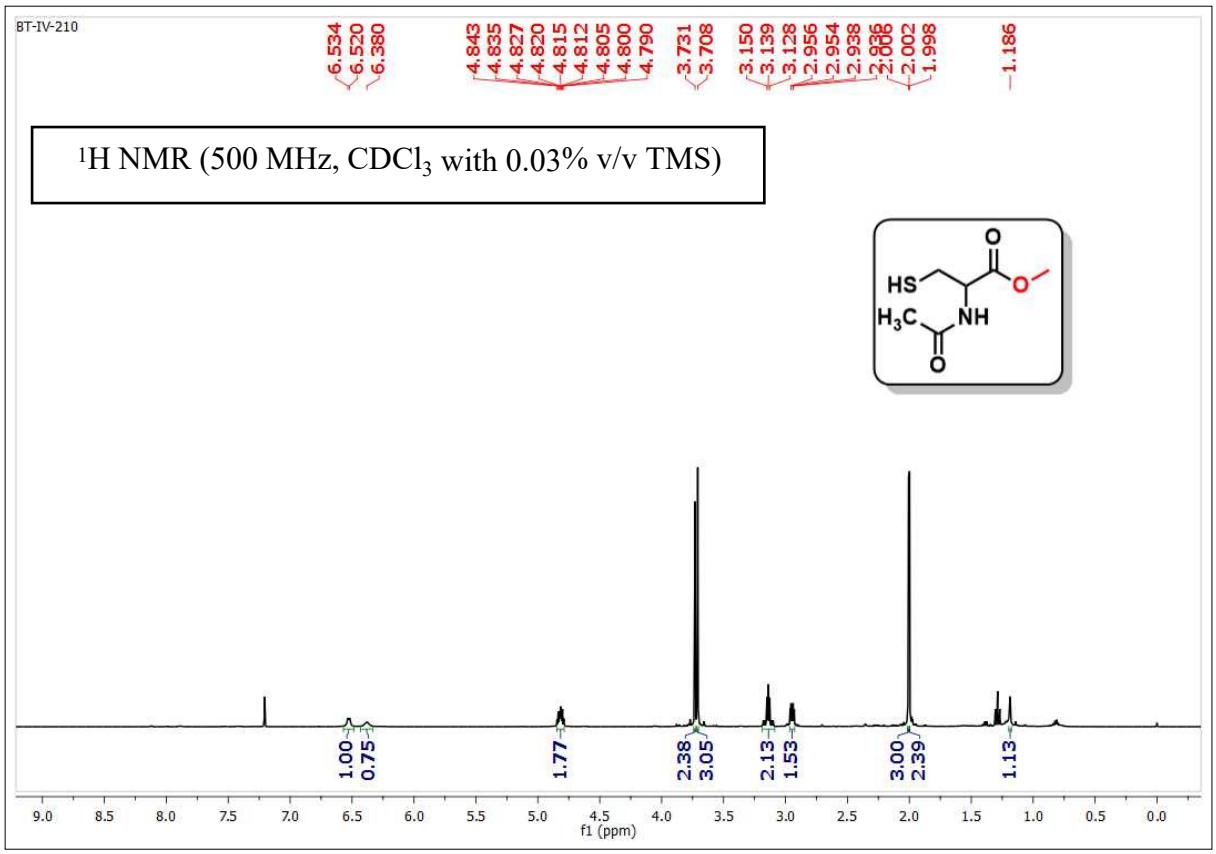

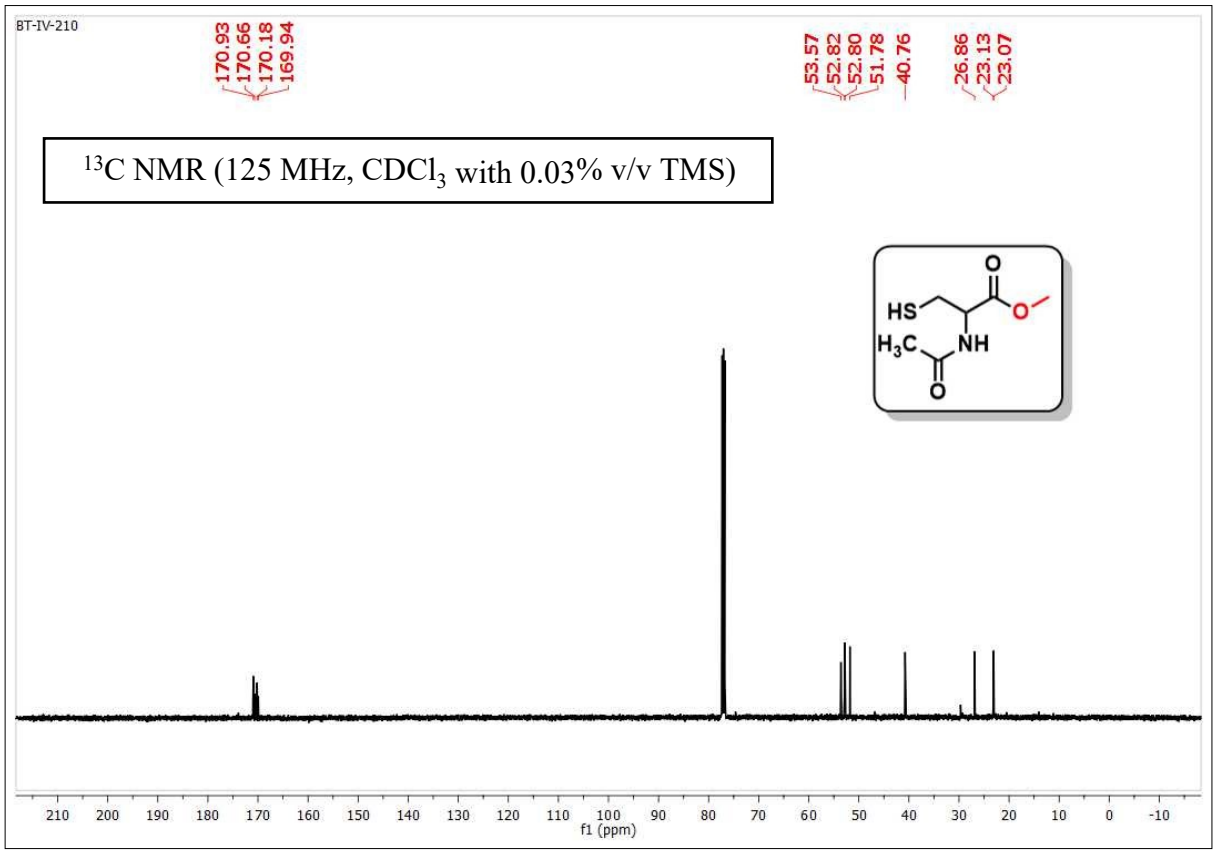

2,2-di(1H-indol-3-yl)ethan-1-ol (53)

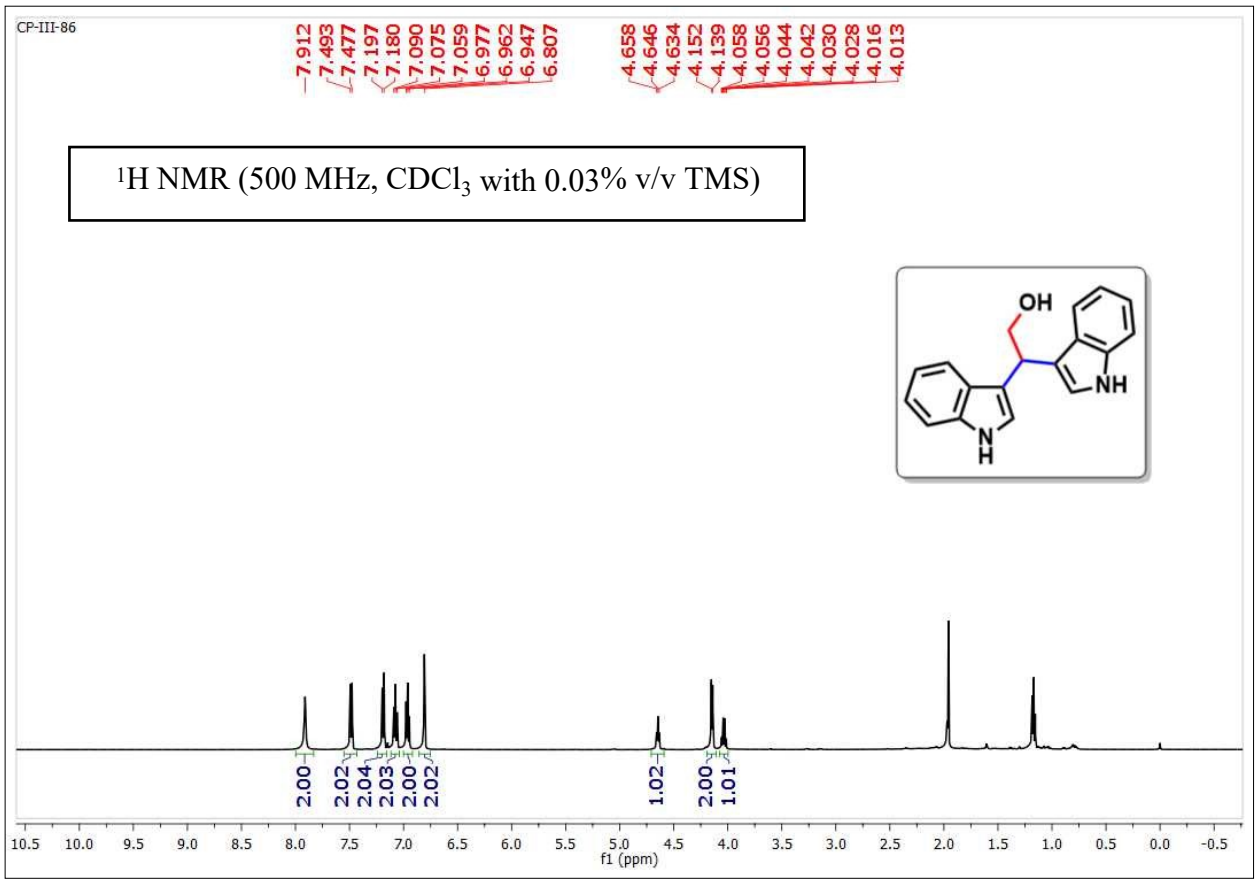

2,2-di(1H-indol-3-yl)ethyl acetate (Streptindole, 54)

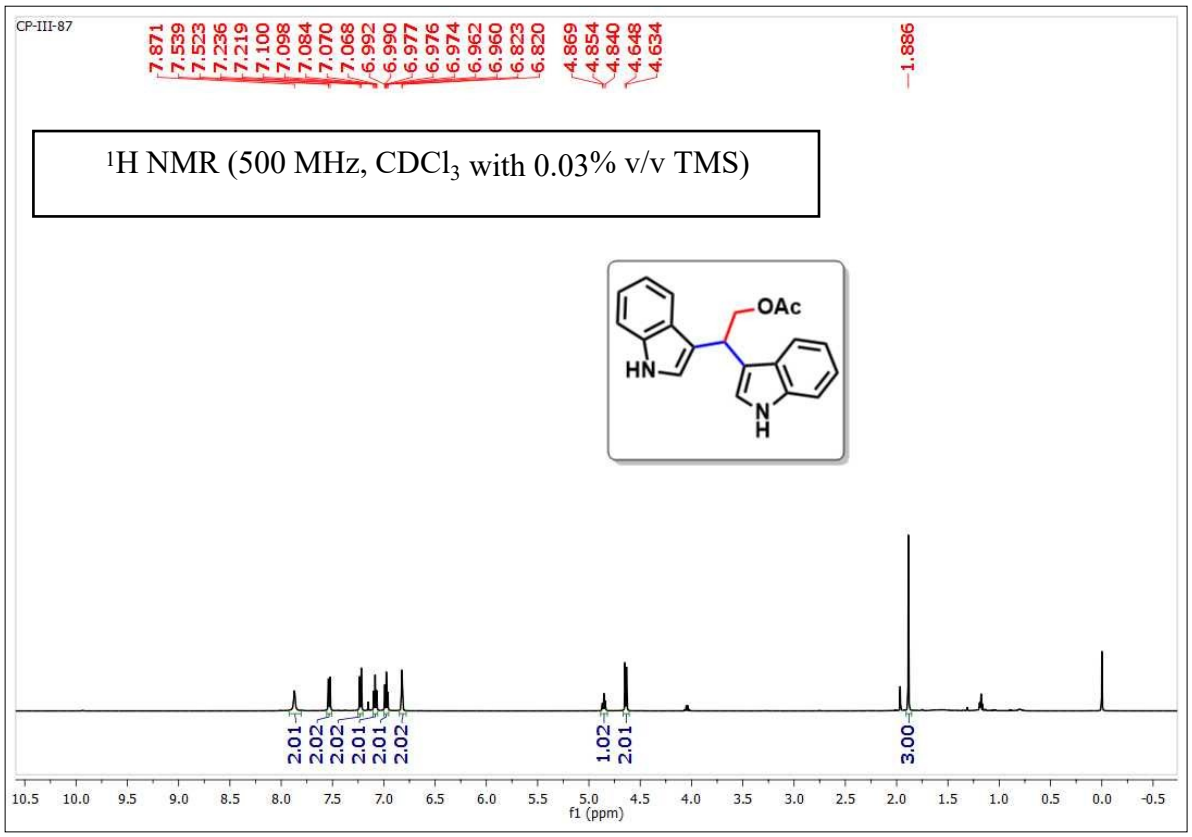

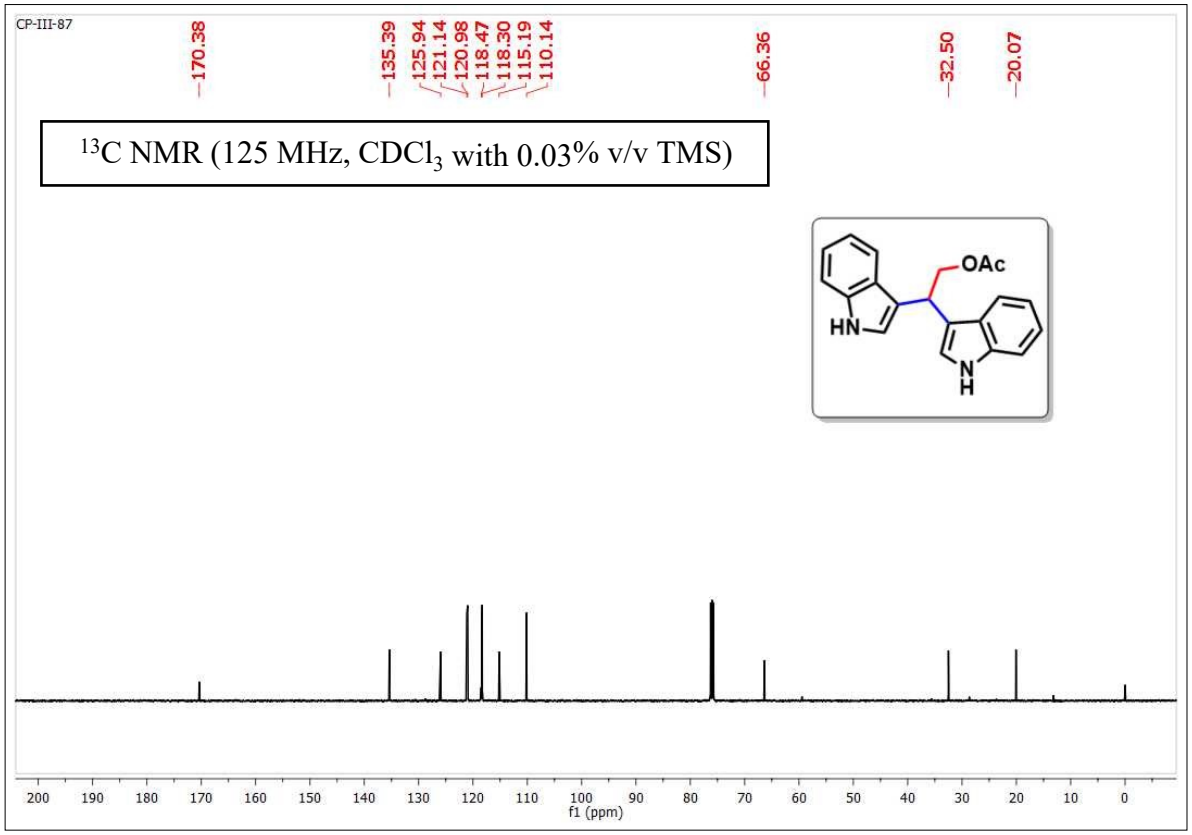

2,2-di(1H-indol-3-yl)ethyl butyrate (Arsindoline B, 55)

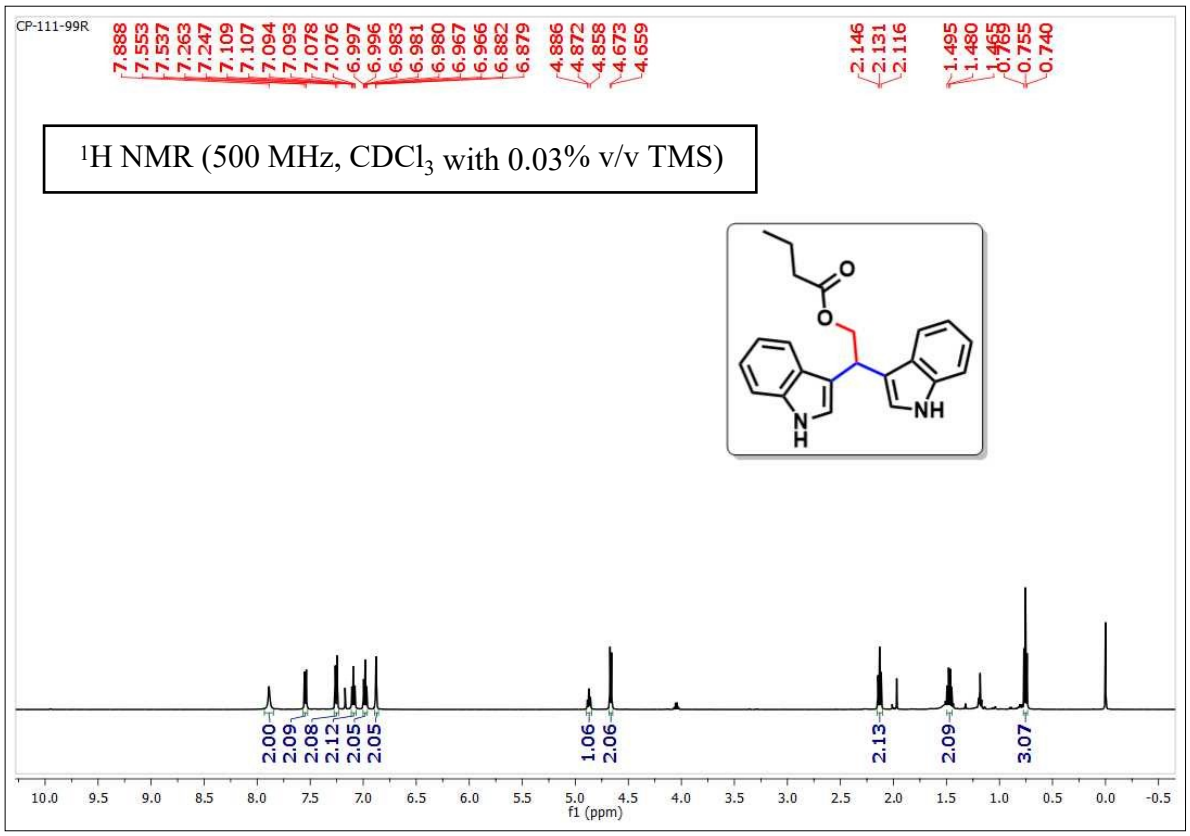

^{1}H NMR (500 MHz, $CDCl_3$ with 0.03% v/v TMS)

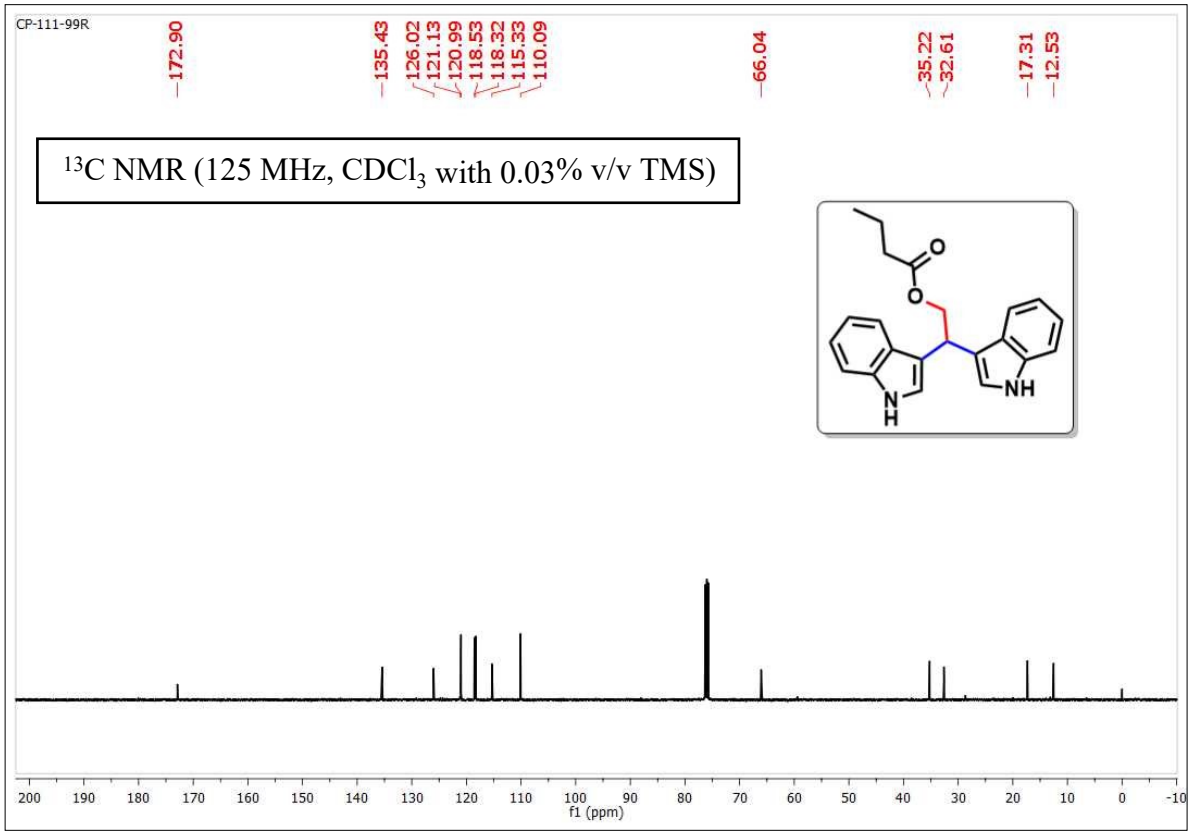

^{13}C NMR (125 MHz, $CDCl_3$ with 0.03% v/v TMS)

11. References

1 X. Guan and R. T. Borchardt, A Convenient Method for the Synthesis of Indole-3-acetic Acids, *Tetrahedron Lett.,* 1994, **35**, 3013–3016.

2 A. M. Davies, S. S. Londhe, E. R. Smith and J. A. Tunge, Single-Step Synthesis of γ–Ketoacids through a Photoredox-Catalyzed Dual Decarboxylative Coupling of α–Oxo Acids and Maleic Anhydrides, *Org. Lett.,* 2023, **25**, 8634–8639.

3 W. Kuldeep, C. Yang, P. R. West, K. C. Deming, S. R. Chemburkar and R. E. Reddy, Synthesis of Arylglyoxylic Acids and Their Collision-Induced Dissociation, *Synth Commun.,* 2008, **38,** 4434–4444.

4 L. Shuangjie, Z. Wei, G. Feng, L. Chunpu, W. Jiang and L. Hong, Palladium-Catalyzed Ortho-Alkoxylation of N-Benzoyl α-Amino Acid Derivatives at Room Temperature, *J. Org. Chem.,* 2017, **82**, 126−134.

5 A. Frisch, Gaussian 09W Reference, 1996.

6 M. G. Valverde, N. A. Cordero and E. S. De la Cal, GAUSSVIEW® as a Tool for Learning Organic Chemistry. In EDULEARN15 Proceedings, 2015, 4366–4370.

7 O. Trott and A. J. Olson, Auto Dock Vina: Improving the Speed and Accuracy of Docking with a New Scoring Function, Efficient Optimization, and Multithreading, *J. Comput. Chem.,* 2010, **31**, 455–461.

8 J. Yang, R. Yan, A. Roy, D. Xu, J. Poisson and Y. Zhang, The I-TASSER Suite: Protein Structure and Function Prediction, *Nat. Methods.,* 2015, **121**, 7–8.

9 L. Jendele, R. Krivak, P. Skoda, M. Novotny and D. Hoksza, PrankWeb: A Web Server for Ligand Binding Site Prediction and Visualization, *Nucleic Acids Res.,* 2019, **47**, 345–349.

10 M. J. Abraham, T. Murtola, R. Schulz, S. Pall, J. C. Smith, B. Hess and E. Lindahl, GROMACS: High Performance Molecular Simulations Through Multi-level Parallelism from Laptops to Supercomputers, SoftwareX 1–2, 2015, 19–25.

11 M. J. Robertson, J. Tirado-Rives and W. L. Jorgensen, Improved Peptide and Protein Torsional Energetics with the OPLS-AA Force Field, *J. Chem. Theory Comput.,* 2015, **11**, 3499–3509.

12 G. Oanca, F. Van der Ent and J. Aqvist, Efficient Empirical Valence Bond Simulations with GROMACS, *J. Chem. Theory Comput.,* 2023, **19**, 6037–6045.

13 (a) J. Haribabu, Y. Tamura, K. Yokoi, C. Balachandran, M. Umezawa, K. Tsuchiya, Y. Yamada, R. Karvembu and S. Aoki, Synthesis and Anticancer Properties of Bis- and mono(cationic peptide) hybrids of Cyclometalated iridium(III) complexes: Effect of the Number of Peptide Units on Anticancer Activity, *Eur. J. Inorg. Chem.,* 2021, **2021**, 1796–1814; (b) S. Swaminathan, J. Haribabu, M. Dharmasivam, N. Maroli, J.P. Jayadharini, N. Balakrishnan, N. Bhuvanesh, C. Echeverria and R. Karvembu, Hinged Bipodal Furoylthiourea-based Ru(II)-arene Complexes: Effect of (ortho, meta, or para)- Substitution on Coordination and Anticancer Activity, *Inorg. Chem.,* 2023, **62**, 3679–3691.

14 T. Lucia, Drug Development: Stages, Challenges, and Importance, *Int. J. of Drug Development and Research.,* 2023, **4**, 1–5.

15 A. Daina, O. Michielin and V. Zoete, SwissADME: A Free Web Tool to Evaluate Pharmacokinetics, Drug-likeness and Medicinal Chemistry Friendliness of Small Molecules, *Sci. Rep.,* 2017, **7**, 42717.

16 A. Daina and V. Zoete, A BOILED-Egg To Predict Gastrointestinal Absorption and Brain Penetration of Small Molecules, *Chem. Med. Chem.,* 2016, **11**, 1117–1121.

17 A. Daina, O. Michielin and V. Zoete, SwissTargetPrediction: Updated Data and New Features for Efficient Prediction of Protein Targets of Small Molecules, *Nucl. Acids Res.,* 2019, **47**, 357–364.
18 D. Gfeller, O. Michielin and V. Zoete, Shaping the Interaction Landscape of Bioactive Molecules, *Bioinformatics.,* 2013, **29***,* 3073–3079.
19 T. Yanai, P. T. David and N. C. Handy, A New hybrid Exchange–Correlation Functional Using the Coulomb-Attenuating Method (CAM-B3LYP), *Chem. Phys. Lett.,* 2004, **393**, 51–57.
20 A. Abkari, I. Chaabane and K. Guidara, DFT (B3LYP/LanL2DZ and B3LYP/6311G+(d,p)) Comparative Vibrational Spectroscopic Analysis of Organic–Inorganic Compound Bis(4-acetylanilinium) tetrachlorocuprate (II), Phys. E Low-Dimensional Syst. *Nanostructures.,* 2016, **81**, 136–144.
21 J. Rafique, Q. Q. Afzal, M. Perveen, J. Iqbal, M. S. Akhter, S. Nazir, M. S. Al-Buriahi, S. Alomairy and Z. A. Alrowaili, Drug Delivery of Carvedilol (Cardiovascular Drug) Using Phosphorene as a Drug Carrier: A DFT Study, *J. Taibah Univ. Sci.,* 2022, **16**, 31–46.
22 M. Vipin, J. Haribabu, N. V. P. Vishnunarayanan, P. Rasin, V. Ramesh, V. S. Kumar, G. Mohit, N. Bhuvanesh, A. Sreekanth, Copper-mediated Cyclization of Thiosemicarbazones Leading to 1,3,4-thiadiazoles: Structural Elucidation, DFT Calculations, in Vitro Biological Evaluation and in Silico Evaluation Studies, *Spectrochim. Acta - Part A Mol. Biomol. Spectrosc.,* 2024, **313**, 124117.
23 S. Bangaru, G. Madhu, M. Srinivasan and M. Prasath, Exploring Flexibility, Intermolecular Interactions and ADMET Profiles of Anti-influenza Agent Isorhapontigenin: A Quantum Chemical and Molecular Docking Study, *Heliyon,.* 2022, **8**, e10215.
24 E. J. Hanan, M. Baumgardner, M. C. Bryan, Y. Chen, C. Eigenbrot, P. Fan, X. H. Gu, H. La, S. Malek, H. E. Purkey, G. Schaefer, S. Schmidt, S. Sideris, I. Yen, C. Yu and T. P. Heffron, 4-Aminoindazolyl-dihydrofuro[3,4-d]pyrimidines as Non-covalent Inhibitors of Mutant Epidermal Growth Factor Receptor Tyrosine Kinase, *Bio organic Med. Chem. Lett.,* 2016, **26**, 534–539.
25 N. V. P. Vishnunarayanan, J. Haribabu, V. S. Kumar, J. F. Santibanez, M. Vipin, P. Rasin, G. Mohit, N. Bhuvanesh and A. Sreekanth, Unraveling the Anticancer Efficacy and Biomolecular Properties of Ru(II)-Arene Complexes of Pyrene-Based Thiosemicarbazone Ligands: A Comprehensive In Silico/In Vitro Exploration, *Organometallics.,* 2024, **43**, 242–260.
26 K. M. R. Marques, M. R. Desterro, S. M. Arruda, L. N. A. Neto, M. C. A. Lima, S. M. V. Almeida, E. C. D. Silva, T. M. Aquino, E. F. Silva-Junior, J. X. Araujo-Junior, M. M. Silva, M. D. Dantas, J. C. Santos, I. M. Figueiredo, M. Bazin, P. Marchand, T. G. Silva and F. J. B. Junior, 5-Nitro-Thiophene-Thiosemicarbazone Derivatives Present Antitumor Activity Mediated by Apoptosis and DNA Intercalation, *Curr. Top. Med. Chem.,* 2019, **19**, 1075–1091.
27 T. A. Wani, H. Rabiah, A. H. Bakheit, M. A. Kalam and S. Zargar, Study of Binding Interaction of Rivaroxaban with Bovine Serum Albumin using Multi-Spectroscopic and Molecular Docking Approach, *Chem. Cent. J.,* 2017, **11**, 134.
28 N. M. Anand, D. H. Liya, A. K. Pradhan, N. Tayal, A. Bansal, S. Donakonda and A. K. Jainarayanan, A Comprehensive SARS-CoV-2 Genomic Analysis Identifies Potential Targets for Drug Repurposing, *PLoS One.,* 2021, **16**, e0248553.
29 S. Younus, S. S. V. Chandra and A. S. S. Nair, Docking and Dynamic Simulation Study of Crizotinib and Temozolomide Drug with Glioblastoma and NSCLC Target to Identify Better Efficacy of the Drug, *Futur J Pharm Sci.,* 2021, **7**, 187.
30 H. Congde, W. Cheng, S. Chougu, J. Xiaodong, W. Xicun, C. Wenju and W. Mingxia, Triarylaminium Salt-Initiated Aerobic Double Friedel–Crafts Reaction of Glycine Derivatives with Indoles, *Adv. Synth. Catal.,* 2013, **355**, 1911–1916.

31 D. C. Holland, J. B. Hayton, M. J. Kiefel and A. R. Carroll, Synthesis and Cheminformatics-Directed Antibacterial Evaluation of Echinosulfonic Acid – Inspired Bis-Indole Alkaloids, *Molecules,* 2024, **29**, 2806.
32 S. Lucarini, M. Mari, G. Piersanti and G. Spadoni, Organocatalyzed Coupling of Indoles with Dehydroalanine Esters: Synthesis of Bis(indolyl)propanoates and Indolacrylates, *RSC Adv.,* 2013, **3**, 19135–19143.
33 P. Sharma, S. Rohilla, and N. Jain, Palladium Catalyzed Carbonylative Coupling for Synthesis of Arylketones and Arylesters Using Chloroform as the Carbon Monoxide Source, *J. Org. Chem.,* 2017, **82**, 1105−1113.
34 C. Xu, N. Zhang, X. Li, Y. Ge, P. Diao and C. Guo, Visible Light Promotes Decyanation Esterification Reaction of β-Ketonitriles with Dioxygen and Alcohols to α-Ketoesters, *Synlett.,* 2018, **29**, 1065–1070.
35 S. Roy, G. Kumar and I. Chatterjee, Photoinduced Diverse Reactivity of Diazo Compounds with Nitrosoarenes, *Org. Lett.,* 2021, **23**, 6709−6713.
36 Z. Yang, H. Liu, B. Pan, F. He and Z. Pan, Design and Synthesis of (Aza)indolyl maleimide based Covalent Inhibitors of Glycogen Synthase Kinase 3β, *Org. Biomol. Chem.,* 2018, **16**, 4127–4140.
37 L. M. Despinoy and M. Hamish, 1-Methoxycarbonylpyrrolizin-3-one and Related Compounds, *Org. Biomol. Chem.,* 2009, **7**, 2187–2194.
38 E. R. Kotb, M. A. Salama, M. A. Anwar and M. S. Soliman, Synthesis and Reactions of Some Novel Quinoxalines for Anticancer Evaluation, *Phosphorus, Sulfur, and Silicon,* 2007, **182**, 1119–1130.
39 R. S. Ramony, N. Marionz and S. P. Nolan, [(NHC)AuCl]-Catalyzed Meyer–Schuster Rearrangement: Scope and Limitations, *Tetrahedron.,* 2009, **65**, 1767–1773.
40 S. C. Ghosh, J. S. Y. Ngiam, A. M. Seayad, D. T. Tuan, C. L. L. Chai and A. Chen, Copper-Catalyzed Oxidative Amidation of Aldehydes with Amine Salts: Synthesis of Primary, Secondary, and Tertiary Amides, *J. Org. Chem.,* 2012, **77**, 8007−8015.
41 Z. Hua, Y. Zhanga, Q. And, B. Xua, W. Pana, P. Caoa, C. Liub, Z. Huangc, W. Xiad, J. Qiue, G. Liang, Development of a Practical and Scalable Synthesis of Anti-HBV Drug Y101, *Tetrahedron.,* 2014, **70**, 9592−9600.
42 D. Curran, O. Dada, H. Muller-Bunz, M. Rothemund, G. Sanchez-Sanz, R. Schobert, X. Zhu and M. Tacke, Synthesis and Cytotoxicity Studies of Novel NHC-Gold(I) Complexes Derived from Lepidiline A, *Molecules.,* 2018, **23**, 2031.
43 T. Zhang, S. Li, W. Yuan, Y. Zhang, F. Meng, Design, Synthesis, and Molecular Docking Studies of N- (9,10- anthraquinone- 2- carbonyl)amino Acid Derivatives as Xanthine Oxidase Inhibitors, *Chem Biol Drug Des.,* 2018, **91**, 893–901.
44 Z. Yuan, Y. Xiaorong, Z. Huang, L. Shilin, Z. Yin and L. Ying, Visible Light-induced Aerobic Oxidative Cross-coupling of Glycine Derivatives with Indoles: A Facile Access to 3,3' Bisindolylmethanes, *Org. Chem. Front.,* 2018, **5**, 2120–2125.